ON THE FILM THICKNESS IN GREASE LUBRICATED DEEP GROOVE BALL BEARINGS

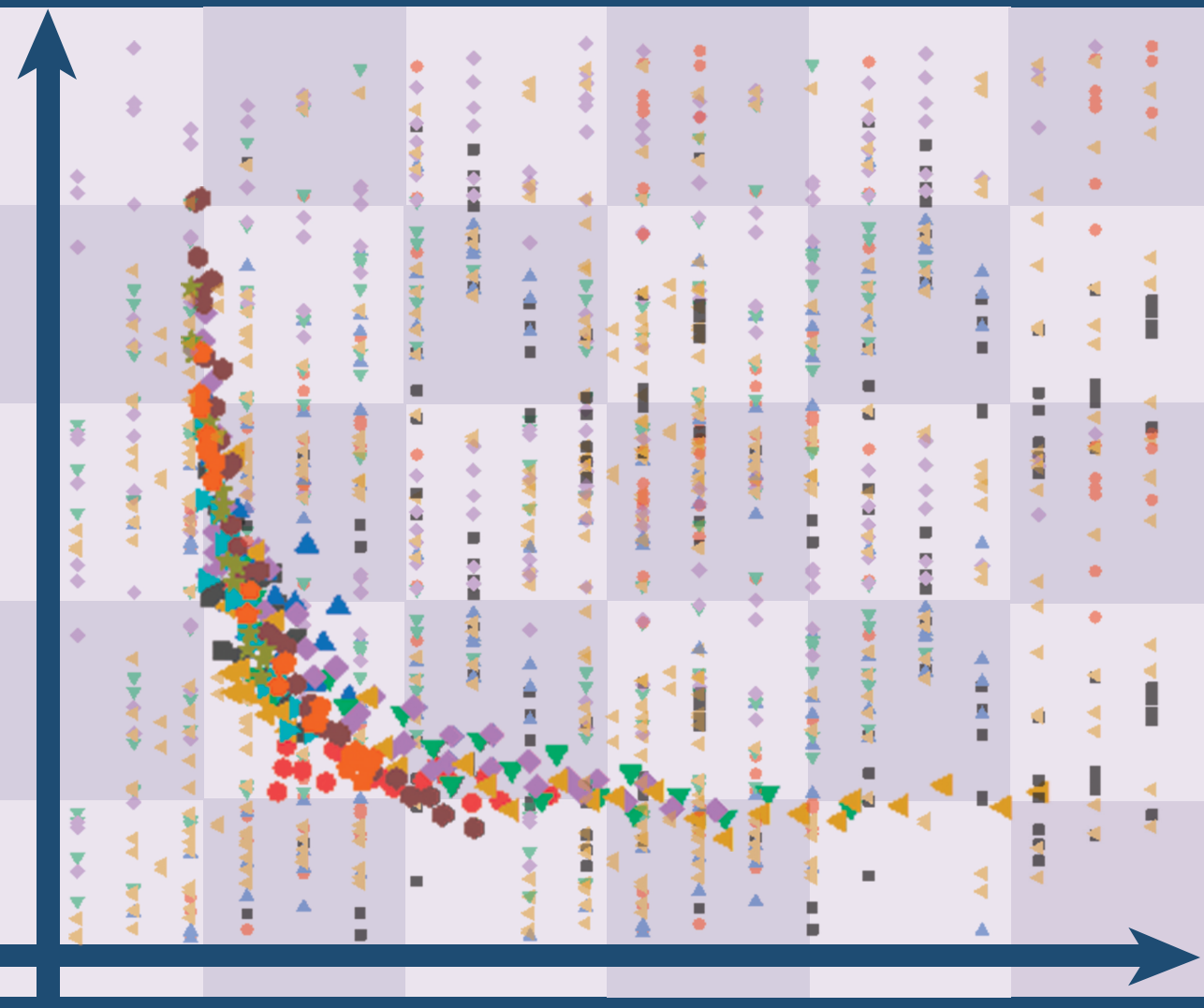

Pramod Shetty

ON THE FILM THICKNESS IN GREASE LUBRICATED DEEP GROOVE BALL BEARINGS

Pramod Shetty

ON THE FILM THICKNESS IN GREASE LUBRICATED DEEP GROOVE BALL BEARINGS

DISSERTATION

to obtain

the degree of doctor at the University of Twente,

on the authority of the rector magnificus,

prof.dr.ir. A.Veldkamp,

on account of the decision of the Doctorate Board

to be publicly defended

on Friday 28^{th} June, 2024 at 12.45 hours

by

Pramod Shetty

born on the 19^{th} of June, 1992

in Udupi, Karnataka, India

This dissertation has been approved by:

Promotor:

Prof.dr.ir. P.M.Lugt

Co-promotor:

Dr. J.A. Osara

This research is supported by SKF RTD, Houten, Netherlands, and Shell Downstream Services International BV, Rotterdam, Netherlands.

Cover design: Pramod Shetty

Printed by: Ipskamp Printing, Enschede

Lay-out: Pramod Shetty

ISBN (print): 978-90-365-6166-2

ISBN (digital): 978-90-365-6167-9

DOI: 10.3990/1.9789036561679

GRADUATION COMMITTEE:

Chair/secretary	Prof. dr. ir. H.F.J.M. Koopman	University of Twente
Promotor	Prof. dr. ir. P.M.Lugt	University of Twente
Co-promotor	Dr. J.A. Osara	University of Twente
Committee members	Prof. dr. R.S. Dwyer-Joyce	University of Sheffield
	Prof. dr. M. Hartl	Brno University of Technology
	Prof.dr.ir. C.H. Venner	University of Twente
	Prof.dr. F.G. Mugele	University of Twente

Dedicated to my Grandpa for inspiring and encouraging my academic journey, and to my mother for her unwavering support.

"Remember that sometimes not getting what you want is a wonderful stroke of luck"

– H.H. The Dalai Lama

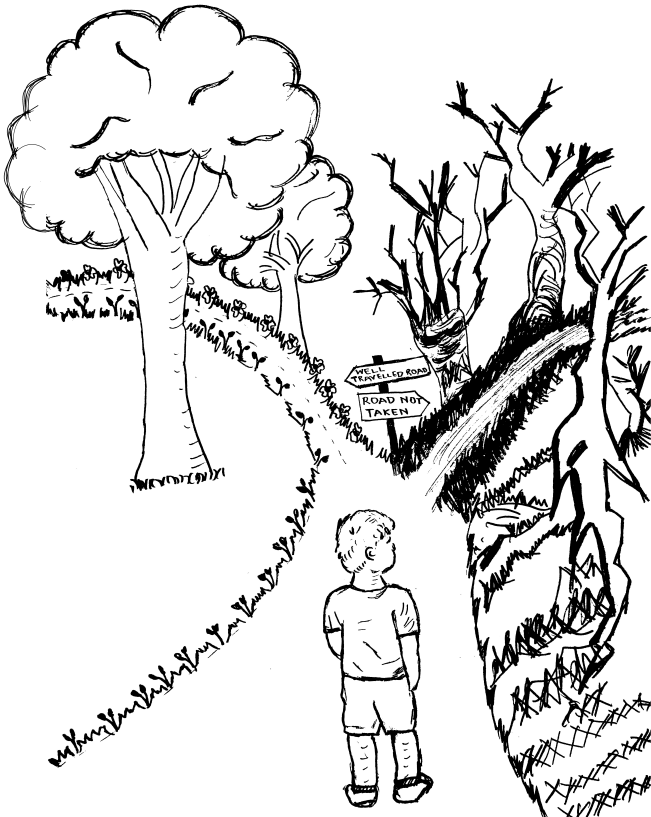

SUMMARY

Most rolling bearings use grease as a lubricant. The service life of a bearing is determined by the bearing fatigue life and grease life. Both are influenced by the quality of lubrication, which is strongly determined by the thickness of the lubricating film. The optimum selection of a lubricating grease and/or the prediction of grease and/or bearing life can only be done properly if the film thickness can be determined. However, until now, there is no equation to predict film thickness in grease lubricated bearings. In practice, the equations that were derived for oil lubrication are used.

In this thesis, the film thickness immediately after the churning phase is studied at various conditions on different bearings and greases. The film thickness is measured after running the bearings for more than 100 hours after freshly filling them, to ensure that the churning phase is finished. It is expected that the bearings then may operate in starved lubrication conditions. An improved electrical capacitance method is developed to measure the film thickness by using an electrical model of the bearing, including the effect of starvation. Excluding starvation would overestimate the film thickness.

It is observed that the film thickness in a grease lubricated bearing initially increases with speed, similar to oil-lubricated contacts. With further increase in speed, the film thickness becomes almost constant; no further increase due to starvation. It also does not decrease with increasing speed due to a balancing replenishment mechanism. Under starvation, the side flow of the lubricant depends on the contact residence time and the over rolling frequency, which balance out at higher speeds.

The film thickness is measured in bearings filled with different grease quantities. It is shown that the film thicknesses differ only during the churning phase of the lubricant. After the churning phase, the self-induced temperatures and film thicknesses are the same irrespective of initial grease amount in the bearing. This implies that the thicknesses of the oil layers left on the track after the clearing phase is independent of the grease volume in the bearing. This suggests that the film thickness immediately after churning is determined by the dynamics of the flow of lubricants in and around the contacts and not by oil released by the grease after churning (bleed).

Contact replenishment is caused by the capillary action around the ball-ring groove contacts. This replenishment is enhanced in the presence of vibrations which cause the balls in the bearings to oscillate curvilinearly on the tracks. This motion makes the balls roll over the ridges formed by the previous balls resulting in increased film thickness. It is also shown that this type of supplementary replenishment by vibrations depends on the load. A model to predict the increase in film thickness due to vibrations is proposed.

It is known that the level of starvation under pure axial load can be well described using only the product of base oil viscosity, half contact width, and linear speed (ηbu).

With the improved film thickness measurement technique, a more accurate power law relationship is proposed to predict the relative film thickness. The dependency of film thickness on load is higher in starved contacts than in fully flooded contacts. It is also observed that bearing size/geometry has little to no influence in determining the level of starvation in the ηub concept.

The film thickness study in radially loaded bearings and bearings under combined (axial+radial) loads showed that there is an additional replenishment at the lower loaded zones. This is due to a larger 'gap' between the ball and the groove in the low load zone causing a reduction in resistance to viscous flow, thereby increasing the flow of lubricant towards the contacts. The level of starvation in bearings under radial and combined loads is lower than in pure axially loaded bearings. The magnitude of the surface tension of the lubricant becomes essential to determine the level of starvation when bearings are running under radial or combined load. It is shown that the surface tension of the lubricant varies with temperature and may differ significantly between base oils for lubricating greases.

Finally, a master curve is created that can be used to calculate the film thickness in grease lubricated ball bearings under radial, axial and combined loads.

SAMENVATTING

In the meeste wentellagers wordt smeervet gebruikt als smeermiddel. De gebruikslevensduur van een lager wordt bepaald door de levensduur van zowel het lager als van het smeervet. Beide worden sterk beïnvloed door de kwaliteit van de smering, die sterk wordt bepaald door de dikte van de smeerfilm. De optimale selectie van een smeervet en/of het voorspellen van de levensduur van het vet en/of het lager kan alleen goed gebeuren als de smeerfilmdikte kan worden uitgerekend. Tot nu toe is er echter geen vergelijking om de smeerfilmdikte in vetgesmeerde lagers te voorspellen. In de praktijk worden de vergelijkingen gebruikt die voor oliesmering zijn afgeleid.

In dit proefschrift wordt de smeerfilmdikte direct na de 'churning fase' bestudeerd onder verschillende condities voor verschillende lagers en smeervetten. De smeerfilmdikte wordt gemeten nadat de lagers meer dan 100 uur hebben gedraaid nadat ze opnieuw zijn gevuld, om er zeker van te zijn dat de churning fase is voltooid. Er wordt verwacht dat de lagers dan onder zogenaamde schrale smeringscondities draaien. Er is een verbeterde elektrische capaciteitsmethode ontwikkeld om de filmdikte te meten door gebruik te maken van een elektrisch model van het lager, inclusief het effect van schrale smering. Het uitsluiten van schrale smering zou de smeerfilmdikte overschatten.

De smeerfilmdikte in een vetgesmeerd lager neemt aanvankelijk toe met de snelheid, vergelijkbaar met oliegesmeerde contacten. Bij een verdere toename van de snelheid wordt de smeerfilmdikte vrijwel constant; geen verdere stijging als gevolg van schrale smering. Ze neemt ook niet af naarmate de snelheid toeneemt, dankzij een aanvulmechanisme ('replenishment'). Bij schrale smering is de zijstroming van het smeermiddel uit de kogel-ring-contacten afhankelijk van de contactverblijftijd en de overrolfrequentie, die bij hogere snelheden in evenwicht komen.

De smeerfilmdikte wordt gemeten in lagers gevuld met verschillende vethoeveelheden. Er wordt aangetoond dat deze alleen verschillen tijdens de churning fase van het smeermiddel. Na de churning fase zijn de zelfgeïnduceerde temperaturen en olielaagdiktes hetzelfde, ongeacht de initiële hoeveelheid vet in het lager. Dit houdt in dat de dikte van de olielagen die na de 'clearing' fase op het spoor achterblijven, onafhankelijk is van het vetvolume in het lager. Dit suggereert dat de filmdikte onmiddellijk na de churning fase wordt bepaald door de dynamiek van de smeermiddelstroming in en rond de contacten en niet door de olie die vrijkomt uit het vet (olie-bloeding uit het smeervet).

Contactreplenishment wordt veroorzaakt door de capillaire werking rond de kogel-ring-contacten. Deze replenishment wordt versterkt door de aanwezigheid van trillingen die ervoor zorgen dat de kogels in de lagers kromlijnig op de loopbanen oscilleren. Deze beweging zorgt ervoor dat de kogels over de 'vloeistofruggen' rollen die door de vorige ko-

gels zijn gevormd, wat resulteert in een grotere smeerfilmdikte. Ook wordt aangetoond dat dit soort olie-aanvulling door trillingen afhankelijk is van de belasting. Er wordt een model afgeleid om de toename van de smeerfilmdikte als gevolg van trillingen te voorspellen.

Het is bekend dat de mate van schrale smering onder puur axiale belasting goed kan worden beschreven door een vergelijking met slechts het product van de viscositeit van de basisolie, de halve contactbreedte en de lineaire snelheid (ηbu). Met de verbeterde techniek voor het meten van de smeerfilmdikte wordt een nauwkeuriger vergelijking afgeleid om de relatieve filmdikte te voorspellen.

De afhankelijkheid van de smeerfilmdikte van de belasting is groter bij schraal gesmeerde contacten dan bij contacten waarbij er veel olie op de loopbanen zit. Er wordt ook vastgesteld dat de afgeleide vergelijkingen onafhankelijk zijn van de grootte van het lager.

Uit het smeerfilmdikteonderzoek bij radiaal belaste lagers en lagers onder gecombineerde (axiale+radiale) belastingen blijkt dat er extra toevoer van olie naar de contacten plaatsvindt in de zone in de omtrek van het lager waar de contactbelastingen lager zijn. Dit komt door een grotere 'opening' tussen de kogel en de groef in de zone met lage belasting, waardoor de weerstand tegen viskeuze stroming afneemt, waardoor de stroming van smeermiddel naar de contacten toeneemt. De mate van schrale smering bij lagers onder radiale en gecombineerde belastingen is lager dan die bij puur axiaal belaste lagers. De waarde van de oppervlaktespanning van het smeermiddel wordt essentieel om de mate van schrale smering te bepalen wanneer lagers onder radiale of gecombineerde belasting draaien. Er wordt aangetoond dat de oppervlaktespanning van het smeermiddel een functie is van de temperatuur en daarnaast aanzienlijk kan verschillen tussen verschillende basisoliën voor smeervetten.

Tenslotte wordt een mastercurve gecreëerd waarmee de smeerfilmdikte in vetgesmeerde kogellagers onder radiale, axiale en gecombineerde belastingen kan worden berekend.

DANKWOORD & ACKNOWLEDGEMENT

This thesis would not have been possible without the support of many people. I would like to express my gratitude to each individual who helped me in one way or another in completing this thesis.

First and foremost, my acknowledgment goes to my mentor, Prof. Dr. Ir. P. M. Lugt. His trust in my work motivated me to overcome hardships. Without his encouragement and guidance, this thesis would not have been possible. I sincerely thank my other mentors, Dr. J. A. Osara, Dr. Rihard Pasaribu, and Ir. Robert Jan Meijer. Their comments and guidance during the project were instrumental in keeping it on track. The amount of knowledge they have passed on to me cannot be expressed in words.

Next, I thank all my committee members, Prof. Dr. R. S. Dwyer-Joyce, Prof. Dr. M. Hartl, Prof. Dr. Ir. C. H. Venner, and Prof. Dr. F. G. Mugele, for accepting our request and dedicating a significant amount of time and effort to reviewing my thesis.

My sincere appreciation goes to Dr. Norbert F. Bader for our numerous discussions. His insights on my models and hypotheses greatly helped refine them. My heartfelt gratitude goes to Dr. Erik de Vries for being with me in the laboratory every time the test rig broke down. I would also like to thank Dries van Swaaij and Leo Tiemersma for their frequent assistance in the laboratory. I thank Belinda Bruinink and Debbie Zimmerman for making my life at the university easier. Profound gratitude to Sip Jan, Geert Mentink, and Jochem Paalman for their assistance in developing the test rig. Without their timely help, I would still be fixing my test rig.

I would like to thank Dr. Pranab Samantha and Mr. Guru Prasad, who introduced me to tribology. Many thanks to Dr. Sathwik Chatra, Faizan Rabbani, and Ashuthosh from SKF for all the support they have given me. I express my gratitude to Dr. Alan Wheatley from Shell for his technical inputs.

My gratitude also goes to Tanmaya Mishra, Alex Vrcek, Mohammad Sattari, Xavier Borras, Melkamu Mekicha, Dmitrii Sergachev, and Pedro Amoroso. I appreciate all the good times we had together.

Special thanks to my brother from another mother, Amit Roy, and my childhood friend, Karthik Rao, for all the moral support they provided. I thank all my TRIBOS friends for the good memories. Many thanks to Jasmin for sending all the research articles I could not access from the Netherlands. Special thanks to Nayan and Marko for all the knowledge they shared with me. I thank all the members of Gada Boys for their inexplicable encouragement to pursue my dream.

I thank all my colleagues and friends who made sure that we had lunch at exactly 12 pm. I thank my lunchmates Farshid, Shubang, Oday, Malek, Atiyeh, Ashkan, Mostafa, Shari, Zara, and Mehdi. I also thank my officemates Min, Femke, and Lieke, who created a good ambiance in the office.

My heartiest thanks to my buddies Ana and Samantha, who made life in the Netherlands adventurous.

I would like to extend my gratitude to my family. Without their encouragement and support, completing this thesis would not have been possible. Thanks to my mom, brother, mother-in-law, father-in-law, Naani, and our cats Navilu and Saint. They made sure that I did not break down during my PhD.

Finally, my sincere appreciation goes to my wife, Shalaka, who was my constant support during my PhD journey.

CONTENTS

LIST OF PUBLICATIONS

(A) Shetty P, Meijer RJ, Osara JA, Lugt PM. Measuring film thickness in starved grease-lubricated ball bearings: an improved electrical capacitance method. Tribology Transactions. 2022 Aug 25;65(5):869-79. https://doi.org/10.1080/10402004.2022.2091067

(B) Shetty P, Meijer RJ, Osara JA, Pasaribu R, Lugt PM. Effect of Grease Filling on the Film Thickness in Deep-Groove Ball Bearings. Tribology Transactions. 2023 Dec 8:1-8. https://doi.org/10.1080/10402004.2023.2282632

(C) Shetty P, Meijer RJ, Osara JA, Pasaribu R, Lugt PM. Vibrations and film thickness in grease-lubricated deep groove ball bearings. Tribology International. 2024 May 1;193:109325. https://doi.org/10.1016/j.triboint.2024.109325

(D) Shetty P, Meijer RJ, Osara JA, Pasaribu R, Lugt PM. Effect of bearing size on film thickness in grease-lubricated axially loaded deep groove ball bearings. Tribology International. 2024 May 8:109748. https://doi.org/10.1016/j.triboint.2024.109748

(E) Shetty P, Meijer RJ, Osara JA, Pasaribu R, Lugt PM. Film thickness in grease-lubricated deep groove ball bearings–a master curve.

The next paper is a publication that is not related to the research on film thickness in deep groove ball bearings but has been added to complete the overview of the work that was done by me at the University of Twente.

(F) Shetty P, Meijer RJ, Lugt PM. An evaporation model for base oil from grease-lubricated rolling bearings including breathing. Tribology Transactions. 2021 Sep 3;64(5):891-902. https://doi.org/10.1080/10402004.2021.1943088

NOMENCLATURE

ϵ_0	Permittivity constant	$[Fm^{-1}]$
α	Viscosity–pressure coefficient	$[\mathrm{Pa}^{-1}]$
β	Temperature-viscosity coefficient	$[1/^\circ C]$
β'	Contact angle	[deg]
δ_i	Elastic deformation in ball-inner ring contact	[m]
δ_o	Elastic deformation in ball-outer ring contact	[m]
ϵ_{air}	Dielectric constant of air	[-]
ϵ_{oil}	Dielectric constant of oil	[-]
η	Dynamic viscosity of the base oil	$[\mathrm{Pa}\cdot\mathrm{s}]$
η_{T_i}	Dynamic viscosity of the base oil at the inner ring	$[\mathrm{Pa}\cdot\mathrm{s}]$
η_{T_o}	Dynamic viscosity of the base oil at the outer ring	$[\mathrm{Pa}\cdot\mathrm{s}]$
$\hat{a}$	Vibration acceleration	$[\mathrm{ms}^{-2}]$
$\hat{a}_0$	Vibration acceleration without unbalancing mass	$[\mathrm{ms}^{-2}]$
$\rho(p)$	Density at pressure p	$[\mathrm{kgm}^{-3}]$
ρ_0	Density at atmospheric pressure	$[\mathrm{kgm}^{-3}]$
σ	Surface tension	$[\mathrm{Nm}^{-1}]$
a	Half contact along the rolling direction for inner ring-ball contact	[m]
A_{Hertz}	Hertzian contact area	$[m^2]$
A_{lv}	Experimentally determined constant in Pelofsky's equation	$[\mathrm{Nm}^{-1}]$
b	Half contact width across the rolling direction for inner ring-ball contact	[m]
B_{lv}	Experimentally determined constant in Pelofsky's equation	$[\mathrm{Pa}\cdot\mathrm{s}]$
Br	Brinkman number	[-]
C_i	Ball-inner ring capacitance	[F]
C_L	Load dependent parameter	[-]
C_o	Ball-outer ring capacitance	[F]
C_T	Non-dimensional thermal correction factor	[-]

$C_{background}$	Background capacitance	[F]
C_{cav}	Capacitance at the outlet	[F]
$C_{flooded}$	Flooded area capacitance	[F]
$C_{i,Hertz}$	Inner ring Hertz capacitance for single contact	[F]
C_{inner}	Total inner ring capacitance	[F]
$C_{o,Hertz}$	Outer ring Hertz capacitance for single contact	[F]
$C_{o,outside}$	Outer ring outside capacitance for single contact	[F]
C_{outer}	Total outer ring capacitance	[F]
$C_{outside}$	Outside capacitance of a single contact	[F]
C_{total}	Total calculated bearing capacitance	[F]
E'	Reduced elastic modulus	[Pa]
F	Load on the contact	[N]
G	Dimensionless material parameter $G = \alpha E'$	[-]
h_∞	Oil layer thickness	[m]
h_g	Grease film thickness	[m]
h_c	Central film thickness	[m]
H_{ff}	Dimensionless fully flooded film thickness	[-]
h_{ff}	Calculated fully flooded base oil film thickness	[m]
$h_{g,\hat{a}_0}$	Film thickness at vibration acceleration $\hat{a}_0$	[m]
$h_{g,\hat{a}}$	Film thickness at vibration acceleration $\hat{a}$	[m]
h_{gap}	Distance between the ball and the surface	[m]
h_m	Minimum film thickness	[m]
h_{st}	Starved film thickness	[m]
K	Thermal conductivity of the lubricant	$[Wm^{-1\circ}C^{-1}]$
k_d	Ellipticity parameter $k_d = 1.03\left(\frac{R_y}{R_x}\right)^{0.63}$	[-]
m	Dimensionless meniscus length from the center of the contact	[-]
m^*	Dimensionless inlet distance at the boundary between fully flooded and starved condition	[-]
m_1	Unbalancing mass	[kg]
m_2	Unbalancing mass	[kg]

n	Number of balls	[-]
ndm	Speed number	[mm × min^{-1}]
p	Pressure	[Pa]
P_d	Diametrical clearance	[m]
p_m	Maximum Hertzian pressure	[Pa]
R_b	Ball radius	[m]
R_i	Inner ring radius in the rolling direction	[m]
R_o	Outer ring radius in the rolling direction	[m]
R_x	Reduced radius in the direction of motion	[m]
R_y	Reduced radius normal to the direction of motion	[m]
SD	Dimensionless starvation parameter	[-]
SRR	Slip-to-roll ratio	[-]
T	Temperature	[$^\circ C$]
U	Dimensionless speed parameter $U = \frac{\eta u}{2E'R_x}$	[-]
u	Entrainment velocity (average velocity)	[m s^{-1}]
W	Dimensionless load parameter $W = \frac{F}{E'(R_x)^2}$	[-]
z_r	Radial distance between the ball top and the outer ring groove	[m]

1

INTRODUCTION

1.1 ROLLING BEARINGS

Rolling element bearings are among the most widely used machine elements in the world [1]. There are more than 50 billion bearings operating in the world at any moment in time [1]. They are used in almost every device that has a rotating component, including skateboards, computers, automobiles, aircraft, space crafts, sea vessels, and so on. More than 80-90% of these bearings are grease lubricated [2]. Unlike plain bearings or journal bearings which include significant sliding, rolling bearings are based on rolling and therefore consume very little frictional energy.

1.2 LUBRICATING GREASE IN ROLLING BEARINGS

Grease is made by blending base oil (typically 80-90%) with a thickening agent (10-20%) such as lithium soap, calcium soap, or polyurea [2, 3]. This semi-solid, colloidal material possesses unique rheological and lubricating characteristics. In practice, grease does not move unless the applied force overcomes its yield stress, shows shear thinning behavior, and may release oil from the thickener which is called bleeding. Traditionally grease is considered as a sponge filled with oil, with the sponge being the thickener, and whenever stress is applied, the oil is released from the thickener [3, 4]. The classical lubrication mechanism suggests that it is the bled oil from these stationary locations that replenishes the contact [5]. Once a newly filled bearing starts to rotate, the grease is redistributed in the bearing via a process known as churning [6]. During this process, most of the grease is deposited on the shield, and the rest of the grease settles on the shoulder and cage. The remaining heavily worked grease stays on the track [6]. Pictorially, this is shown in Figure 2.3. The churning process is divided into two sub-phases named (a) channeling: the first phase where grease is pushed aside and a channel is formed, and (b) clearing: the subsequent phase in which the remaining grease on the track is removed [7, 8]. After the end of the churning phase, typically 1-24 hours, the bleeding phase begins. This phase is by far the longer phase in the lifetime of the bearing and is characterized by a semi-steady state where oil may be released by the above mentioned

bleed process.

1.3 FILM THICKNESS IN GREASE LUBRICATED BEARINGS

The life and friction torque of grease lubricated rolling bearings are mainly determined by the quality of the lubricating film (partially or completely) separating the rolling element from the inner and outer rings of the bearings. If the surfaces are fully separated by a lubricant film then the bearing is running in "full film lubrication" conditions. The thickness of the film, commonly called "film thickness", is determined by the lubricant viscosity, contact geometry, and operating conditions. Predicting the film thickness facilitates the selection of the bearing size and lubricant for specific applications.

As mentioned above, grease consists mainly of oil and it is primarily this oil that lubricates the bearing contacts. There are equations to calculate the film thickness for oil-lubricated contacts when there is abundant oil around the contacts [9, 10]. In those conditions, the contacts are considered "fully flooded" [11] (see Figure 2.1). When the lubricant quantity influences the film thickness, the bearing is running under so-called "starved lubrication" conditions [11, 12]. The film thickness will therefore be smaller.

In grease lubricated bearings, the supply of oil towards the contacts is limited. This is not relevant at very low speeds, when there will be enough time for the oil to flow and provide fully flooded conditions. Actually, at very low speeds the film thickness will even be larger than the value calculated for fully flooded conditions. At moderately higher speeds, the film thickness will be almost equal to that calculated for fully flooded conditions. The explanation for this can be found in [13]. At moderate and higher speeds, the supply of oil from grease towards the contacts is limited, therefore, grease lubricated bearings mostly operate under starved lubrication [2].

So far, there are no models to predict the film thickness in grease lubricated bearings. The available models are based on starved EHL models. These models require the thickness of the oil layers "feeding the contacts", or the meniscus distance in front of the ball-race contacts, in addition to the properties that are needed to calculate the fully flooded film thickness. There are models that calculate the film thickness by calculating the side flow in the full contact domain (inlet and Hertzian contact) [14, 15], or only in the Hertzian contact area [16, 17]. These models are used to calculate the thickness of the layers in the outlet which forms the inlet for the next contact. These models predict a decreasing film thickness in time. By contrast, measurements on ball bearings running under constant operating conditions show that the film thickness is constant [18, 19], which indicates that there must also be a supply of lubricant to the contact.

On ball-on-disc machines, it has been shown that the relative film thickness (the ratio of grease film thickness to the calculated fully flooded film thickness) can be described by a dimensionless number containing the base oil viscosity and contact dimensions [20]. For axially loaded 6209 bearings, a more-or-less similar relationship was found between the relative film thickness and the product of viscosity (η), half contact width (b), and linear speed (u) [19]. This is the starting point of the research described in this thesis.

The important questions that are explored in this thesis are:

- How does the film thickness vary with speed in a ball bearing?
- Does the film thickness depend on the initial quantity of grease filled in the bearing?
- Does the film thickness depend on the bearing size?
- Does the film thickness depend on the type of load, i.e., axial load, radial load, and/or combined load?
- Immediately after the churning phase, what are the significant loss and replenishment mechanisms?
- Does the film thickness depend on the vibration level of the machine?
- Can one predict the film thickness immediately after the churning phase?

1.4 OUTLINE OF THE THESIS

This thesis is divided into two parts. In the first part, the study is summarized and the important results are discussed. In the second part, the complete peer-reviewed publications are attached. The remaining chapters in the first part include:
Chapter 2: In this chapter, the film thickness theory and the available models associated with the grease lubricated bearings are summarized.
Chapter 3: Here, methods to measure the film thickness in ball bearings are discussed. We show why a new method is required compared to the works of Wilson and Jablonka. We also discuss other experimental tools used in the study.
Chapter 4: Film thickness dependency on the initial grease quantity is discussed. Here, we show that film thickness immediately after the churning phase does not depend on the bleeding, and that there is no bulk reflow of grease.
Chapter 5: The influence of vibrations on film thickness is presented. We induce additional vibrations to prove the dependency of the film thickness on vibration.
Chapter 6: The film thickness in axially loaded bearings of various sizes is shown.
Chapter 7: The film thicknesses in a bearing under radial loads and combined (radial + axial) loads are presented. The effect of surface tension is shown.
Chapter 8: The conclusions from this research work and some recommendations for future studies are presented.

2

FILM THICKNESS THEORY FOR GREASE LUBRICATED BEARINGS

This chapter will briefly describe the theory and existing models that will be used in this thesis. It starts with the theory developed for oil-lubricated contacts and how this is applied to grease lubricated contacts. The chapter will finish with a description of how this theory is used in a novel film thickness measurement method.

2.1 FILM THICKNESS IN OIL LUBRICATED CONTACTS

2.1.1 FULLY FLOODED CONDITIONS

In 1886, Reynolds developed the hydrodynamic lubrication theory which described the lubrication mechanisms in conformal contacts [21]. When this was applied to non-conformal contacts, such as in bearings and gears, the film thicknesses obtained were too low to explain the successful operation of these machine elements. In 1945, Ertel showed that in non-conformal contacts, due to high pressure, there is a local elastic deformation in the contact, as well as a drastic increase in the lubricant viscosity. This helps to build the lubricant film in the non-conforming contacts [22]. This particular type of hydrodynamic lubrication is denoted by Elasto-Hydrodynamic Lubrication (EHL). After this breakthrough discovery, a lot of effort was put into obtaining the solutions for line contact problems numerically. The next milestone discovery happened in the 1960s when Dowson and Higginson proposed the (engineering) equations for film thickness based on the curve-fitted regression analysis for line contact problems [23]. Ertel and Petrusevich predicted a local drop in film thickness, a constriction at the contact exit, and a corresponding spike in pressure. The calculations of Dowson and Higginson confirmed this spike in pressure and the restriction in film thickness which gives the minimum film thickness [23–25]. Figure 2.1 shows the elastic deformation of the contacts, the constriction formed at the exit, the central film thickness h_c, minimum film thickness h_m, and the pressure distribution.

After solving the line contact problem, the solution for the elliptical contact problem was achieved more than a decade later because of the higher computing power required for the 2-dimensional nature of the problem [26]. In 1976-1977, Hamrock and Dowson published, for fully flooded conditions, the following equations for the central and minimum film thicknesses, which are still widely used today [10, 27–29]:

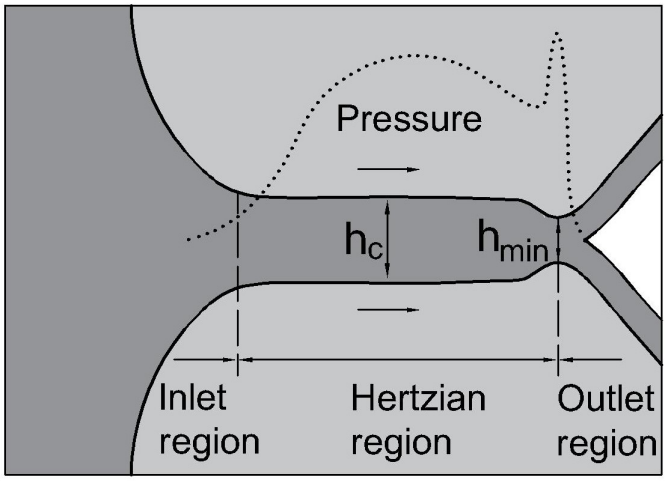

Figure 2.1: A fully flooded EHL contact showing the central and minimum film thickness. The dotted line shows the pressure profile in the contact.

$$\frac{h_c}{R_x} = 2.69U^{0.67}G^{0.53}W^{-0.067}(1-0.61e^{-0.73k_d}), \tag{2.1}$$

$$\frac{h_m}{R_x} = 3.63U^{0.68}G^{0.0.49}W^{-0.073}(1-e^{-0.68k_d}). \tag{2.2}$$

Here, h_c is the central film thickness (often written as h_{ff} where ff stands for "fully flooded"), h_m is the minimum film thickness, R_x is the reduced radius in x direction, k_d is the ellipticity parameter, G, U, and W are dimensionless material, speed, and load parameters, respectively. In deep groove ball bearings, elliptical contacts prevail.

2.1.2 STARVED CONDITIONS

In 1970, Wedeven observed that the film thickness also depends on the amount of oil in the inlet of the contacts, a lubrication condition called "starved lubrication" [11, 30]. The film generation in EHL contacts mainly depends on the pressure generated in the inlet region: if this region is supplied with a limited quantity of oil, the length over which shear flow towards the contact can take place is smaller, leading to a lower film thickness than in the case of fully flooded conditions [30]. Figure 2.2 shows the limited supply of oil in front of the contact, the meniscus position, central and minimum film thickness, and pressure distribution.

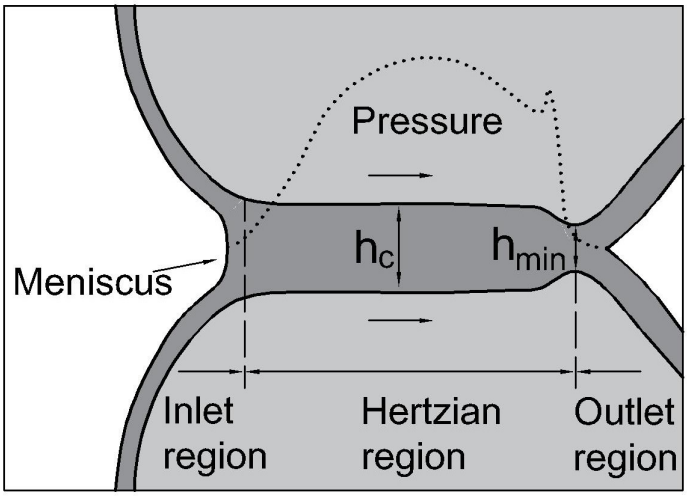

Figure 2.2: A starved EHL contact showing the central and minimum film thickness. The dotted line shows the pressure profile.

Wedeven showed that the film thickness in starved contacts can be correlated to the inlet meniscus position and proposed an equation to estimate the film thickness based on this. Later, an improved model for the film thickness based on this meniscus position was given by Hamrock and Dowson [31]. Finding the inlet meniscus position in a bearing is practically impossible/difficult, although great progress has been made in measuring this using ultrasonic sensors [32, 33]. Also, in the case of heavily starved contacts, the inlet meniscus coincides with the Hertzian contact radius, which makes this parameter of limited use [14]. Therefore, a model that uses the oil layer thickness on the track in front of the contact as a measure for the level of starvation was proposed by Damiens et al. [14]. This model uses a parameter called γ which determines the loss of lubricant from the contact by side-flow. By curve fitting the results of numerous simulations, they correlated γ with the operating parameters. In real bearings, the contacts are much wider than those for which they have calculated the γ values so the model cannot be used here directly.

Van Zoelen [34] recognized that the oil in the above mentioned layers that are feeding the EHL contacts with oil, not only flows due to the interaction with the balls but also by centrifugal shear stresses on the layers caused by the rotating rings and balls. He showed, with pure rotation and "planetary rotation" of the balls, that characterizing this behavior is not trivial.
In addition, Van Zoelen developed a semi-analytical model for side flow of oil from the Hertzian area in lubricated contacts [16]. Neglecting inlet side flow means that their model is only valid for severely starved contacts (i.e., very short inlets). Again, the outlet layer thickness of an EHL contact determines the inlet layer thickness of the next contact. The result was an equation to predict the film thickness in the full bearing based on

side flow from the Hertzian contacts without considering replenishment [16, 17]. The absence of contact replenishment caused a decreasing film thickness. However, via this model, they showed that the film thickness decay rate is lower at increased load and is independent of speed. This appears counter-intuitive. Later in this thesis, we will show that the film thickness is independent of speed at higher speeds.

Both the Van Zoelen and the Damiens models predict a film thickness decay. However, the measurements in real bearings show a constant film thickness, indicating the presence of contact replenishment, i.e., (re-)flow of lubricants towards the center of the running tracks. Studies on the replenishment mechanisms will be further discussed in the next section.

2.2 REPLENISHMENT MECHANISMS

The lubricant enters the contact at the inlet region. The increase of pressure in the inlet will cause some side flow. The very high pressure inside the contact also causes some side flow but much of it is compressed, traveling through the contact, and leaving the contact at the outlet where it is decompressed. When the lubricant leaves the contact, it forms two almost equally thick layers on the two contacting surfaces and continues to lubricate the next contact [16, 34, 35]. Oil volumes next to the track caused by side flow are not lost from the bearing but provide contact replenishment, leading to relatively stable film thicknesses. Some fundamental work was done on this mechanism and will be listed below.

Pemberton and Cameron [36] visualized the flow of lubricant around an EHL contact on a ball-on-disc machine. They showed that the outlet layer thickness is not uniform and that ridges are formed. They showed that replenishment mainly happens at the inlet of the contact by squeezing the oil ridges resulting in oil feed to the center of the contacts. This is enhanced by capillary effects.

In an axially loaded ball bearing, the balls will not only rotate but may also spin. The experiments conducted by Åstrom et al. [37] on a thrust ball bearing, Larsson [38] on deep groove ball bearing test rig, and Cann et al. [39] on a ball-on-disc machine showed the significance of ball spin in replenishment. They claimed that due to ball spin, lubricant will be pulled towards the contact region which would help contact replenishment.

Track replenishment could also be due to out-of-contact replenishment, which is a result of replenishment between successive over-rollings [20]. In 1974, Chiu [40] modeled replenishment by assuming that there is sufficient oil available from the ridges along the track, and presumed that replenishment mainly occurs in-between the balls in a bearing due to surface tension forces [40]. However, later, Gershuni et al. [41] and Jacod et al. [42] showed that this out-of-contact replenishment is negligible in ball bearing applications because of the very short duration available to replenish the contacts between successive over-rolling. There is nowadays an agreement that out-of-contact replenishment within the bearing is generally too slow and therefore not relevant [18, 20, 41]. Therefore, it is evident that capillary pressure forces cause the

in-contact replenishment which drives the lubricant towards the center of the ball-ring contacts.

Recently, using computational fluid dynamics (CFD) simulations, Nogi [43, 44] and Fischer et al. [45] simulated replenishment in starved EHL contacts. They found that starvation was dependent on the capillary number which is a function of viscosity and surface tension. Then they determined the transition from fully flooded conditions to starved lubrication based on this.

In radially loaded bearings, the load distribution along the circumference is not uniform, hence, a ball continuously moves from the loaded zone where the Hertzian contact size and pressure are large, to the unloaded zone where the Hertzian contact size and pressure are small, and back again. The significance of this motion on replenishment was studied by Cann and Lubrecht [46] on a ball-on-disc machine. They showed that unloading the ball, which resulted in a smaller contact width, facilitated the lubricant flow, resulting in higher film thickness. This shows that in addition to the properties of the lubricant, and bearing parameters, the dynamic conditions arising during the operation of the bearings may also play a role in determining the film thickness in ball bearings.

2.3 FILM THICKNESS IN GREASE LUBRICATED CONTACTS

2.3.1 FULLY FLOODED CONDITIONS

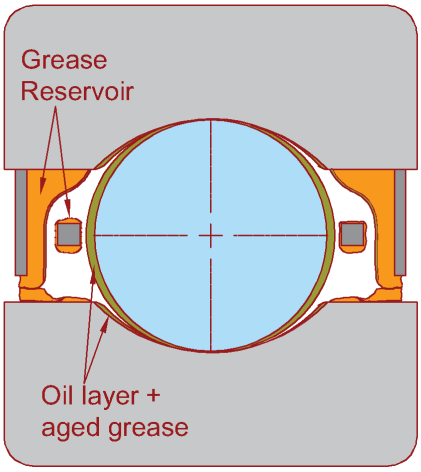

Figure 2.3: A grease lubricated bearing showing grease reservoirs on the seal, shoulder, and cage.

Grease film thickness measurements under fully flooded conditions on ball-on-disc machines or on two-disc machines showed that the film thickness could be greater than the base oil film thickness [11, 47–50]. If the test was set-up such that starvation could occur, then the initial film thickness was again initially higher than the oil film thickness but subsequently dropped to values below the base oil film thickness [51–53].

The observation of a grease lubricated EHL contact using a high-speed camera by Åstrom et al. [53] showed that some of the thickener particles passed through the contact which explains the above mentioned larger films. This was further confirmed by the experiments carried out by Cann et al. [50]. Several studies have led to models for fully flooded grease lubricated contacts. One of the first models, by Sasaki et al. [54], considered grease as a Bingham fluid. The models by Greenwood and Kauzlarich [55], Yang and Qian [56], and Jonkisz et al. [47] use a Herschel-Bulkley rheology model. These models might be relevant during the churning phase of the grease, and if the operating speed is low. As the speed increases, shear thinning behavior/structural breakdown of the grease leads to the viscosity approaching the base oil viscosity [57]. Cen et al. [13] and Kaneta et al. [58] showed that this only applies to extremely low speeds. At moderate speeds, the films are almost equal to the base oil film thickness. A recent study by Cyriac et al. [59] showed that for moderate speeds, the grease film thickness does not depend on any grease rheological properties. They also showed that the increase in film thickness due to thickener entrapment is related to the thickener volume fraction and the size of the thickener fibers. In another study, Couronne et al. [60] showed a relationship between the grease elastic modulus and the film thickness.

At higher speeds, starvation occurs and the film thickness becomes smaller than the fully flooded base oil film thickness. This is described further in the next section.

2.3.2 STARVED CONDITIONS

The grease film thickness study on a ball-on-disc machine showed that if the grease is not pushed back to the contact, starvation occurs resulting in an initially decreasing film thickness which later becomes stable [46, 61, 62]. Cann et al. [62] also showed that the decay rate is similar to the base oil decay rate. Merieux et al. [63] showed in their ball-on-disc measurements that grease replenishment depends on the shear stability of the grease. The least shear-stable grease showed a constant film thickness with time whereas the film thickness in the stable grease dropped with time. The film thickness in intermediately stable grease initially dropped and then recovered. They ascribed this to a difference in oil release rate: the least shear-stable grease quickly releases the oil, generating more oil for replenishment [63]. They postulated that the film consisted of a thickener deposited layer in combination with a hydrodynamic film. In the case of a stable film, there will be a balance between the loss and feed of lubricant from and to the contacts [42, 62].

Based on the replenishment mechanisms discussed above, Miettinen [64] categorized the lubrication mechanism in grease lubricated bearings into three categories. The bearing geometry, grease properties, and operating conditions determine which parameter will dominate and determine the film thickness [64]:

(a) Film build-up is due to both thickener and base oil, and could also include the bulk movement of grease [61, 62].

(b) Grease reservoirs formed during churning release the base oil [5].

(c) Film formation is due to heavily worked grease, whereas the rest of the grease simply seals the bearing [65].

Finally, using experimental results from the ball-on-disc machine, and considering that replenishment is a local phenomenon driven by capillary forces, Cann et al. [20] proposed a dimensionless parameter called the *SD* parameter. This parameter relates the relative film thickness (the ratio of measured film thickness to calculated fully flooded film thickness) to the viscosity, half contact width, linear speed, and oil layer thickness. Using this parameter, we can identify the boundary between the fully flooded and starved regimes, and determine the film thickness in the starved regime [20].

These single-contact measurements are helpful in understanding some of the fundamentals of grease lubrication in bearings. However, they may not include all the possible replenishment mechanisms as would occur in real bearings. We have now reached a point where further understanding can only be done by directly studying the film thickness in a grease lubricated bearing.

2.4 FILM THICKNESS MEASUREMENT IN A BEARING - STATE OF THE ART

The very first film thickness measurements in rolling bearings lubricated with grease were done in 1979 by Wilson [66] using the electrical capacitance method. This method was first used by Lewicki [67], then by Crook [68], and Dyson and Wilson [69]. They measured film thickness on a two-disc machine. Currently, the electrical capacitance method is considered the most suitable method available to measure film thickness in bearings. In the EHL contacts, due to the high load applied, the ball-ring contact will elastically deform and resemble a parallel plate capacitor when voltage is applied across them. The separating oil film between the ball-ring contact acts as a dielectric material, the thickness of which (called the film thickness) determines the capacitance of the contact. When the film thickness changes, correspondingly, the capacitance also changes.

When an EHL contact acts as a capacitor, it is not just the Hertzian region contributing to the total capacitance; the region around the Hertzian contact also contributes. The method was therefore later refined by including the contribution to the capacitance of this region. In this study, we call this the “outside capacitance”. Barz et al. [70] used a correction factor to compensate for this outside capacitance and measured film thickness in an angular contact ball bearing. They showed that the relative film thickness is governed by a power law relationship with speed. The film thickness measured by Baly et al. [71] in an angular contact ball bearing showed that the film thickness initially increases with increasing speed similar to the base oil film thickness. Further increase in speed led to starvation, after which a small drop in film thickness was observed. Even further increasing the speed made the film thickness constant (independent of speed) up to a certain speed. Additional increase in speed gave a higher irregular film thickness [71]. Similar results are also obtained in our measurements which will be presented in the later chapters.

Using the calibration method developed by Wilson [66] which intrinsically includes the outside capacitance in the calibration process, the film thickness in a full bearing at ultra-low speeds was measured by Morales-Espejel et al. [13]. They reported that the film thickness is notably greater compared to the film thickness in base oil lubrication.

Similarly, for moderate speed conditions, Cen and Lugt [19] showed that the relative film thickness follows a power law relation with ηbu (the product of viscosity, half contact width and speed) for various greases and loads.

Jabloka et al. [72–74] computed the contribution of the outside capacitance for single contact measurements as well as for full bearings under fully flooded conditions only. Here, we extend this method to starved lubrication conditions, which are dominant in grease lubricated bearings. In addition, in our new method, the dielectric constant of the lubricant, which is load-dependent, can be obtained directly from the test rig which makes it easier. The new method is discussed in the next Chapter.

3

EXPERIMENTS

In this chapter, we briefly describe all the experimental methods and setups used in this research. First, we list the greases used, then describe our two film thickness measurement test rigs. Then we describe the electrical capacitance method. We briefly explain the previously developed methods and their advantages and shortcomings. Then, we introduce our new improved capacitance method. Surface tension measurement is subsequently described. For a more detailed description of the new film thickness measurement methods, the reader is referred to Paper 1 in Appendix A.

3.1 GREASES

Three lithium-thickened greases with mineral oil as the base oil are chosen for this study: one with base oil viscosity of 100 cSt at 40 $^{\circ}C$ and consistency of NLGI grade 2.5, named "LiM-100-2.5" grease; another grease with a base oil viscosity of 474.5 cSt at 40 $^{\circ}C$ having consistency of NLGI grade 1.5 is called "LiM-460-1.5" grease; a third grease with the same base oil viscosity of 474.5 cSt at 40 $^{\circ}C$ but with higher thickener percentage resulting in NLGI grade 3 is named "LiM-460-3". Other properties of these greases are given in Table 3.1. Based on the measured outer ring temperature, the base oil viscosities at other temperatures are estimated using Walther's equation [2].

3.2 TEST RIGS

In this study, two test rigs are used to measure film thickness in ball bearings. Using test rig 1, we can measure film thickness in a 6209 bearing under an axial load and up to a speed of 4000 rpm. The outer ring of the bearing is isolated from the rest of the rig using polymers. The test bearing is driven by an electric motor, attached through a magnetic coupling. A mercury contact is used to establish an electrical contact with the rotating inner ring of the bearings. Axial load is applied through pneumatic bellows, and the resulting force is measured using a load cell. This test rig is used in obtaining results presented in papers A and B (in the appendix). The schematic diagram of the test rig

Property	LiM-100-2.5	LiM-460-1.5	LiM-460-3
Kinematic viscosity @ 40 °C (cSt)	102.8	474.5	474.5
Kinematic viscosity @ 100 °C (cSt)	10.3	31.4	31.4
Density @ 15 °C (g/cm^3)	0.891	0.902	0.902
Pressure-viscosity coefficient @ 40 °C (GPa^{-1})	31.8	27.4	27.4
Thickener content (% mass)	13	13	17
Surface tension @ 61 °C (N/m)	0.0171	0.0276	0.0276
A_{lv} (N/m)	0.0330	0.0327	0.0327
B_{lv} (Pa.s)	-0.0217	-0.0219	-0.0219

Table 3.1: Properties of greases used in this study. A_{lv} and B_{lv} are used in Pelofsky's equation to determine surface tension at various temperatures.

with critical parts listed is shown in Figure 3.1.

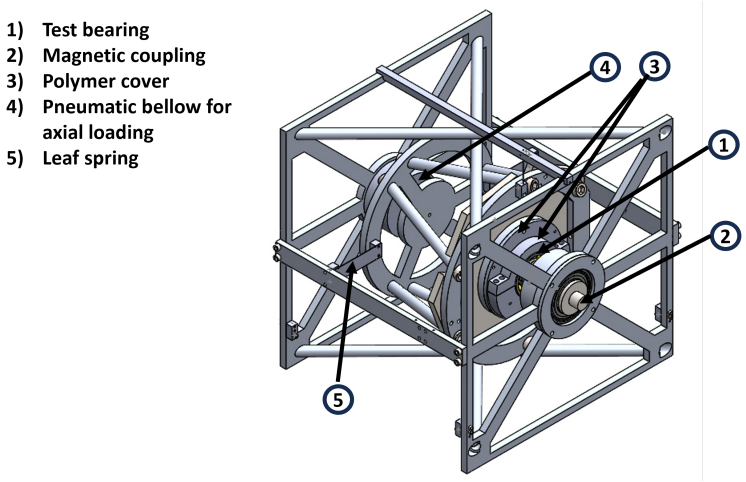

Figure 3.1: Schematic diagram of a portion of test rig 1. The driving motor is not shown.

Using test rig 2, we can run ball bearings of three different sizes, i.e., 6204, 6206, and 6209 bearings. We can apply axial load, radial load, and combined loads. This test rig can operate up to 14000 rpm shaft speed. The applied load is measured using a load cell. Similar to test rig 1, the voltage across the inner ring and outer ring is measured using a mercury contact fitted on the rotating shaft. Hybrid bearings are used as support bearings. The schematic drawing of the test rig 2 used in this study is shown in Figure 3.2.

In both test rigs, the outer ring temperatures of the test bearings are measured using an

electrically insulated thermocouple. The temperatures of the bearings are controlled by passing hot/cold air around the test bearings. All the bearings used in our study have C3 clearance. The capacitances of the test bearings are measured using 'Lubcheck MK3', a specialized device developed at SKF. A schematic diagram showing the electrical connection between the test bearings and 'Lubcheck MK3' is shown in Figure 3.3. For axially loaded test conditions, an unmodified all-steel-ball bearing is used. For radial load measurements, a hybrid bearing with a single steel ball is used.

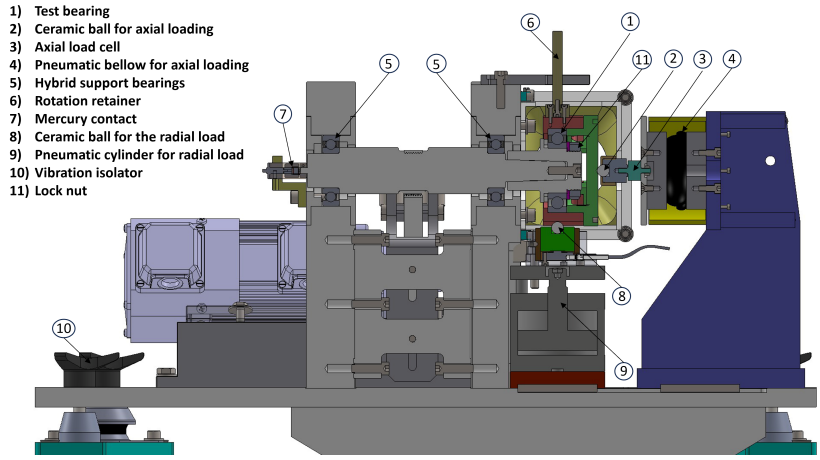

Figure 3.2: Schematic diagram of test rig 2.

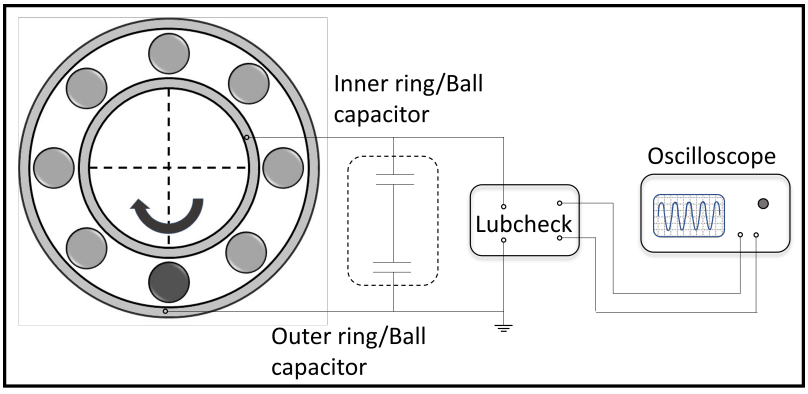

Figure 3.3: Schematic representation of the film thickness measurement interface on a single steel ball bearing using Lubcheck [75].

3.3 JABLONKA'S ELECTRICAL CAPACITANCE METHOD

The electrical capacitance method is one of the most convenient methods now available to measure film thickness in deep groove ball bearings. Figure 3.3 shows that the

capacitance is measured by applying a voltage over the bearing where the bearing is part of a test rig. The measured electrical capacitance includes the contribution of the capacitance of the EHL contacts between balls and rings, and contribution from the rest of the test rig. The latter is here called the "background capacitance". The grease film thickness here only affects the capacitance formed at the EHL contacts. Basically, the background capacitance does not change, which is very convenient.

The simplest way to model the electrical capacitance in a bearing would be to consider the EHL contacts as parallel plate capacitors with surface area A_{Hertz} (the Hertzian contact area), separated by a dielectric material, the compressed oil, with thickness h_c.

The capacitance is then given by

$$C_{Hertz} = \frac{\epsilon_0 \epsilon_{oil} A_{Hertz}}{h_c}, \tag{3.1}$$

where ϵ_0 is the permittivity constant ($8.85 \times 10^{-12} F/m$), ϵ_{oil} is the dielectric constant of the dielectric material (which in our study is lubricating oil).

This needs to be extended by including the contribution to the capacitance by the area around the Hertzian contact, which is here called the 'outside capacitance'.
This was earlier modeled by Jablonka et al. [72–74] for fully flooded conditions. In starved contacts, only part of the "outside capacitance area" is filled with oil. By not taking this effect into account, the film thickness will be over-predicted. The method to measure the film thickness in this thesis is based on an extension/improvement of the approach by Jablonka et al. [72–74], with the effect of starvation now included. As mentioned above, Jablonka measured on fully flooded contacts, as shown in Figure 3.4.

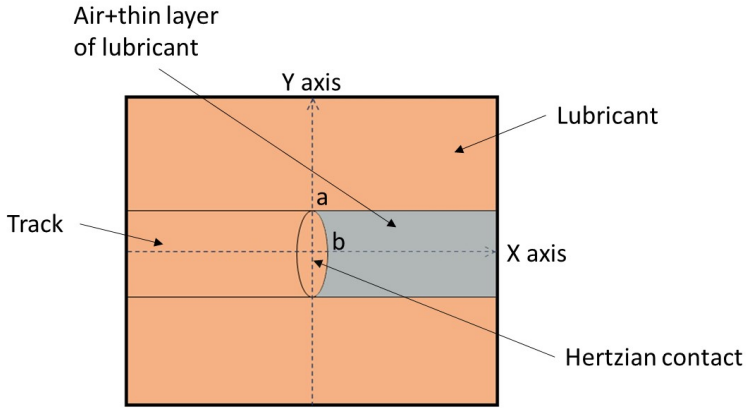

Figure 3.4: A simplified fully flooded contact condition showing oil around the contact. (Depicted regions are not to scale).

The outside capacitance has two regions, one filled with the oil ($C_{flooded}$), and another

at the exit side of the contact where layers of oil separated by air fill the gap between the contacts (C_{cav}). Therefore, the outside capacitance can be calculated as

$$C_{outside} = C_{flooded} + C_{cav} \tag{3.2}$$

where $C_{flooded}$ and C_{cav} are given by

$$C_{flooded} = \iint_{A_{flooded}} \frac{\epsilon_0 \epsilon_{oil} dxdy}{h_c + h_{gap}(x,y)} \tag{3.3}$$

and

$$C_{cav} = \iint_{A_{cav}} \frac{\epsilon_0 dxdy}{\frac{h_c}{\epsilon_{oil}} + h_{gap}(x,y)\frac{1}{\epsilon_{air}}}, \tag{3.4}$$

where h_c is the central film thickness and h_{gap} is the distance between the ball and ring surfaces away from the Hertzian contact.

First, an approximate film thickness was used to predict the outside capacitance. Then, using this capacitance, the film thickness was obtained. The dielectric constants at different loads and temperatures are predicted using the Clausius-Mossotti equation.

The integration limits were chosen based on the following assumptions:

1. On the inlet side of the contact, the capacitance was calculated up to the point where the gap between the surfaces is nine times the central film thickness. The oil level beyond this point gives fully flooded conditions [30].
2. In a bearing, to know the limits in the transverse (to the rolling) direction, it was assumed that oil fills the gap between the ball and the bearing ring up to the shoulder.

3.4 THE NEW CAPACITANCE METHOD INCLUDING STARVATION

When a bearing with n balls is axially loaded, all the balls will carry the same load. This results in equal film thicknesses at every ball. The electrical circuit connecting the inner and outer rings therefore involves a setup of n capacitors arranged in parallel. Additionally, each of these capacitors is composed of two capacitors in series, formed by the contact between the ball and inner ring as well as the contact between the ball and outer ring. The corresponding electrical circuit is shown in Figure 3.5.

For a single ball, the capacitance between the ball and the inner ring is

$$C_i = C_{i,Hertz} + C_{i,outside} \tag{3.5}$$

and the capacitance between the ball and the outer ring is

$$C_o = C_{o,Hertz} + C_{o,outside}, \tag{3.6}$$

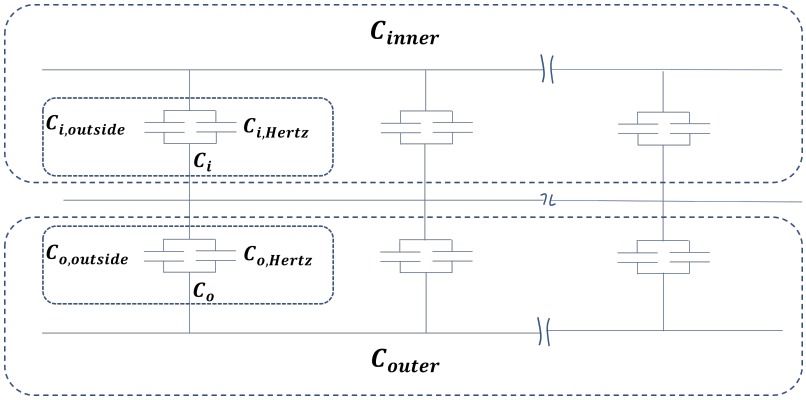

Figure 3.5: A simplified electrical circuit showing capacitors at the ball-ring interfaces.

where the subscripts $Hertz$ and $outside$ stand for the Hertzian and outside capacitances respectively, calculated using equation 3.1. For a bearing with n number of balls, the capacitance at the inner ring can be obtained by

$$C_{inner} = nC_i \tag{3.7}$$

and the outer ring capacitance is obtained by

$$C_{outer} = nC_o. \tag{3.8}$$

The inner ring and outer ring capacitances are in series, therefore, the equivalent/total capacitance of the bearing is given by

$$C_{total} = \frac{1}{\frac{1}{C_{inner}} + \frac{1}{C_{outer}}} + C_{background}. \tag{3.9}$$

The total capacitance in the bearing is then

$$C_{total} = \frac{1}{\frac{1}{n(\epsilon_0\epsilon_{oil}\frac{A_{i,Hertz}}{h_{c,i}} + C_{i,outside})} + \frac{1}{n(\epsilon_0\epsilon_{oil}\frac{A_{o,Hertz}}{h_{c,o}} + C_{o,outside})}} + C_{background}, \tag{3.10}$$

where $h_{c,i}$ and $h_{c,o}$ are inner ring and outer ring central film thicknesses; $C_{i,outside}$ and $C_{o,outside}$ are outside capacitances of the ball-inner and ball-outer ring contacts; $A_{i,Hertz}$ and $A_{o,Hertz}$ are the Hertzian contact areas on the inner ring and outer ring. The background capacitance can be measured using a hybrid bearing. Hybrid bearings are made with ceramic balls which do not form capacitors with bearing ring contacts, hence, the measured capacitance will simply be the background capacitance.

Our new method uses Jablonka et al.'s capacitance model as a foundation. However, in addition to the above considerations, we will here determine the dielectric constant

of the oil within the experimental setup, without using any pressure-and temperature-dielectric constant relationships. Additionally, we do not need an approximate film thickness for calculating the outside capacitance. In this study, we include the effect of starvation which is crucial in grease lubricated bearings.

3.4.1 FINDING DIELECTRIC CONSTANT

Finding the dielectric constant is similar to the calibration process proposed by Wilson [66, 76]. Here, we fill the bearing with sufficient oil to ensure fully flooded conditions. Then, we measure the capacitance and the bearing temperature at a particular operating condition (for example, 513 N and 4000 rpm). Using Hamrock and Downson's film thickness equation 2.1, we calculate the inner ring film thickness ($h_{ff,i}$) and outer ring film thickness ($h_{ff,o}$). Subsequently, these film thickness values are used to obtain the outside capacitance using the equations 3.2, 3.3 and 3.4. By substituting the measured total capacitance (C_{total}) into equation 3.10 and rearranging, we can solve for the dielectric constant ϵ_{oil}. We repeat the same procedure to obtain the dielectric constant for every different lubricant and load.

The same dielectric constant should be found for a specific lubricant and load at any given speed. This is verified in Figure 3.6, showing the measured and calculated total capacitances. The obtained dielectric constant in this condition is $\epsilon_{oil} = 4.06$.

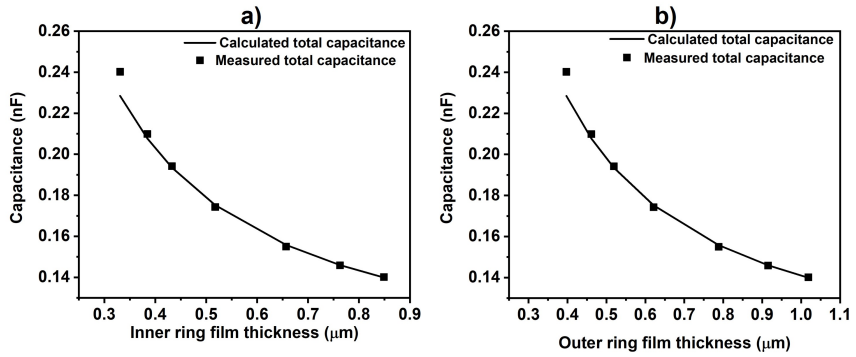

Figure 3.6: Calculated and measured total capacitances versus film thickness for (a) inner ring and (b) outer ring film thickness. F_a =513 N; LiM-100-2.5 grease bled oil. Here the dielectric constant was determined using a single speed of 400 rpm.

3.4.2 OBTAINING THE GREASE FILM THICKNESS

3.4.2.1 STARVATION

During starvation, the inlet of the contact will be filled up to an inlet meniscus, and the rest of the gap will be filled with two layers of oil and air. This is schematically shown in Figure 3.7.

The outside capacitance now depends on the dimensionless meniscus position m, which can be obtained using Hamrock and Dowson's starved film thickness equation [31]

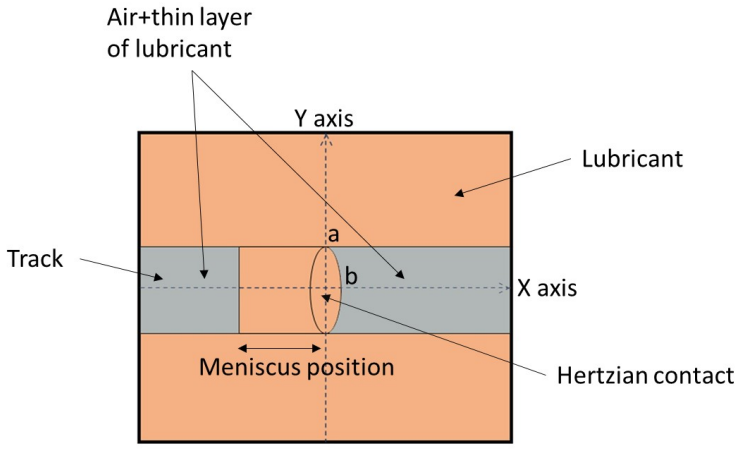

Figure 3.7: A simplified depiction of the regions in starved contact conditions, illustrating the position of the meniscus on the track. (Regions are not to scale).

$$h_{st} = H_{ff} R_x \left(\frac{m-1}{m^*-1} \right)^{0.29}, \tag{3.11}$$

where m^* is the dimensionless inlet position at the boundary between the fully flooded and starved regions. This can be obtained from

$$m^* = 1 + 3.06 \left[\left(\frac{R_x}{b} \right)^2 H_{ff} \right]^{0.58}. \tag{3.12}$$

Here, $H_{ff} = h_{ff}/R_x$ can be calculated using equation 2.1. Equation 3.11 contains two unknowns m and h_{st} both of which can be obtained by an iterative approach using the measured capacitance. The relation between the outer ring film thickness and the inner ring film thickness is obtained from [77]:

$$h_{st,o} = h_{st,i} \left[\frac{R_o(R_i + R_b)}{R_i(R_o - R_b)} \right]^{0.476} \left(\frac{\eta_{T_o}}{\eta_{T_i}} \right)^{0.67}, \tag{3.13}$$

where it is assumed that the relation between outer and inner ring film thicknesses during starvation is the same as that under fully flooded conditions. The iterative procedure to find the starved film thickness is shown in Figure 3.8

3.4.2.2 FULLY FLOODED GREASE FILM THICKNESS

In a grease lubricated bearing, at low rotating speeds, the film thickness can be larger than the base oil fully flooded film thickness. In this case, we assume that the lubricant completely fills the gap between the ball and the ring other than in the outlet region as shown in Figure 3.4. Here, the total capacitance is only a function of the central film

thickness. Now, we iteratively determine H_{ff} until the measured and calculated total capacitances (C_{total}) become sufficiently close. The iterative procedure is described in the flow chart shown in Figure 3.8.

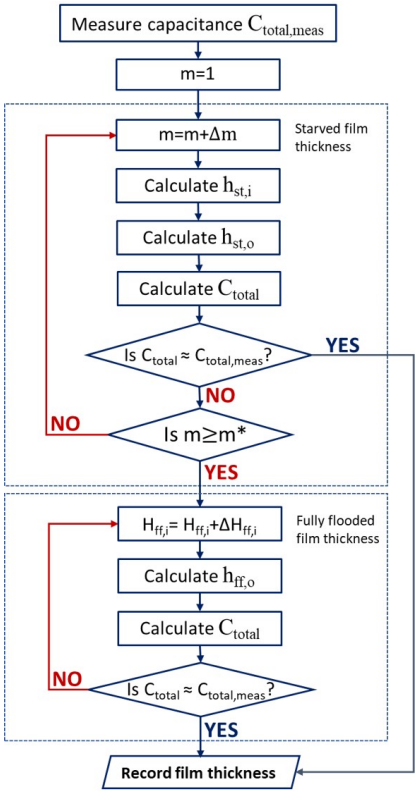

Figure 3.8: Flow chart showing the procedure for determining the film thickness in grease lubricated bearings using the new method.

3.5 MEASURING SURFACE TENSION

The surface tension of each base oil is measured using a Dynamic Contact Angle (DCAT) machine, following a Wilhelmy plate method. A clean thin plate is immersed in the test lubricant heated to a specific temperature. The force on the plate that is a result of wetting is measured, which gives the surface tension. A picture of the DCAT machine is shown in Figure 3.9.

The surface tension σ of the lubricants changes with temperature, therefore, Pelofsky's equation [78] is used to predict it at other temperatures:

$$ln\,\sigma = ln\,A_{lv} + \frac{B_{lv}}{\eta}. \tag{3.14}$$

Here, constants A_{lv} and B_{lv} are experimentally determined by curve fitting the measured surface tension at two or more temperatures and η is the dynamic viscosity of the base oil (which depends on temperature). The values of these constants and the surface tensions of the base oils are listed in Table 3.1. All measurements were repeated at least twice for statistical significance.

Figure 3.9: DCAT machine used to measure the surface tension of the base oil.

4

FILM THICKNESS DEPENDENCE ON INITIAL GREASE QUANTITY

This chapter discusses the impact of the initial grease-filling quantity on the film thickness after the churning phase. Here 6209 bearings are filled up to 30%, 15%, and 7.5% of the free volume of the bearings using two different greases. The film thickness and temperatures are measured on test rig 1 (see previous chapter for test rig description). These two greases have very different consistency, and base oil viscosity but are made out of the same thickener material with the same percentage of thickener. The different initial filling quantities are expected to result in different grease reservoir sizes. Traditionally, it is speculated that from these stable reservoirs grease bleeds, replenishes the contacts and reduces the level of starvation. Our results show that in both the greases, after the churning phase, the temperature and film thickness are the same for all three different initial fillings. This indicates that the quantity of heavily worked grease or oil layer left on the track after churning is the same and does not depend on the initial filling quantity. Afterwards, the film thickness is measured at controlled temperatures and at various speeds under three loads. The results show that initially, the film thickness increases with the speed, and at higher speeds, it becomes almost constant. The film thickness in all three different initial levels of filling is the same at all loads and speeds. This implies that grease bleed does not contribute to contact replenishment during the first hours after the churning phase.

The work in this chapter has been published. The paper can be found in Appendix B.

4.1 CHURNING RESULTS FOR DIFFERENT FILLINGS

The greases used in this effect of filling study are LiM-100-2.5 and LiM-460-1.5. The properties of these greases are in Table 3.1 in Chapter 3.

The temperature in the bearing is determined by the frictional heat generated and the heat dissipation from the bearings. The sources of friction in the bearings are a) rolling

friction, b) sliding friction, c) seal friction, and d) viscous drag. In our study non-contacting seals are used, therefore the seal friction can be neglected.

The churning temperature and film thickness profiles are shown in Figure 4.1. We can notice that the temperature and film thickness profiles for both the greases mirror each other. A high temperature leads to a low viscosity and therefore low film thickness.
At the start of the churning phase (channeling phase [6]), the temperature for 30% filling is higher for both greases, this is due to the higher drag forces. However, after the churning phase, the temperature and film thicknesses of all three conditions, for both the greases become almost the same.

The difference in temperatures between the LiM-100-2.5 and LiM-460-1.5 greases during and after churning is due to the difference in viscous drag forces, caused by both a difference in base oil viscosity and in consistency.

During churning, most of the grease is pushed out of the bearing swept area by the balls leaving behind a heavily worked grease/oil layer on the track that is generally thinner than the EHL fully flooded film thickness. The same temperature and film thickness after the churning phase indicates therefore that the level of starvation/lubricant layer thickness is the same after churning for all three different fillings.

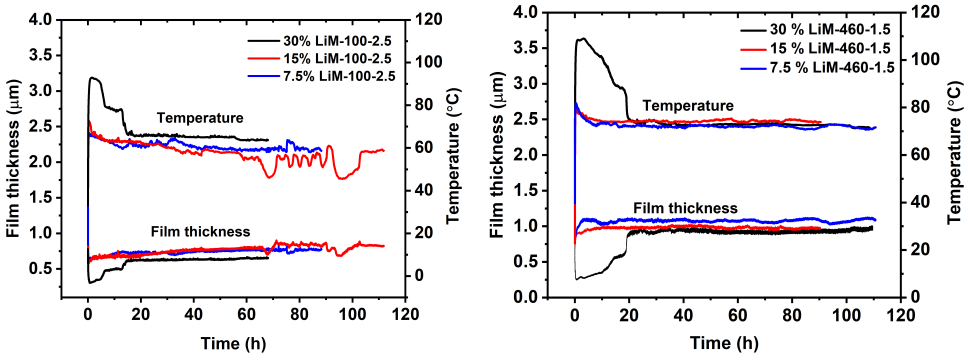

(a) LiM-100-2.5

(b) LiM-460-1.5

Figure 4.1: Instantaneous temperature and film thickness during grease churning in 6209 bearing with (a) LiM-100-2.5 and (b) LiM-460-1.5 greases at 30%, 15% and 7.5% initial filling, load = 513 N, speed = 4000 rpm.

The amount of grease left on the bearing seals after churning is shown in Figure 4.2. Traditional grease lubrication mechanisms suggest oil bleeds from these stationary positions to replenish the contact. If the reservoir sizes are small, then the bleed would also be small. The grease from the stationary position is here the grease attached to the seals and the amount of this is given in Table 4.1 showing that the grease on the seals for the bearings filled 7.5% is very low compared to 15% and 30% fillings. The amount of grease left in the bearing (excluding the grease located on the seals) after churning is given in Table 4.2 showing an independence on the initial filling quantity, the excess grease will be pushed out of the bearing swept area during the churning process.

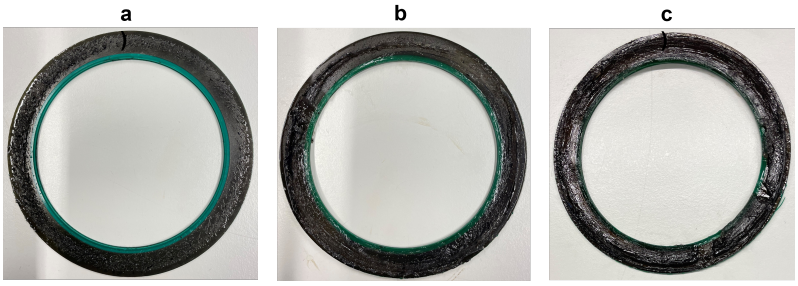

(a) LiM-100-2.5 with a) 7.5%, b) 15%, and 30% fillings

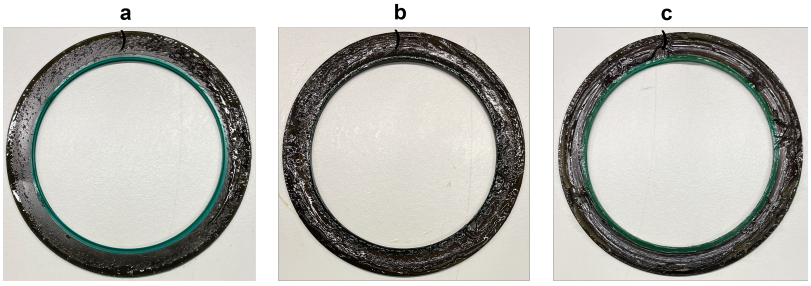

(b) LiM-460-1.5 with a) 7.5%, b) 15%, and 30% fillings

Figure 4.2: The tested bearing seals showing the grease left on them for different percentages of initial grease filling.

Mass of grease on the seals		
Filling (%)	LiM-100-2.5 (g)	LiM-460-1.5 (g)
7.5	0.24	0.28
15	1.46	1.36
30	2.35	1.96

Table 4.1: Mass of grease left on the bearing seals, measured after the experiments. The initial filling (mass) of grease is 6.2 g, 3.1 g, and 1.55 g.

	Mass of grease in the bearings		Volume percentage of grease in the bearings	
Filling (%)	LiM-100-2.5 (g)	LiM-460-1.5 (g)	LiM-100-2.5 (%)	LiM-460-1.5 (%)
7.5	1.31	1.01	6.48	4.99
15	1.21	1.04	5.98	5.14
30	1.37	2.27	6.77	11.71

Table 4.2: Mass and volume percentage of grease left in the bearings, measured after the experiments, after taking off the seals. Here, the volume percentage is the fraction of the bearing's free volume occupied by the grease.

4.2 FILM THICKNESS RESULTS FOR DIFFERENT FILLINGS

In this section, film thickness results in different speeds and loads measured at a constant temperature of $61\pm0.5^{\circ}C$ are presented. An example film thickness measurement is shown in Figure 4.3. We can notice from this figure that the film thickness initially shows a transient behavior but becomes stable after 2-3 minutes. The film thicknesses reported here are taken after this.

Figure 4.4 shows the film thickness for the different filling percentages measured at 513 N, 700 N, and 900 N from 400 rpm to 4000 rpm for both greases. We can see that for both the greases and for all the different filling percentages, the film thickness initially increases with speed and becomes almost constant after a certain speed. This was predicted by Van Zoelen et al. [16, 34, 35]. In severely starved contacts, at higher speeds, the film thickness depends on side flow out from the Hertzian contacts, determined by the residence time and the overrolling frequency. As the speed increases, these two balance out making film thickness almost independent of speeds [34, 79]. We can notice that the film thicknesses are load dependent under starved lubrication, whereas they barely vary with the load in the fully flooded conditions [18, 20]. In starved contacts, replenishment at the exit center becomes smaller with increasing contact widths. Therefore, the film thickness correlates well with the half-contact width. More on the transition to starvation and parameters determining the level of starvation will be discussed in the later chapters.

In Figure 4.4 we see that for both greases, under all the loads and at all the speeds (both low and high speeds), film thickness is the same in the bearings initially filled with the different quantities of grease. This shows that the replenishment rates in all the conditions are the same even though the grease reservoir sizes are different. The oil bleed from these stationary reservoirs apparently did not contribute to replenishment. Cen and Lugt [19] showed that the starvation levels in greases with different bleed properties were the same indicating that the bleed did not play a role in the bearings immediately after churning. Recently, Lugt et al. [80] showed that oil bleeding starts only after the point in time where the oil layer thickness is reduced. In their case, this was at the point in time when oxidation started. In our experiments, the film thicknesses are measured immediately after the churning phase, i.e., well before the onset of oxidation. Therefore film thickness also did not depend on the bled oil from the stationary grease reservoirs. The replenishment of the contacts is apparently only determined by the heavily worked grease/oil layer left on the track after the churning phase.

LiM-460-1.5 grease is chosen for this study, presuming that because of its low consistency, it might form lumps that would fall back onto the track, leading to a film thickness that depends on the filling quantity. However, contrary to this expectation, the experimental results demonstrate that this is not the case. Figure 4.4d-4.4f shows that for all three different loads and all the speeds, 7.5%, 15%, and 30% grease fillings yield the same film thickness similar to the behavior of the high consistency LiM-100-2.5 grease. From this result, we rule out the bulk re-flow of grease lumps onto the track as the predominant replenishment mechanism during the early post-churning phase.

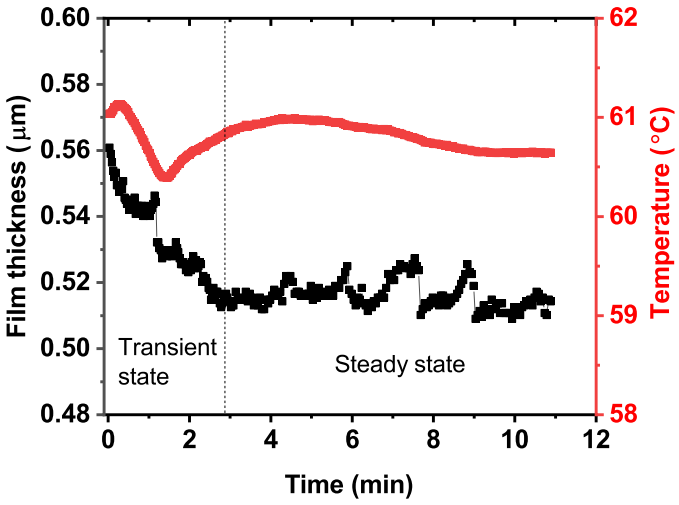

Figure 4.3: An example film thickness measurement at 3000 rpm, Load: 900 N, Grease: LiM-100-2.5, filling percentage: 30%.

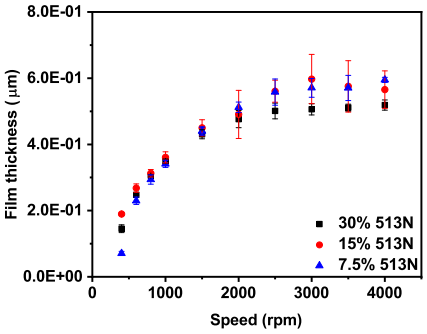

(a) LiM-100-2.5, 513 N

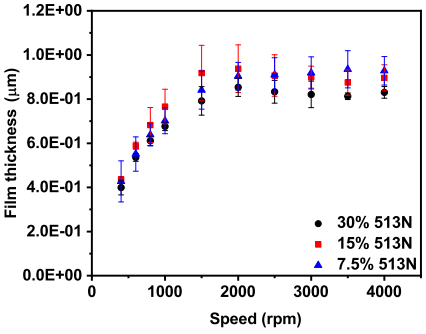

(d) LiM-460-1.5, 513 N

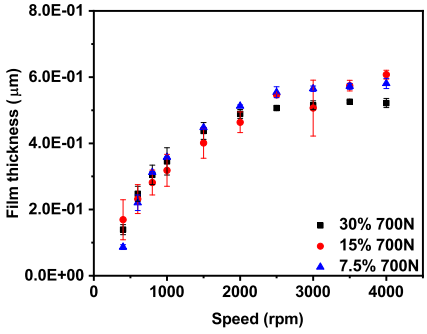

(b) LiM-100-2.5, 700 N

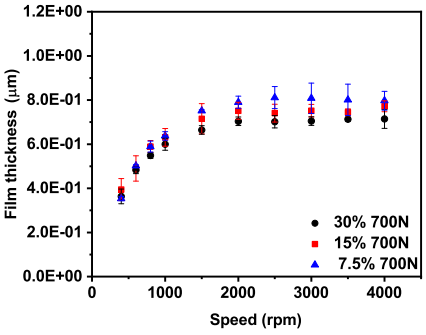

(e) LiM-460-1.5, 700 N

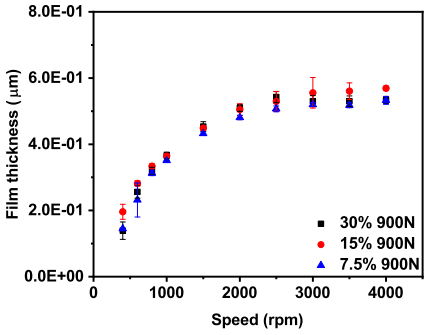

(c) LiM-100-2.5, 900 N

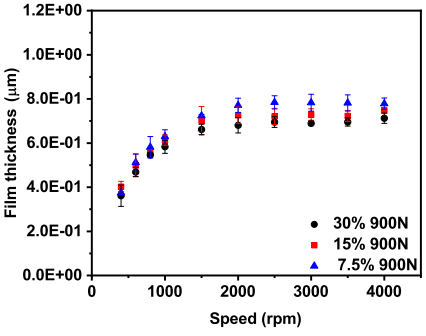

(f) LiM-460-1.5, 900 N

Figure 4.4: Film thickness in 6209 bearings lubricated with LiM-100-2.5 and LiM-460-1.5 greases.

It can be argued that if the amount of heavily worked grease left on the track after churning is already enough to yield a fully flooded film thicknesses, then the film thickness would not be influenced by the initial filling quantities. This is verified by calculating the relative film thickness (the ratio of measured grease film thickness h_g to the calculated

base oil film thickness h_{ff}) at different conditions. If the relative film thickness is equal or lager than one, the contacts are fully flooded, else they are starved. Figure 4.5 shows that at higher ηbu values both "LiM-100-2.5" and "LiM-460-1.5" greases show starvation.

These results shed some light on the significance of some of the replenishment mechanisms, but do not infer that a lower quantity of grease filling is better. Previous experiments have shown that the grease life is proportional to the grease quantity in the bearings [81, 82], hence, lower filling will result in shorter grease life.

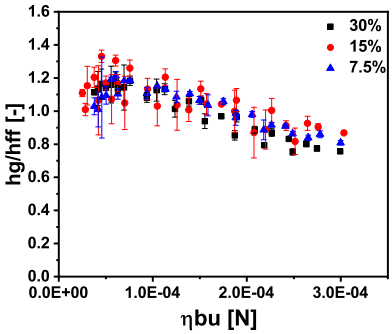

(a) 30%, 15% and 7.5% filling of LiM-100-2.5

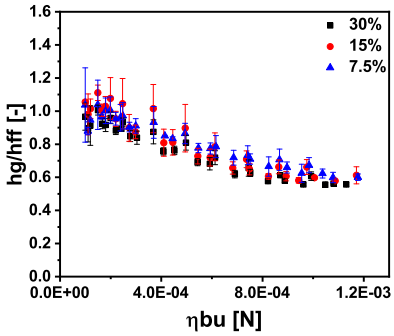

(b) 30%, 15% and 7.5% filling of LiM-460-1.5

Figure 4.5: Relative film thickness vs product of viscosity, speed, and contact width.

5

VIBRATIONS AND FILM THICKNESS

Vibrations in a machine are frequently occurring and may serve as a replenishment mechanism in grease lubricated bearings [39, 83]. A study on a ball-on-disc machine lubricated with grease showed that the lubricant film thickness increases with the lateral vibrations [84]. In this chapter, we will show the significance of vibrations on the film thickness in grease lubricated deep groove ball bearings. Additionally, we will show that an increase in film thickness due to lateral vibration also depends on the axial load on the bearings. The mechanism that causes the increase in film thickness due to vibrations is identified and explained using an analytical model. Finally, we show that film thickness does not decrease at high speeds (up to 0.8 million ndm) in grease lubricated deep groove ball bearings. The results shown in this chapter are based on the experiments done using test rig 2.

In this study, 6209 bearings are lubricated with LiM-100-2.5 grease (see Table 3.1 in Chapter 3 for the grease properties). The film thickness is measured after running the bearings for more than 100 hours to ensure the completion of the churning phase. An accelerometer, horizontally mounted on the bearing housing, measures the vibration acceleration. The film thicknesses and the vibrations are measured alternately to avoid electrical signal interference without changing the test bearing set-ups. The work in this chapter has been published. The paper can be found in Appendix C.

5.1 VIBRATIONS-INDUCED FILM THICKNESS CHANGES

Figure 5.1 presents film thickness measured on test rig 1 and test rig 2 with the same bearing under an axial load of 513 N showing the same film thickness in both the rigs up to 4000 rpm. As mentioned before, in test rig 1 we can measure film thickness only up to 4000 rpm. The film thickness in test rig 2 between 3000 rpm and 6000 rpm is almost constant, increasing to a peak value at 8000 rpm. Two potential sources of this increase are electrical signal interference and mechanical vibrations. The background capacitance should ideally be constant under all conditions i.e. at all speeds and loads. If any electrical artifacts influence the measurements, then the background capacitance will

vary. The background capacitance measured at different speeds remains stable, indicating that there was no electrical interference. Therefore, vibration is the likely reason for the anomalous film thickness behavior. The accelerometer, to measure vibration acceleration, is mounted on the bearing housing using a magnet. The root mean square (rms) values of the measured acceleration are calculated and plotted in Figure 5.1 showing that at 8000 rpm there is a sudden rise in vibration acceleration signal, which subsequently becomes almost stable. Film thickness and vibrations show a good correlation with each other. Via power spectral density (PSD) analysis, we can identify some vibration characteristics. Figure 5.2 shows the PSD of vibration signal at various speeds. For any speed, the first harmonic frequency is its rotational frequency. Also, except for 2000, 4000, and 8000 rpm the amplitudes of subsequent harmonics are lower than the first dominant/fundamental frequency. We can see from Figure 5.2 that the 266 Hz peak, at a speed of 8000 rpm, has the highest amplitude in comparison with other speeds/frequencies. This could be the machine resonance frequency. Also, unlike other speeds, at 8000 rpm, the second harmonic is orders of magnitude greater than the first harmonic. If the amplitudes of succeeding harmonics are lower than 15% of the first dominant frequency, then the cause of vibration is likely due to the unbalanced rotating system [85]. The measured vibration levels on our test rig are still within acceptable limits.

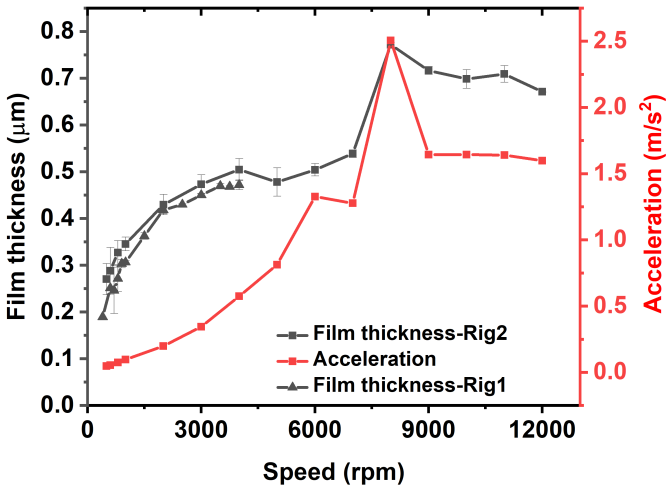

Figure 5.1: Film thickness and vibration acceleration for different speeds. Grease: LiM-100-2.5; bearing: 6209, axial load: 513 N; Temperature: 61 °C.

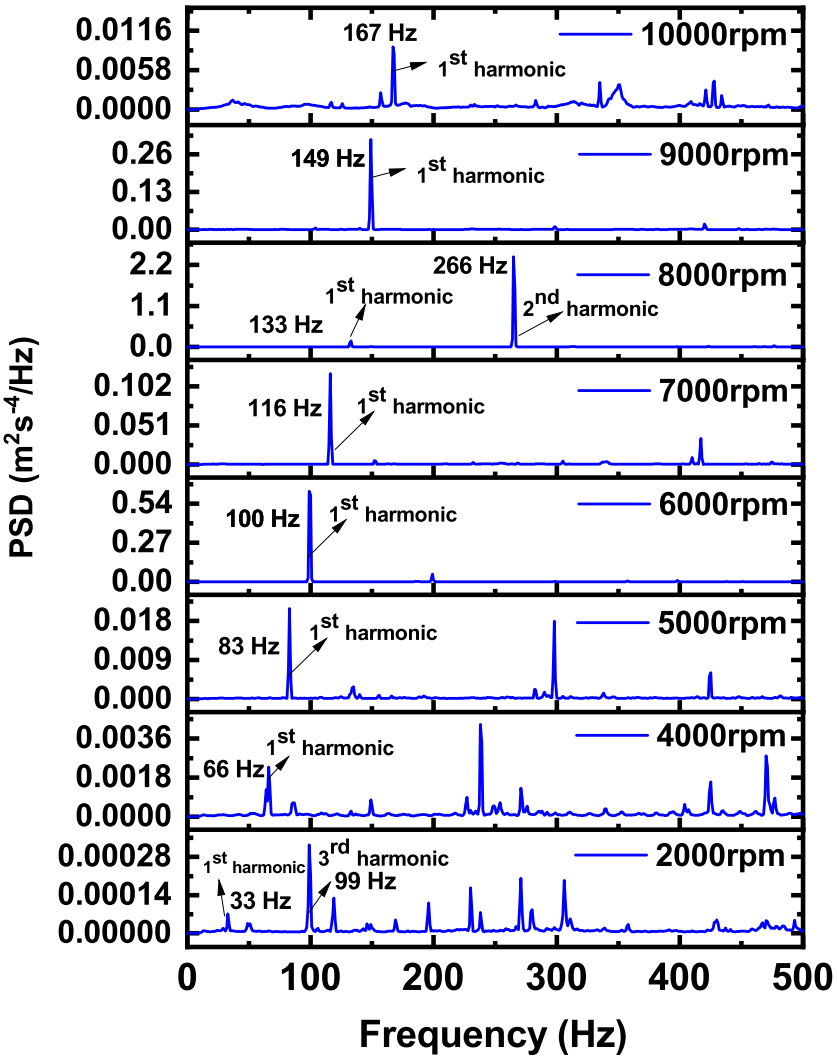

Figure 5.2: Power spectral density (PSD) plots for different speeds. Grease: LiM-100-2.5; bearing: 6209, axial load: 513 N; Temperature: 61 °C. Self-induced vibrations (i.e., no unbalance mass added).

5.2 CHARACTERIZING VIBRATION EFFECT ON FILM THICKNESS

To further confirm whether film thickness increases with vibration, we induced additional vibrations at lower speeds by adding unbalancing masses on the main shaft. The

vibration acceleration measured without any additional mass is denoted as $\hat{a}_0$; acceleration measured with mass m_1 is denoted as $\hat{a}_1$, and acceleration measured with m_2 is denoted as $\hat{a}_2$. Figure 5.3a shows the accelerations at different speeds due to these unbalancing masses; distinctive vibration acceleration can be seen above 2000 rpm for all three configurations. The corresponding film thicknesses measured in these setups are shown in Figure 5.3b. It is evident from these results that the film thickness is higher at higher vibration levels.

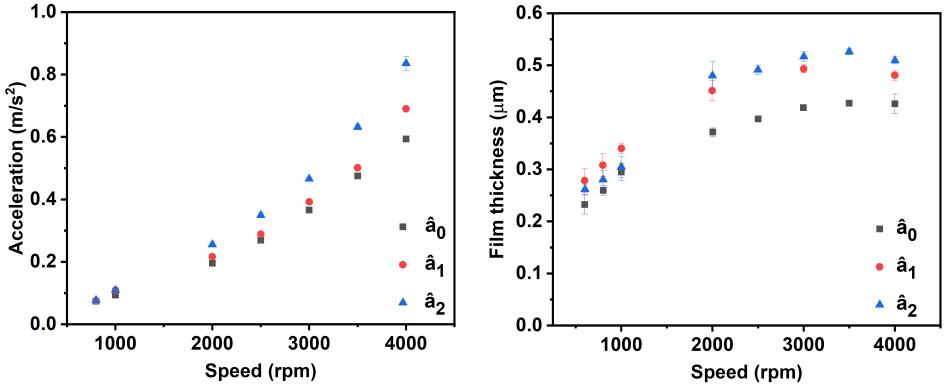

(a) (b)

Figure 5.3: (a) Vibration measurement showing the difference in vibration acceleration for the three configurations. $\hat{a}_0$, $\hat{a}_1$ and $\hat{a}_2$ correspond to the accelerations induced by masses m_0, m_1 and m_2 respectively. (b) Variation of film thickness under corresponding vibration conditions. Bearing axial load = 513 N, Grease: LiM-100-2.5.

The next question that arises is whether we can quantify the increase in film thickness due to vibrations; also, is there a dependence on the applied axial load? To answer these questions, similar to the 513 N study, we measured the film thickness at 900 N axial load under three different levels of vibrations by adding unbalancing mass m_1 and m_2.

Then, we correlate measured film thickness $h_{g,\hat{a}}$ to vibration acceleration $\hat{a}$ to obtain a characteristic fit. The film thickness $h_{g,\hat{a}_0}$ measured without any additional unbalancing mass on the shaft corresponding to vibration acceleration $\hat{a}_0$ is considered as the reference. Figure 5.4 plots the normalized increase in vibration acceleration $\frac{\hat{a}-\hat{a}_0}{\hat{a}_0}$ against the normalized film thickness $\frac{h_{g,\hat{a}}}{h_{g,\hat{a}_0}}$ for axial bearing loads of 513 N and 900 N, fitting well with:

$$\frac{h_{g,\hat{a}}}{h_{g,\hat{a}_0}} = C_L \left(\frac{\hat{a}-\hat{a}_0}{\hat{a}_0} \right)^{1/5} + 1, \tag{5.1}$$

where the parameter C_L varies with loads. Here, $C_L = 0.15$ for 900 N load and $C_L = 0.3$ for 513 N load, with correlation coefficient R^2 values of 0.73 and 0.90 respectively.

All the film thickness and the vibration points shown in Figure 5.3 are plotted in Figure

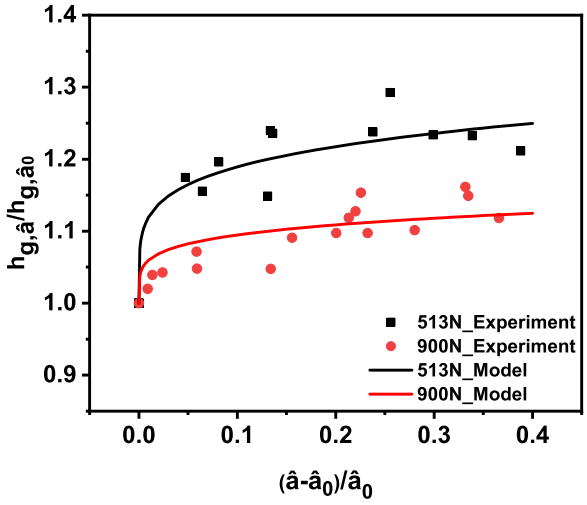

Figure 5.4: Variation of normalized film thickness with relative increase in vibration acceleration, under accelerations $\hat{a}_0$, $\hat{a}_1$, and $\hat{a}_2$ and various speeds. Bearing axial load = 513 N and 900 N.

5.4 in addition to the 900 N measurements. Figure 5.4 infers that the increase in film thickness due to vibration depends on the load. At higher loads, the replenishment due to vibrations is lower than at lower loads. This is attributed to the contact width: at higher loads, the contact width will be larger, and replenishing the center of the contact needs a larger vibration amplitude. One can use equation 5.1 to correct the anomalous film thickness measured at higher speeds due to effects such as resonance (shown in Figure 5.1).

5.3 MECHANISM BY WHICH VIBRATIONS INCREASE FILM THICKNESS

Vibrations can increase film thickness via several possible mechanisms, one of which is increase in resultant entrainment velocity due to lateral vibrations. The lateral vibrations produced could alter the resultant entrainment velocity resulting in increased film thickness [86]. We measured the lateral velocity due to vibrations by integrating the measured vibration acceleration to estimate the velocity due to vibrations. This velocity is four orders of magnitude lower than the main entrainment velocity. Therefore, this mechanism is not considered to be the main reason for the increase in film thickness.

Another mechanism is rapid fluctuation in contact width due to rapid changes in the normal load leading to an increase in entrainment velocity [87, 88]. The increase in film thickness due to rapid change in load is calculated using the analytical solution from Glovnea and Zhang [87, 88]. The unbalancing mass m_2 is used for the calculations. It is found that the film thickness variation due to this effect is just 1%. Hence, this mecha-

nism is also considered to be insignificant.

One more mechanism that could increase the film thickness due to vibrations is when the rolling elements roll on the ridges formed by the previous balls due to lateral displacements [84]. The approximate axial displacement of the outer ring of the bearing can be estimated by double integrating the measured vibration acceleration. Figure 5.5 shows an excellent correlation between the film thickness (black plot) and the estimated axial displacement (red plot). Note that the axial displacement estimated from the measured vibration acceleration is a conservative estimate because it also includes the effects from other parts of the test rig.

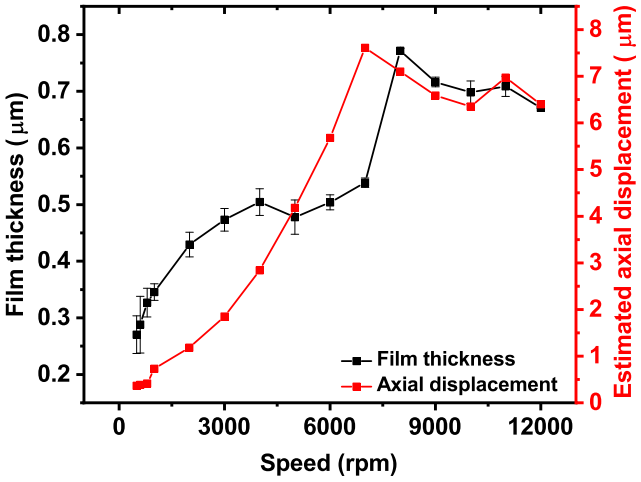

Figure 5.5: Film thickness (left axis) and estimated axial displacement (right axis) as functions of speed. Bearing axial load (static) = 513 N.

Next, we show by solving analytical equations how a small unbalancing mass (m_1=0.41 g or m_2 = 0.84 g) could cause lubricant replenishment via over-rolling on the ridges formed by the preceding balls. The load on the rolling elements changes continuously when the unbalancing mass rotates. This causes the contact angle β' to change correspondingly. The resulting contact angle due to the applied axial load and the unbalancing radial load can be calculated using the equations proposed by Harris and Kotzalas [89, 90]. The change in contact angle results in the curvilinear motion of the balls along the groove, transverse to the rolling direction. This curvilinear displacement is given by $2\pi r_o \Delta\beta'/360$, where $\Delta\beta'$ represents the change in contact angle due to unbalance only, and r_o is the outer ring groove radius. This is graphically shown in Figure 5.6.

We estimate the displacement of the contacts due to unbalancing masses m_1 and m_2 which causes 2.24 N and 4.27 N additional cyclic forces at 4000 rpm. The axial load considered is 513 N, it is assumed that the radial load varies sinusoidally with a frequency of $2\pi n/60$. Figure 5.7 shows that the shift in contact due to unbalancing force is also

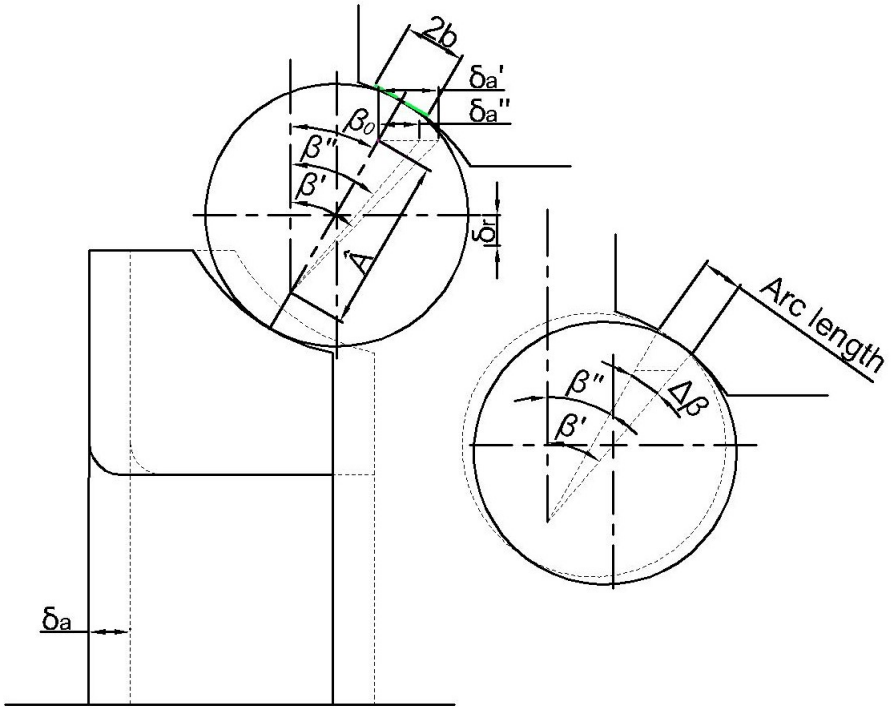

Figure 5.6: Contact geometry showing the axial and radial displacements and the resulting curvilinear transverse displacement (arc length) at the contact.

sinusoidal with amplitudes of 4.21 μm and 8.06 μm for the 2.24 N and 4.27 N loads, respectively. During this curvilinear displacement, the balls over-roll on the grease ridges formed by the previous balls. This pushes the lubricant back towards the center of the contact increasing the film thickness [84].

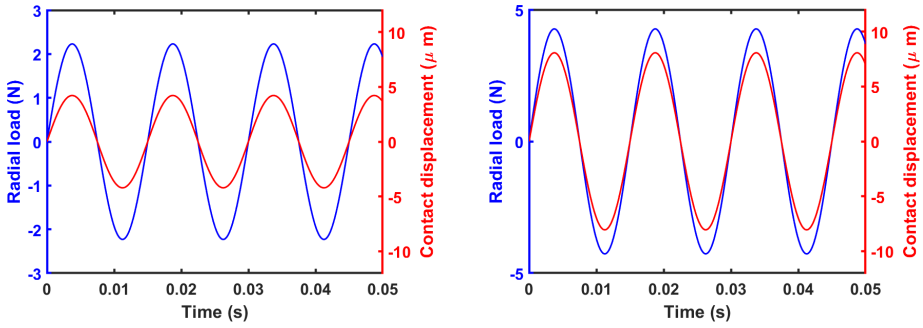

(a) (b)

Figure 5.7: Cyclic radial loads and resulting shifts in contact due to unbalancing mass (a) m_1 with unbalancing force amplitude of 2.24 N, and (b) m_2 with unbalancing force amplitude of 4.27 N. Bearing axial load (static) = 513 N.

6

UNIVERSAL MODEL FOR FILM THICKNESS IN AXIALLY LOADED BEARINGS

It has been speculated that the film thickness evolution in bearings with different sizes would be different. This is ascribed to the different distances between the grease reservoirs and the EHL contacts [39]. In Chapter 2 we showed the relationship between the relative film thickness and the product of viscosity, half contact width, and velocity (ηbu) using only 6209 deep groove ball bearings. In this chapter, we will show that the ηbu concept is also valid for bearings of different sizes. Here, film thickness is measured in 6204, 6206, and 6209 bearings lubricated with the LiM-100-2.5 and LiM-460-3 greases, the latter with much higher viscosity. These are the widely used bearings in electric vehicles, motors, and general-purpose machines. For more details on the bearing sizes and greases used, refer to Chapter 3. Finally, an empirical equation is proposed to determine film thickness in the axially loaded deep groove ball bearings. An analysis is done on the significance of speed and load's contribution towards the film build-up. All the results shown in this chapter are obtained using test rig 2. All film thickness measurements are done at $61\pm0.5^{\circ}C$. The work presented in this chapter has been submitted to be published as a technical paper. The paper can be found in Appendix D.

6.1 FILM THICKNESS IN 6204, 6206, AND 6209 BEARINGS

Figures 6.1a and 6.1b show the film thickness in 6204 bearings lubricated with LiM-100-2.5 and LiM-460-3 greases, respectively. The film thickness is measured from 1500 to 14000 rpm giving a maximum of 0.469 million ndm. The bearing lubricated with LiM-100-2.5 grease is loaded with 300 N, 400 N, and 500 N axial load. The bearing lubricated with LiM-460-3 grease is loaded with 400 N, 500 N, and 600 N axial loads. The loads are randomly chosen below the maximum rating of the test rig and bearings. The resulting contact pressure, and half contact width across 'b' and along 'a' are shown in Table 6.1.

The film thickness in both the bearings increases with speed up to 4000 rpm then it becomes almost constant up to 6000 rpm. The film thickness abruptly increases after 6000 rpm with a spike at 8000 rpm. The spike at 8000 rpm and the scattered film thickness at higher speeds are due to vibration effects. The reason for the increase in film thickness due to vibrations was described in the previous chapter. The film thickness of LiM-100-2.5 lubricated bearings shows a stable value after high speeds whereas the LiM-460-3 lubricated bearings show a higher contribution of vibrations to the film thickness at higher speeds. This appears to be due to the higher viscosity of the LiM-460-3 base oil.

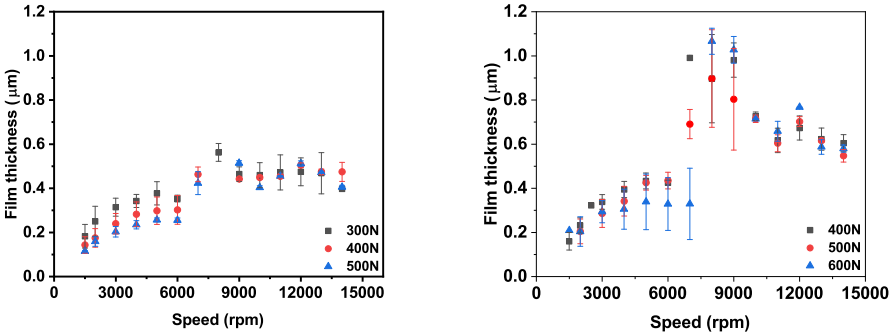

(a) Lubricated with LiM-100-2.5 grease.

(b) Lubricated with LiM-460-3 grease.

Figure 6.1: Variation of film thickness with speed in 6204 bearings lubricated with (a) LiM-100-2.5 grease and (b) LiM-460-3 grease.

Load (N)	Half contact width b (mm)	Half contact width a (mm)	Contact pressure (GPa)
300	0.849	0.064	1.20
400	0.925	0.069	1.31
500	0.987	0.074	1.39
600	1.041	0.078	1.47

Table 6.1: Bearing loads, half contact widths (across and along the running direction, giving ellipticity ratio = 0.0748), and maximum contact pressures for 6204 bearing inner ring-ball contact.

Figure 6.2 shows the film thickness in 6206 bearings. In these bearings, the film thickness is measured up to 9000 rpm, corresponding to 0.41 million ndm. The film thicknesses are measured at 310 N, 460 N, and 620 N axial loads, and the resulting contact pressures and contact widths are shown in Table 6.2. Similar to 6204 bearings, the increase in film thickness due to vibrations at about 8000 rpm can also be seen in these bearings.

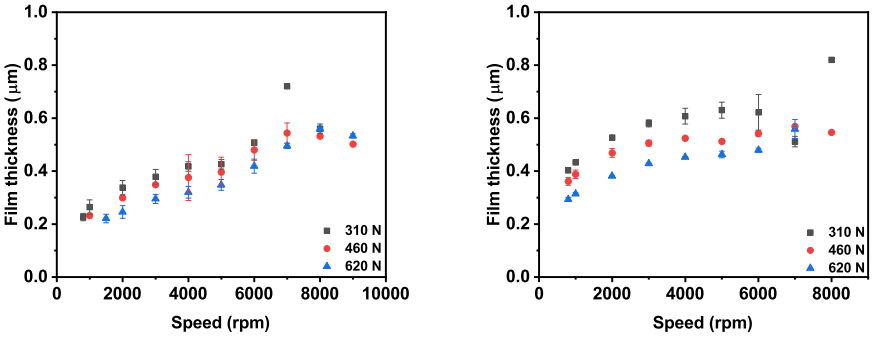

(a) Lubricated with LiM-100-2.5 grease.

(b) Lubricated with LiM-460-3 grease.

Figure 6.2: Variation of film thickness with speed in 6206 bearings lubricated with (a) LiM-100-2.5 grease and (b) LiM-460-3 grease.

Load (N)	Half contact width b (mm)	Half contact width a (mm)	Contact pressure (GPa)
310	0.855	0.068	1.03
460	0.962	0.077	1.16
620	1.050	0.084	1.27

Table 6.2: Bearing loads, half contact widths (across and along the rolling direction, giving ellipticity ratio = 0.0797), and maximum contact pressures for 6206 bearing inner ring-ball contact.

Figure 6.3 shows the film thickness in 6209 bearings, the largest bearing we tested. The film thickness is measured from 500 rpm up to 12000 rpm shaft rotational speed. This corresponds to 0.78 million ndm for the highest tested speed. The film thicknesses are measured at 513 N, 700 N, and 900 N axial loads. The resulting contact pressures and contact widths are shown in Table 6.3. The increase in film thickness after 6000 rpm and a peak film thickness at 8000 rpm can also be seen in these bearings.

In all the tested bearings, film thickness becomes almost constant at higher speeds. This is because, in severely starved contacts, the film thickness is mainly determined by the side flow, a function of residence time and the over-rolling frequency in combination with contact replenishment. As the speed increases, these two effects balance out reducing the dependency of film thickness on the speeds [16, 34, 79]. In all the bearings the film thicknesses at different loads are also different. Under fully flooded conditions, the dependency of film thickness on the load is minimal ($h_{ff} \propto W^{0.067}$) whereas it is more significant under starved lubrication conditions. Replenishment at the center of

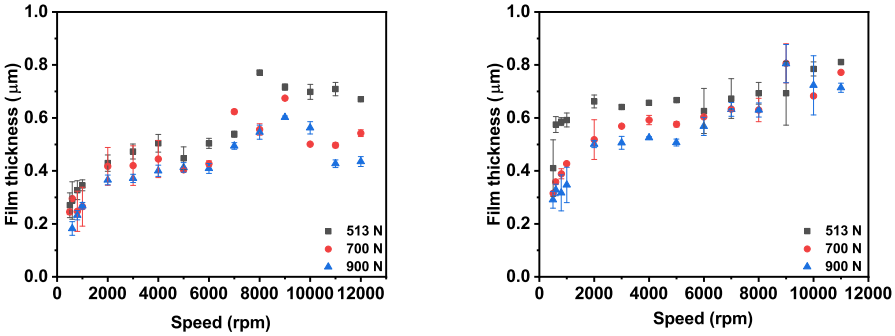

(a) Lubricated with LiM-100-2.5 grease.

(b) Lubricated with LiM-460-3 grease.

Figure 6.3: Variation of film thickness with speed in 6209 bearings lubricated with (a) LiM-100-2.5 grease and (b) LiM-460-3 grease.

Load (N)	Half contact width b (mm)	Half contact width a (mm)	Contact pressure (GPa)
513	1.087	0.085	0.97
700	1.194	0.093	1.07
900	1.286	0.100	1.15

Table 6.3: Loads, half contact widths (across and along the running direction, giving ellipticity ratio = 0.0779) and maximum contact pressures for 6209 bearing inner ring-ball contact.

the contact in the starved contacts is less attainable for larger contacts. The higher loads will increase the contact width, increasing the dependency of the film thickness on the load [20, 39]. In all the tested conditions, the film thicknesses of LiM-460-3 lubricated bearings are higher than the ones lubricated with LiM-100-2.5 greases. This is due to the higher viscosity of the LiM-460-3 base oil. Later we will show that, even though the absolute film thickness of LiM-460-3 grease is higher, the level of starvation, denoted by the relative film thickness, is lower than the LiM-100-2.5 lubricated bearings.

In the next section, we will use all these results to obtain an empirical equation for the film thickness.

6.2 FILM THICKNESS MODEL FOR AXIALLY LOADED BEARINGS

Most grease lubricated bearings operate under starved lubrication. The level of starvation in the bearings is given by the relative film thickness, the ratio of the measured grease film thickness (h_g) to the calculated fully flooded base oil film thickness (h_{ff}). The fully flooded film thickness is calculated based on Hamrock and Dowson's fully flooded film thickness equation 2.1. However, the film thickness obtained at higher speeds using this equation will deviate from the actual film thickness due to the inlet shear heating effects [91–93]. Therefore, a correction factor "C_T" proposed by Gupta et

al. [91] is used with Hamrock and Downson's film thickness equation:

$$C_T = \frac{1 - 13.2(p_m/E')Br^{0.42}}{1 + 0.213(1 + 2.23SRR^{0.83})Br^{0.64}}, \tag{6.1}$$

where Br is the Brinkman number given by $Br \approx -\beta\eta_0 u^2/K$, SRR is the slide-to-roll ratio (which is assumed as zero in our calculations), β is the temperature-viscosity coefficient obtained from $\eta = \eta_0 e^{-\beta(T-T_0)}$, K is the thermal conductivity of the lubricant, and p_m is the maximum Hertzian pressure. The C_T in our tests varied between 0.98 and 0.63.

A relative film thickness lower than 1 denotes starved lubrication conditions. In grease lubricated contacts, the relative film thickness can be greater than 1, because at low speeds, the shear rates are lower hence the grease apparent viscosity is more than the base oil viscosity resulting in higher film thickness. It is shown by Cann et al. [20] on a ball-on-disc machine, and later by Cen and Lugt [19] on full bearings, that the relative film thickness correlates well with the product of base oil viscosity (η), half contact width (b), and linear speed (u).

In Figure 6.4 we present the correlation between the relative film thickness and ηbu for three different bearing sizes, each lubricated with two different greases and each under three different loads at various speeds as mentioned in the previous section. The film thickness influenced by vibrations is either corrected as mentioned in the previous chapter or excluded from further analysis in this chapter. Even though vibration is one of the important replenishment mechanisms, including this effect would hinder the identification of any parameter related to the bearing geometry and dimensions. Figure 6.4 shows the corrected film thickness for 6209 bearings lubricated with LiM-100-2.5 grease for 513 N and 900 N loads. Data points above 6000 rpm for 6204–LiM-460-3 grease and 6209–LiM-100-2.5 grease (under 700 N load) are excluded.

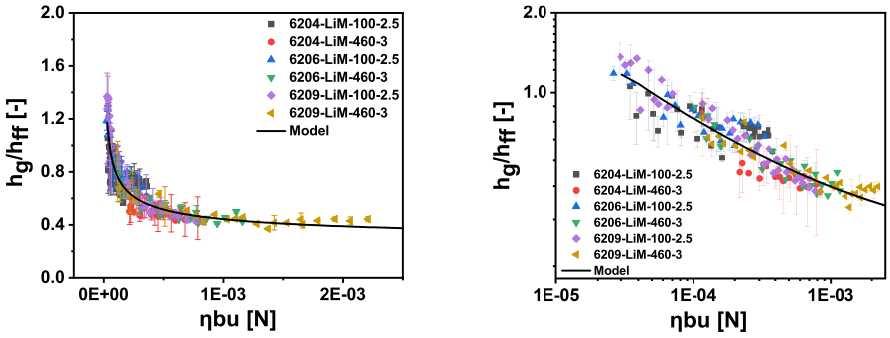

(a) Linear scale.

(b) Log-log scale.

Figure 6.4: Relative film thickness in 6204, 6206, and 6209 bearings lubricated with LiM-100-2.5 (100 cSt) and LiM-460-3 (460 cSt) greases.

A power law relationship can be established between the relative film thickness and ηbu

as shown in Figure 6.4. The curve-fitted equation obtained from the measured film thicknesses is

$$\frac{h_g}{h_{ff}} = 0.0544\,(\eta b u)^{-0.2945}, \tag{6.2}$$

with a goodness of fit R^2 of 86%. The collapse of film thickness data from all three different bearings lubricated with two greases and at three different loads and speeds on a single curve indicates that none of the bearing geometry-related parameters are necessary to describe the film thickness. In fully flooded conditions, the film thickness h_{ff} is related to speed u by

$$h_{ff} \propto u^{0.67}.$$

The inlet shear heating correction C_T (Eqn. 6.1) also depends on the speed, approximated for a moderate speed condition as

$$C_T \propto u^{-0.25},$$

which yields

$$h_{ff} \propto u^{0.42}.$$

The starved film thickness then reads:

$$h_g \propto u^{0.12}, \tag{6.3}$$

indicating that in the starved contacts, the film thickness has a weak dependency on speed. This agrees with the work of Van Zoelen et al. [16, 34, 35]. The proposed equation 6.2 is not validated for ultra-low speed conditions. At ultra-low speed conditions, it has been shown that the relative film thickness could be more than 1000 due to the very high grease viscosity at low shear rates. This is because, at ultra-low-speed conditions, the shear rates are very low.

Equation 6.2 shows that the transition from fully flooded to starved lubrication conditions can be estimated only with the base oil viscosity, half contact width, and linear speed and does not depend on the grease bleed rate, the bearing geometry parameters or grease rheological properties. Also, it confirms again that replenishment is a local phenomenon. Equation 6.2 indicates that the level of starvation increases with the base oil viscosity, speed, and load. The replenishment in the bearing lubricated with higher viscosity base oil would be difficult due to its lower mobility.

The fully flooded grease film thickness measurements on a ball-on-disc machine by Cen et al. [94] and Kochi et al. [95] showed that the film thickness at higher speeds (the conditions in which we tested our bearings) follows the base oil film thickness irrespective of grease rheological properties. In full bearings, similar results can be seen. At higher speeds, the inlet shear rates are so high that the grease viscosity is almost equal to the base oil viscosity.

Recently it was found by Okal et al. [96] that conformity–the ratio of the inner and outer race radii to the ball diameter – influences the film thickness in starved lubrication conditions. In our bearings, the outer ring conformity is different for different bearing sizes but their effect on the film thickness could not be identified in our experiments.

The difference in bearing size would induce different centrifugal forces on the lubricant, but since the replenishment is similar in all the bearing sizes, the effect of centrifugal force on the lubricant flow seems not to be significant. This was also theoretically expected from the work of Van Zoelen et al. [34, 35]. They showed that the side flow induced by the EHL action is more significant than the centrifugal force-induced flow.

Another parameter that influences the film thickness is the oil layer thickness on the track and the balls [14, 20]. It was shown by Van Zoelen et al. [16, 34, 35] that the oil layer at the exit of the EHL contacts divides equally between two rolling surfaces. Using the equations proposed by Chevalier and Damiens, we can estimate the oil layer thickness on the track h_∞ after the churning phase using the equation $h_\infty = \frac{h_g \rho(p)}{2\rho_0}$. Here, we use the measured grease film thickness h_g and the stable temperature after the churning phase as inputs. The calculated oil layer thickness is given in Table 6.4. The oil left on the track is almost the same in all three bearings and for both the greases. Therefore the degree of starvation for all the bearings and greases has the same dependency on the ηbu values.

Grease	6204	6206	6209
LiM-100-2.5	0.3	0.4	0.4
LiM-460-3	0.4	0.3	0.4

Table 6.4: Thicknesses, in μm, of the oil layers left on the track after churning.

7

FILM THICKNESS MODEL: THE MASTER CURVE

In the previous chapter, we established a power law relationship between the relative film thickness and ηbu for axially loaded bearings. Unlike axially loaded bearings, in bearings under radial or combined axial and radial loads, the load distribution among the balls will not be uniform and, hence, the film thickness at the ball-ring interfaces along the bearing circumference is not uniform. Consequently, an all steel ball bearing is not suitable for measuring film thickness via electric capacitance. Therefore, a 6209-type hybrid bearing is assembled with one ceramic ball replaced by a steel ball. This facilitates the measurement of instantaneous film thickness as the steel ball moves along the circumferential groove, given the ceramic balls are not electrically conductive.

The capacitance is a measure of film thickness, hence, it varies as the single steel ball moves along the groove. The film thickness which is inversely proportional to the measured capacitance is highest at the lowest loaded ball, and lowest at the highest loaded contact. The film thickness at this highest loaded point is considered in our analysis (see Figure 7.1b and Figure 7.3b). Here, all the film thicknesses are measured after running the bearing with freshly filled grease for 100 hours to ensure the churning phase has finished. Similar to the axially loaded bearings, the post-churning film thickness is stable when the operating conditions are held constant. The average film thickness from a 10- to 15-minute run at the highest loaded ball-ring contact is considered in our analysis.

The load distribution depends on the radial clearance in the bearing. In our experiments, we used a hybrid bearing with C3 radial clearance.

LiM-100-2.5 and LiM-460-3 greases are chosen for the study. The film thickness is measured at $61\pm0.5^{\circ}C$ on rig 2. Three different radial loads are tested for each grease. A set of three different combinations of radial and axial loads is used to study the film thickness under the combined load conditions.

In this chapter, we demonstrate that the product ηbu is not sufficient to predict the level

of starvation when a radial load is present. This is ascribed to a varying gap between balls and rings along the circumference where the contact with the largest gap dominates lubricant replenishment. We then show that the relative film thickness can be described well with $\frac{\eta bu}{z_r \sigma}$ where z_r is the radial gap between the ball and the outer ring groove at the zenith of the unloaded zone.

The work presented in this chapter has been submitted to be published as a technical paper. The paper can be found in Appendix E.

7.1 FILM THICKNESS

7.1.1 RADIAL LOAD

Three levels of radial loads are used in the tests: 700 N, 900 N, and 1200 N. The resulting highest normal load in the bearing contact, corresponding contact width, and maximum Hertzian pressure are shown in Table 7.1. An example capacitance measurement and resulting normal contact load profile for the bearing under radial load is shown in Figure 7.1a. It is observed that the capacitance follows the load distribution. Figure 7.1b shows the cyclic variation of capacitance with time and the (peak) capacitance values selected for subsequent analyses.

Radial load (N)	Highest load (N)	a (mm)	b (mm)	Contact pressure (GPa)
700	414.8	0.110	1.417	1.27
900	515.3	0.119	1.523	1.36
1200	662.8	0.129	1.657	1.48

Table 7.1: Applied radial load on the 6209-type bearing and the resulting normal contact load on the heaviest loaded ball, half contact widths along, a, and across, b, the running direction, giving ellipticity ratio = 0.0779) and contact pressure for 6209 bearing inner ring-ball contact.

The film thicknesses from the highest loaded point for different speeds and loads are shown in Figure 7.2 for both LiM-100-2.5 and LiM-460-3 grease lubricated bearings. We can see that, similar to the axial load conditions, the film thickness initially increases as the speed increases and becomes constant after a certain speed. For the LiM-100-2.5 lubricated bearing, the film thickness is stable after 2500 rpm whereas for the LiM-460-3 lubricated bearing, the film thickness became stable after 1000 rpm. We also notice that the film thickness of LiM-100-2.5 grease is lower than that of LiM-460-3 grease because of the former's lower base oil viscosity. We will show in section 7.2.1 that even though the absolute film thickness is lower for LiM-100-2.5 grease, the level of starvation is higher. Unlike axially loaded bearings, the film thickness under radial load does not show much variation with the load. We will explain the reason for this behavior in the next section.

7.1.2 COMBINED LOAD

Three sets of axial and radial load combinations are used in this study. The film thicknesses measured with (a) 500 N axial + 900 N radial load are denoted as 'A500R900'; (b) 900 N axial + 900 N radial load are denoted as 'A900R900'; (c) 900 N axial + 500 N radial

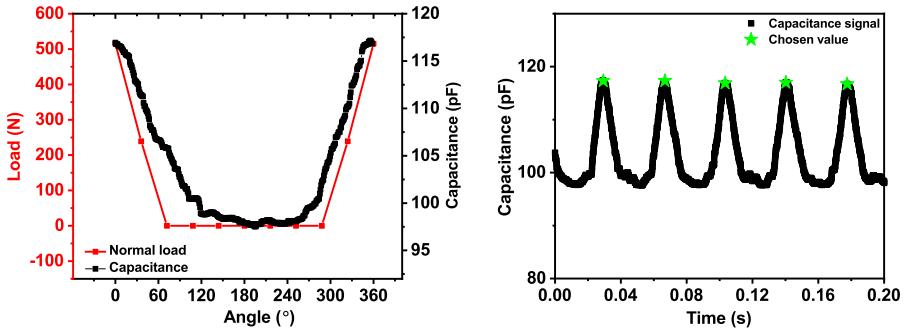

(a) Calculated load distribution and the capacitance signal

(b) Capacitance signal showing the chosen value

Figure 7.1: (a) Calculated ball-ring normal load variation and capacitance signal at different angular locations as the steel ball moves along the bearing circumference, (b) cyclic capacitance signal showing the selected peaks for a LiM-100-2.5 grease lubricated 6209 bearing under 900 N applied radial load.

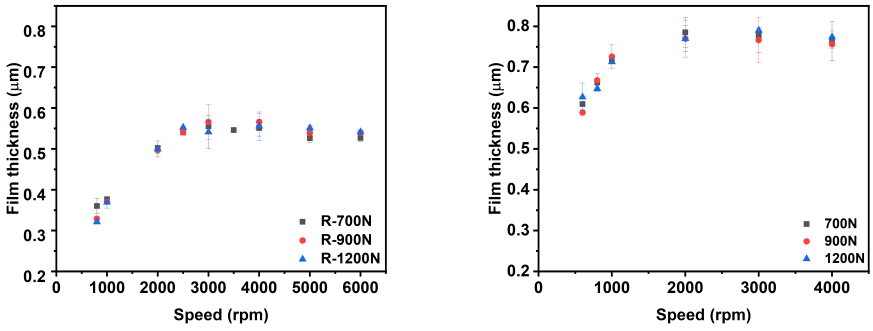

(a) Lubricated with LiM-100-2.5 grease.

(b) Lubricated with LiM-460-3 grease.

Figure 7.2: Variation of film thickness with speed for radially loaded bearings and lubricated with (a) LiM-100-2.5 grease and (b) LiM-460-3 grease.

load are denoted as 'A900R500'. The resulting highest load on the ball, its contact widths, and maximum Hertzian pressure are given in Table 7.2. An example load distribution calculation for balls at different circumferential positions and the corresponding capacitance signal is shown in Figure 7.3a, and an example cyclic capacitance profile with the chosen (peak) values is shown in Figure 7.3b. It is evident that the lowest loaded ball is at an angular position of 108 ° from the highest loaded ball. The capacitance also follows the same profile as the load variation along the bearing circumference.

Axial load (N)	Radial load (N)	Highest load (N)	a (mm)	b (mm)	Contact pressure (GPa)
500	900	586.7	0.1239	1.590	1.42
900	900	658.4	0.1287	1.652	1.47
900	500	477.7	0.1157	1.485	1.32

Table 7.2: Applied combined load on the bearing and the resulting load on the heavily loaded ball, half contact widths along, *a* and across, *b* the running direction, (giving ellipticity ratio = 0.0779) and contact pressure for 6209 bearing inner ring-ball contact.

The film thickness versus speed measurements at three different loads are shown in Figures 7.4. Similar to axial and radial load conditions, the film thickness increases with the speed initially and becomes almost stable. As we noticed in the radially loaded conditions, starvation for the LiM-100-2.5 grease lubricated bearing starts at a higher speed than that for the LiM-460-3 grease lubricated bearing. Under combined load conditions also, we do not see much load dependence for LiM-100-2.5 lubricated bearings.

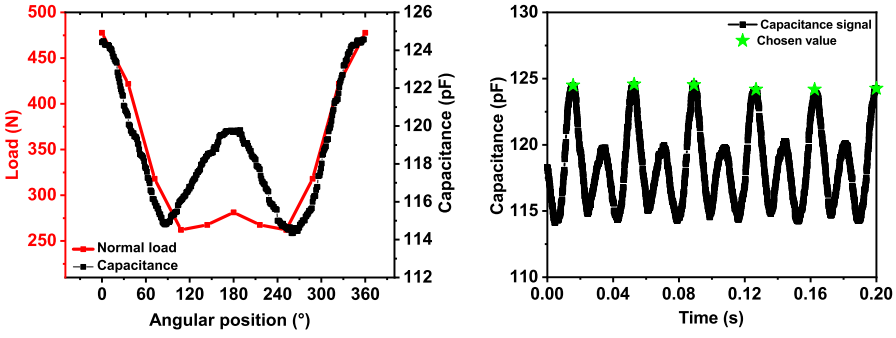

(a) Calculated load distribution and the capacitance signal

(b) Capacitance signal showing the chosen value

Figure 7.3: (a) Load distribution and the variation of capacitance at different angular positions, (b) capacitance signal and the chosen value for bearings lubricated with LiM-100-2.5 grease at 4000 rpm under 900 N axial load and 500 N radial load.

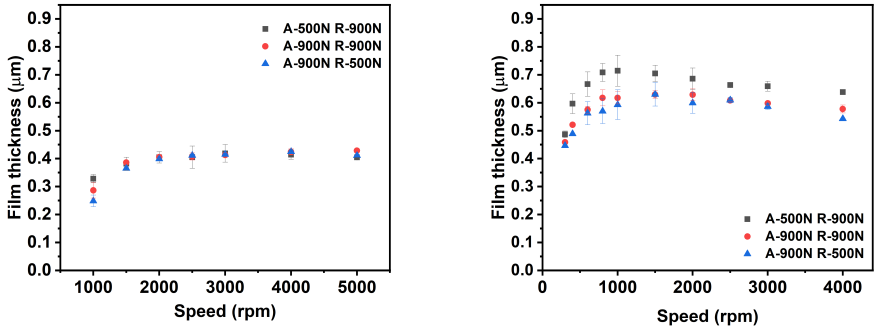

(a) Lubricated with LiM-100-2.5 grease.

(b) Lubricated with LiM-460-3 grease.

Figure 7.4: Film thickness variation with speed for combined axially and radially loaded bearings and lubricated with (a) LiM-100-2.5 grease and (b) LiM-460-3 grease.

7.2 RELATIVE FILM THICKNESS

Figure 7.5 shows how the relative film thickness varies in radial and combined load conditions for two different greases at various speeds and loads. Unlike axial load conditions, here, the relative film thickness for LiM-100-2.5 grease and LiM-460-3 grease do not merge to follow a unique power law relationship with ηbu in both radial load and combined load conditions. This indicates that there are some additional parameters required to fully define the degree of starvation in the presence of radial loads.

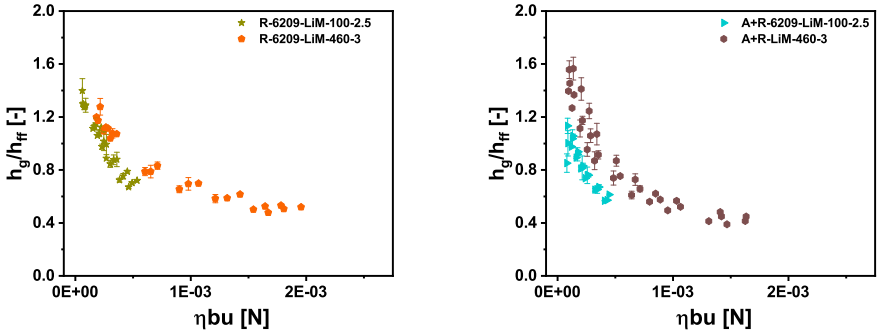

(a) Radial load

(b) Combined load

Figure 7.5: Variation of relative film thickness with ηbu for (a) radially loaded bearings, and (b) combined axially and radially loaded bearings, and lubricated with LiM-100-2.5 and LiM-460-3 greases.

7.2.1 THE EFFECT OF SURFACE TENSION

Previous studies [19, 39, 41] have shown that replenishment happens due to the capillary action at the ball and the groove contacts. The capillary action depends on the surface tension of the lubricant.

For pure axial load there was no need to include surface tension to describe the level of starvation. This does not mean that it is not relevant, it means that it may vary so little, compared to the speed, contact width and viscosity, that it can be considered constant. To identify if it does become relevant for radial and combined load, we measured it at 61 $^{\circ}C$, the test temperature, and found values of 0.0171 and 0.0276 N/m for LiM-100-2.5 and LiM-460-3 grease respectively (see Table 3.1) .

Now we plot the relative film thickness h_g/h_{ff} against $\eta bu/\sigma$ for both LiM-100-2.5 and LiM-460-3 greased bearings in Figure 7.6. We can see that the relative film thicknesses of both the greases merge together on a single curve for pure radial, and combined load. Comparing the axial load results from Figure 7.6c with Figure 7.6c shows that the results for axial load do not change significantly by adding σ.

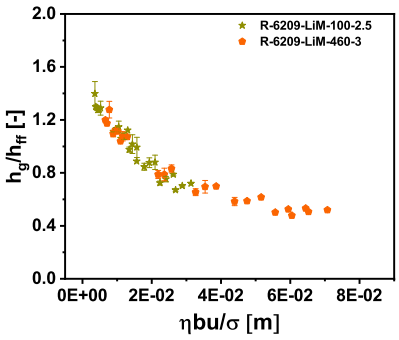

(a) Radial load

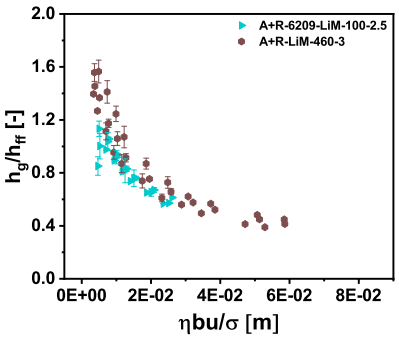

(b) Combined load

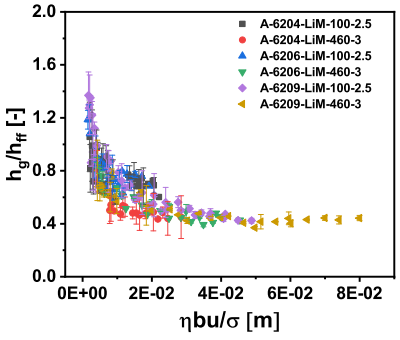

(c) Axial load

Figure 7.6: Variation of relative film thickness with $\eta bu/\sigma$ for (a) radial, (b) combined, and (c) axial load lubricated with LiM-100-2.5 grease and LiM-460-3 grease.

To see whether the degree of starvation in each loading type follows the same power law profile, we plot all results from axial, radial, and combined loads in Figure 7.7. The degree of starvation is observed to be highest for axial load (i.e., lowest h_g/h_{ff} profile), followed by combined and radial load conditions. This begs the question of why/how the degree

of starvation depends on the loading types and why we had to include surface tension when radial load is present. This is answered in the next section.

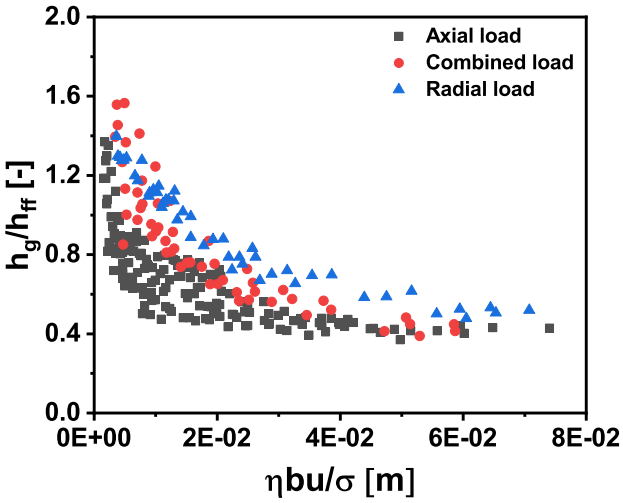

Figure 7.7: Relative film thickness h_g/h_{ff} vs $\eta bu/\sigma$ for all three different loading types.

7.2.2 FILM THICKNESS MODEL FOR BEARINGS UNDER PURE RADIAL LOAD

The film thickness results under pure radial load (Figure 7.2) show that they do not vary with the load magnitudes. To verify this, we plot in Figure 7.8 the relative film thickness as a function of capillary number alone i.e. without including half contact width b of the highest loaded ball. We can fit the data points for both LiM-100-2.5 and LiM-460-3 lubricated bearings under radial loads with a power law curve

$$\frac{h_g}{h_{ff}} = 1.8\left(\frac{\eta u}{\sigma}\right)^{-0.31} \tag{7.1}$$

with $R^2 = 0.93$. The fact that the contact width b of the highest loaded ball is not important confirms that the level of starvation is independent of load for pure radial load. It indicates that the replenishment in the radially loaded bearing is dominated by the balls in the unloaded region. However, this replenishment mechanism is not present in axially loaded bearings. To address this, and include all the relevant mechanisms for all the load types, we derive an universal expression, which is explained in the next section.

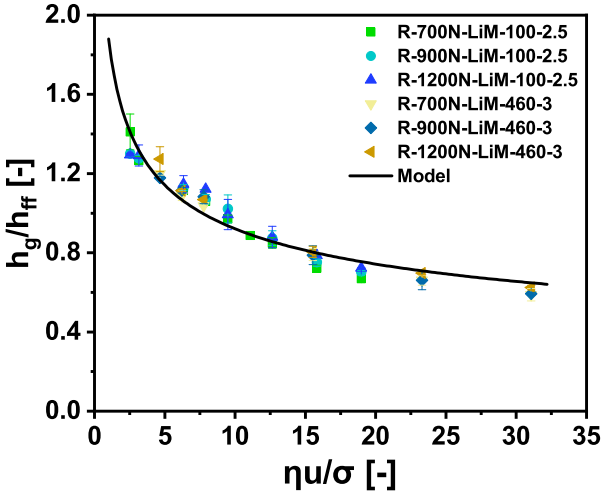

Figure 7.8: Relative film thickness as a function of capillary number ($\eta u/\sigma$) for three different radial loads and two different greases.

7.2.3 THE RADIAL GAP EFFECT

As mentioned above, when a radial load is applied, the load distribution among the balls in the bearing is not uniform (see Figure 7.1a and Figure 7.3a). Due to this load variation among the balls, the Hertzian contact width b also varies, affecting the replenishment of the contacts.

The oil replenishment in the ball-ring contacts is facilitated by the capillary pressure and the hydraulic resistance. The capillary pressure is primarily determined by the surface tension of the lubricant and the 'fluid curvature' [97, 98], which depends on the distance between the surfaces outside the Hertzian contact. The smaller the distance between the surfaces, the more replenishment is expected. But this capillary flow is also balanced by the hydraulic resistance. This hydraulic resistance also depends on the distance between the surfaces but this dependency is much higher than that of the driving capillary force.

In the highest loaded contact, this fluid curvature is largest due to smaller gap between the surfaces, hence, higher capillary pressure is expected. But the hydraulic resistance is also larger due to the increased contact width and the smaller gap between the surfaces. In the lowest loaded contacts, the capillary pressure is expected to be lower than in the highest loaded ball because of decreased curvature (increased gap), but the hydraulic resistance reduces more significantly than the capillary pressure. Therefore a net increase in oil replenishment is observed in the lowest loaded contacts.

Quantifying this effect is not trivial. Particularly under combined load, the gap between ball and ring will be different on the left and right side of the contacts. The gap and contact width will be different for each ball, it varies in 3 dimensions, there will be an in-

teraction between the inner ring and outer ring contact etc. As an engineering approach we select the vertical distance between the apex of the ball and the outer ring groove and call this z_r.

This distance is straightforward in the case of pure radial load. In that case it is given by $z_r = P_d + \delta_i + \delta_o$, where P_d is the diametrical clearance, δ_i and δ_o are the inner ring- and outer ring-ball contact deformation, respectively. When the radial load increases, the gap z_r also increases. When axial loads and combined loads (axial+radial load) are applied, the ball shifts axially and its vertical axis makes a contact angle β' with the contact normal (see Figure 7.9b). Here, the gap between the top of the ball and the groove center depends on the axial, radial, and angular deflections of the inner ring; and the contact angle. The procedure to obtain the ball center and inner ring groove center positions is explained in reference [89]. The gap can then be calculated by assuming the ball is perfectly circular away from the Hertzian contact, the outer ring is stationary, and the inner ring moves. This is a static load analysis, hence, centrifugal force is neglected to render the contact angle at the inner ring-ball contact and at the ball-outer ring contact equal.

The gaps calculated for all the loads are listed in Table 7.3. For combined loads and radial loads, the gap varies along the circumference of the bearing. An example calculation of the gap z_r for combined load condition is shown in Figure 7.10. We consider the largest gap between the ball and the groove in our analysis. This largest gap happens to always be radially opposite to the highest loaded ball. In the case of axial loads, the gap does not vary much with the loads whereas the gap depends on the load when radial load is applied. Since radial loads have an opposing impact on contact width, this explains why the film thickness in radially loaded bearings do not vary much with the load magnitudes. The gap z_r also depends on the type of load i.e. axial, radial, or combined. It is lowest for the axially loaded bearings, and highest for the radial load condition, and in between for combined load. All these observations suggest that an increasing gap z_r leads to a decreasing degree of starvation.

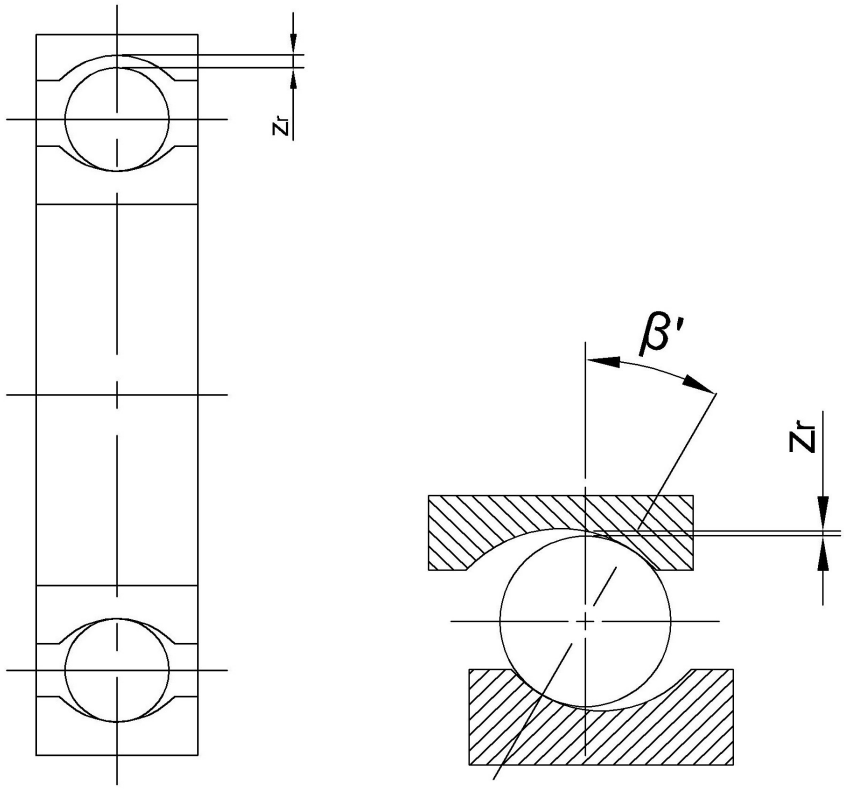

(a) Radial load

(b) Axial load and Combined load

Figure 7.9: Ball-ring diagram showing the gap z_r between the top of the ball and the outer ring groove.

Bearing	Axial load (N)	Radial load (N)	z_r (μm)
6209	513	0	10.00
6209	700	0	10.16
6209	900	0	10.30
6206	310	0	7.50
6206	460	0	7.65
6206	620	0	7.80
6204	300	0	8.27
6204	400	0	8.43
6204	500	0	8.57
6209	0	700	37.62
6209	0	900	39.28
6209	0	1200	41.52
6209	500	900	26.95
6209	900	900	25.31
6209	900	500	20.15

Table 7.3: Applied load on different bearings and the gap z_r calculated.

7.2.4 MASTER CURVE

Now, we have identified that the level/degree of starvation increases with increasing ηbu and decreasing $z_r\sigma$. In Figure 7.11 we plot the relative film thickness for all the results shown so far —axial, radial, combined loads, all bearings and both greases—against the non-dimensional number $\eta bu/z_r\sigma$. The relative film thickness is observed to correlate well with $\eta bu/z_r\sigma$ for axial, radial and combined loads and merges onto a single power law relation. A curve fit to these measurement points results in a power law relationship as follows

$$\frac{h_g}{h_{ff}} = 7.305\left(\frac{\eta bu}{z_r\sigma}\right)^{-0.34}. \tag{7.2}$$

The goodness of curve fit is 87.7%. It is astonishing to see that different bearing sizes with different lubricants, and different combinations of loads follow a single power law curve. We can see that the transition from fully flooded to starvation begins when the non-dimensional starvation parameter is more than 375. These results are only valid for moderately low to high-speed conditions. At extremely low speeds, it is observed that the film thickness increases several times more than the base oil film thickness [13, 94].

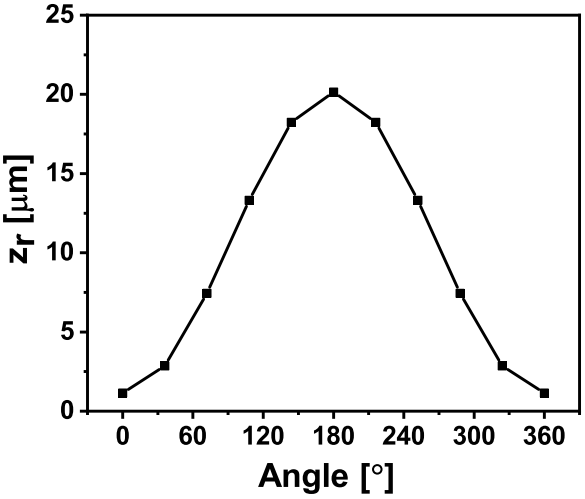

Figure 7.10: Vertical distance between the top of the ball and the outer ring groove for all the balls in the bearing for combined load comprising an axial load of 900 N and a radial load of 500 N in a 6209 bearing.

At extremely low speeds, the shear rates are low, hence, the grease's apparent viscosity could be higher resulting in a higher film thickness. When the speed increases, the shear rate increases, and the grease viscosity approaches the base oil viscosity, therefore, we only need base oil viscosity to estimate the film thickness and it does not depend on the grease rheological properties.

As discussed in the previous chapter, we can also observe that the dependency on the speed is lower when starved than when fully flooded. The film thickness dependency on the load depends on the type of loading i.e. for axial load conditions, it depends on the contact width 'b' but in the presence of radial load, the dependency on load decreases. This is also reflected in the non-dimensional starvation parameter $\eta bu/z_r\sigma$. Since both b and z_r increase linearly with the load under radial load condition as shown in Figure 7.12, they balance out and the dependency on the load reduces.

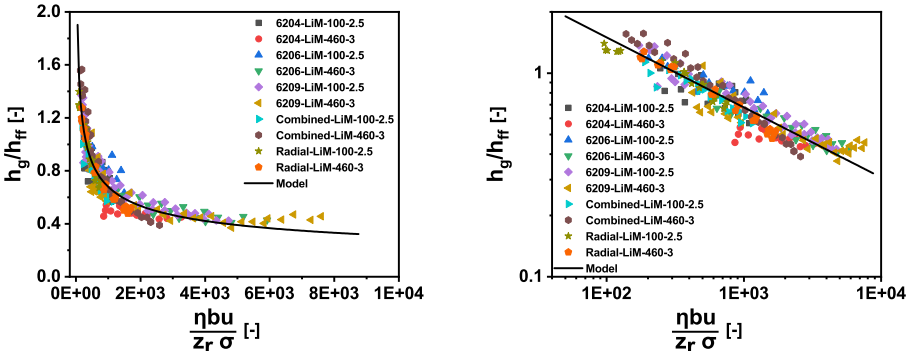

(a) Linear scale

(b) Log-log scale

Figure 7.11: Variation of relative film thickness with non-dimensional starvation parameter.

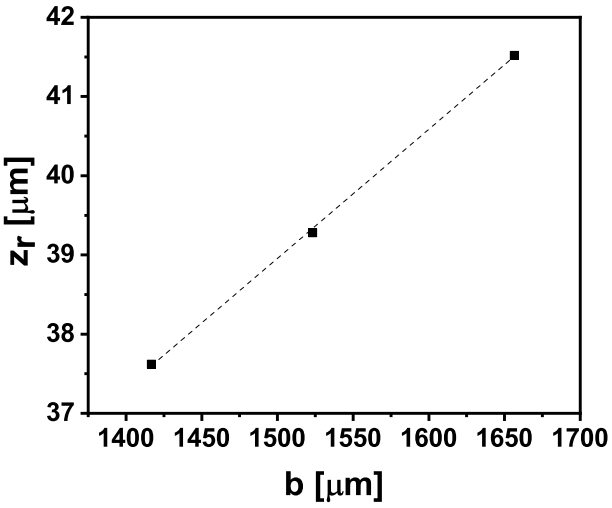

Figure 7.12: Contact width of the highest loaded ball vs gap z_r for pure radial load, showing a linear relationship between b and z_r.

8

CONCLUSIONS AND RECOMMENDATIONS

8.1 CONCLUSIONS

Despite film thickness being one of the important parameters in grease lubricated bearings, there are no equations to predict it. In this thesis, a systematic study on the film thickness immediately after the churning phase was carried out. The primary findings from the thesis are outlined below.

The conclusions that are discussed here apply to good quality ball bearings and greases in the operational domain in which the underlying tests have been performed.

A new method to measure the starved film thickness in grease lubricated bearings using an electrical capacitance method was developed, wherein the ball-ring contacts are the capacitors. An electrical capacitance model of the bearing was used, making it possible to calculate the impact of starvation on capacitance. This is relevant because the 'calibration' is done with oil lubrication, i.e., with fully flooded contacts. The result is that thinner films are found.

It was shown that the film thickness after the end of the churning phase is independent of the initial grease-filling quantity. We demonstrated that the clearing sub-phase leaves oil layers with thicknesses that are solely determined by the dynamics of the oil flow in and around the contacts facilitated by contact pressure driven side flow (loss) and capillary action (replenishment). The film thickness does not depend on the oil bleed from the grease reservoirs located outside the swept area of the bearing. We know that grease looses its base oil during the life-time of the bearing. Apparently, bleed only

takes place when oil-layers in the raceway are consumed (by evaporation, leakage, etc.), i.e., after longer running times.

Contact replenishment is enhanced by vibrations. The film measurements with vibrations showed that there was an increase in film thickness depending on the load on the bearings. Due to vibrations, the ball on the track oscillates curvilinearly causing it to roll over the ridges formed by the previous ball, resulting in increased contact replenishment. A model to predict the increase in film thickness due to vibrations was also proposed.

The film thickness in a grease lubricated ball bearing does not decrease with increasing speeds but is almost constant after a certain critical speed. This is contrary to what was often observed on ball-on-disc (single contact) machines. This means that grease lubrication can be safely applied at higher speed applications such as in bearings for electric motors in electric vehicles. The film thickness in an axially loaded ball bearing can be estimated using the equation

$$\frac{h_g}{h_{ff}} = 0.0544\ (\eta b u)^{-0.2945}$$

with 86% accuracy. The film thickness dependency on the load is higher than in the case of fully flooded conditions. Increasing the viscosity increases the level of starvation. In moderate to high-speed conditions, the film thickness does not depend on the grease's rheological properties but only on the base oil properties.

Applying radial or combined load changes the side flow and replenishment due to a variation of the contact width b in the circumference of the bearing. This introduces an additional dynamic effect but also makes the distance over which contact replenishment needs to take place different for each ball-ring contact in the bearing. Moreover, it is unlikely that the available volume of oil for replenishment is equal for each ball. This volume determines the capillary pressure, that drives the flow for contact replenishment.

Contact replenishment is driven by the balance of capillary pressure and hydraulic resistance. The resistance depends on the length over which replenishment needs to take place, i.e., the contact width b, and viscosity. The capillary pressure depends on surface tension and the 'fluid curvature' which is given by the gap between ball and ring outside the Hertzian contact, at the air-oil interface (side-ways meniscus). The fact that the surface tension is not relevant for determining the level of starvation in the case of axial load showed that this capillary pressure does not change considerably with bearing load and speed. However, this does not apply in the case of radial/combined load. This means that the height of the gap determining the meniscus curvature (and therefore the capillary pressure) is determined by a location/position that does not change considerably for pure axial load but does change in the case for radial/combined load. It was shown in this thesis that this position is at the apex of the balls. So the capillary pressure

effects can be represented using the radial gap between ball and ring at the ball-apex position.

The film thickness dependency on load magnitude in the presence of radial load is lower than for axial load conditions. The surface tensions of the base oils vary with temperatures, so it is essential to include them to determine the transition from fully flooded conditions to starved conditions when radial loads are present. The relative film thickness in radially loaded bearings can be found using

$$\frac{h_g}{h_{ff}} = 1.8\left(\frac{\eta u}{\sigma}\right)^{-0.31}.$$

a function of capillary number only with a confidence of 93%.

Finally, the film thickness in a deep groove ball bearing under axial, radial, or combined load conditions can be estimated with a confidence of 87.7% using the equation

$$\frac{h_g}{h_{ff}} = 7.305\left(\frac{\eta b u}{z_r \sigma}\right)^{-0.34}.$$

8.2 RECOMMENDATIONS FOR FUTURE RESEARCH

- The film thickness equation developed in this thesis applies to 'good quality' ball bearings and greases. These include 'metal-soap' thickened greases and polyurea greases. It is recommended to continue this work with lubricating greases with a different lubrication mechanism such a calcium-sulponate complex greases.
- Film thickness behaviors in ultra-low speed conditions were not considered in this study since the focus was to identify the beginning of starvation and the parameters controlling it. The film thickness at ultra-low speed might depend not only on the base oil properties of the grease. This study would help to understand the film thickness in ultra-low-speed applications such as wind turbines.
- Modern electrical motors are anticipated to operate at higher rotational speeds than tested here (0.8 million ndm). It is recommended to measure film thickness at higher speeds (2-3 million ndm).
- The maximum speed (reference speed) in bearings is a function of the grease type. It is recommended to find the favorable properties of high speed greases by using film thickness measurements.
- The film thickness studies in this thesis were performed after only 100 hours of running the bearing after being filled with fresh grease. The replenishment mechanisms might change after a very long duration of bearing operation. Therefore, a study on the film thickness in bearings after running for an extended period is necessary.
- The effect of vibrations on the film thickness in a bearing can be studied further by using a laser vibrometer which enables direct measurement of relative displacement in the bearing outer ring.
- The film thickness in very low-consistency grease was not measured in our experiments (Lower than 1.5). The lower consistency greases could give a different level of starvation.
- The film thickness behavior might be different in different types of rolling element bearings. The level of starvation in each bearing type, e.g. cylindrical roller bearings, etc., needs to be studied individually.
- Three different deep groove ball bearing sizes were tested in this thesis. It was shown that lubrication mechanism did not essentially change within this variation of bearing size. It is recommended to investigate/find the largest size of bearing to which the derived film thickness equation applies.
- All the tested bearings had C3 radial clearance. It is known that the radial load distribution changes with radial clearance. Film thickness variation for bearings with different clearance needs to be studied.
- The film thickness equation that was developed in this work is empirical. It is recommended to develop a physical model for side flow and contact replenishment

for single contacts, and apply this to the complex geometry of a full grease lubricated bearing to refine the equation.

BIBLIOGRAPHY

[1] McQueen, A., 2010. "Stathis ioannides, devoted to the fight against friction". *Evolution: The Business and Technology Magazine from SKF*, pp. 18–20.

[2] Lugt, P. M., 2012. *Grease lubrication in rolling bearings*. John Wiley & Sons.

[3] Gow, G., 2010. "Lubricating grease". *Chemistry and Technology of Lubricants*, pp. 411–432.

[4] Saatchi, A., Shiller, P. J., Eghtesadi, S. A., Liu, T., and Doll, G. L., 2017. "A fundamental study of oil release mechanism in soap and non-soap thickened greases". *Tribology International,* **110**, pp. 333–340.

[5] Baker, A. E., 1958. "Grease bleeding—a factor in ball bearing performance". *NLGI spokesman,* **22**(9), pp. 271–277.

[6] Chatra, S. K. R., and Lugt, P. M., 2021. "The process of churning in a grease lubricated rolling bearing: Channeling and clearing". *Tribology International,* **153**, p. 106661.

[7] Chatra, S. K. R., and Lugt, P. M., 2020. "Channeling behavior of lubricating greases in rolling bearings: Identification and characterization". *Tribology International,* **143**, p. 106061.

[8] Chatra, S. K. R., 2023. "The process of churning in grease lubricated bearings: Identification and thermo-mechanical characterization". PhD thesis, University of Twente.

[9] Lubrecht, A. A., Venner, C. H., and Colin, F., 2009. "Film thickness calculation in elasto-hydrodynamic lubricated line and elliptical contacts: the dowson, higginson, hamrock contribution". *Proceedings of the Institution of Mechanical Engineers, Part J: Journal of Engineering Tribology,* **223**(3), pp. 511–515.

[10] Hamrock, B. J., and Dowson, D., 1977. "Isothermal elastohydrodynamic lubrication of point contacts: part iii—fully flooded results". *Journal of Lubrication Technology,* **99**(2), pp. 264–275.

[11] Wedeven, L. D., Evans, D., and Cameron, A., 1971. "Optical analysis of ball bearing starvation". *Journal of Lubrication Technology,* **93**(3), pp. 349–361.

[12] Svoboda, P., Kostal, D., Krupka, I., and Hartl, M., 2013. "Experimental study of starved EHL contacts based on thickness of oil layer in the contact inlet". *Tribology International,* **67**, pp. 140–145.

[13] Morales-Espejel, G. E., Lugt, P. M., Pasaribu, R., and Cen, H., 2014. "Film thickness in grease lubricated slow rotating rolling bearings". *Tribology International,* **74**, pp. 7–19.

[14] Damiens, B., Venner, C. H., Cann, P. M., and Lubrecht, A. A., 2004. "Starved lubrication of elliptical EHD contacts". *J. Trib.,* **126**(1), pp. 105–111.

[15] Chevalier, F., Lubrecht, A. A., Cann, P. M., Colin, F., and Dalmaz, G., 1998. "Film thickness in starved EHL point contacts". *Journal of Tribology,* **120**.

[16] Van Zoelen, M. T., Venner, C. H., and Lugt, P. M., 2009. "Prediction of film thickness decay in starved elasto-hydrodynamically lubricated contacts using a thin layer flow model". *Proceedings of the Institution of Mechanical Engineers, Part J: Journal of Engineering Tribology,* **223**(3), pp. 541–552.

[17] Venner, C. H., Van Zoelen, M. T., and Lugt, P. M., 2012. "Thin layer flow and film decay modeling for grease lubricated rolling bearings". *Tribology International,* **47**, pp. 175–187.

[18] Cen, H., and Lugt, P. M., 2019. "Film thickness in a grease lubricated ball bearing". *Tribology International,* **134**, pp. 26–35.

[19] Cen, H., and Lugt, P. M., 2020. "Replenishment of the EHL contacts in a grease lubricated ball bearing". *Tribology International,* **146**, p. 106064.

[20] Cann, P. M., Damiens, B., and Lubrecht, A. A., 2004. "The transition between fully flooded and starved regimes in EHL". *Tribology International,* **37**(10), pp. 859–864.

[21] Reynolds, O., 1885. "On the theory of lubrication and its application to Mr. Beauchamp Tower's experiments, including an experimental determination of the viscosity of olive oil". *Philosophical Transactions of the Royal Society of London,* **177**, p. 157.

[22] Ertel, A. M., 1945. "Die Berechnung der hydrodynamischen Schmierung gekrümmter Oberflächen unter hoher Belastung und Relativbewegung". *Fortschr. Ber. VDIZ, Reihe,* **1**.

[23] Dowson, D., and Higginson, G. R., 1959. "A numerical solution to the elasto-hydrodynamic problem". *Journal of Mechanical Engineering Science,* **1**(1), pp. 6–15.

[24] Dowson, D., and Higginson, G. R., 1960. "The effect of material properties on the lubrication of elastic rollers". *Journal of Mechanical Engineering Science,* **2**(3), pp. 188–194.

[25] Dowson, D., Higginson, G. R., and Whitaker, A. V., 1962. "Elasto-hydrodynamic lubrication: a survey of isothermal solutions". *Journal of Mechanical Engineering Science,* **4**(2), pp. 121–126.

[26] Spikes, H. A., 2006. "Sixty years of EHL". *Lubrication Science,* **18**(4), pp. 265–291.

[27] Hamrock, B. J., and Dowson, D., 1976. "Isothermal elastohydrodynamic lubrication of point contacts: Part 1—theoretical formulation". *Journal of Lubrication Technology,* **98**(2).

[28] Hamrock, B. J., and Dowson, D., 1977. "Isothermal elastohydrodynamic lubrication of point contacts: part iii—fully flooded results". *Journal of Lubrication Technology,* **99**(2).

[29] Hamrock, B. J., and Dowson, D., 1976. "Isothermal elastohydrodynamic lubrication of point contacts: Part ii—ellipticity parameter results". *Journal of Lubrication Technology,* **98**(3).

[30] Wedeven, L. D., 1970. "Optical measurements in elastohydrodynamic rolling-contact bearings". PhD thesis, Imperial College London.

[31] Hamrock, B. J., and Dowson, D., 1977. "Isothermal elastohydrodynamic lubrication of point contacts: Part iv—starvation results". *Journal of Lubrication Technology,* **99**(1).

[32] Dwyer-Joyce, R., Drinkwater, B., and Donohoe, C., 2003. "The measurement of lubricant–film thickness using ultrasound". *Proceedings of the Royal Society of London. Series A: Mathematical, Physical and Engineering Sciences,* **459**(2032), pp. 957–976.

[33] Gray, W., and Dwyer-Joyce, R., 2022. "In-situ measurement of the meniscus at the entry and exit of grease and oil lubricated rolling bearing contacts". *Frontiers in Mechanical Engineering,* **8**, p. 1056950.

[34] Van Zoelen, M. T., 2009. "Thin layer flow in rolling element bearings". PhD thesis, University of Twente.

[35] Van Zoelen, M. T., Venner, C. H., and Lugt, P. M., 2010. "The prediction of contact pressure–induced film thickness decay in starved lubricated rolling bearings". *Tribology Transactions,* **53**(6), pp. 831–841.

[36] Pemberton, J., and Cameron, A., 1976. "A mechanism of fluid replenishment in elastohydrodynamic contacts". *Wear,* **37**(1), pp. 185–190.

[37] Åström, H., Östensen, J. O., and Höglund, E., 1993. "Lubricating grease replenishment in an elastohydrodynamic point contact". *Journal of Tribology,* **115**.

[38] Larsson, P.-O., 1996. "Lubricant replenishment in the vicinity of an EHD contact". PhD thesis, Luleå Tekniska Universitet.

[39] Cann, P. M., and Lubrecht, A. A., 2007. "Bearing performance limits with grease lubrication: the interaction of bearing design, operating conditions and grease properties". *Journal of Physics D: Applied Physics,* **40**(18), p. 5446.

[40] Chiu, Y. P., 1974. "An analysis and prediction of lubricant film starvation in rolling contact systems". *ASLE Transactions,* **17**(1), pp. 22–35.

[41] Gershuni, L., Larson, M. G., and Lugt, P. M., 2008. "Lubricant replenishment in rolling bearing contacts". *Tribology Transactions,* **51**(5), pp. 643–651.

[42] Jacod, B., Pubilier, F., Cann, P. M., and Lubrecht, A. A., 1999. "An analysis of track replenishment mechanisms in the starved regime". In *Tribology Series*, Vol. 36. Elsevier, pp. 483–492.

[43] Nogi, T., 2015. "An analysis of starved EHL point contacts with reflow". *Tribology Online,* **10**(1), pp. 64–75.

[44] Nogi, T., 2015. "Film thickness and rolling resistance in starved elastohydrodynamic lubrication of point contacts with reflow". *Journal of Tribology,* **137**(4), p. 041502.

[45] Fischer, D., von Goeldel, S., Jacobs, G., and Stratmann, A., 2021. "Numerical investigation of effects on replenishment in rolling point contacts using CFD simulations". *Tribology International,* **157**, p. 106858.

[46] Cann, P. M., and Lubrecht, A. A., 2003. "The effect of transient loading on contact replenishment with lubricating greases". In *Tribology Series*, Vol. 43. Elsevier, pp. 745–750.

[47] Jonkisz, W., and Krzemiński-Freda, H., 1979. "Pressure distribution and shape of an elastohydro-dynamic grease film". *Wear,* **55**(1), pp. 81–89.

[48] Muennich, H. C., and Gloeckner, H. J. R., 1980. "Elastohydrodynamic lubrication of grease-lubricated rolling bearings". *ASLE Transactions,* **23**(1), pp. 45–52.

[49] Palacios, J. M., Cameron, A., and Arizmendi, L., 1981. "Film thickness of grease in rolling contacts". *ASLE Transactions,* **24**(4), pp. 474–478.

[50] Cann, P. M., Williamson, B. P., Coy, R. C., and Spikes, H. A., 1992. "The behaviour of greases in elastohydrodynamic contacts". *Journal of Physics D: Applied Physics,* **25**(1A), p. A124.

[51] Cann, P. M., 1996. "Understanding grease lubrication". In *Tribology Series*, Vol. 31. Elsevier, pp. 573–581.

[52] Aihara, S., and Dowson, D., 1978. "A study of film thickness in grease lubricated elastohydrodynamic contacts". In Proc of the 5th Leeds-Lyon Symposium on Tribology, pp. 104–115.

[53] Åström, H., Isaksson, O., and Höglund, E., 1991. "Video recordings of an EHD point contact lubricated with grease". *Tribology International,* **24**(3), pp. 179–184.

[54] Sasaki, T., Mori, H., and Okino, N., 1960. "Theory of grease lubrication of cylindrical rooler bearing". *Bulletin of JSME,* **3**(10), pp. 212–219.

[55] Kauzlarich, J. J., and Greenwood, J. A., 1972. "Elastohydrodynamic lubrication with Herschel-Bulkley model greases". *ASLE Transactions,* **15**(4), pp. 269–277.

[56] Yang, Z., and Qian, X., 1987. "A solution to grease lubricated EHD film thickness in an elliptical rolling contact". In ImechE Conference Publication, Vol. 1, pp. 97–104.

[57] Jonkisz, W., and Krzeminski-Freda, H., 1982. "The properties of elastohydrodynamic grease films". *Wear,* **77**(3), pp. 277–285.

[58] Kaneta, M., Ogata, T., Takubo, Y., and Naka, M., 2000. "Effects of a thickener structure on grease elastohydrodynamic lubrication films". *Proceedings of the Institution of Mechanical Engineers, Part J: Journal of Engineering Tribology,* **214**(4), pp. 327–336.

[59] Cyriac, F., Lugt, P. M., Bosman, R., Padberg, C. J., and Venner, C. H., 2016. "Effect of thickener particle geometry and concentration on the grease EHL film thickness at medium speeds". *Tribology Letters,* **61**, pp. 1–13.

[60] Couronné, I., Vergne, P., Mazuyer, D., Truong-Dinh, N., and Girodin, D., 2003. "Effects of grease composition and structure on film thickness in rolling contact". *Tribology Transactions,* **46**(1), pp. 31–36.

[61] Cann, P. M., 1996. "Starvation and reflow in a grease-lubricated elastohydrodynamic contact". *Tribology Transactions,* **39**(3), pp. 698–704.

[62] Cann, P. M., Chevalier, F., and Lubrecht, A. A., 1997. "Track depletion and replenishment in a grease lubricated point contact: a quantitative analysis". In *Tribology Series*, Vol. 32. Elsevier, pp. 405–413.

[63] Mérieux, J. S., Hurley, S., Lubrecht, A. A., and Cann, P. M., 2000. "Shear-degradation of grease and base oil availability in starved EHL lubrication". In *Tribology Series*, Vol. 38. Elsevier, pp. 581–588.

[64] Miettinen, J., Andersson, P., and Wikström, V., 2001. "Analysis of grease lubrication of a ball bearing using acoustic emission measurement". *Proceedings of the Institution of Mechanical Engineers, Part J: Journal of Engineering Tribology,* **215**(6), pp. 535–544.

[65] Scarlett, N. A., 1967. "Paper 21: use of grease in rolling bearings". In Proceedings of the Institution of Mechanical Engineers, Conference Proceedings, Vol. 182, SAGE Publications Sage UK: London, England, pp. 585–624.

[66] Wilson, A. R., 1979. "The relative thickness of grease and oil films in rolling bearings". *Proceedings of the Institution of Mechanical Engineers,* **193**(1), pp. 185–192.

[67] Lewicki, W., 1955. "Some physical aspects of lubrication in rolling bearings and gears". PhD thesis, University of London (Birkbeck College).

[68] Crook, A. W., 1961. "The lubrication of rollers II. Film thickness with relation to viscosity and speed". *Philosophical Transactions of the Royal Society of London. Series A, Mathematical and Physical Sciences,* **254**(1040), pp. 223–236.

[69] Dyson, A., and Wilson, A. R., 1969. "Film thicknesses in elastohydrodynamic lubrication of rollers by greases". In Proceedings of the Institution of Mechanical Engineers, Conference Proceedings, Vol. 184, SAGE Publications Sage UK: London, England, pp. 1–11.

[70] Barz, M., 1996. "Die Schmierfilmbildung in fettgeschmierten schnellaufenden Spindellagern". PhD thesis, Verlag nicht ermittelbar.

[71] Baly, H., Poll, G., Cann, P. M., and Lubrecht, A. A., 2006. "Correlation between model test devices and full bearing tests under grease lubricated conditions". In IUTAM Symposium on Elastohydrodynamics and Micro-elastohydrodynamics: Proceedings of the IUTAM Symposium held in Cardiff, UK, 1–3 September 2004, Springer, pp. 229–240.

[72] Jablonka, K., Glovnea, R., and Bongaerts, J., 2012. "Evaluation of EHD films by electrical capacitance". *Journal of Physics D: Applied Physics,* **45**(38), p. 385301.

[73] Jablonka, K., Glovnea, R., and Bongaerts, J., 2018. "Quantitative measurements of film thickness in a radially loaded deep-groove ball bearing". *Tribology International,* **119**, pp. 239–249.

[74] Jablonka, K., Glovnea, R., Bongaerts, J., and Morales-Espejel, G., 2013. "The effect of the polarity of the lubricant upon capacitance measurements of EHD contacts". *Tribology International,* **61**, pp. 95–101.

[75] Jablonka, K., Glovnea, R., Bongaerts, J., and Morales-Espejel, G., 2012. "Comparative measurements of EHD film thickness in ball-on-flat rig and rolling element bearing". In STLE 67th Annual Meeting, pp. 6–10.

[76] Dyson, A., and Wilson, A. R., 1965-66. "Film thicknesses in elastohydrodynamic lubrication by silicone fluids". *Proceedings of the Institution of Mechanical Engineers,* **180**, pp. 97–112.

[77] Zhang, X., and Glovnea, R., 2021. "Grease film thickness measurement in rolling bearing contacts". *Proceedings of the Institution of Mechanical Engineers, Part J: Journal of Engineering Tribology,* **235**(7), pp. 1430–1439.

[78] Pelofsky, A. H., 1966. "Surface tension-viscosity relation for liquids.". *Journal of Chemical and Engineering Data,* **11**(3), pp. 394–397.

[79] Shetty, P., Meijer, R. J., Osara, J. A., and Lugt, P. M., 2022. "Measuring film thickness in starved grease-lubricated ball bearings: An improved electrical capacitance method". *Tribology Transactions,* **65**(5), pp. 869–879.

[80] Lugt, P. M., Holgerson, M., and Reinholdsson, F., 2023. "Impact of oxidation on grease life in rolling bearings". *Tribology International,* **188**, p. 108785.

[81] Lugt, P. M., and Berens, F., 2022. "The grease life factor concept for ball bearings". *Tribology International,* **169**, p. 107460.

[82] Gafitanu, M., Silicon, D., Ianus, G., and Olaru, D., 1993. "A general model for grease deterioration in ball bearings". In Proceedings of the 6th international congress on tribology. Budapest: EUROTRIB, Vol. 2, pp. 355–9.

[83] Cann, P. M., and Lubrecht, A. A., 1999. "An analysis of the mechanisms of grease lubrication in rolling element bearings". *Lubrication Science,* **11**(3), pp. 227–245.

[84] Nagata, Y., Kalogiannis, K., and Glovnea, R., 2012. "Track replenishment by lateral vibrations in grease-lubricated EHD contacts". *Tribology Transactions,* **55**(1), pp. 91–98.

[85] Mais, J., 2002. "Spectrum analysis: The key features of analyzing spectra". *SKF USA, Inc.*

[86] Kalogiannis, K., 2013. "Behaviour of elastohydrodynamic films subjected to oscillatory motion". PhD thesis, University of Sussex United Kingdom.

[87] Glovnea, R., and Zhang, X., 2018. "Elastohydrodynamic films under periodic load variation: an experimental and theoretical approach". *Tribology Letters,* **66**(3), p. 116.

[88] Zhang, X., Glovnea, R., Morales-Espejel, G. E., and Félix-Quiñonez, A., 2020. "The effect of working parameters upon elastohydrodynamic film thickness under periodic load variation". *Tribology Letters,* **68**, pp. 1–10.

[89] Harris, T. A., and Kotzalas, M. N., 2006. *Advanced concepts of bearing technology.* CRC press.

[90] Harris, T. A., and Kotzalas, M., 2006. "Rolling bearing analysis, 5^{th} edition". *A Wiley-Interscience Publication. USA.*

[91] Gupta, P. K., Cheng, H. S., Zhu, D., Forster, N. H., and Schrand, J. B., 1992. "Viscoelastic effects in mil-l-7808-type lubricant, Part I: analytical formulation". *Tribology Transactions,* **35**(2), pp. 269–274.

[92] Jang, J. Y., Khonsari, M. M., and Bair, S., 2007. "On the elastohydrodynamic analysis of shear-thinning fluids". *Proceedings of the Royal Society A: Mathematical, Physical and Engineering Sciences,* **463**(2088), pp. 3271–3290.

[93] Kumar, P., and Khonsari, M. M., 2008. "EHL circular contact film thickness correction factor for shear-thinning fluids". *Journal of Tribology,* **130**(4).

[94] Cen, H., Lugt, P. M., and Morales-Espejel, G., 2014. "On the film thickness of grease-lubricated contacts at low speeds". *Tribology Transactions,* **57**(4), pp. 668–678.

[95] Kochi, T., Sakai, M., Nogi, T., Dong, D., and Kimura, Y., 2019. "Experimental study on the physics of thick EHL film formation with grease at low speeds". *Tribology Letters,* **67**(2), p. 55.

[96] Okal, M., Kostal, D., Sperka, P., Krupka, I., and Hartl, M., 2022. "Effect of contact conformity on grease lubrication". *Lubricants,* **10**(11), p. 289.

[97] Lucas, R., 1918. "Über das Zeitgesetz des kapillaren Aufstiegs von Flüssigkeiten". *Kolloid-Zeitschrift,* **23**(1), pp. 15–22.

[98] Chakraborty, S., 2005. "Dynamics of capillary flow of blood into a microfluidic channel". *Lab on a Chip,* **5**(4), pp. 421–430.

APPENDIX A

TRIBOLOGY TRANSACTIONS
2022, VOL. 65, NO. 5, 869–879
https://doi.org/10.1080/10402004.2022.2091067

Measuring Film Thickness in Starved Grease-Lubricated Ball Bearings: An Improved Electrical Capacitance Method

Pramod Shetty[a], Robert Jan Meijer[a], Jude A. Osara[a], and Piet M. Lugt[a,b]

[a]Engineering Technology, University of Twente; [b]SKF Research and Technology Development

ABSTRACT

Presented in this article is a new method to measure the film thickness in a rolling bearing running under starved conditions, such as in grease-lubricated bearings, using the electrical capacitance method. The method was used to study the impact of speed on film thickness. Results show that fully flooded conditions prevail at lower speeds where the film thickness increases with increasing speed. At higher speeds, where grease-lubricated bearings run under starved lubrication conditions, this increase is less pronounced. At even higher speeds, the film thickness becomes almost independent of the speed.

ARTICLE HISTORY
Received 23 February 2022
Accepted 14 June 2022

KEYWORDS
Rolling bearings; grease; film thickness; elastohydrodynamic lubrication; capacitance method

Introduction

There are more than 18 billion rolling element bearings currently in use. By far, most of them are grease lubricated *(1)*. Bearing life is determined by fatigue life and is reduced when lubrication is ineffective *(2, 3)*. This reduction does not takes place when the contacting surfaces are fully separated, preventing metal-to-metal contact. For fully flooded conditions the (elastohydrodynamic, EHL) film thickness can be predicted using Hamrock and Dowson's equations *(4, 5)* or Nijenbanning's equation *(6)*. These fully flooded conditions typically occur in oil-lubricated bearings. In the case of grease lubrication, at medium and higher speeds, starvation occurs and the films can no longer be predicted using these equations. The existing models for starved lubrication, such as those from Wedeven et al. *(7)*, Damiens et al. *(8)*, Hamrock and Dowson *(9)*, and Van Zoelen et al. *(10)*, all require some measure of the volume of oil in the inlet as input, an unknown for grease-lubricated bearings. The full problem is very complex and the development of models can be greatly supported by having accurate film thickness measurements.

Early studies on grease film thickness by Poon *(11)*, Wilson *(12)*, and Dyson and Wilson *(13)* using twin-disc machines showed that grease forms a thicker film than its base oil at the beginning of operation but the film thickness decreases quickly over a period of time before stabilizing. Point contact measurements and model calculations by Jonkisz and Krzeminski-Freda showed that the pressure distribution and the shape of a grease film can be predicted using the base oil properties *(14)*. Åstrom et al. *(15)* showed that the film thickness inside the Hertzian contact is not uniform and were the first to show that thickener fibers pass through the EHL contact under fully flooded conditions. This was confirmed by Cann and Spikes *(16)*.

The studies by Booser and Wilcock *(17)*, Baker *(18)*, and Wikström and Jacobson *(19)* showed that the film thickness in a grease-lubricated bearing is determined by the lubricant feed and loss mechanism. They listed various replenishment mechanisms such as grease bleed, centrifugal force–induced flow, and capillary forces. The loss mechanisms identified are pressure-induced side flow, centrifugal force–induced side flow, evaporation, cage scraping, oxidation, drop loss, and polymerization *(1)*. These replenishment mechanisms were studied for single point contacts and for full bearings *(20–24)*. Today these replenishment mechanisms are yet to be fully understood.

In 1974, Chiu postulated that replenishment mainly occurs in between the balls in a bearing, denoted by "out of contact replenishment". He developed a model based on surface tension, which he used to predict the onset of starvation *(25)*. In Chiu's model, it is assumed that there is sufficient oil available from the ridges along the track. Guangteng and Spikes *(26)* studied film thickness under extremely starved conditions, denoted by "parched lubrication," and showed that, at high speeds, the film thickness levels off. They built a model in which the film thickness is a function of the disjoining pressure. They concluded that replenishment in the thick-film regime is dominated by surface tension and that the disjoining pressure inhibits the complete collapse of the film.

CONTACT Pramod Shetty p.shetty@utwente.nl
Review led by D. Nelias.

Nomenclature

n	Number of balls	ϵ_{air}	Dielectric constant of air
C	Capacitance F	$C_{outside}$	Outside capacitance of a single contact [F]
ϵ_0	Permittivity constant $[Fm^{-1}]$	A_{Hertz}	Hertzian contact area $[m^2]$
ϵ_{oil}	Dielectric constant of oil	R_x	Reduced radius in the direction of motion [m]
A	Area of the plate $[m^2]$	U	Dimensionless speed parameter
h	Distance between the parallel plate $[m]$	G	Dimensionless material parameter
C_i	Ball–inner ring capacitance $[F]$	W	Dimensionless load parameter
$C_{i,outside}$	Inner ring outside capacitance for single contact $[F]$	ν_{cSt}	Kinematic viscosity [cSt]
$C_{i,Hertz}$	Inner ring Hertz capacitance for single contact [F]	c	Constant in Walther equation [loglogcSt/logK]
C_o	Ball-outer ring capacitance $[F]$	K	Constant in Walther equation [loglogcSt]
$C_{o,outside}$	Inner ring outside capacitance for single contact $[F]$	T	temperature [K]
$C_{o,Hertz}$	Outer ring Hertz capacitance for single contact [F]	η_0	Base oil viscosity [Pa.s]
C_{inner}	Total inner ring capacitance [F]	u_s	Entrainment velocity $[ms^{-1}]$
C_{outer}	Total outer ring capacitance [F]	E'	Reduced elastic modulus [Pa]
C_{total}	Total calculated bearing capacitance [F]	F	Force [N]
$C_{total,meas}$	Total measured bearing capacitance [F]	R_y	Reduced radius in y direction [m]
$C_{background}$	Background capacitance [F]	R_x	Reduced radius in x direction [m]
$C_{flooded}$	Flooded area capacitance [F]	m^*	Dimensionless inlet distance at the boundary between fully flooded and starved condition
h_c	Central film thickness [m]		
h'	Ratio of outer ring to inner ring film thickness	m	Dimensionless meniscus length from the centre of the contact
h_{gap}	Distance between the ball and the surface [m]		
$h_{ff,i}$	Fully flooded inner ring central film thickness [m]	b	Half contact width in x direction [m]
$h_{ff,o}$	Fully flooded outer ring central film thickness [m]	a	Half contact width in y direction [m]
$h_{g,i}$	Inner ring grease film thickness [m]	$H_{i,ff}$	Dimensionless inner ring fully flooded film thickness
$h_{g,o}$	Outer ring grease film thickness [m]	R_o	Outer ring radius in the rolling direction [m]
h_{st}	Starved film thickness [m]	R_i	Inner ring radius in the rolling direction [m]
A_i	Inner ring Hertzian contact area $[m^2]$	R_b	Ball radius [m]
A_o	Outer ring Hertzian contact area $[m^2]$	η_{T_o}	Outer ring dynamic viscosity [Pa.s]
C_{cav}	Capacitance at the outlet [F]	η_{T_i}	Inner ring dynamic viscosity [Pa.s]

Recently, Nogi *(27, 28)* simulated the starved EHL point contact to study the effect of capillary number on starved film thickness, considering the unevenly distributed oil film in the inlet of the contact. In their simulations, instead of assuming the inlet meniscus as a straight line as done by Hamrock and Downson, they used a Coyne-Elrod theory to obtain the inlet film thickness. The inlet meniscus position was evaluated based on the inlet oil film thickness using the Elrod algorithm. Fischer et al. *(29)* derived a parameter to determine the transition to starved lubrication from fully flooded condition based on the capillary number and therefore the contact angle of the base oil. The authors found that starvation was controlled by the capillary number, a function of the base oil surface tension.

Single contact measurements may not properly include possible replenishment effects caused by preceding contacts or, in general, by the thin-film flow on all surfaces in a bearing such as described by Van Zoelen et al. *(30)*. These single contact measurements are very useful to understand some of the basics in grease-lubricated bearings. However, we have now reached a point where we can only achieve further understanding by studying the film thickness in the grease-lubricated bearing itself. The film thickness in a full bearing at ultra-low speeds was measured by Morales-Espejel et al. *(31)*. They found that the film thickness is significantly larger than that for base oil lubrication. For moderate speed conditions, Cen and Lugt *(32)* reported that the relative film thickness follows a power law relation with the product of viscosity, speed, and half contact width.

To measure the film thickness in rolling bearings, the most suitable method currently available is the electrical capacitance method. The ball–ring interface resembles a parallel-plate capacitor where the capacitance is determined by the lubricant film thickness that separates the ball and the ring. The capacitance method was first used by Lewicki *(33)* and then by Crook *(34)*, Dyson and Wilson *(13)*, and Wilson *(12)*. Later, the method was refined by including the capacitance formed outside the Hertzian zone. In this article, we call this the "outside capacitance." Barz *(35)* used a correction factor to compensate for this outside capacitance. Cen and Lugt *(36)* used the calibration method developed by Wilson *(12)*, who neglected this effect. Jabloka et al. *(37–39)* calculated the outside capacitance for fully flooded conditions for a single point contact as well as for the full bearing. In our work, we further developed their approach for starved contacts; that is where the contact is not fully flooded with lubricant. In addition, in our new method we do not need to know the dielectric constant of the lubricant. Finally, we do not need to make use of a density–pressure relationship.

We will first describe the new method and later employ it to study the film thickness in a grease-lubricated deep-groove ball bearing as a function of speed for three different temperatures. It was found that the film thickness at low speeds is similar to or higher than the film thickness from using just the base oil. Beyond a certain transitional speed, we will show that the film thickness is almost independent of speed.

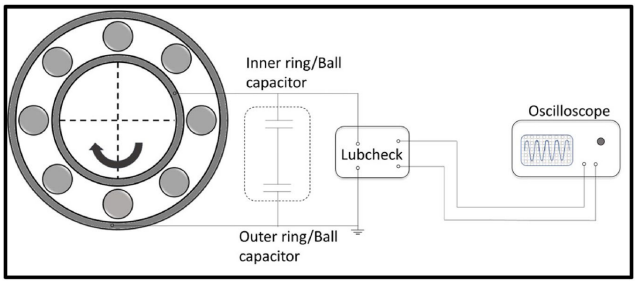

Figure 1. Schematic representation of the bearing with Lubcheck *(46)*.

Film thickness measurement using electrical capacitance

An in-house-made bearing test rig was used for measuring the film thickness. The electrical capacitance was measured using Lubcheck Mk3, a device developed by Heemskerk et al. *(40)*; see Fig. 1. Here, the test bearing is electrically isolated, the stationary outer ring is directly connected to the Lubcheck Mk3, and the rotating inner ring is connected through a mercury contact. The detailed description of the test rig is given by Cen and Lugt *(36)*. The relation between the Lubcheck output voltage V_{cap} and the electrical capacitance of the bearing reads

$$C_{total,\,meas} = (10 - V_{cap})C_{ref}/V_{cap}, \qquad [1]$$

where C_{ref} is a Lubcheck reference capacitance.

In this article, all measurements were performed with a standard lithium hydroxystearate–thickened grease with a mineral oil with a viscosity of 100 and 10 cSt at 40 and 100°C, respectively.

There are two commonly used methods to evaluate the film thickness in a bearing using the electrical capacitance method: *(1)* the calibration curve, method developed by Dyson and Wilson *(13)* (which was also used by Cen and Lugt *(36)*) and *(2)* a capacitance model method developed by Jablonka et al. *(37)*. Here, we review both because we will use components of each in our new method.

Method 1 by Wilson

Because the measured bearing capacitance is influenced by the outside capacitance, as discussed previously, and the dielectric constant of the oil is pressure dependent, obtaining the central film thickness from measurements is not straightforward. Wilson *(12)* and, subsequently, Cen and Lugt *(36)* made a calibration curve for a certain load by performing a speed sweep with base oil, during which they measured both the capacitance and the bearing temperature and then calculated the film thickness for each speed using Hamrock and Dowson's fully flooded film thickness equation. This then gives a relation between film thickness and capacitance for a specific bearing load and speed. The Hamrock and Dowson film thickness equation is

$$\frac{h_c}{R_x} = 2.69U^{0.67}G^{0.53}W^{-0.067}(1 - e^{-0.73k_d}), \qquad [2]$$

where h_c is the central film thickness (also subsequently rewritten as h_{ff}, where *ff* stands for fully flooded); R_x is the reduced radius in the x direction; U, G, and W are the dimensionless speed, material, and load parameters; and k_d is the ellipticity parameter. The temperature was measured on the outer ring of the bearing, and for each speed the kinematic viscosity of the oil was calculated using Walther's equation:

$$\log_{10}\log_{10}(\nu_{cSt} + B) = K - c\log T, \qquad [3]$$

where B is a fluid-specific constant. For oil, $B = 0.7$. The constants c and K can be calculated from the known viscosities of the oil at two different temperatures via

$$c = \frac{\log_{10}\log_{10}(\nu_{cSt1} + B) - \log_{10}\log_{10}(\nu_{cSt2} + B)}{\log_{10}T_2 - \log_{10}T_1} \qquad [4]$$

$$K = \log_{10}\log_{10}(\nu_{cSt1} + B) + c\log_{10}T_1. \qquad [5]$$

The calibration for measuring the grease film thickness is done with oil. It is uncertain to what extent thickener will enter the contact and influence the dielectric constant. To compensate for this, Wilson *(12)* added a small quantity of di-(2-ethylhexyl) sebacate to the mineral oil.

However, we have not used any additives to compensate for the dielectric constant because this difference was very low (about 10%), as well as to avoid any changes in the original grease properties.

The approach is simple and easy to use. However, one cannot distinguish between the film thickness on the outer-ring and inner ring with this method. In addition, there is no compensation in the calibration curve for the effect of starvation.

Method 2 by Jablonka et al.

In the above method from Wilson *(12)*, the test rig, including the bearing, was modeled as a single capacitor. Jablonka et al. *(37, 38)* developed a more advanced electrical model of the bearing, with the work of Barz *(35)* as a starting point, including the Hertzian contact capacitance, outside capacitance, and background capacitance. The outside capacitance

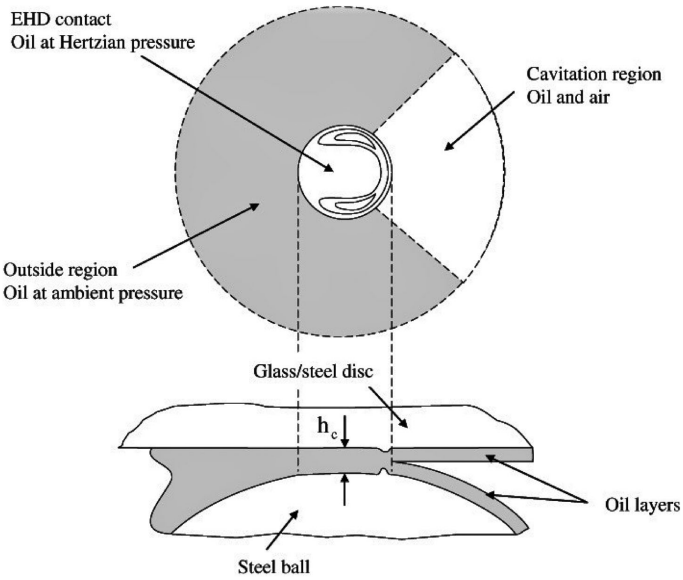

Figure 2. Pictorial representation of a single point contact showing the flooded and cavitated regions around the Hertzian contact. Reproduced from Jablonka et al. *(37)* with permission.

is the contribution to the total capacitance of the gap between the ball and ring outside the Hertzian contact, denoted here by h_{gap}. The background capacitance is the capacitance of the rig except for the contribution of the EHL contacts. This background capacitance is independent of the operating conditions of the bearing and can be regarded as constant.

For a purely axially loaded ball bearing with n balls, all balls are equally loaded and the film thickness between the balls and rings can be considered equal for all balls. The electrical circuit between the inner and outer rings therefore consists of n capacitors in parallel where each of these again consists of two capacitors in series, formed by the ball–inner ring contact and the ball–outer ring contact. The film thickness in the Hertzian contact is assumed to be uniform and each contact can therefore be simulated by a parallel-plate capacitor.

For a parallel-plate capacitor, the capacitance is given by

$$C = \frac{\epsilon_0 \epsilon_{oil} A}{h}, \quad [6]$$

where ϵ_0 is the permittivity constant $(8.85 \times 10^{-12} F/m)$, ϵ_{oil} is the dielectric constant of the dielectric material (for example, lubricating oil), A is the area of the capacitor plate, and h is the distance between the parallel plates.

Figure 2 shows a single contact. It is evident that the total capacitance is not only due to the Hertzian contact region, but also includes the capacitance due to the outside regions.

The equivalent electrical circuit for a ball bearing with a metal cage is shown in Fig. 3. For each ball, the ball–inner ring capacity is

$$C_i = C_{i,Hertz} + C_{i,outside} \quad [7]$$

and the ball–outer ring capacity is

$$C_o = C_{o,Hertz} + C_{o,outside}, \quad [8]$$

where the subscripts *Hertz* and *outside* indicate the Hertzian and outside capacitances, respectively. For n number of balls, the inner ring capacity reads

$$C_{inner} = nC_i \quad [9]$$

and the outer ring capacity is

$$C_{outer} = nC_o. \quad [10]$$

Because the inner and outer ring capacitances are in series, the equivalent/total capacitance of the bearing is given by

$$C_{total} = \frac{1}{\frac{1}{C_{inner}} + \frac{1}{C_{outer}}} + C_{background}, \quad [11]$$

where $C_{background}$ is the capacitance of the test rig itself, which can be assumed constant.

For a single contact they calculated the outside capacitance as

$$C_{outside} = C_{flooded} + C_{cav}, \quad [12]$$

where, as illustrated in Fig. 6, $C_{flooded}$ and C_{cav} are the flooded region capacitance and the cavitated region capacitance, respectively, given by

$$C_{flooded} = \iint_{A_{flooded}} \frac{\epsilon_0 \epsilon_{oil} dxdy}{h_c + h_{gap}(x,y)} \quad [13]$$

and

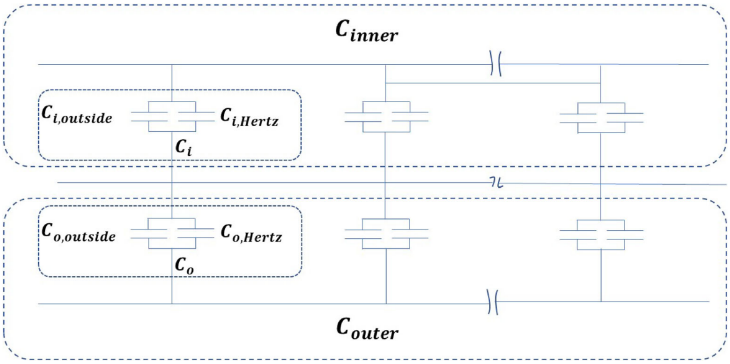

Figure 3. Equivalent electrical circuit showing capacitances at the ball–ring interfaces.

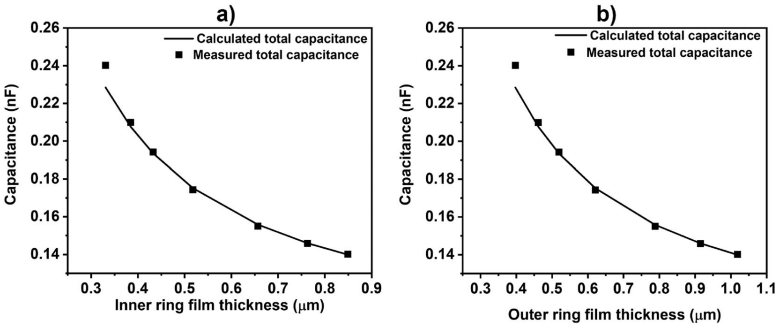

Figure 4. Calculated and measured total capacitance versus film thickness for (a) inner ring and (b) outer ring film thickness. F_a =513 N; Li/M bled oil. Here the dielectric constant was determined using a single speed.

$$C_{cav} = \int\int_{A_{cav}} \frac{\epsilon_0 dxdy}{\frac{h_c}{\epsilon_{oil}} + h_{gap}(x,y)\frac{1}{\epsilon_{air}}}. \quad [14]$$

The integration limits $A_{flooded}$ and A_{cav} are calculated based on the following assumptions:

(1) On the inlet side of the contact, capacitance was calculated up to the point where the separation of the surface is nine times the central film thickness assuming the fully flooded condition.
(2) To calculate the capacitance on the side of the contacts, it was assumed that oil fills the gap between the ball and the bearing ring up to the shoulder.
(3) In the cavitation region, the capacitance was calculated up to the distance where surface separation reaches nine times the central film thickness.

It is assumed that the central film splits into two equal halves, neglecting the effect of decompression at the outlet (see Fig. 2). The Hertzian capacitance–film thickness relationship, from Eq. [6], reads

$$C_{Hertz} = \frac{\epsilon_0 \epsilon_{oil} A_{Hertz}}{h_c}, \quad [15]$$

where h_c is the central film thickness and A_{Hertz} is the Hertzian contact area. The dielectric constant ϵ_{oil} at normal pressure and temperature was obtained from published values in the literature. Jablonka et al. *(37)* used pressure– and temperature–-dielectric constant relationships to obtain the dielectric constant of the oil at higher pressure and temperature. The background capacity $C_{background}$, in Eq. [11], was measured with a hybrid bearing (i.e., with ceramic balls). In their experiments, they used a single steel ball and the other balls were ceramic. They roughly estimated the film thickness using Hamrock and Dowson's film thickness equation to calculate the outside capacitance and measured the background capacitance. The final film thickness was then obtained by considering the inner and outer ring capacitances in series, as done in Eq. [11]; thus,

$$C_{total} = \frac{1}{\frac{1}{n\left(\epsilon_0\epsilon_{oil}\frac{A_{i,Hertz}}{h_{c,i}} + C_{i,outside}\right)} + \frac{1}{n\left(\epsilon_0\epsilon_{oil}\frac{A_{o,Hertz}}{h_{c,i}h'} + C_{o,outside}\right)}} + C_{background}, \quad [16]$$

where $h' = \frac{h_{c,o}}{h_{c,i}}$, $A_{i,Hertz}$ and $A_{o,Hertz}$ are the Hertzian contact area on the inner ring and outer ring, and $C_{i,outside}$ and

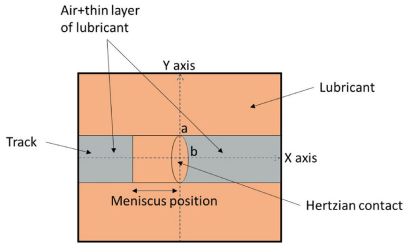

Figure 5. A simplified starved contact condition showing meniscus position on the track.

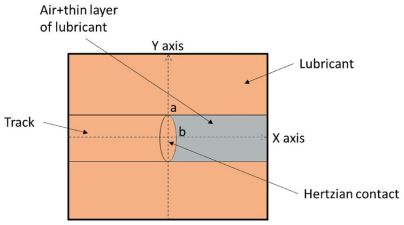

Figure 6. A simplified fully flooded contact condition showing oil around the contact.

$C_{o,outside}$ are outside capacitances of the ball–innerring and ball–outer ring contacts.

So far, all methods are calibrated by assuming fully flooded conditions. However, grease-lubricated bearings usually run under starved lubrication conditions, leading to a somewhat lower capacitance for the same film thickness. In the method by Jablonka et al. *(37, 38)*, the outside capacitance is overestimated if the bearings are running under starved lubrication.

The new method

The starting point of our new method is Jablonka et al.'s *(37, 38)* capacitance model. However, we will determine the dielectric constant of the oil within the set of experiments without using any pressure– and temperature– dielectric constant relationships. We also do not require a rough estimate of film thickness otherwise required to calculate the outside capacitance. In this study, we include the effect of starvation, which is a very significant consideration in grease lubrication.

Determination of the dielectric constant

Similar to Jablonka et al. *(38)*, we will use an electrical model in combination with a capacitance measurement for a fully flooded bearing lubricated with base oil. This is done via the following procedure:

(a) Measure the background capacitance using a ceramic bearing.
(b) Measure the capacitance and temperature in the test bearing using the base oil at a particular load and speed (for example, 513 N and 400 rpm).
(c) Calculate the fully flooded inner ring film thickness ($h_{ff,i}$) and outer ring film thickness ($h_{ff,o}$) using the Hamrock and Dowson film thickness equation (Eq. [2], with viscosity estimated from the measured outer ring temperature). Then substitute these into the capacity–film thickness equations for the outside and the Hertzian regions (Eqs. [12]–[14]).
(d) Substitute the measured total capacitance (C_{total}) from step (2) into Eq. [16] and rearrange to solve for the dielectric constant ϵ_{oil}.

We can now verify whether the obtained dielectric constant is valid for any film thickness measurement under this specific load by making a constant load speed sweep, while measuring the capacitance and temperature at each speed. Figure 4 shows that there is indeed a good correlation between measured and calculated total capacitances for both inner and outer film thicknesses, indicating that the same grease–oil dielectric constant can be used to obtain film thickness (or speed) for a particular load.

The measured dielectric constant via this method was $\epsilon_{oil} = 4.06$. The literature gives values for various greases varying between 2.88 to 4.76 at atmospheric pressure *(41)*. Pressure increases the dielectric constant *(42)*, so finding a somewhat higher value is plausible.

Determination of the film thickness

Obtaining grease film thickness during starvation

Under starved lubrication conditions, the inlet of the contact will be partially filled up to an inlet meniscus. This is illustrated in Fig. 5. The contribution to the capacitance in the inlet of the contacts will therefore be given by part of the gap filled with oil and part of the gap filled with air and oil layer. The outside capacitance is therefore now a function of the severity of starvation and can only be calculated if the inlet meniscus position is known.

The equation used to calculate the film thickness h_{st} as a function of the meniscus position, also called 'inlet distance', is from Dowson and Hamrock *(9)* and reads

$$h_{st} = H_{ff} R_x \left(\frac{m-1}{m^*-1} \right)^{0.29}, \qquad [17]$$

where $m = x/b$ is the dimensionless inlet meniscus position (x is the meniscus position and b is the half contact width in the x direction); m^* is the limit of the dimensionless meniscus distance beyond which fully flooded film thickness occurs, obtained from

$$m^* = 1 + 3.06 \left[\left(\frac{R_x}{b} \right)^2 H_{ff} \right]^{0.58}, \qquad [18]$$

and $H_{ff} = h_{ff}/R_x$ is the dimensionless fully flooded film thickness, calculated using Eq. [2]. The dimensionless meniscus position m will be calculated using an iterative approach. The central film thicknesses for the inner ring is then obtained from Eq. [17]. The outer ring film thickness

is calculated assuming the film thickness ratio for starved and fully flooded conditions are equal. Using this film thickness and meniscus position, C_{total} is calculated. When the contact runs starved, it is assumed that the region outside the running track is still completely filled with oil. The inlet side of the track behind the meniscus is also assumed to be completely filled with oil. The gap between the ball and ring up to the meniscus is filled with air and a layer of oil. The gap between the ball and ring at the outlet across the track is also filled with air and a layer of oil. As mentioned previously, it is assumed that the central lubricant film splits into two equal halves, neglecting the effect of decompression at the outlet. The same dielectric constant of the oil is used for the Hertzian region (pressurized region) and the outside region (depressurized region). The iterative process to find the inlet meniscus position for calculating the starved central film thickness is

(1) Assume $m = 1$.
(2) Calculate the inner ring starved film thickness $h_{st,i}$ using Eq. [17].
(3) Assume that the ratio of outer and inner ring film thicknesses during starvation is equal to that under fully flooded conditions

$$h\prime = \frac{h_{c,o}}{h_{c,i}} = \left[\frac{R_o(R_i + R_b)}{R_i(R_o - R_b)}\right]^{0.476} \left(\frac{\eta_{T_o}}{\eta_{T_i}}\right)^{0.67} \quad [19]$$

and calculate the outer ring film thickness $h_{st,o}$.
(4) Using the dimensionless meniscus position and the film thicknesses, calculate the C_{total}.
(5) Compare the measured and calculated C_{total}.

If the difference is not sufficiently small (e.g., less than 1% difference), check whether the contact is starved or fully flooded by comparing m and m^*. When $m \geq m^*$ the contact is fully flooded; otherwise, it is starved. For starved conditions, repeat the process by slightly increasing the meniscus position. For fully flooded conditions, follow the steps described in the next section.

Stop the iteration when the difference is sufficiently small.

Measuring fully flooded grease film thickness

In grease lubrication, the film thickness could be greater than the fully flooded base oil film thickness. This is caused by a higher viscosity of the grease than its base oil, generally observed at low shear rates, hence at very low bearing speeds. In this case, the area around the contact excluding the outlet region is considered to be filled with oil. At the outlet region the space between the ball and ring across the track is considered entirely filled with a layer of oil and air. This is depicted in Fig. 6. Now, the total capacitance is only a function of central film thickness. Here, we vary H_{ff} in Eq. [17] until the calculated total capacitance (C_{total}) matches the measured capacitance. The iterative process to find the fully flooded film thickness is

(1) Increase the $H_{ff,i}$ in Eq. [17].
(2) Use Eq. [19] to calculate the outer ring film thickness $h_{ff,o}$.

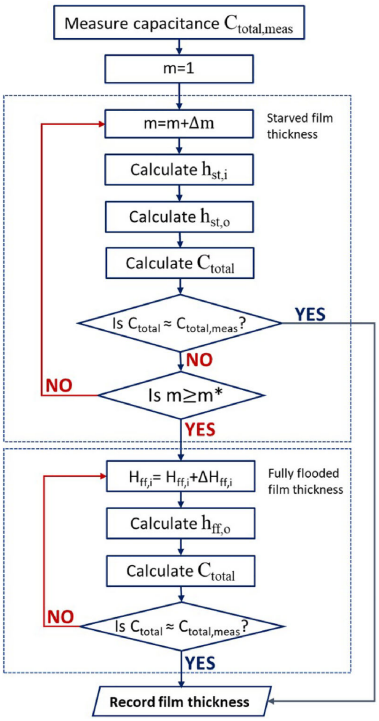

Figure 7. Flowchart of the newly proposed procedure for determining film thickness in grease lubricated roller bearings.

(3) Use these film thicknesses to calculate the total capacitance C_{total}.
(4) Compare the measured and calculated C_{total}. If the difference is sufficiently small (less than 1% difference), the film thickness is correct. If not, slightly increase $H_{ff,i}$ and repeat the process.

The flow chart of the newly proposed film thickness measurement procedure is shown in Fig. 7.

To demonstrate the effect of starvation on the film thickness estimation, a worst case (severe starvation) example calculation is performed. For this, a 6209 deep-groove ball bearing with 513 N axial load and Li/M bled oil was selected. For a set of assumed capacitances, the film thicknesses were calculated using Wilson's method. Next, using the new method, the film thicknesses were calculated for the same assumed capacitances considering inlet of the contact as severely starved. Here, we considered that the gap between the ball and track in the inlet side is filled with air and a layer of oil while calculating the total capacitance C_{total}. Figure 8 shows a significant increase in the predicted/estimated film thicknesses if the starvation effect is excluded. The percentage deviation of the calculated film thicknesses without considering starvation was up to 20% in this particular case.

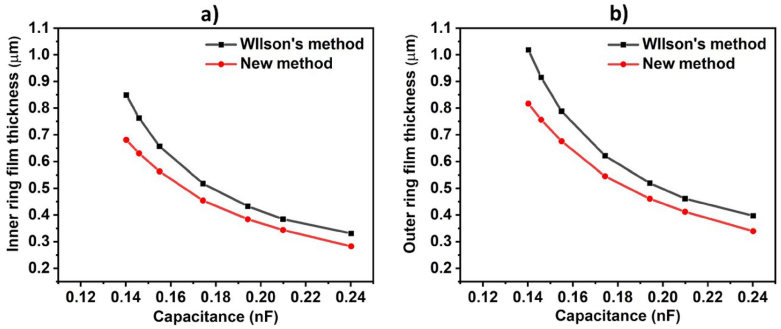

Figure 8. Difference in calculated film thickness from Wilson's method and the new method. Note that this is for an extremely starved condition. (a) Inner ring and (b) outer ring.

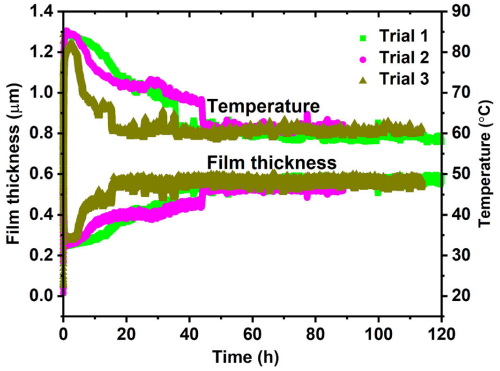

Figure 9. Example of three film thickness and temperature measurements showing that the film thickness is stable after about 60 h. After each measurement the grease was replaced with fresh grease. 6209-2RZ bearing running under self-induced temperature conditions with Li/M grease; load = 513 N, speed = 4,000 rpm.

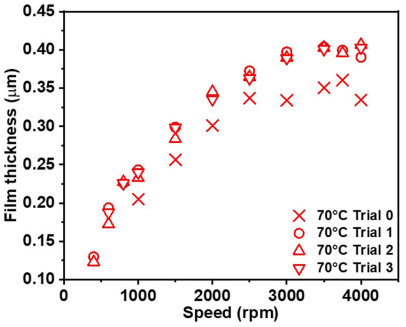

Figure 10. Comparison of film thickness between fresh grease (Trial 0)—in which each measurement uses fresh grease—to without fresh grease (Trials 1, 2, and3)—in which the same grease is re-used throughout. 6209-2RZ bearing with Li/M grease; load = 513 N.

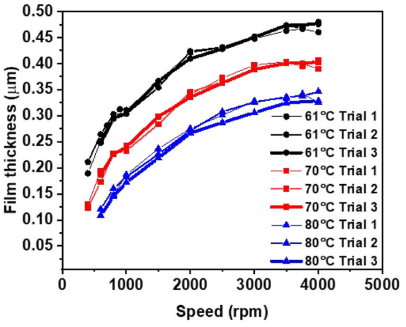

Figure 11. Film thickness versus speed for three different temperatures. 6209-2RZ bearing with Li/M grease; load = 513 N.

Measurement results

Grease film thickness was measured on 6209-2RZ bearing using Li/M grease with 30% of the free volume filling. The bearing was run for 100h to allow completion of the churning phase. Without replacing the grease, all of the following film thickness measurements were made. The speed was varied from 600 to 4,000 rpm. At every speed, film thickness was measured at three different temperatures. A heat gun and a fan were used to control the temperature. At every speed, the temperature and film thickness were allowed to reach a stable value, and average temperature and film thickness were considered for analysis. The measurements were repeated three times to ensure repeatability.

Figure 9 shows that the film thickness is low during the churning phase due to the high temperatures caused by drag and viscous forces leading to high friction and therefore heat generation. After the churning phase, the film thickness becomes steady. This steady phase is the region of interest. The operating conditions are very mild where no significant grease degradation will take place. Moreover, the films are much larger than the surface roughness and the loads are low, causing no bearing damage. Hence, we can use the same bearing for all of our measurements without re-filling the bearing with fresh grease for every measurement.

To check whether using the same bearing that has completed the churning phase without freshly re-filling for each subsequent measurement influences the results, a series of measurements was made with freshly filled grease at each speed. After each fresh filling, the bearing ran for 20h, and film thickness was averaged over the last hour. The temperature was maintained at 70°C for every measurement. It can be seen from Fig. 10 that the film thicknesses of the freshly filled grease (Trial 0) and those without fresh grease (Trials 1, 2, and 3) are very similar, with the freshly filled grease having slightly lower film thickness than those without freshly filled grease. This is because each fresh grease measurement was taken after only 20h of running; it is evident from Fig. 9 that at 20h duration, film building may be incomplete.

Figure 11 plots the film thickness versus speed for three temperatures. For each temperature, the film thickness increases up to a certain speed, after which it becomes almost constant. At low speeds, the curves typically follow fully flooded behavior: they increase linearly with the speed on a log-log scale (refer to Fig. 12). At higher speeds, when the oil supply and/or replenishment is limited to the contact, the slope decreases up to a certain speed, a result of starved lubrication after which it becomes almost zero. This behavior is similar to what was found earlier in single contact measurements, such as those from Guangteng et al. *(43)* and Cann et al. *(20)*. They also found that the film thickness became constant with increasing speed at some point. However, in these single contact film thickness measurements, this happened under severe starvation. We see here that this phenomenon already occurs when the film thickness is about 30% of the fully flooded values. A possible explanation for the deviation from the single contact measurements could be due to differences in lubricant supply and loss mechanisms to the contacts. Some of these are the differences in grease reservoir adjacent to the tracks, osculation, and the fact that the contacts are elliptical in real ball bearings as opposed to the circular contacts in the single contact setups.

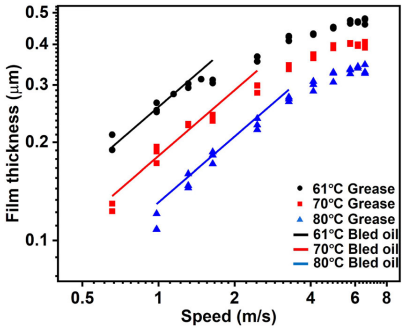

Figure 12. Film thickness versus speed on a log-log scale; 6209-2RZ bearing with Li/M grease; load = 513 N.

The film thickness becoming independent of speed was previously observed by De Laurentis et al. *(44)*, Barz *(35)*, and Cen and Lugt *(36)*. This effect was already predicted by Van Zoelen et al. *(10)* in their starved EHL model without replenishment. They showed that side flow out from the Hertzian contacts is governed by the time the lubricant spends in the contact (residence time) and the frequency of overrolling. These effects cancel each other out and the net result is that the film thickness is independent of speed. Van Zoelen's model applies to severely starved conditions and also results in a continuously decreasing film in time, none of which occurs here. Hence, the model cannot be applied to predict the film thickness in a grease-lubricated bearing. In our study, we see a supply of lubricant towards the contacts that is enough to maintain a film. This supply is independent of the space between balls and must therefore be a local replenishment effect *(36)*.

Figure 13 shows the relative film thickness h_g/h_{ff} versus speed at the three test temperatures. When $h_g/h_{ff} \geq 1$, fully flooded conditions persist; when $h_g/h_{ff} < 1$, lubrication is starved. Figure 13a shows the results at 61°C. At speeds lower than 1,000 rpm, relative film thickness is greater than one. After 1,000 rpm, the relative film thickness is less than one, indicating starved lubrication. For 70 and 80°C measurements, a similar behavior is observed but with different transition speeds for each temperature. The transition from fully flooded condition to starved condition takes place at about 1,500 rpm for 70°C and at 2,500 rpm for 80°C. This indicates that the transition from fully flooded condition to starved condition depends on the viscosity of the base oil as well (given that viscosity is a function of temperature).

A further analysis of the film thickness was carried out as shown in Fig. 12, which shows that the slope of the film

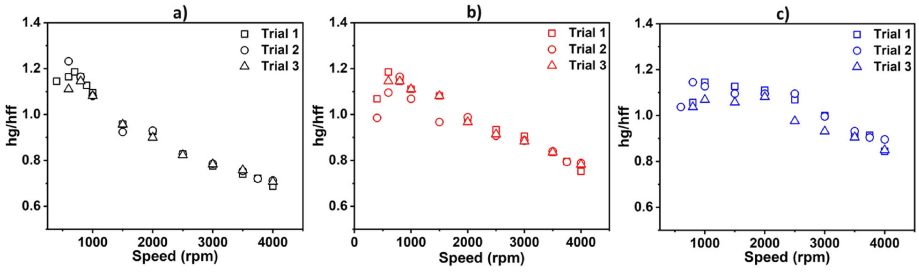

Figure 13. Relative film thickness versus speed at (a) 61°C, (b) 70°C, and (c) 80°C. 6209-2RZ bearing with Li/M grease; load = 513 N.

thickness versus speed on log-log plot is 0.67 at lower speeds for all three tested temperatures. From this we can conclude that we can safely use the fully flooded oil film thickness equations to estimate the grease film thickness in bearings using the base oil properties at lower speeds. It should be noted that the real film thickness could be slightly higher than the calculated value. As mentioned above, the film thickness at very low speed is larger than the fully flooded base oil film thickness because of the higher grease viscosity at very low shear rates (and therefore very low speeds in a bearing). The viscosity approaches the base oil viscosity at high shear rates (so higher bearing speeds) *(31)*, so here the film thickness is quite similar to values predicted using the base oil viscosity. In addition to this shear thinning effect, the film thickness could be larger due to thickener particle entrainment in the contact *(45)*. Single contact measurements on ball-on-disc rigs using optical interferometry have shown that lumps of thickener enter the contact at very low speeds *(15)*. This gives a nonuniform film thickness, varying in time. The electrical capacitance is inversely proportional to the thickness of the film, which implies that even small local thin areas of the film have a large impact on the measured film thickness. These "perturbations" will therefore cause much "spread" in the measured film thickness. The combination of film nonuniformity and the non-Newtonian grease rheology leads to very thick films with fluctuating minimum thickness at very low speed, thereby leading to a spread in measured values.

A major difference between our measurements (with pure axial load—hence, all balls are equally loaded, giving equal contact widths) and the measurements that use optical interferometry is that the latter are performed in contacts where one of the surfaces is flat. This means that there is a very large osculation and that grease can flow freely sideways. In bearings the osculation is small and grease is trapped in between seals/shields and the track. The contacts in real bearings are therefore not getting starved as easily as in these "model configurations." It takes much longer before starvation occurs. We expect therefore that starvation will start to occur at higher speeds and that the replenishment rates will be different, leading to a different film thickness–speed relation. Note that the basic physics is similar; only the ratio of side flow to replenishment is expected to be different between single contact measurements and actual bearing measurements. This leads to similar film thickness versus speed curves, but with different coefficients.

Conclusions

An improved film thickness measurement method, based on an electric capacitance model, including the effect of starvation, has been developed. Under an extremely starved condition, film thickness estimation/prediction could be about 20% higher when starvation effects are excluded. The newly developed method has been used to measure the film thickness in grease-lubricated deep-groove ball bearings as a function of speed at three different temperatures. It is shown that at lower speeds the grease film thickness increases with speed, similar to the base oil film thickness. After a critical speed, the grease film thickness becomes almost independent of speed.

Funding

We thank SKF Research and Technology Development and Shell for funding this work and for their approval to publish this article.

ORCID

Pramod Shetty http://orcid.org/0000-0001-6946-2201
Robert Jan Meijer http://orcid.org/0000-0002-0270-4218
Jude A. Osara http://orcid.org/0000-0001-7186-2765
Piet M. Lugt http://orcid.org/0000-0001-9356-7599

References

(1) Lugt, P. M. (2012), *Grease Lubrication in Rolling Bearings*, John Wiley & Sons: Chichester, UK.

(2) Bonnett, A. H. (1993), "Cause and Analysis of Anti-Friction Bearing Failures in AC Induction Motors," *Conference Record of 1993 Annual Pulp and Paper Industry Technical Conference*, pp 36–46, IEEE. doi:10.1109/PAPCON.1993.255813

(3) Liu, W. (2014), "The Prevalent Motor Bearing Premature Failures Due to the High Frequency Electric Current Passage," *Engineering Failure Analysis*, **45**, pp 118–127. doi:10.1016/j.engfailanal.2014.06.021

(4) Lubrecht, A., Venner, C. H., and Colin, F. (2009), "Film Thickness Calculation in Elasto-Hydrodynamic Lubricated Line and Elliptical Contacts: The Dowson, Higginson, Hamrock Contribution," *Proceedings of the Institution of Mechanical Engineers - Part J: Journal of Engineering Tribology*, **223**(3), pp 511–515. doi:10.1243/13506501JET508

(5) Hamrock, B. J. and Dowson, D. (1977), "Isothermal Elastohydrodynamic Lubrication of Point Contacts: Part III—Fully Flooded Results," *Journal of Tribology*, **99**(2), pp 264–275. doi:10.1115/1.3453074

(6) Nijenbanning, G., Venner, C. H., and Moes, H. (1994), "Film Thickness in Elastohydrodynamically Lubricated Elliptic Contacts," *Wear*, **176**(2), pp 217–229. doi:10.1016/0043-1648(94)90150-3

(7) Wedeven, L. D., Evans, D., and Cameron, A. (1971), "Optical Analysis of Ball Bearing Starvation," *Journal of Lubrication Technology*, **93**(3), pp 349–361. doi:10.1115/1.3451591

(8) Damiens, B., Venner, C. H., Cann, P., and Lubrecht, A. (2004), "Starved Lubrication of Elliptical EHD Contacts," *Journal of Tribology*, **126**(1), pp 105–111. doi:10.1115/1.1631020

(9) Hamrock, B. J. and Dowson, D. (1977), "Isothermal Elastohydrodynamic Lubrication of Point Contacts: Part IV—Starvation Results," *Journal of Tribology*, **99**(1), pp 15–22. doi:10.1115/1.3452973

(10) Van Zoelen, M., Venner, C. H., and Lugt, P. M. (2009), "Prediction of Film Thickness Decay in Starved Elasto-Hydrodynamically Lubricated Contacts Using a Thin Layer Flow Model," *Proceedings of the Institution of Mechanical Engineers - Part J: Journal of Engineering Tribology*, **223**(3), pp 541–552. doi:10.1243/13506501JET524

(11) Poon, S.-Y. (1972), "An Experimental Study of Grease in Elastohydrodynamic Lubrication," *Journal of Lubrication Technology*, **94**(1), pp 27–34. doi:10.1115/1.3451631

(12) Wilson, A. (1979), "The Relative Thickness of Grease and Oil Films in Rolling Bearings," *Proceedings of the Institution of Mechanical Engineers*, **193**(1), pp 185–192. doi:10.1243/PIME_PROC_1979_193_019_02

(13) Dyson, A. and Wilson, A. (1969), "Film Thicknesses in Elastohydrodynamic Lubrication of Rollers by Greases,"

Proceedings of the Institution of Mechanical Engineers, Conference Proceedings, Vol. 184, pp 1–11. SAGE: London. doi:10.1243/PIME_CONF_1969_184_137_02

(14) Jonkisz, W. and Krzeminski-Freda, H. (1979), "Pressure Distribution and Shape of an Elastohydro-Dynamic Grease Film," *Wear*, **55**(1), pp 81–89. doi:10.1016/0043-1648(79)90181-9

(15) Åström, H., Isaksson, O., and Höglund, E. (1991), "Video Recordings of an EHD Point Contact Lubricated with Grease," *Tribology International*, **24**(3), pp 179–184. doi:10.1016/0301-679X(91)90024-4

(16) Cann, P. and Spikes, H. (1992), "Fourier-Transform Infrared Study of the Behavior of Grease in Lubricated Contacts," *Lubrication Engineering*, **48**, pp 335–343.

(17) Booser, E. and Wilcock, D. (1953), "Minimum Oil Requirements of Ball Bearings," *Lubrication Engineering*, **9**(3), pp 140–143.

(18) Baker, A. (1958), "Grease Bleeding—A Factor in Ball Bearing Performance," *NLGI Spokesman*, **22**(9), pp 271–277.

(19) Wikström, V. and Jacobson, B. (1997), "Loss of Lubricant from Oil-Lubricated Near-Starved Spherical Roller Bearings," *Proceedings of the Institution of Mechanical Engineers - Part J: Journal of Engineering Tribology*, **211**(1), pp 51–66. doi:10.1243/1350650971542318

(20) Cann, P., Damiens, B., and Lubrecht, A. (2004), "The Transition between Fully Flooded and Starved Regimes in EHL," *Tribology International*, **37**(10), pp 859–864. doi:10.1016/j.triboint.2004.05.005

(21) Cann, P., Chevalier, F., and Lubrecht, A. (1997), "Track Depletion and Replenishment in a Grease Lubricated Point Contact: A Quantitative Analysis," *Tribology Series*, Vol. 32, pp 405–413. Elsevier. doi:10.1016/S0167-8922(08)70469-3

(22) Gershuni, L., Larson, M. G., and Lugt, P. M. (2008), "Lubricant Replenishment in Rolling Bearing Contacts," *Tribology Transactions*, **51**(5), pp 643–651. doi:10.1080/10402000802192529

(23) Jacod, B., Pubilier, F., Cann, P., and Lubrecht, A. (1999), "An Analysis of Track Replenishment Mechanisms in the Starved Regime," *Tribology Series*, Vol. 36, pp 483–492. Elsevier. doi:10.1016/S0167-8922(99)80069-8

(24) Mérieux, J., Hurley, S., Lubrecht, A., and Cann, P. (2000), "Shear-Degradation of Grease and Base Oil Availability in Starved EHL Lubrication," *Tribology series*, Vol. 38, pp 581–588. Elsevier. doi:10.1016/S0167-8922(00)80162-5

(25) Chiu, Y. (1974), "An Analysis and Prediction of Lubricant Film Starvation in Rolling Contact Systems," *ASLE Transactions*, **17**(1), pp 22–35. doi:10.1080/05698197408981435

(26) Guangteng, G. and Spikes, H. (1996), "The Role of Surface Tension and Disjoining Pressure in Starved and Parched Lubrication," *Proceedings of the Institution of Mechanical Engineers - Part J: Journal of Engineering Tribology*, **210**(2), pp 113–124. doi:10.1243/PIME_PROC_1996_210_487_02

(27) Nogi, T. (2015), "An Analysis of Starved EHL Point Contacts with Reflow," *Tribology Online*, **10**(1), pp 64–75. doi:10.2474/trol.10.64

(28) Nogi, T. (2015), "Film Thickness and Rolling Resistance in Starved Elastohydrodynamic Lubrication of Point Contacts with Reflow," *Journal of Tribology*, **137**(4), p 041502. doi:10.1115/1.4030203

(29) Fischer, D., von Goeldel, S., Jacobs, G., and Stratmann, A. (2021), "Numerical Investigation of Effects on Replenishment in Rolling Point Contacts Using CFD Simulations," *Tribology International*, **157**, p 106858. doi:10.1016/j.triboint.2021.106858

(30) Van Zoelen, M. T., Venner, C. H., and Lugt, P. M. (2008), "Free Surface Thin Layer Flow on Bearing Raceways," *Journal of Tribology*, **130**(2), pp 021802–1–021802-10. doi:10.1115/1.2805433

(31) Morales-Espejel, G. E., Lugt, P. M., Pasaribu, H., and Cen, H. (2014), "Film Thickness in Grease Lubricated Slow Rotating Rolling Bearings," *Tribology International*, **74**, pp 7–19. doi:10.1016/j.triboint.2014.01.023

(32) Cen, H. and Lugt, P. M. (2020), "Replenishment of the EHL Contacts in a Grease Lubricated Ball Bearing," *Tribology International*, **146**, p 106064. doi:10.1016/j.triboint.2019.106064

(33) Lewicki, W. (1955), *Some Physical Aspects of Lubrication in Rolling Bearings and Gears*, PhD Thesis, University of London (Birkbeck College).

(34) Crook, A. (1961), "The Lubrication of Rollers II. Film Thickness with Relation to Viscosity and Speed," *Philosophical Transactions of the Royal Society of London. Series A, Mathematical and Physical Sciences*, **254**(1040), pp 223–236.

(35) Barz, M. (1996), *Die Schmierfilmbildung in Fettgeschmierten Schnellaufenden Spindellagern*, PhD Thesis, Verlag Nicht Ermittelbar.

(36) Cen, H. and Lugt, P. M. (2019), "Film Thickness in a Grease Lubricated Ball Bearing," *Tribology International*, **134**, pp 26–35. doi:10.1016/j.triboint.2019.01.032

(37) Jablonka, K., Glovnea, R., and Bongaerts, J. (2012), "Evaluation of EHD Films by Electrical Capacitance," *Journal of Physics D: Applied Physics*, **45**(38), p 385301. doi:10.1088/0022-3727/45/38/385301

(38) Jablonka, K., Glovnea, R., and Bongaerts, J. (2018), "Quantitative Measurements of Film Thickness in a Radially Loaded Deep-Groove Ball Bearing," *Tribology International*, **119**, pp 239–249. doi:10.1016/j.triboint.2017.11.001

(39) Jablonka, K., Glovnea, R., Bongaerts, J., and Morales-Espejel, G. (2013), "The Effect of the Polarity of the Lubricant upon Capacitance Measurements of EHD Contacts," *Tribology International*, **61**, pp 95–101. doi:10.1016/j.triboint.2012.11.016

(40) Heemskerk, R., Vermeiren, K., and Dolfsma, H. (1982), "Measurement of Lubrication Condition in Rolling Element Bearings," *ASLE Transactions*, **25**(4), pp 519–527. doi:10.1080/05698198208983121

(41) Wittek, E., Kriese, M., Tischmacher, H., Gattermann, S., Ponick, B., and Poll, G. (2010), "Capacitances and Lubricant Film Thicknesses of Motor Bearings under Different Operating Conditions," *The XIX International Conference on Electrical Machines-ICEM 2010*, pp 1–6. IEEE. doi:10.1109/ICELMACH.2010.5608142

(42) Mopsik, F. I. (1967), "Dielectric Constant of n-Hexane as a Function of Temperature, Pressure, and Density," *Journal of Research of the National Bureau of Standards. Section A, Physics and Chemistry*, **71**(4), p 287.

(43) Guangteng, G., Cann, P., and Spikes, H. (1992), "A Study of Parched Lubrication," *Wear*, **153**(1), pp 91–105. doi:10.1016/0043-1648(92)90263-8

(44) De Laurentis, N., Liang, H., Lugt, P. M., and Kaderic, A. (2019), "Investigation into the Influence of Bearing Operational Conditions on Grease Film Thickness Using a Model Rolling Bearing Rig," *Extended Abstract International Tribology Conference,Sendai, Japan*.

(45) Cyriac, F., Lugt, P. M., Bosman, R., Padberg, C. J., and Venner, C. H. (2016), "Effect of Thickener Particle Geometry and Concentration on the Grease EHL Film Thickness at Medium Speeds," *Tribology Letters*, **61**(2), pp 1–13

(46) Jablonka, K., Glovnea, R., Bongaerts, J., and Morales-Espejel, G. (2012), "Comparative Measurements of EHD Film Thickness in Ball-on-Flat Rig and Rolling Element Bearing," *STLE 67th Annual Meeting*, pp 6–10, St. Louis, USA.

APPENDIX B

TRIBOLOGY TRANSACTIONS
2024, VOL. 67, NO. 1, 62–69
https://doi.org/10.1080/10402004.2023.2282632

Effect of Grease Filling on the Film Thickness in Deep-Groove Ball Bearings

Pramod Shetty[a], Robert Jan Meijer[a], Jude A. Osara[a], Rihard Pasaribu[b], and Piet M. Lugt[a,c]

[a]Engineering Technology, University of Twente, Enschede, Netherlands; [b]Shell Downstream Services International B.V., Rotterdam, Netherlands; [c]SKF Research and Technology Development, Houten, Netherlands

ABSTRACT

Determining the film thickness during the bleeding phase of grease lubrication in a bearing is difficult due to the various replenishment and loss mechanisms involved. An additional factor that could influence the film thickness is the amount of grease in the bearing. In this study, film thickness is measured in deep-groove ball bearings using two different greases, each with initial grease filling percentages of 7.5%, 15%, and 30% of the bearing's free volume. Film thickness is measured during the early stage of the bleeding phase at various loads and speeds using the electrical capacitance method. Results show that, after churning, values of temperature and film thickness are similar for the three different filling quantities. This indicates that bulk grease flow or oil bleed from the reservoirs formed in the unswept region does not impact the lubricant film thickness in the early stage of bearing operation.

ARTICLE HISTORY
Received 1 May 2023
Accepted 8 November 2023

KEYWORDS
Rolling bearings; grease; film thickness; oil bleeding; grease filling

Introduction

Grease is a colloid consisting of base oil, thickener, and additives *(1)*. Grease is one of the most preferred lubricants in a bearing because of its excellent sealing properties and long-term lubrication (most deep- groove ball bearings are lubricated for life). When a bearing is filled with grease, the grease is located on the track, between the ball and cage, distributed unevenly in the bearing. Once the bearing starts to run, the grease starts to redistribute in the bearing in a process known as churning. At the end of the churning phase, most of the grease will settle on the shield and cage while the rest of the worked grease stays on the raceway track *(2)*.

Chatra and Lugt *(2)* studied grease churning and showed that this phase consists of two subphases, namely, channeling and clearing. They described channeling as "a process where grease is moved from the area between the balls to the unswept area." They studied the grease left on the track during the churning process in SKF 6204 bearings and found that, within 10 min of running the bearing, only 35% of the original grease was left in the swept area of the bearing; the rest of the grease either leaked out or was located on the bearing shoulders/shields. During the clearing phase, another 5% to 10% is moved to the unswept volume, finally leaving only 20% to 25% of the total initial grease quantity in the swept area.

After churning, grease lubrication is believed to operate in the starved lubrication regime; that is, the film thickness depends on the thickness of oil layers in the inlet region of the contacts *(3–5)*. It has been suggested that reservoirs formed during the churning phase subsequently bleed the oil and help to replenish the contacts. Along with the bled oil, a small quantity of worked grease could also lubricate the contact *(6)*. Predicting grease film thickness during this stage—called the bleeding phase—wherein the bearing operates for most of its service life, is crucial to avoid metal-to-metal contact. Estimating the grease film thickness is difficult because of the complex time-dependent grease rheology, starvation, and multiple replenishment mechanisms during grease bleeding *(1)*.

There are three different grease lubrication mechanisms, the dominant one of which depends on the bearing geometry, grease properties, and operating conditions *(7)*:

a. Film formation is due to both thickener and base oil, including the bulk movement of grease *(6,8)*.
b. Grease reservoirs formed during churning releases the base oil in a controlled manner *(9)*.
c. Film formation is due to heavily worked grease, whereas the rest of the grease simply seals the bearing *(10)*.

In addition to these mechanisms, there have been discussions on how the lubricant is driven toward the contact *(11–15)*. Cann et al. distinguished grease lubrication mechanisms as in-contact replenishment (due to capillary action) and out-of-contact replenishment (due to replenishment between successive overrolling) *(13)*. Of these two

CONTACT Pramod Shetty p.shetty@utwente.nl

mechanisms, there is a clear consensus that out-of-contact replenishment within the bearing is too slow and not relevant *(13, 16, 17)*. Hence, in-contact replenishment, facilitated by surface tension, is considered to be the mechanism that drives the lubricant toward the tribological contacts in rolling bearings. Understanding which mechanism governs film replenishment under which conditions remains to be studied.

Film thickness measurements at extremely low speeds studied by Morales-Espejel et al. *(18)*, Cen et al. *(19)*, and Concalves et al. *(20)* showed that the grease film is thicker than the "base oil–only film" at low speeds. In the current study, we are interested in the medium-speed range where starved lubrication conditions may be prevalent. Cann et al. studied used bearings from R2F and R0F test rigs and observed that both bearings had the same grease distribution pattern but the supply of lubricant was dependent on the bearing geometry and operating conditions *(21,22)*. Both tests showed that only a small quantity of heavily worked grease was found on the track or on the cage, whereas most of the remaining grease was on the seals.

Cann et al. grouped the elements determining the grease lubrication mechanisms in bearings into three categories. (1) Lubrication parameters: grease rheology, base oil and thickener properties, oxidation, thermal stability, etc.; (2) Operational conditions: speed, load, temperature, and vibrations; and (3) bearing parameters: cage design, size, surface finish, and material of the bearings.

Most bearings are initially filled with grease up to 30% to 50% of the free volume *(23,24)*. For high-speed applications, bearings are filled with grease up to about 20% of the free volume *(1,25)*. Past studies have shown that overfilling is adverse to bearing operation due to the higher levels of dissipative viscous drag forces overheating the bearings *(24)*. Overfilling could result in faster thermo-mechanical grease degradation.

Grease life studies have shown that inadequate initial quantity of grease in a bearing results in shorter grease life *(1)*. Chatra and Lugt showed that churning duration will vary in a population of bearings running under the same conditions with the same (amount of) grease, which they ascribed to small differences in the initial grease positioning during filling *(2)*. Ward et al. found that a low initial grease volume resulted in film thickness similar to the base oil film thickness, whereas a high initial volume led to a longer run-in with thicker films *(26)*.

The question that then arises is: Does grease filling—the initial quantity of grease—in the bearing play a role in film formation during the bleed phase? If lubrication mechanism (a) is true—that is, both the thickener and bled oil lubricate the contact by the bulk movement of grease—then the film thickness would indeed depend on the quantity of grease filled. The filling quantity would also influence mechanism (b) because the total oil released *via* bleeding from a small quantity of grease would be low. Mechanism (c), however, will not be affected by the grease filling quantity. In this article, the impact of grease filling quantity is systematically studied using two different commonly used grease types.

Materials and methods

Grease

Two lithium-thickened greases were selected for this study: one with base oil viscosity of 100 cSt at 40°*C* and a consistency of NLGI grade 2.5, henceforth called "LiM-100-2.5" grease, and the other grease with a base oil viscosity of 474.5 cSt at 40°*C* with consistency of NLGI grade 1.5, henceforth called "LiM-460-1.5" grease. Both greases have the same thickener weight percentage of 13%. Details of the grease properties are given in Table 1.

Measuring film thickness in deep-grove ball bearings

The film thickness in a deep-groove ball bearing was measured by using an electrical capacitance method in an in-house-built bearing test rig. The detailed construction and working principle of the test rig were explained by Cen and Lugt *(17)*. The measured capacitance is converted to film thickness using a new method described in our previous paper *(27)*, which includes the effects of starvation on the measured capacitance. In this study, the same method is used but with a faster algorithm for the iteration loop. In our previous paper, we described a linear iteration algorithm to obtain the appropriate meniscus position. Here, we use the secant method to speed up the iteration instead of the ordinary linear iteration.

SKF 6209 bearings with C3 clearance were chosen for this study. 30%, 15%, and 7.5% of the free volumes of the bearings were filled with grease. The filling percentage is indicated with a prefix in the corresponding grease designation. These bearings were run for about 80 to 100 h until grease churning was finished. The bearings ran under self-induced temperature during the churning phase, with the temperature profile used to identify when the churning phase ended. After the churning phase, the temperature of the bearing was controlled to 61° C, using an electric heat gun and a fan. Here, the bearing temperature was measured on the outer ring of the bearings (away from the heat gun and fan). Next, the film thickness was measured for 10 min and the average value was taken for further analysis. The film thickness was measured from 400 to 4,000 rpm with 513, 700, and 900 N loads. These loads resulted in contact pressures of 1.03, 1.15, and 1.25 GPa, respectively, on the inner ring ball contact. All measurements were repeated thrice and the results are presented as averages and standard deviations.

Table 1. Properties of greases used in this study.

Property	LiM-100-2.5	LiM-460-1.5
Kinematic viscosity @ 40° C (cSt)	102.8	474.5
Kinematic viscosity @ 100° C (cSt)	10.31	31.4
Density @ 15° C (g/cm^3)	0.891	0.902
Pressure–viscosity coefficient @ 40° C (GPa^{-1})	31.8	27.4
Thickener content (% mass)	13	13

Results and discussion

Churning

Figure 1 shows the self-induced temperature and film thickness during the churning phase of LiM-100-2.5 grease. The temperature induced in a bearing is due to frictional heat generation in the bearing. The sources of friction in the bearing include (a) rolling friction, (b) sliding friction, (c) seal friction, and (d) friction due to viscous drag, churning, and splashing *(28)*. In this study, noncontacting seals were used, so seal friction can be neglected.

The temperature during churning is high due to high viscous dissipation and heat generation *(29,30)*. During the bleeding phase, the friction torque is the result of rolling and sliding friction only, leading to a lower, steady-state temperature. Except for the initial channeling subphase of churning, the instantaneous film thickness profile appears to mirror the temperature profile. This is due to a decrease in both grease and base oil viscosities at high temperatures, yielding low film thickness, and vice versa (low temperature yields high viscosity and film thickness). The initial instantaneous normalized film thickness (first 20–30 min) is very high (typically more than 1.8) during the channeling subphase of churning even though the temperature is high, which is ascribed to thickener entrapment in the contacts. During the subsequent clearing subphase wherein the grease is pushed to the sides to form reservoirs, the temperature of the bearing is still high but the film thickness is low because of lower base oil viscosity. After churning, the temperature drops to a relatively steady value, leading to a corresponding increase in film thickness. The percentage of grease filling (i.e. the initial quantity of grease) has a clear impact on the churning behavior. It can be seen that 30% filling yielded the highest peak temperature of 95° C, whereas 15% and 7.5% fillings resulted in 73°C and 67°C peak temperatures, respectively. As expected, a higher filling results in higher viscous drag forces. In addition, the duration of the churning phase seems to be affected by the level of filling. Note that the final steady temperature for all filling percentages is the same. This means that rolling and sliding friction are identical (rolling friction is given by viscosity and level of starvation) and that the levels of starvation are the same at the end of churning for all of these cases. This is reflected in the bleeding phase film thickness, which is indeed also practically the same for all three different fillings.

Figure 2 shows the churning behavior of LiM-460-1.5 grease with a very high-viscosity base oil (viscosity of 474.5 cSt) and low consistency (NLGI grade 1.5). This figure shows that the channeling phase is somewhat longer and has a peak temperature that is higher than that of LiM-100-2.5 grease (with base oil viscosity of 100 cSt and consistency of NLGI grade 2.5). Note that both greases have the same thickener concentration but different base oil viscosities. The high base oil viscosity of the LiM-460-1.5 grease could induce high viscous drag forces during churning. The low consistency of LiM-460-1.5 could cause it to fall back more easily onto the track, leading to more viscous heat generation. After churning—that is, during the bleeding phase—the temperature of LiM-460-1.5 grease is higher than that of LiM-100-2.5 grease. This indicates that the base oil viscosity primarily determines the bleeding phase temperature and film thickness. After churning, only a small quantity of worked grease is left on the track. Subsequently, we show that, under all of the different operating conditions, the film thicknesses in all three different fillings are the same for both greases tested.

Figure 3 shows the grease left on the seals after the churning phase. It is observed that the bearing with 7.5% filling left a small amount of grease on the seal, whereas 15% and 30% fillings deposited considerable amounts. During the churning phase, most of the grease is expelled from the swept area and deposited on the empty unswept region including the seals. Hence, a smaller grease layer is anticipated on the seals with lower fillings as these experiments verify. Table 2 shows the amount of grease left on the bearing seals after churning. It is evident that the higher the grease filling, the higher the grease layer deposited on the seals for both greases tested. Though the quantity of grease left on the seals after churning is as predicted, its effect on film thickness might be different depending on the prevalent replenishment mechanism(s). It is generally believed that, from these stationary positions, grease will release the oil by bleeding, similar to a sponge releasing water. If the quantity of grease in these stationary positions is small, the contacts will receive a low oil supply and, hence, have a low film thickness.

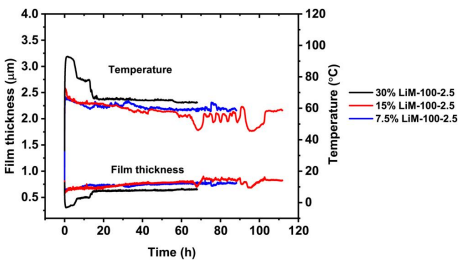

Figure 1. Instantaneous temperature and film thickness during grease churning in 6209 bearing with LiM-100-2.5 grease, 30%, 15%, and 7.5% initial filling, load = 513 N, speed = 4,000 rpm.

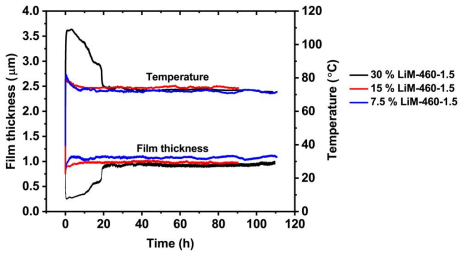

Figure 2. Instantaneous temperature and film thickness during grease churning in 6209 bearing with LiM-460-1.5 grease, 30%, 15%, and 7.5% initial filling, load = 513 N, speed = 4,000 rpm. (a) LiM-100-2.5 with (a) 7.5%, b) 15%, and 30% fillings, (b) LiM-460-1.5 with (a) 7.5%, (b) 15%, and 30% fillings.

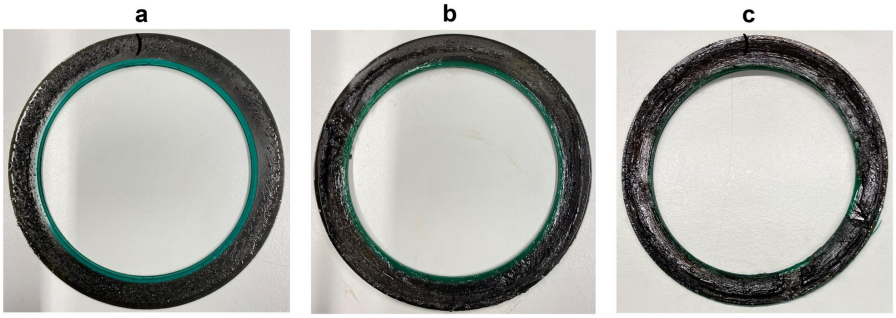

(a) LiM-100-2.5 with a) 7.5%, b) 15%, and 30% fillings

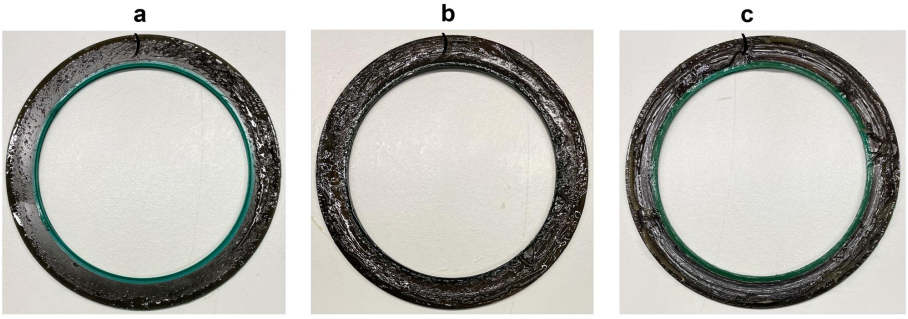

(b) LiM-460-1.5 with a) 7.5%, b) 15%, and 30% fillings

Figure 3. Tested bearing seals with different amounts of initial grease. (a) 513 N, (b) 700 N, (c) 900 N.

Table 2. Mass of grease left on the seals, measured after the experiments.

Mass of grease on the seals (g)			
S/N	Filling %	LiM-100-2.5	LiM-460-1.5
1	7.5	0.24	0.28
2	15	1.46	1.36
3	30	2.35	1.96

Table 3 shows the mass of grease left inside the bearings after the tests, including the grease located on the bearing shoulders, raceways, cage bars, and cage pockets. This is measured by removing the seals from the bearings and measuring the bearing weight with grease, which is then subtracted from the bearing weight without grease. Chatra and Lugt found that, after churning in 6204 bearings (filled with grease up to 30% of the bearing's free volume), about 20% to 25% of the initial filling is left in the bearings *(2)*. Similarly, the 30%-filled LiM-100-2.5 and 30%-filled LiM-460-1.5 greases left 22.8% and 37.8% of the initial grease amount in the bearings, respectively. With the measured mass of grease left in the bearings, we can calculate the percentage of the free volume occupied by grease; that is, the percentage of grease in the bearing relative to the free volume of the bearing. We notice that for all of the fillings, only 4.99% to 11.71% of the free space in the bearing is occupied by grease at the end of the test.

In the next section, we will discuss these effects on film thickness. We will attempt to determine whether there is indeed a bulk flow of lubricants from the unswept region to the swept region.

Film thickness

In our previous paper *(27)*, we showed that film thickness is almost independent of speed during the bleeding phase of the grease. In this article, we present film thicknesses measured during the bleeding phase for different initial grease filling percentages. Here, the measurements are taken at a constant temperature of 61° C. This temperature selection is arbitrary. After the churning phase of grease lubrication, the film thickness depends only on the operating conditions; that is, load, speed, and temperature. During the speed sweep, in the first few minutes after changing the speed, the film thickness is transient. Subsequently, after a few more minutes, the film thickness becomes steady at that speed and load, varying with temperature only (which here is also held constant). The instantaneous film thickness is then recorded for 10 min in the steady region and averaged to give one discrete data point for further analysis. A sample film thickness measurement is shown in Figure 7.

Table 3. Mass and volume percentage of grease left in the bearings, measured after the experiments.

		Mass of grease in the bearings (g)		Volume percentage of grease in the bearings (%)	
S/N	Filling %	LiM-100-2.5 (g)	LiM-460-1.5 (g)	LiM-100-2.5 (%)	LiM-460-1.5 (%)
1	7.5	1.31	1.01	6.48	4.99
2	15	1.21	1.04	5.98	5.14
3	30	1.37	2.27	6.77	11.71

The volume percentage is the fraction of the bearing's free volume occupied by the grease.

It is evident in Fig. 4 that for the three different fillings of LiM-100-2.5 grease, film thickness remains the same at low and high speeds. It can also be seen that film thickness becomes almost constant at higher speeds for all three fillings. This accords with our previous observation *(27)*. The film thickness in a severely starved contact is governed by the side flow of the lubricant from the contact. This side flow is determined by the residence time and frequency of over-rolling. As the speed increases, these two mechanisms balance out making film thickness almost independent of speed *(14,27,31,32)*.

We repeated the measurements at three different loads to check whether the film thickness would change. Under fully flooded conditions, film thickness weakly depends on the load by an exponent of only −0.067 for point contacts *(5)*. Cen and Lugt showed that the normalized film thickness during the bleeding phase of grease lubrication is related to the contact width (contact width changes with load) *(14)*. This indicates that the relationship between film thickness and load under starved conditions is different from that during fully flooded conditions. In this study, we investigate whether this relationship is impacted by different initial grease fillings. Figure 4 shows the three different loading conditions. The contact widths for these three conditions are 1.154 mm, 1.281 mm, and 1.392 mm for the inner ring-ball contact across the running direction.

Cann et al. *(13)* studied the effect of starvation on lubricant film thickness using a ball-on-disc machine. They showed that the normalized film thickness can be related to the product: viscosity (η) × speed (u)× load $^{1/3}$ × lubrication level^{-1} × surface tension^{-1}, or viscosity × speed × contact width (b) × lubrication level^{-1} × surface tension^{-1}. On a deep groove ball bearing, Cen and Lugt *(17)* showed that in grease-lubricated bearings, with greases having very different bleeding rates, base oil viscosities and thickener types, the level of starvation was determined by base oil viscosity × contact width × speed—ηbu—indicating that bleeding did not play a major role during this phase of the lubrication. Recently Lugt et al. *(33)* found that grease does not bleed before oxidation starts, and oxidation starts only after all the anti-oxidants are consumed from the grease. It was observed in their experiments that until 500 h, grease did not bleed. Their experiments were conducted at higher temperatures (110° C). It can therefore be expected that in our tests bleed will not take place for even much longer times. Figures 4 and 5 show that the filling does not change the film thickness in any of the loading conditions. These results indicate that immediately after the churning phase, the level of lubricant remaining on the track does not depend on the initial filling quantity. The excess grease will

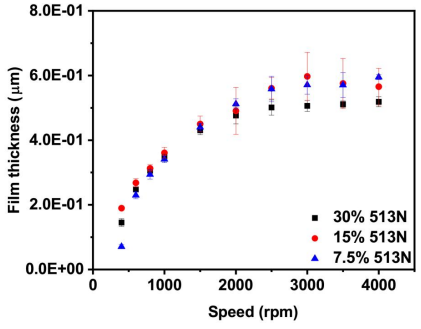

(a) 513N

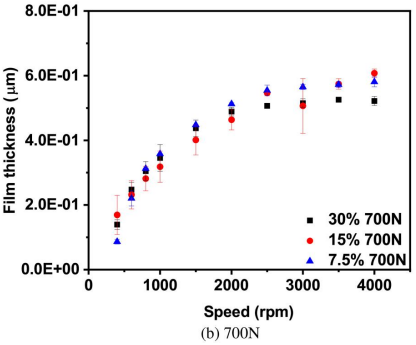

(b) 700N

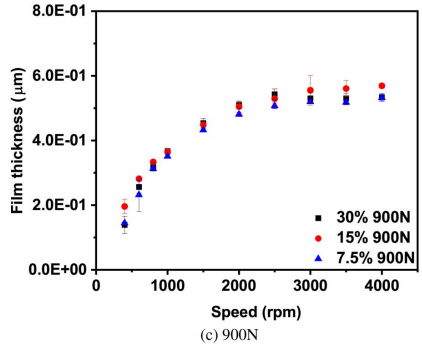

(c) 900N

Figure 4. LiM-100-2.5 grease film thickness as a function of speed and initial filling quantity. (a) 513 N, (b) 700 N, (c) 900 N.

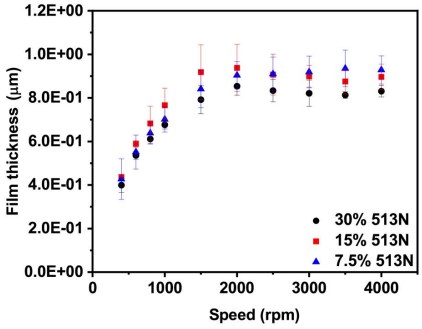

(a) 513N

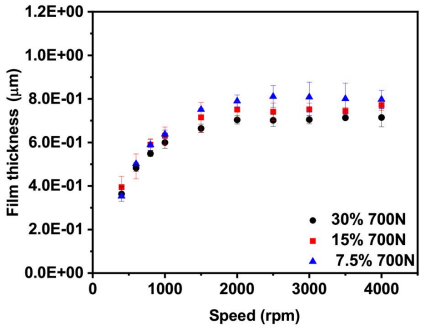

(b) 700N

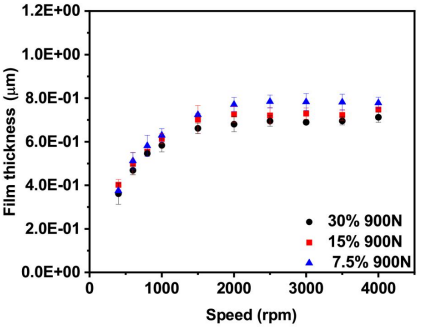

(c) 900N

Figure 5. LiM-460-1.5 grease film thickness as a function of speed and initial filling quantity. (a) 30%, 15% and 7.5% filling of LiM-100-2.5, (b) 30%, 15% and 7.5% filling of LiM-460-1.5.

be cleared from the track during churning. The reservoirs formed near the contact also do not play a role in lubricating the contact. If the reservoirs were contributing to the replenishment *via* either increased bleed or assisting the cage scraping/lubricant reflow between overrollings, an increase in film thickness would have been observed.

Replenishment

A classical explanation of grease lubrication says that during the churning phase, grease is moved to the side of the rolling elements, where it remains due to its stiffness and from where it bleeds the oil behind the contact and replenishes the next rolling element *(11,34)*. Studies by Baly et al. *(35)*, Gershuni et al. *(16)*, and Cen et al. *(14)* showed that this is indeed not the relevant replenishment mechanism. Cann et al. *(13)* and Jacod et al. *(36)* suggested that replenishment is a local phenomenon caused by the interaction between the oil and the contact itself. The different filling results in this study show the same. Both tested greases under all three different loads and at various speeds showed that film thickness does not change with different fillings. If replenishment was not local, the higher filling would have resulted in higher film thickness. The churning results (refer to Figs. 1 and 2) show that the level of lubricant remaining on the track is the same for all fillings for both greases. Because the level of lubricant on the track is the same and replenishment is due to interaction between the oil and the contact, a change in the filling will not alter the film thickness.

As mentioned above, the replenishment rate of a lubricant depends on the viscosity of the base oil, irrespective of the replenishment mechanism; that is, in-contact replenishment or out-of-contact replenishment *(14)*. Point contact results and deep- groove ball bearing film thickness results from Cann et al. and Cen et al. have shown that the higher the viscosity, the higher the starvation level. Figure 5 shows that LiM-460-1.5 grease with a high-viscosity base oil also shows similar behavior as LiM-100-2.5 grease. It was originally speculated that low-consistency greases might have lumps that continue to fall back onto the track, so film thickness might also depend on the filling quantity. However, to our surprise, experimental results show that this is not the case. Figure 5 shows that for all three loading conditions and speeds, 7.5%, 15%, and 30% grease fillings give the same film thickness. From this result, we rule out the bulk reflow of grease lumps onto the track as the predominant replenishment mechanism.

In the case of oil lubrication, if the inlet of the contact is filled with abundant lubricant—that is, under fully flooded conditions—the film thickness developed will not change with a further increase in oil level *(3)*. It can be argued that if the quantity of worked grease left on the track is high enough even with 7.5% and 15% fillings, then the film thickness would be independent of fillings. To check whether this is the case, the relative film thickness was calculated. Relative film thickness is the ratio of measured grease film thickness to the film thickness calculated using base oil properties. We use Hamrock and Dowson's equations to calculate the base oil film thickness using the bearing's outer ring temperature. If this ratio is greater than or equal to 1, the contacts are fully flooded. If the ratio is less than 1, the contacts are starved. Figure 6 shows that both greases were under starved lubrication at higher ηbu values, indicating that even during starved conditions, the film thickness is independent of grease filling in deep-groove ball bearings at moderate speeds.

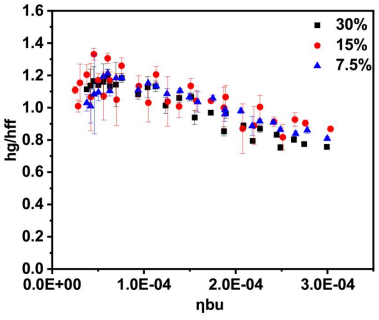

(a) 30%, 15% and 7.5% filling of LiM-100-2.5

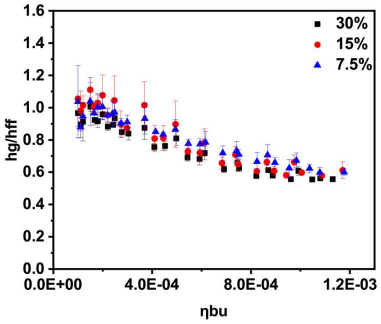

(b) 30%, 15% and 7.5% filling of LiM-460-1.5

Figure 6. Relative film thickness vs. product of viscosity, speed, and contact width.

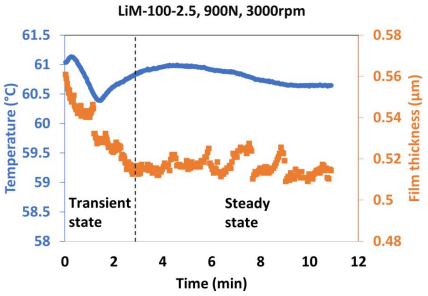

Figure 7. Sample film thickness measurement showing the initially transient instantaneous film thickness stabilizing after a few minutes, at a set speed. The instantaneous film thickness values in the steady region are averaged to yield each discrete data point plotted in Figs. 4–6. Grease: LiM-100-2.5, speed: 3000 rpm, load: 900 N, filling percentage: 30%.

These results only show the lubrication mechanism in the deep-groove ball bearings in the early operating hours. One should not conclude that lower grease filling is indeed better. It was shown earlier that grease life is proportional to the volume of grease filled *(36–38)*. Hence, lower or inadequate grease filling would result in shorter grease life.

Conclusion

- Bearings filled with different initial quantities of grease showed different temperature and film thickness profiles only during the churning phase.
- After the churning phase, the self-induced temperature was the same in all three cases (30%, 15%, and 7.5% filling). This indicates that the oil level left on the track is the same irrespective of the filling.
- The film thickness at different speeds and loads was the same for the various fillings.
- Similar results were obtained for both greases tested, indicating that the results are applicable for greases with various base oil viscosities and consistencies.
- Bulk reflow of grease lumps or by the bleeding of base oil from the reservoirs formed on the shoulder and seals is not significant during the early stages of bearing operation. Only the oil left on the track after churning appears to lubricate the contacts.
- The thickness of the layers of oil on the tracks is independent of the filling.
- We showed here that the early film thickness is independent of filling. This means that clearing (the last phase in the churning process) leaves oil layers with thicknesses determined solely by the dynamics of oil flow in and around the contact (side flow and replenishment) and not by bleed from the grease reservoirs.

Disclosure statement

No potential conflict of interest was reported by the author(s).

Acknowledgments

We thank Min Gao for performing some of the experiments. We also thank SKF Research and Technology Development and Shell for funding this work and for their approval to publish this article.

ORCID

Pramod Shetty http://orcid.org/0000-0001-6946-2201
Robert Jan Meijer http://orcid.org/0000-0002-0270-4218

References

(1) Lugt, P. M. (2012), *Grease Lubrication in Rolling Bearings*, John Wiley & Sons: Chichester, UK.
(2) Chatra, K. R. S., and Lugt, P. M. (2021), "The Process of Churning in a Grease Lubricated Rolling Bearing: Channeling and clearing," *Tribology International*, **153**, pp 106661. doi:10.1016/j.triboint.2020.106661
(3) Wedeven, L. D., Evans, D., and Cameron, A. (1971), "Optical Analysis of Ball Bearing Starvation," *Journal of Lubrication Technology*, **93**, pp 349–361. doi:10.1115/1.3451591
(4) Cheng, H., and Sternlicht, B. (1965), "A Numerical Solution for the Pressure, Temperature, and Film Thickness between Two Infinitely Long, Lubricated Rolling and Sliding Cylinders, under

Heavy Loads," *Journal of Mechanical Engineering Science*, **87**, pp 695–704.

(5) Dowson, D., and Whitaker, A. (1965), "Paper 4: A Numerical Procedure for the Solution of the Elastohydrodynamic Problem of Rolling and Sliding Contacts Lubricated by a Newtonian Fluid," Proceedings of the Institution of Mechanical Engineers, vol. 180, pp 57–71, SAGE Publications. London doi:10.1243/PIME_CONF_1965_180_064_02

(6) Cann, P. (1996), "Starvation and Reflow in a Grease-Lubricated Elastohydrodynamic Contact," *Tribology Transactions*, **39**, pp 698–704. doi:10.1080/10402009608983585

(7) Miettinen, J., Andersson, P., and Wikström, V. (2001), "Analysis of Grease Lubrication of a Ball Bearing Using Acoustic Emission Measurement," *Proceedings of the Institution of Mechanical Engineers - Part J: Journal of Engineering Tribology*, **215**, pp 535–544. doi:10.1243/1350650011543781

(8) Cann, P., Chevalier, F., and Lubrecht, A. (1997), "Track Depletion and Replenishment in a Grease Lubricated Point Contact: A Quantitative Analysis," *Tribology Series*, Vol. 32. pp 405–413, Elsevier.

(9) Baker, A. (1958), "Grease Bleeding—A Factor in Ball Bearing Performance," *NLGI Spokesman*, **22**, pp 271–277.

(10) Scarlett, N. (1967), "Paper 21: Use of Grease in Rolling Bearings," Proceedings of the Institution of Mechanical Engineers, Vol. 182, pp585–624, SAGE Publications. London. doi:10.1243/PIME_CONF_1967_182_045_02

(11) Chiu, Y. (1974), "An Analysis and Prediction of Lubricant Film Starvation in Rolling Contact Systems," *A S L E Transactions*, **17**, pp 22–35. doi:10.1080/05698197408981435

(12) Cann, P., and Lubrecht, A. (1999), "An Analysis of the Mechanisms of Grease Lubrication in Rolling Element Bearings," *Lubrication Science*, **11**, pp 227–245. doi:10.1002/ls.3010110303

(13) Cann, P., Damiens, B., and Lubrecht, A. (2004), "The Transition between Fully Flooded and Starved Regimes in EHL," *Tribology International*, **37**, pp 859–864. doi:10.1016/j.triboint.2004.05.005

(14) Cen, H., and Lugt, P. M. (2020), "Replenishment of the EHL Contacts in a Grease Lubricated Ball Bearing," *Tribology International*, **146**, pp 106064. doi:10.1016/j.triboint.2019.106064

(15) Guangteng, G., and Spikes, H. (1996), "The Role of Surface Tension and Disjoining Pressure in Starved and Parched Lubrication," *Proceedings of the Institution of Mechanical Engineers - Part J: Journal of Engineering Tribology*, **210**, pp 113–124. doi:10.1243/PIME_PROC_1996_210_487_02

(16) Gershuni, L., Larson, M. G., and Lugt, P. M. (2008), "Lubricant Replenishment in Rolling Bearing Contacts," *Tribology Transactions*, **51**, pp 643–651. doi:10.1080/10402000802192529

(17) Cen, H., and Lugt, P. M. (2019), "Film Thickness in a Grease Lubricated Ball Bearing," *Tribology International*, **134**, pp 26–35. doi:10.1016/j.triboint.2019.01.032

(18) Morales-Espejel, G. E., Lugt, P. M., Pasaribu, H., and Cen, H. (2014), "Film Thickness in Grease Lubricated Slow Rotating Rolling Bearings," *Tribology International*, **74**, pp 7–19. doi:10.1016/j.triboint.2014.01.023

(19) Cen, H., Lugt, P. M., and Morales-Espejel, G. (2014), "Film Thickness of Mechanically Worked Lubricating Grease at Very Low Speeds," *Tribology Transactions*, **57**, pp 1066–1071. doi:10.1080/10402004.2014.933936

(20) Gonçalves, D., Graça, B., Campos, A. V., Seabra, J., Leckner, J., and Westbroek, R. (2015), "On the Film Thickness Behaviour of Polymer Greases at Low and High Speeds," *Tribology International*, **90**, pp 435–444. doi:10.1016/j.triboint.2015.05.007

(21) Cann, P., Doner, J., Webster, M., and Wikstrom, V. (2001), "Grease Degradation in Rolling Element Bearings," *Tribology Transactions*, **44**, pp 399–404. doi:10.1080/10402000108982473

(22) Cann, P., Webster, M., Doner, J., Wikstrom, V., and Lugt, P. (2007), "Grease Degradation in R0F Bearing Tests," *Tribology Transactions*, **50**, pp 187–197. doi:10.1080/10402000701261003

(23) Lugt, P. M. (2009), "A Review on Grease Lubrication in Rolling Bearings," *Tribology Transactions*, **52**, pp 470–480. doi:10.1080/10402000802687940

(24) Chatra, K. R. S., Osara, J. A., and Lugt, P. M. (2022), "Impact of Grease Churning on Grease Leakage, Oil Bleeding and Grease Rheology," *Tribology International*, **176**, pp 107926. doi:10.1016/j.triboint.2022.107926

(25) FAG. (2002), "Rolling Bearing Lubrication," Technical Report, Publ. No. WL 81 115/4.

(26) Ward, P., Leveille, A., and Frantz, P. (2008), "Measuring the EHD Film Thickness in a Rotating Ball Bearing," *Proceedings of the 39th Aerospace Mechanisms Symposium*, NASA, Vol. 107, Citeseer.

(27) Shetty, P., Meijer, R. J., Osara, J. A., and Lugt, P. M. (2022), "Measuring Film Thickness in Starved Grease-Lubricated Ball Bearings: An Improved Electrical Capacitance Method," *Tribology Transactions*, **65**, pp 869–879. doi:10.1080/10402004.2022.2091067

(28) SKF. (2003), *Skf General Catalogue*, p 87, SKF: Gothenburg.

(29) Chatra, K. R. S. (2023), "The Process of Churning in Grease Lubricated Bearings: Identification and Thermo-Mechanical Characterization," PhD thesis. doi:10.3990/1.9789036555081.

(30) Chatra, K. R. S., and Lugt, P. M. (2020), "Channeling Behavior of Lubricating Greases in Rolling Bearings: Identification and Characterization," *Tribology International*, **143**, pp 106061. doi:10.1016/j.triboint.2019.106061

(31) Van Zoelen, M., Venner, C. H., and Lugt, P. M. (2009), "Prediction of Film Thickness Decay in Starved Elasto-Hydrodynamically Lubricated Contacts Using a Thin Layer Flow Model," *Proceedings of the Institution of Mechanical Engineers - Part J: Journal of Engineering Tribology*, **223**, pp 541–552. doi:10.1243/13506501JET524

(32) Venner, C. H., Van Zoelen, M., and Lugt, P. M. (2012), "Thin Layer Flow and Film Decay Modeling for Grease Lubricated Rolling Bearings," *Tribology International*, **47**, pp 175–187. doi:10.1016/j.triboint.2011.10.019

(33) Lugt, P. M., Holgerson, M., and Reinholdsson, F. (2023), "Impact of Oxidation on Grease Life in Rolling Bearings," *Tribology International*, **188**, pp 108785. doi:10.1016/j.triboint.2023.108785

(34) Damiens, B., Lubrecht, A. A., and Cann, P. (2001), "Lubrication Regimes in Rolling Element Bearings," *Tribology and Interface Engineering Series*, **39**, pp 295–301.

(35) Baly, H., Poll, G., Cann, P., and Lubrecht, A. (2006), "Correlation between Model Test Devices and Full Bearing Tests under Grease Lubricated Conditions," IUTAM Symposium on Elastohydrodynamics and Micro-Elastohydrodynamics, pp 229–240, Springer: Dordrecht.

(36) Jacod, B., Pubilier, F., Cann, P., and Lubrecht, A. (1999), "An Analysis of Track Replenishment Mechanisms in the Starved Regime," *Tribology Series*, Vol. 36, pp 483–492, Elsevier: Amsterdam.

(37) Lugt, P. M., and Berens, F. (2022), "The Grease Life Factor Concept for Ball Bearings," *Tribology International*, **169**, pp 107460. doi:10.1016/j.triboint.2022.107460

(38) Gafitanu, M., Silicon, D., Ianus, G., and Olaru, D. (1993), "A General Model for Grease Deterioration in Ball Bearings," Proceedings of the 6th International Congress on Tribology, Vol. 2, pp 355–359, EUROTRIB: Budapest.

APPENDIX C

Tribology International 193 (2024) 109325

Contents lists available at ScienceDirect

Tribology International

journal homepage: www.elsevier.com/locate/triboint

Full Length Article

Vibrations and film thickness in grease-lubricated deep groove ball bearings

Pramod Shetty [a,*], Robert Jan Meijer [a], Jude A. Osara [a], Rihard Pasaribu [b], Piet M. Lugt [a,c]

[a] Engineering Technology, University of Twente, The Netherlands
[b] Shell Downstream Services International B.V, The Netherlands
[c] SKF Research and Technology Development, The Netherlands

ARTICLE INFO

Keywords:
Grease
Film thickness
Elastohydrodynamic lubrication
Vibrations
Rolling bearings

ABSTRACT

Understanding the relevance and significance of the various replenishment mechanisms in grease-lubricated bearings is very important in choosing the appropriate lubrication strategy. This study shows that the lubricant film thickness in the ball-ring contacts of a deep groove ball bearing may increase by 10%–25% due to vibrations. The possible mechanisms behind this film thickness increase are discussed. Of the proposed contact replenishment mechanisms, the micro-lateral motion of the contact edge across the tracks caused by in-operation vibrations appears crucial. Results show that in the starved contacts, vibration plays a vital role in determining the film thickness.

1. Introduction

Rolling bearings reduce friction and wear in rotating machinery via the lubricant film developed at the bearing contacts. Estimating the film thickness during the bleeding phase of a grease-lubricated bearing is critical for smooth, reliable operation since most bearings primarily run in this phase during their life cycle. Various lubricant loss and replenishment mechanisms impact the film thickness during the bleeding phase. Studies by Cann et al. [1–4], Cen and Lugt [5], and Gershuni et al. [6] showed that the oil replenishment is primarily local, i.e., only around the contact. The force driving the oil toward the contact could be due to capillary action, though this needs further verification.

Cen and Lugt [5] and Shetty et al. [7,8] studied the film thickness behavior in different ball bearings with different speeds, loads, greases, filling quantities, and temperatures. They showed that the relative film thickness—the ratio of measured film thickness to the estimated fully-flooded film thickness—correlates well with the product of viscosity, speed, and half contact width via a power law curve, demonstrating that the dependence of film thickness on load is more significant in starved contacts than under fully flooded conditions. The film thickness was also observed to be almost independent of speed as speed increased ($\geq$ 2000 rpm) and contacts became more starved. These studies shed some light on the relevance of replenishment and loss mechanisms in grease-lubricated bearings.

Recent studies have attempted to propose models for the film thickness in lubricant-starved contacts based on capillary flow replenishment [9–13]. Understanding the significance of each replenishment or loss mechanism is important for accurate model development.

Cann et al. [3,14] classified the mechanisms determining the lubrication in a bearing into three categories. (1) Lubricant parameters: grease rheology, base oil viscosity, oxidation, and thermal stability; (2) Operating parameters: speed, load, temperature, and vibrations; and (3) Bearing parameters: size, surface finish, material, cage design, etc. Among these mechanisms, vibrations—the primary focus of this article—appear significant.

Vibrations are inherent in all rotating machinery. In ball bearings, vibrations could result from various sources such as: variable compliance [15,16]; geometric deviations such as raceway waviness, rolling elements spheroidicity, and roughness [17]; and external sources such as shaft misalignment, unbalance, and loose mechanical interfaces [18,19]. The dynamic analysis of a shaft-bearing system showed that the lubricant film thickness impacts the resonance frequency, damping and stiffness of the system [20–22]. Studies on ball-on-disk machines with varying load and oscillatory motion indicated that vibrations impact the film thickness in an Elastohydrodynamic Lubrication (EHL) contact [23–26]. Numerical studies also showed that surface waviness and indentation exacerbate vibrations, further impacting the film thickness [17,27,28]. It is, therefore, anticipated that vibrations will also influence the film thickness in ball bearings having multiple EHL contacts.

Vibrating machines can induce unpredictable forces and displacements in EHL contacts. A study by Félix Quinonez and Morales-Espejel [29] showed that due to normal vibrations (fluctuations in normal load), the lubricant entrainment velocity changes as the contact radius changes. This change in entrainment velocity, combined with the

* Corresponding author.
E-mail address: p.shetty@utwente.nl (P. Shetty).

https://doi.org/10.1016/j.triboint.2024.109325
Received 28 November 2023; Received in revised form 9 January 2024; Accepted 21 January 2024
Available online 22 January 2024

Nomenclature

β	Contact angle [°]
β_0	Free contact angle [°]
δ_a	Axial displacement [m]
δ_r	Radial displacement [m]
$\hat{a}$	Vibration acceleration [ms^{-2}]
$\hat{M}$	Total mass of the system [kg]
λ	Damping coefficient [$N\,s\,m^{-1}$]
ω	Angular velocity [$rad\,s^{-1}$]
ψ	Angular distance between the rolling elements [°]
Â	Gap between the raceway groove curvature centers [m]
θ	Bearing misalignment angle [°]
b	Half contact width in across the rolling direction [m]
C_L	Load dependent parameter [/]
d_m	Bearing pitch diameter [m]
F_a	Axial force [N]
F_r	Applied radial load [N]
$h_{g,\hat{a}}$	Film thickness at vibration acceleration $\hat{a}$ [m]
k	Stiffness [$N\,m^{-1}$]
K_n	Load–deflection factor [$Nm^{-1.5}$]
M	Applied Moment [Nm]
m	Unbalancing mass [kg]
N	Speed [rpm]
R_i	Centers of the inner-ring raceway groove curvature radii [m]
t	Time [s]
u_s	Entrainment velocity [m/s]
u_{res}	Resultant entrainment velocity [ms^{-1}]
x	Displacement [m]

squeeze effect, can have an impact on the (fully flooded) film thickness in the contact. Glovnea and Zhang developed an analytical model for the change in fully flooded film thickness due to load variations [24]. Later, Zhang et al. [30] developed an improved semi-analytical method and numerical method to describe this phenomenon, and showed that the larger the load amplitude, the larger the deviation of film thickness from the steady-state value.

Experiments on a ball-on-disk machine, lubricated with oil, revealed that when the contact is subjected to oscillatory rolling motion, high frequencies raise the starvation level, thereby impacting the central film thickness [31]. When the contact is subjected to lateral vibrations, Kalogiannis et al. observed that film thickness perturbations occur only at high lateral frequencies and low main entrainment velocities [26]. At lower lateral frequencies and higher main entrainment velocities, film thickness variation is not significant. This derives directly from the *resultant* entrainment velocity which is the vector sum of the main entrainment velocity and the lateral velocity [23,26]: the impact of lateral vibrations—indicated by the lateral velocity (or frequency)—on resultant entrainment velocity is expectedly low when the main velocity is significantly higher. In addition, an experimental study by Fryzs et al. [23] and a numerical study by A. Félix Quiñonez [32] showed that there would be fluctuations in the film thickness within the central region at higher lateral vibration frequencies.

Recently, Nagata et al. [33] and Kalogianni et al. [26] studied the effect of vibration on the film thickness in a ball-on-disk machine lubricated with grease by inducing lateral motion between the ball and the plate. They found a significant increase in film thickness due to the imposed vibrations. During the lateral vibrations, grease from the side band is pushed/taken back onto the track, replenishing the contacts. The authors stated that "Because many grease-lubricated machine elements experience vibrations during their operation, it is possible that these vibrations play a positive role in the lubrication mechanisms" [33]. Their study was constrained to a fixed stroke length (355 μm) and a vibration frequency of 10 Hz.

It is evident that much has been done on oil-lubricated EHL contacts in fully flooded conditions. In this article, we will show the result of a study on the influence of vibrations on the film thickness in a grease-lubricated deep groove ball bearing, under starved lubrication conditions.

Table 1
Properties of the base oil and thickener content of the grease used in this study.

Property	LiM-100-2.5
Kinematic viscosity @ 40 °C (cSt)	102.8
Kinematic viscosity @ 100 °C (cSt)	10.31
Density @ 15 °C (g/cm^3)	0.891
Pressure–viscosity coeff. @ 40 °C (GPa^{-1})	31.8
Thickener content (% mass)	13

2. Materials and methods

2.1. Grease

A lithium-thickened grease, denoted as "LiM-100-2.5 grease", is selected for this study. It has a base oil viscosity of 100 cSt at 40 °C and a consistency of NLGI grade 2.5. Detailed properties are described in Table 1.

2.2. Measuring film thickness in deep groove ball bearings (DGBB)

The film thickness in the bearing contacts is measured on a new in-house built bearing test rig. A sectional view of the test rig is shown in Fig. 1 identifying various salient parts. The film thickness is measured using a device called "Lubcheck MK3" developed by Heemskerk et al. [34]. It uses an electrical capacitance method to measure the film thickness in an electrically isolated test bearing loaded on a shaft supported by two hybrid bearings (bearings with ceramic balls and steel rings). The inner ring which rotates with the shaft is connected to the Lubcheck device via a mercury contact, while the stationary outer ring is directly connected with a wire. The detailed procedure to convert measured capacitance into film thickness including the effect of starvation is described in our previous paper [7]. An encoder is used to measure the shaft rotation speed which can reach 15000 rpm. The axial and radial loads are applied using a pneumatic bellow and a pneumatic cylinder, respectively, with load cells attached to measure the applied load. Although this test rig can support both radial and axial loads, only axial load is used in the present study. The temperature of the outer ring is measured using a thermocouple. An electrically insulating but thermally conductive gel is used to electrically isolate the bearing from the thermocouple. The temperature of the test bearing can be controlled by forcing air around the test bearing using an air duct, as shown in Fig. 10. In our setup, the bearing temperature can be controlled to a minimum value of approximately 40 °C by using laboratory air at room temperature and high flow rates; and to a maximum value of 120 °C by first heating up the laboratory air.

In this study, all the experiments are conducted on an SKF 6209 bearing with C3 clearance, filled with LiM-100-2.5 grease up to 30% of the bearing's free volume. The test loads are 513 N and 900 N axial loads (dimensionless load $C/P = 34$ and $C/P = 21.8$, respectively), yielding contact pressures of 0.972 GPa and 1.28 GPa, respectively,

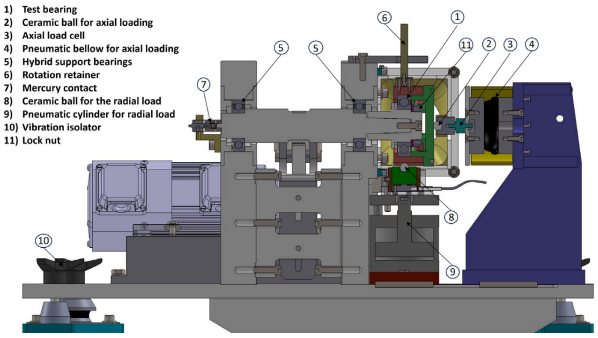

Fig. 1. Side sectional view of the test rig. See Appendix A for a three-dimensional view.

between the inner ring and each ball. The bearing initially runs at 4000 rpm and 513 N for 100 h to complete grease churning. The end of grease churning and start of grease bleeding phase is identified using the bearing's instantaneous self-induced temperature and film thickness profiles. This study focuses on the film thickness in the bleeding phase where the bearing operates for most of its service life.

All the film thickness measurements are performed in the post-churning phase at a temperature of 61 °C for 10–15 min. Film thickness reaches a stable value within 1–2 min after the initial transient effects [8]. The time average of the stable film thickness is considered in the analysis. All the experiments herein are repeated at least twice and average values are used. The plotted error bars represent the standard deviations of the measurements.

2.3. Inducing and measuring vibrations

Vibration in a rotating shaft-bearing assembly with unbalancing mass m, modeled using a spring–mass–damper system, is governed by $\hat{M}\ddot{x} + \lambda\dot{x} + kx = me\omega^2 \sin(\omega t)$, where $\hat{M}$ is the total mass of the system, x is the displacement, λ is the damping coefficient, k is the spring stiffness coefficient, m is the rotating unbalance mass, e is the eccentricity (i.e., distance between the center of rotation and center of the mass m), ω is the angular velocity and t is time. The right-hand side of the equation represents the force due to the rotating unbalance and the left-hand side of the equation represents the dynamic response of the system [35]. Here, we induce two different levels of vibrations by adding two different unbalancing masses to the lock-nut of the shaft-bearing assembly. An accelerometer to measure the vibration of the test bearing is mounted horizontally via a magnet on the test bearing housing. The initial/reference condition without any additional mass is labeled 'm_0', and conditions with unbalance masses added are denoted by 'm_1' and 'm_2'. The unbalancing force generated depends on the speed, eccentricity and mass. Here, the unbalancing force is estimated at 4000 rpm. The lock nut radius is taken as the eccentric distance for the calculation. The resulting forces for $m_1 = 0.44g$ and $m_2 = 0.84g$ are 2.2 N and 4.2 N, respectively.

Due to signal interference between the accelerometer and the capacitance measurement equipment, we are unable to measure vibration acceleration and film thickness simultaneously. So, the vibration and film thickness measurements presented here are performed alternately i.e., first, we measure the vibration of the test rig under a specific condition, then remove the accelerometer from the rig and measure the film thickness capacitance on the same set-up and condition, before changing to the next operating condition.

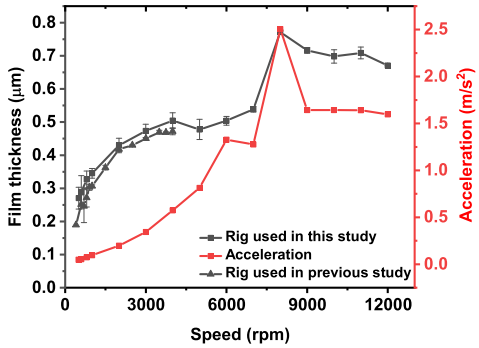

Fig. 2. Variation of film thickness (black lines) and vibration acceleration (red line) for different speeds, axial load = 513 N, Temperature = 61 °C. The results from the previous study are detailed in [7].

3. Results

Our previous study [7] showed that the film thickness is almost independent of speed in severely starved grease-lubricated contacts. Under the same conditions as the tests done in this current study, with the same grease, at a temperature of 61 °C, this negligible dependence of film thickness on speed was observed after 2500 rpm. In that (previous) study, the test rig was limited to speeds up to 4000 rpm. We subsequently built a new test rig to study the film thickness behavior at higher speeds. In this current study, film thickness is measured at speeds up to 12000 rpm (corresponding to a product of the pitch diameter of the bearing in millimeters and speed in rpm, denoted as ndm, equal to 0.8 million), under the same 513 N axial load; see Fig. 2. The film thickness values obtained on both test rigs are similar at speeds up to 4000 rpm. At higher speeds, > 6000 rpm, film thickness values unexpectedly and significantly increase.

To investigate this distinctive film thickness increase with speed, the vibration signature of the test rig is measured. The vibration is measured for one minute in the horizontal direction, and root mean square (rms) values are evaluated. Fig. 2 shows that the vibration acceleration increases with the speed, as expected. But at 8000 rpm, there is a significant increase in vibration acceleration, followed by a drop to a stable value. Vibration and film thickness appear to follow a similar pattern. To identify the possible cause of the vibration,

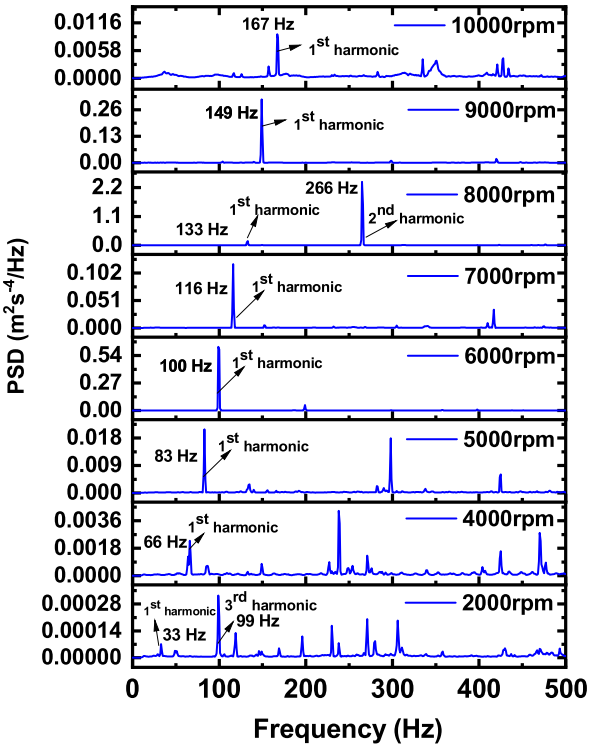

Fig. 3. Power spectral density (PSD) plots for different speeds. Axial load = 513 N. Self-induced vibrations (i.e., no unbalance mass added).

the power spectral densities (PSD) (also called acceleration spectral densities) are calculated and plotted for different speeds in Fig. 3. PSD is used to identify the dominating frequencies in a vibration signal. It describes the distribution of power in a frequency domain in the signal. Here, power is the mean square value of the vibration acceleration. The y-axis is the power normalized with the frequency bin width, making it independent of the duration of the measurements. This will facilitate comparing different measurements regardless of their measurement duration. It can be seen from Fig. 3 that, for a particular speed, the first harmonic frequency is its rotational frequency; the amplitudes of other harmonics are lower than the first dominant/fundamental frequency (except for 2000, 4000 and 8000 rpm). It is also evident from Fig. 3 that the 266 Hz peak, at a speed of 8000 rpm, has the highest amplitude in comparison with other speeds/frequencies. This 8000 rpm/266 Hz could be the speed/frequency at which the machine resonates. For 8000 rpm, the amplitude of the second harmonic is orders of magnitude higher than the first harmonic, which could be due to this resonance. It should be noted that if the subsequent harmonics are 15% lower than the first dominant frequency, the cause of vibration is likely unbalancing [36]. In our test rig, the vibration level is high enough to have an impact on the film thickness but low enough to not cause any considerable damage.

3.1. Isolating vibration effect on film thickness

Changes in the output signal from the electrical sensors can be due to actual interactions at the bearing contacts or due to electrical artifacts from interferences or other uncontrollable factors. So, we first determine the extraneous effects in the electrical signal, to properly isolate actual vibration impact on film thickness.

3.1.1. External effects outside the EHL contacts

To check whether the increase in film thickness is caused by any vibration-induced electrical effects, we measured the *background capacitance* using a hybrid bearing. The background capacitance is the total measured capacitance excluding the contribution from the EHL contact [37]. This capacitance is test rig-dependent and usually constant for all conditions [7]. Fig. 4 plots background capacitance for a speed sweep without additional mass, labeled 'Bg cap m_0', and with unbalance mass m_1, labeled 'Bg cap m_1'. The speed is varied from 0 to 12000 rpm. The background capacitance is evidently not affected by vibrations, indicating that any observed change in measured film thickness capacitance in the presence of vibrations in the bearing is therefore induced by actual changes in EHL film thickness.

Fig. 4 also shows the actual film thickness capacitance, labeled "Film cap m_0", for an all-steel bearing. This capacitance, much higher than the background capacitance, decreases with speed as expected, at low to medium speeds. Hence, we anticipate that any consistently observed changes in film thickness due to vibrations are not induced by external electrical effects, but are actual phenomena-induced variations in film thickness in the bearing's contacts.

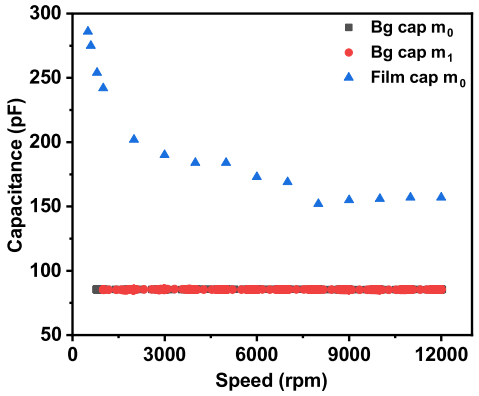

Fig. 4. Background capacitance (Bg cap) at different speeds, with and without an additional mass on the shaft. Bearing axial load = 513 N. Bg cap m_0 represents measurements under self-induced vibration (unbalance mass = 0); Bg cap m_1 represents measurements under vibration with an unbalancing mass m_1 (unbalance mass = 0.44 g). Film cap m_0 is actual film thickness capacitance measurement.

3.1.2. Vibrations-induced film thickness changes

Fig. 5(a) shows vibration acceleration versus speed for the three vibration levels studied: $\hat{a}_0$ (self-induced vibrations with no unbalance mass), $\hat{a}_1$ (vibrations including the additional impact of unbalance mass m_1) and $\hat{a}_2$ (vibrations including the additional impact of unbalance mass m_2). It is evident that each configuration yields a distinct vibration acceleration profile, with $\hat{a}_2 > \hat{a}_1 > \hat{a}_0$ (at speeds $\geq$ 2000 rpm).

Fig. 5(b) shows the film thickness profiles for the three vibration configurations. Above 1000 rpm, the film thickness under $\hat{a}_2$ vibration is the highest, followed by $\hat{a}_1$, then $\hat{a}_0$. This corresponds to $\hat{a}_2$ having the highest vibration acceleration, followed by $\hat{a}_1$, then $\hat{a}_0$, indicating the dependence of film thickness on vibration levels. The test was repeated with an axial bearing load of 900 N, showing similar results. In addition, the PSD analysis (Fig. 3) shows that until 5000 rpm, the maximum PSD amplitude is only 0.02 m^2s^{-4}, after which the amplitude increases exponentially, reaching values up to 2.5 m^2s^{-4} at 8000 rpm. This increase in vibration corresponds to an increase in measured film thickness (see Fig. 2).

3.2. Characterizing vibration effect on film thickness

In this section, we derive an equation for the film thickness $h_{g,\hat{a}}$ as a function of vibration acceleration level $\hat{a}$. This work is empirical, hence vibrations cannot be completely removed, so measuring film thickness under zero vibrations is impossible. We, therefore, define a reference film thickness ($h_{g,\hat{a}_0}$) under 'minimum vibrations', obtained here at lower speeds. Measurements for this reference are at the self-induced vibration level $\hat{a}_0$. Fig. 6 plots the normalized increase in vibration acceleration $\frac{\hat{a}-\hat{a}_0}{\hat{a}_0}$ against the normalized film thickness $\frac{h_{g,\hat{a}}}{h_{g,\hat{a}_0}}$ for axial bearing loads of 513 N and 900 N, fitting well with:

$$\frac{h_{g,\hat{a}}}{h_{g,\hat{a}_0}} = C_L \left(\frac{\hat{a}-\hat{a}_0}{\hat{a}_0} \right)^{1/5} + 1, \quad (1)$$

where C_L is a load-dependent parameter. Here, C_L = 0.3 for 513 N load and C_L = 0.15 for 900 N load, with correlation coefficient R^2 values of 0.90 and 0.73, respectively. The slopes of the initial sharp increase and the subsequent asymptotic increase in film thickness are different for both loads. These are related to the ratio of displacement (a measure of the vibration amplitude) to the contact size, which is larger for lower load. Same-amplitude vibrations cause more contact replenishment in smaller contacts, leading to thicker films, than in large contacts. Further study into the influence of load on vibration-induced film replenishment [38] is recommended.

Using Eq. (1), we can correct the measured film thicknesses for vibration effects, as shown in Fig. 7. For every speed, the vibration level $\hat{a}$ is measured and substituted into Eq. (1) to obtain the corrected value of the grease film thickness $h_{g,\hat{a}}$. We fit the curves with the measured vibration levels up to 4000 rpm and extrapolate to higher speeds to get the reference vibration acceleration $\hat{a}_0$. Vibrations at speeds $\leq$ 2000 rpm (where fully flooded condition persists) are minimal, coinciding with the reference vibrations; as such, no correction is done in that regime. Above 2000 rpm (where starved lubrication persists), the measured film thickness at 2000 rpm (0.43 μm) is used as the reference film thickness $h_{\hat{a}_0}$. Fig. 7 presents the originally measured film thickness (black plot) and the vibrations-corrected film thickness (red plot), showing a significant impact of high-speed (over 7000 rpm) vibrations on film thickness. Fig. 7 verifies previous findings that, in grease-lubricated bearings, film thickness becomes independent of speed at high speeds [5,7] (as shown by the red plot), and that vibrations can skew film thickness measurements (as shown by the black plot).

In the next section, we attempt to understand **how** vibration influences the film thickness in grease-lubricated bearings. We will discuss possible mechanisms behind this phenomenon and examine which mechanism plays the most vital role.

4. Discussion

4.1. Vibrations-induced increase in film thickness

Three possible mechanisms that could increase the EHL film thickness due to vibrations have been proposed in the literature. These were briefly discussed in the above *Introduction* section. In this section, we analyze our measurements based on all three theories and identify the most relevant.

4.1.1. Change in resultant entrainment velocity

In the presence of lateral vibrations, the resultant entrainment velocity u_{res} is the vector sum of the main entrainment velocity u_s and the lateral velocity v, i.e., $u_{res} = \sqrt{u_s^2 + v^2}$. In this study, the lateral velocities in the contact at various shaft speeds are estimated conservatively as time integrals of the measured vibration accelerations, and the rms values of the velocities are used for subsequent calculations. Results show that lateral velocities (v) due to vibration are four magnitude orders lower than the main entrainment velocities u_s, having negligible impact on the resultant contact entrainment velocities, similar to the observations by Kalogiannis et al. [26] for low lateral frequencies. Therefore, in our study, increase in entrainment velocity is not the active mechanism responsible for the higher film thickness due to vibrations.

4.1.2. High-frequency fluctuations in contact force

Vibrations can also exert an additional force on the contacts. The film thickness in an EHL regime is mainly determined by the inlet conditions at the contact. Rapid changes in loads impact contact dimensions. When the contact edge moves against the lubricant entrainment direction, the lubricant advances towards the contact at a relative velocity given by the sum of the main entrainment velocity and the rate of change of contact dimension. The resultant entrainment velocity is higher than the main entrainment velocity. When high enough, it may increase the film thickness. We estimate the contribution of this mechanism to film thickness replenishment using the analytical model developed by Glovnea and Zhang [24,30]. For an unbalancing load of 4.27 N (resulting from the added mass m_2 at 4000 rpm), the predicted change in film thickness is 1%. Hence, the rate of contact load fluctuations due to vibrations does not contribute considerably to the observed increase in film thickness.

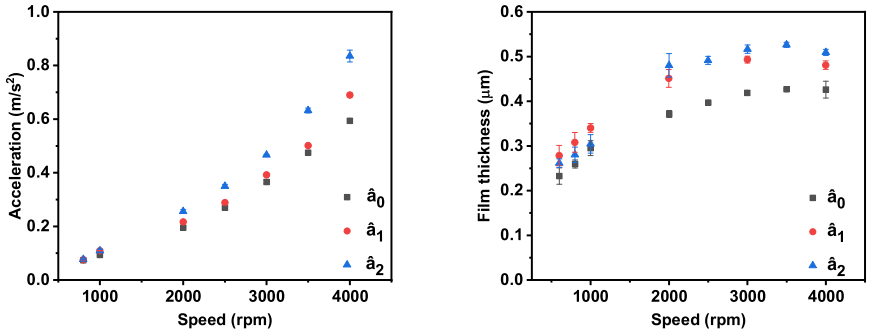

Fig. 5. (a) Vibration measurement showing the difference in vibration acceleration for the three different configurations. $\hat{a}_0$, $\hat{a}_1$ and $\hat{a}_2$ correspond to the accelerations induced by m_0, m_1 and m_2, respectively. (b) Variation of film thickness with speed, under different vibrating conditions. Axial bearing load = 513 N, Grease:LiM-100-2.5.

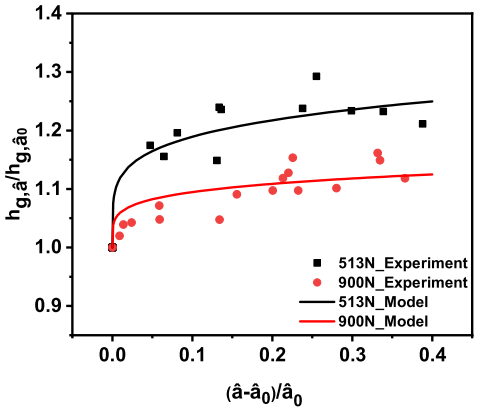

Fig. 6. Variation of normalized film thickness with relative increase in vibration acceleration, under accelerations $\hat{a}_0$, $\hat{a}_1$, and $\hat{a}_2$ and various speeds. Axial bearing load = 513 N and 900 N.

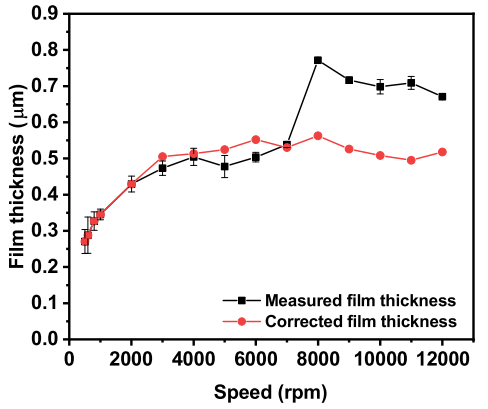

Fig. 7. Corrected and measured film thickness variation with speed, under different vibrating conditions. Axial bearing load = 513 N.

4.1.3. Shift in ball-ring contact position

Nagata et al. [33] showed that in grease-lubricated point contacts, the film thickness is higher when lateral vibrations are present. The lateral motion of the ball facilitates contact replenishment by pushing the grease ridges formed by side flow in/around the EHL region of the preceding contact back into the track. A similar phenomenon is probable in a full bearing. By double integrating the measured vibration acceleration with respect to time, we estimate the lateral displacement of the outer ring. Fig. 8 plots this axial displacement (red plot) and the (uncorrected) measured film thickness versus speed (black plot). At low to medium shaft speeds, the displacement increases monotonously with speed, roughly correlating with film thickness. At high speeds (≥8000 rpm), the displacement varies directly as film thickness, decreasing with speed. Even though the applied load is axial, due to misalignment/unbalancing, a small component of the load acts radially on the bearings. To balance this additional time-varying radial force, the bearing ring moves axially due to a shift in contact angle. The sudden increase in film thickness after 7000 rpm is possibly due to significant increase in the lateral displacement. This effect, a function of the ratio of displacement to contact size, will facilitate high replenishment. Fig. 6 shows that vibrations have higher impact under lower loads (hence, for smaller contacts). The center of a wider contact is harder to replenish. Note that the displacement (in Fig. 8) obtained from the measured vibration acceleration includes effects from other parts of the rig, such as support bearings and bearing housings. Hence, this estimated displacement is a qualitative measure of the ball-ring contact movement.

To further verify this mechanism, we estimate *quantitatively* the displacement due to the unbalance masses, using a system of equations proposed by Harris and Kotzalas [39,40]. The results are shown in Fig. 9 and the details of this analysis are presented in Appendix B. In Fig. 9, the radial loads due to unbalance are plotted with blue lines and the resulting contact displacements at the highest loaded contact are represented with red lines. The displacement amplitudes are 4.21 μm and 8.06 μm for the 2.24 N and 4.27 N loads, respectively.

It appears that due to additional forces caused by vibrations, the contact angle fluctuates, continuously displacing the ball-ring contacts

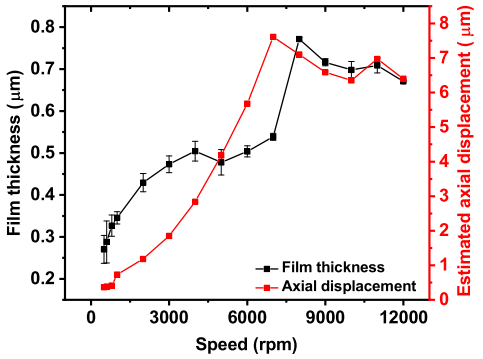

Fig. 8. Film thickness (left axis) and estimated axial displacement (right axis) as functions of speed. Axial bearing load (static) = 513 N.

along a curvilinear path (see Appendix B for more). As this occurs, the ball rolls over the ridges created by the preceding contacts and drags the lubricant towards the center of the contact causing higher film thickness, similar to the observation by Nagata et al. [33] on a ball-on-disk machine.

5. Summary, conclusions, and recommendations

Our newly developed test rig showed quite a distinct rise in film thickness at speeds around 8000 rpm for SKF 6209 DGBB (grease lubricated and axially loaded with two different loads) running in starved conditions. Vibrations measured with a horizontally mounted accelerometer showed a clear correlation between the unexpected increase in film thickness and level of vibration. To further investigate this, additional unbalancing forces were generated with two different masses attached to the lock-nut, in order to quantify the change in film thickness, up to 4000 rpm shaft speed. Then, an empirical model was developed to correlate the relative increase in the film thickness with the relative increase in acceleration for two different axial loads. The model was used to correct the measured film thickness at shaft speeds up to 12000 rpm, corresponding to 0.8 million ndm in the SKF 6209 bearing used here. This led to the following findings:

- An increase in the vibration acceleration shows a clear increase in the starved film thickness.
- This increase in starved film thickness is not due to changes in resultant entrainment velocity, because the lateral velocities caused by the vibrations are four orders of magnitude lower than the main entrainment velocity. The same argument holds for fluctuations in the contact force, which are too small to have considerable effect.
- A model to estimate the lateral displacements due to the unbalancing forces shows that these displacements could reach values up to 8 μm (for our conditions), which is potentially enough to replenish the contacts by pulling grease and/or oil from the side of the track into the contacts (when the ball rolls over the ridges formed by the preceding ball).
- After correcting the measured film thickness with the derived *film thickness-vibration level* empirical relationship, results show that the (corrected) film thickness is almost independent of speed above 2000 rpm, further verifying observations previously reported in our earlier work and other studies.

Some recommendations for future experiments to better understand vibrations-induced film thickness changes:

- Perform ball-on-disk measurements similar to Nagata et al. [33] but with an oil/grease layer and a very small oscillation amplitude.
- Measure the actual displacement between the inner and outer ring of the test bearing using a laser vibrometer to obtain a directly measured relative displacement. An additional advantage here is that the film thickness and displacement can be measured simultaneously, because the laser does not interfere with the capacitative film thickness measurement.

CRediT authorship contribution statement

Pramod Shetty: Writing – original draft, Validation, Methodology, Formal analysis, Data curation, Conceptualization. **Robert Jan Meijer:** Writing – review & editing, Supervision, Methodology, Conceptualization. **Jude A. Osara:** Writing – review & editing, Supervision, Methodology, Conceptualization. **Rihard Pasaribu:** Writing – review & editing, Supervision, Methodology, Funding acquisition, Conceptualization. **Piet M. Lugt:** Writing – review & editing, Supervision, Methodology, Funding acquisition, Conceptualization.

Declaration of competing interest

The authors declare that they have no known competing financial interests or personal relationships that could have appeared to influence the work reported in this paper.

Data availability

Data will be made available on request.

Acknowledgments

We thank SKF Research and Technology Development and Shell Downstream Services International B.V for funding this work and approving this publication. We also thank Dr. Norbert F. Bader for the insightful discussions during the study.

Appendix A

Fig. 10 shows the three-dimensional CAD of the film thickness measurement test rig used in this study.

Appendix B

Here, we analytically quantify the lateral motion induced by the unbalancing masses, as a second verification of the impact of this mechanism on film thickness replenishment. See Fig. 9 for the analysis results.

The natural misalignment/unbalance in the shaft is used as the reference. In this analysis, the radial forces emanate from the unbalancing masses m_1 and m_2 only. Due to this additional radial force along with the applied axial load, three parameters change: (a) relative axial displacement of the rings, (b) contact angle, and (c) contact width. When radial and axial loads are applied to a ball bearing, the ring-ball contact deforms and the relative displacements of the inner and outer raceways are defined by relative axial displacement δ_a, radial displacement δ_r, angular displacement θ, and contact angle β, all of which can be obtained by numerically solving Eqs. (2)–(5)—proposed by Harris and Kotzalas [39,40]. More information can be found in [39,40].

Axial force

$$F_a = -K_n \hat{A}^{1.5} \sum_{\psi=0}^{\psi=\pm\pi} \times \frac{\left\{\left[(\sin\beta_0 + \bar{\delta}_a + R_i\bar{\theta}\cos\psi)^2 + (\cos\beta_0 + \bar{\delta}_r\cos\psi)^2\right]^{0.5} - 1\right\}^{1.5} (\sin\beta_0 + \bar{\delta}_a + R_i\bar{\theta}\cos\psi)}{\left[(\sin\beta_0 + \bar{\delta}_a + R_i\bar{\theta}\cos\psi)^2 + (\cos\beta_0 + \bar{\delta}_r\cos\psi)^2\right]^{0.5}} \quad (2)$$

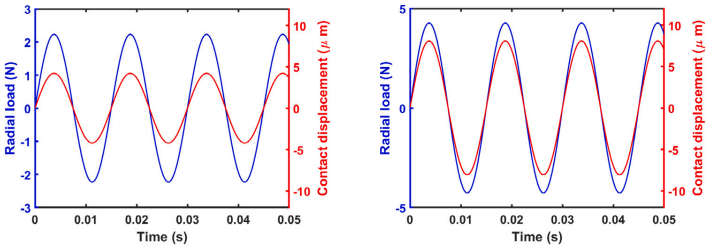

Fig. 9. Cyclic radial loads and resulting shifts in contact due to unbalancing mass (a) m_1 with unbalancing force amplitude of 2.24 N, and (b) m_2 with unbalancing force amplitude of 4.27 N. Axial bearing load (static) = 513 N.

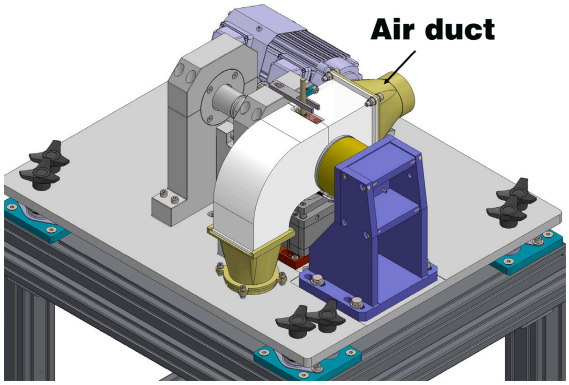

Fig. 10. Isometric view of the test rig showing air duct for temperature control.

$$M = -\frac{d_m}{2} K_n \hat{A}^{1.5} \sum_{\psi=0}^{\psi=\pm\pi} \frac{\left\{[(\sin\beta_0 + \bar{\delta_a} + R_i\bar{\theta}\cos\psi)^2 + (\cos\beta_0 + \bar{\delta_r}\cos\psi)^2]^{0.5} - 1\right\}^{1.5} (\sin\beta_0 + \delta_a + R_i\bar{\theta}\cos\psi)\cos\psi}{[(\sin\beta_0 + \bar{\delta_a} + R_i\bar{\theta}\cos\psi)^2 + (\cos\beta_0 + \bar{\delta_r}\cos\psi)^2]^{0.5}} \tag{4}$$

Box I.

Radial force

$$F_r = -K_n \hat{A}^{1.5} \sum_{\psi=0}^{\psi=\pm\pi} \times \frac{\left\{[(\sin\beta_0 + \bar{\delta_a} + R_i\bar{\theta}\cos\psi)^2 + (\cos\beta_0 + \bar{\delta_r}\cos\psi)^2]^{0.5} - 1\right\}^{1.5} (\cos\beta_0 + \bar{\delta_r}\cos\psi)\cos\psi}{[(\sin\beta_0 + \bar{\delta_a} + R_i\bar{\theta}\cos\psi)^2 + (\cos\beta_0 + \bar{\delta_r}\cos\psi)^2]^{0.5}} \tag{3}$$

Angular displacement is given in Box I.

Contact angle

$$\beta = \cos^{-1} \frac{\cos\beta_0 + \bar{\delta_r}\cos\psi}{[(\sin\beta_0 + \bar{\delta_a} + R_i\bar{\theta}\cos\psi)^2 + (\cos\beta_0 + \bar{\delta_r}\cos\psi)^2]^{0.5}} \tag{5}$$

When bearing loads are both radial and axial (here, the radial load is due to unbalance and the axial load is the applied load), the load distribution along the circumference of the bearing will not be uniform. Calculations are here performed for the highest-loaded ball.

When the radial load varies over time due to unbalance, the contact angle β—the angle formed between the line that passes through the center of the ball-ring contact and an axis perpendicular to the bearing rotational axis—will change correspondingly as the contact rotates along the ring interfaces. See Fig. 11. The motion of the balls along the curved path on the grooves, transverse to the rolling direction, i.e., the curvilinear displacement, is given by $2\pi r_o \Delta\beta/360$, where $\Delta\beta$ represents the change in contact angle due to unbalance only, and r_o is the outer ring groove radius.

Using these equations, we estimate the contact displacements for the 2.24 N and 4.27 N unbalancing force conditions resulting from the m_1 and m_2 masses added to the shaft. The axial force used is 513 N and the shaft speed is 4000 rpm. The radial force varies sinusoidally with time at a frequency equal to $2\pi N/60$.

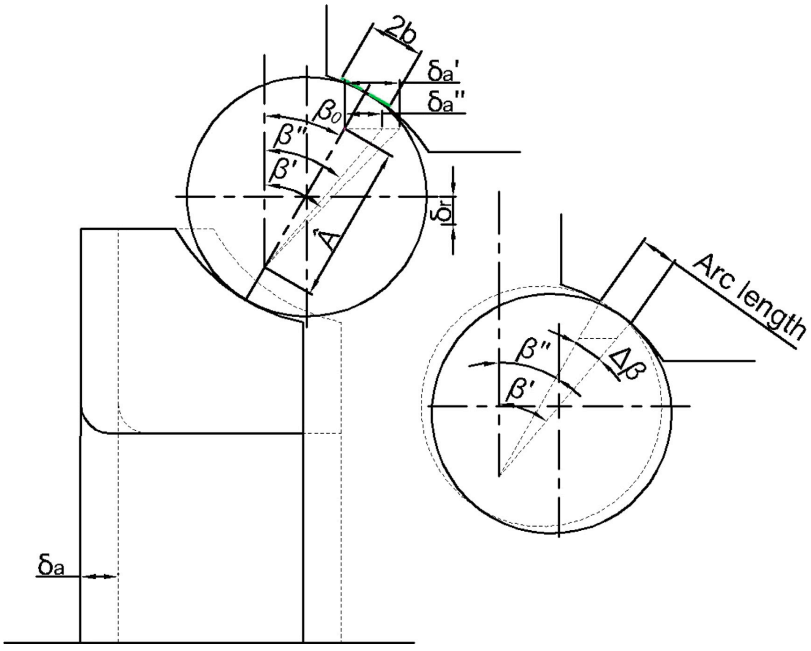

Fig. 11. Contact geometry showing the axial and radial displacements and the resulting curvilinear transverse displacement (arc length) at the contact.

References

[1] Cann P, Damiens B, Lubrecht A. The transition between fully flooded and starved regimes in EHL. Tribol Int 2004;37(10):859–64.

[2] Cann P, Chevalier F, Lubrecht A. Track depletion and replenishment in a grease lubricated point contact: A quantitative analysis. In: Tribology series, vol. 32. Elsevier; 1997, p. 405–13.

[3] Cann P, Lubrecht A. An analysis of the mechanisms of grease lubrication in rolling element bearings. Lubr Sci 1999;11(3):227–45.

[4] Cann P, Doner J, Webster M, Wikstrom V. Grease degradation in rolling element bearings. Tribol Trans 2001;44(3):399–404.

[5] Cen H, Lugt PM. Replenishment of the EHL contacts in a grease lubricated ball bearing. Tribol Int 2020;146:106064.

[6] Gershuni L, Larson MG, Lugt PM. Lubricant replenishment in rolling bearing contacts. Tribol Trans 2008;51(5):643–51.

[7] Shetty P, Meijer RJ, Osara JA, Lugt PM. Measuring film thickness in starved grease-lubricated ball bearings: An improved electrical capacitance method. Tribol Trans 2022;65(5):869–79.

[8] Shetty P, Meijer RJ, Osara JA, Pasaribu R, Lugt PM. Effect of grease filling on the film thickness in deep groove ball bearings. Tribol Trans 2023;1–12, published online.

[9] Nogi T. An analysis of starved EHL point contacts with reflow. Tribol Online 2015;10(1):64–75.

[10] Fischer D, von Goeldel S, Jacobs G, Stratmann A, König F. Investigation of lubricant supply in rolling point contacts under starved conditions using CFD simulations. In: IOP conference series: Materials science and engineering, vol. 1097, no. 1. IOP Publishing; 2021, 012007.

[11] Zhang S, Jacobs G, von Goeldel S, Vafaei S, König F. Prediction of film thickness in starved EHL point contacts using two-phase flow CFD model. Tribol Int 2023;178:108103.

[12] Nogi T, Shiomi H, Matsuoka N. Starved elastohydrodynamic lubrication with reflow in elliptical contacts. J Tribol 2018;140(1):011501.

[13] Nogi T. Film thickness and rolling resistance in starved elastohydrodynamic lubrication of point contacts with reflow. J Tribol 2015;137(4):041502.

[14] Cann P, Lubrecht A. Bearing performance limits with grease lubrication: the interaction of bearing design, operating conditions and grease properties. J Phys D: Appl Phys 2007;40(18):5446.

[15] Wensing JA. On the dynamics of ball bearings. University of Twente; 1998.

[16] Tandon N, Choudhury A. A review of vibration and acoustic measurement methods for the detection of defects in rolling element bearings. Tribol Int 1999;32(8):469–80.

[17] Cupu D, Stratmann A, Jacobs G. Analysis of transient elastohydrodynamic lubrication of point contact subjected to sinusoidal dynamic loads. In: IOP conference series: Materials science and engineering, vol. 539, no. 1. IOP Publishing; 2019, 012030.

[18] SKF. SKF general catalogue 5000/i EN. 2003, p. 87.

[19] Lacey SJ. An overview of bearing vibration analysis. Maint Asset Manag 2008;23(6):32–42.

[20] Bal H, Aktürk N. Vibration modeling of wind turbine shaft as rigid shaft supported by EHL contact ball bearings with overhung disc system. Tribol Int 2020;151:106481.

[21] Akturk N. Dynamics of a rigid shaft supported by angular contact ball bearings. Imperial College London (University of London); 1993.

[22] Harsha SP. Non-linear dynamic response of a balanced rotor supported on rolling element bearings. Mech Syst Signal Process 2005;19(3):551–78.

[23] Fryza J, Sperka P, Krupka I, Hartl M. Effects of lateral harmonic vibrations on film thickness in EHL point contacts. Tribol Int 2018;117:236–49.

[24] Glovnea R, Zhang X. Elastohydrodynamic films under periodic load variation: an experimental and theoretical approach. Tribol Lett 2018;66(3):116.

[25] Kalogiannis K, Mares C, Glovnea RP, Ioannides S. Elastohydrodynamic film thickness response to harmonic vibrations. In: International multi-conference on engineering and technological innovation. 2008.

[26] Kalogiannis K. Behaviour of elastohydrodynamic films subjected to oscillatory motion [Ph.D. thesis, Doctoral dissertation], University of Sussex United Kingdom; 2013.

[27] Ai X, Cheng HS. The influence of moving dent on point EHL contacts. Tribol Trans 1994;37(2):323–35.

[28] Venner C, Lubrecht A. Numerical simulation of waviness in a circular EHL contact, under rolling/sliding. In: Tribology series, vol. 30. Elsevier; 1995, p. 259–72.

[29] Félix-Quiñonez A, Morales-Espejel GE. Film thickness fluctuations in time-varying normal loading of rolling elastohydrodynamically lubricated contacts. Proc Inst Mech Eng C 2010;224(12):2559–67.

[30] Zhang X, Glovnea R, Morales-Espejel GE, Félix-Quiñonez A. The effect of working parameters upon elastohydrodynamic film thickness under periodic load variation. Tribol Lett 2020;68:1–10.

[31] Nishikawa H, Handa K, Kaneta M. Behavior of EHL films in reciprocating motion. JSME Int J C 1995;38(3):558–67.
[32] Quiñonez AF. Numerical analysis of transverse reciprocating velocity effects in EHL point contacts. Tribol Int 2018;126:1–8.
[33] Nagata Y, Kalogiannis K, Glovnea R. Track replenishment by lateral vibrations in grease-lubricated EHD contacts. Tribol Trans 2012;55(1):91–8.
[34] Heemskerk R, Vermeiren K, Dolfsma H. Measurement of lubrication condition in rolling element bearings. ASLE Trans 1982;25(4):519–27.
[35] Rao SS. Mechanical vibrations. John Wiley and Sons; 2001.
[36] Mais J. Spectrum analysis: the key features of analyzing spectra. SKF USA, Inc; 2002, p. 11.
[37] Jablonka K, Glovnea R, Bongaerts J. Evaluation of EHD films by electrical capacitance. J Phys D Appl Phys 2012;45(38):385301.
[38] Cen H, Lugt PM. Effect of start-stop motion on contact replenishment in a grease lubricated deep groove ball bearing. Tribol Int 2021;157:106882.
[39] Harris TA, Kotzalas MN. Advanced concepts of bearing technology. CRC Press; 2006.
[40] Harris TA, Kotzalas M. Rolling bearing analysis. fourth ed.. USA: A Wiley-Interscience publication; 2001.

APPENDIX D

Tribology International 197 (2024) 109748

Contents lists available at ScienceDirect

Tribology International

journal homepage: www.elsevier.com/locate/triboint

Full Length Article

Effect of bearing size on film thickness in grease-lubricated axially loaded deep groove ball bearings

Pramod Shetty [a,*], Robert Jan Meijer [a], Jude A. Osara [a], Rihard Pasaribu [b], Piet M. Lugt [a,c]

[a] Engineering Technology, University of Twente, The Netherlands
[b] Shell Downstream Services International B.V, The Netherlands
[c] SKF Research and Technology Development, The Netherlands

ARTICLE INFO

Keywords:
Grease
Film thickness
Elastohydrodynamic lubrication
Electrical capacitance method
Deep groove ball bearing
Bearing size

ABSTRACT

Estimating the film thickness in a grease lubricated bearing in the post-churning phase is complex because of the prevalent starved lubrication conditions. In our earlier work, we showed that the relative film thickness (h_g/h_{ff}) in an axially loaded 6209 deep groove ball bearing (DGBB) depends on the product of viscosity, load and linear speed (ηbu). In this article, we present the results of experiments performed using bearings of different sizes – 6204, 6206, 6209 – and show that the relative film thickness maintains a power-law relationship with ηbu, independent of the bearing size.

1. Introduction

Grease-lubricated bearings operate under starved lubrication conditions during most of the operational period. Determining the film thickness during this period facilitates optimization of operating parameters and selection of the right lubricant to prevent failures caused by seizure.

Models to predict film thickness under starved lubrication conditions have been proposed by Wedeven et al. [1], Hamrock and Dowson [2], Damiens et al. [3], and Van Zoelen et al. [4]. These models require either the meniscus distance from the center of the contact or the oil layer thickness on the track. These values are impossible to obtain in full bearings, making these models directly inapplicable to an industrial bearing. Accurate prediction of film thickness in a grease-lubricated bearing under various conditions remains a paramount need in the bearing and lubricants industry.

The film thickness in deep groove ball bearings has been shown to depend on temperature, load, speed and base oil viscosity during the post-churning phase [5–7]. If these parameters are held constant, film thickness is observed to reach a pseudo-steady state condition within a few minutes [6,8]. During this stage, we can measure the film thickness and study various replenishment and loss mechanisms contributing to the film build-up. Jacod et al. [9] and Gershuni et al. [10] identified that the replenishment due to local capillary forces is more significant than the out-of-contact reflow between the successive over-rollings. Ball-on-disc studies and computational fluid dynamics (CFD) simulations by Nogi [11,12] and Fischer et al. [13] considered the reflow of the lubricant back to the contact. They showed that starved film thickness is a function of capillary number, oil layer thickness, and fully flooded film thickness.

Based on ball-on-disc experiments, Cann et al. [14] proposed a non-dimensional parameter named "SD parameter" with which film thickness can be predicted. The SD parameter is the ratio of the product of dynamic viscosity η, half contact width b, and linear speed u to the product of surface tension σ and oil height h_∞ (i.e., $SD = \eta bu/\sigma h_\infty$). This parameter follows a power law relationship with the relative film thickness, the ratio of measured grease film thickness h_g to the calculated (fully flooded) base oil film thickness h_{ff}. Cen and Lugt [5] showed that, in the early post-churning phase of bearing operation, a similar relationship can also be obtained for a deep groove ball bearing. For multiple greases and operating conditions, they demonstrated a power law relationship between the relative film thickness (h_g/h_{ff}) and the product (ηbu) of dynamic viscosity η, half contact width b, and linear speed u. They recognized that the surface tension σ of the commonly used oils in greases does not vary much and therefore omitted this. The oil height h_∞ was kept constant in [14], so was also omitted. Their ηbu concept describes the effect of grease type (base oil viscosity), number of rolling elements, speed, and load very well. However, their study was restricted to a 6209 bearing, hence the effect of bearing size on film thickness remains unknown.

Cann and Lubrecht [15] suggested that contact replenishment is more difficult in larger bearings because of the larger distance between the grease reservoir and the contacts. Conversely, the replenishment

* Corresponding author.
E-mail address: p.shetty@utwente.nl (P. Shetty).

https://doi.org/10.1016/j.triboint.2024.109748
Received 25 February 2024; Received in revised form 24 April 2024; Accepted 6 May 2024
Available online 8 May 2024

Nomenclature

β	Temperature-viscosity coefficient [1/°C]
$\dot{\gamma}$	Shear rate [s^{-1}]
η	Dynamic viscosity [Pa s]
κ	Ellipticity ratio [/]
ω_i	Inner race angular velocity [rad s^{-1}]
$\rho(p)$	Density at pressure p [kg m^{-3}]
ρ_0	Density at atmospheric pressure [kg m^{-3}]
σ	Surface tension [N m^{-1}]
a	Half contact along the rolling direction [m]
b	Half contact width across the rolling direction [m]
Br	Brinkman number [/]
C_T	Non-dimensional thermal correction factor [/]
d	Ball diameter [m]
h_∞	Oil layer thickness [m]
h_c	Central film thickness [m]
h_g	Grease film thickness [m]
h_{ff}	Calculated fully flooded base oil film thickness [m]
K	Thermal conductivity of the lubricant [W $m^{-1}°C^{-1}$]
ndm	Speed number [mm × min^{-1}]
p_m	Maximum Hertzian pressure [Pa]
R_i	Inner race radius [m]
SRR	Slip-to-roll ratio [/]
u	Entrainment velocity (average velocity) [m s^{-1}]

model proposed by Chiu [16] may imply that larger bearings will have more replenishment due to the larger distance between the successive balls, which increases the time available for lubricant replenishment between the contacts. Recently, it was found that the conformity in the bearing contact could play a role in replenishment [17]: the contact with lower conformity showed higher film thickness due to higher induced capillary action. However, this conformity does not change significantly with bearing size. Damiens et al. [18] showed that reducing cage clearance (which typically depends on bearing size) helps in redistributing the grease and increases the film thickness. The effects of centrifugal forces on lubricant loss and supply also depend on the bearing size [19,20]. In this study, we investigate whether the power law relationship between h_g/h_{ff} and ηbu holds for different bearing sizes, doing film thickness measurements with again varying speeds, load, and different greases. By studying the film thickness in differently sized bearings, we can better understand the effect of dimension and geometry on lubricant film formation, replenishment and loss at the bearing contacts.

2. Materials and methods

2.1. Lubricant grease

Two Lithium-thickened greases with mineral oil as the base oil were used in this study. The grease denoted as 'LiM-100-2.5' has a base oil viscosity of 100 cSt at 40 °C and consistency of NLGI grade 2.5. The grease named 'LiM-460-3' has a base oil viscosity of 474.5 cSt at 40 °C and a consistency of NLGI grade 3. More information about these greases is provided in Table 1.

Table 1
Properties of the base oils and thickener contents of the greases used.

Property	LiM-100-2.5	LiM-460-3
Kinematic viscosity @ 40 °C (cSt)	102.8	474.5
Kinematic viscosity @ 100 °C (cSt)	10.31	31.4
Density @ 15 °C (g/cm^3)	0.891	0.902
Pressure-viscosity coeff. @ 40 °C (GPa^{-1})	31.8	27.4
Thickener content (% mass)	13	17

Table 2
Dimensions of the bearings used.

Property	6204	6206	6209
Width (mm)	14	16	19
Bore diameter (mm)	20	30	45
Outside diameter (mm)	47	62	85

2.2. Film thickness measurement

Three bearing sizes are selected for this study: SKF 6204, 6206, and 6209. These are widely used bearing types used in electric motors, electric vehicles (EV), and general-purpose machines. The bearing dimensions are listed in Table 2. The film thicknesses in these bearings are measured using an electrical capacitance method. A device called 'Lubcheck MK3', developed by Heemskerk et al. [21], measures the electrical capacitance. The method to obtain the film thickness from the measured capacitance is detailed in Ref. [6]. The film thickness measurement test rig is described in our previous publication [22]. In this study, film thickness is measured under axial loads. For all the bearings and greases, 30% of the free volume of each bearing is filled with fresh grease after which it is run for more than 80–150 h to finish churning, see Appendix. The film thicknesses reported in this study are measured after the churning phase. See the Appendix for some examples of the measurements. The reported film thickness (h_g) is the inner ring-ball contact film thickness. During the film thickness measurements, the temperature of the outer ring is controlled using hot air flow around the bearing. The temperature is held at 61 ± 0.5 °C. At each set operating point, the film thickness is measured for about 10–15 min. Film thickness stabilizes within 1–2 min after each speed/load change, and the time average value after this is considered for the analysis. All the experiments here are conducted in the full film EHL regime. Measurements are repeated at least twice, and the standard deviations are plotted as error bars in the results figures below.

3. Results

3.1. 6204 bearing

Fig. 1 presents the film thickness in 6204 bearings lubricated with LiM-100-2.5 grease and LiM-460-3 grease. The bearings are tested at a shaft speed range of 1500–14 000 rpm, which results in a maximum of 0.469 million ndm (ndm is the product of speed n in rpm and pitch diameter dm in mm). The loads on the bearing lubricated with LiM-100-2.5 are 300 N, 400 N, and 500 N. These result in a contact pressure range of 1.198 GPa–1.47 GPa and a half contact width range of 0.849 mm–1.041 mm (see Table 3). These calculations are done for the inner ring-ball contacts, and the contact widths are across *'b'* and along *'a'* the running direction of the ball. Fig. 1(a) shows that, for LiM-100-2.5 grease, the film thickness increases with shaft speed up to 4000 rpm and becomes almost constant until 6000 rpm. The spike in film thickness around 8000 rpm is attributed to vibrations in the test rig [22]. After this rise, film thickness drops and again becomes almost constant. The film thickness in 6204 bearings lubricated with LiM-460-3 grease is shown in Fig. 1(b). The applied loads are 400 N, 500 N, and 600 N. The resulting contact pressures and half contact widths are shown in Table 3. Similar to the LiM-100-2.5 grease, film thickness

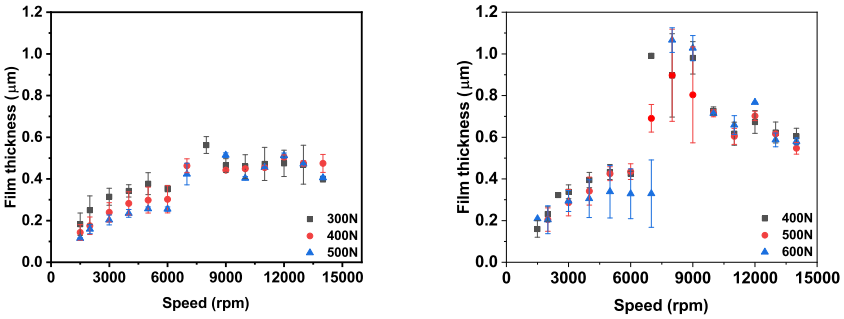

(a) Lubricated with LiM-100-2.5 grease. (b) Lubricated with LiM-460-3 grease.

Fig. 1. Variation of film thickness with speed in 6204 bearings lubricated with (a) LiM-100-2.5 grease and (b) LiM-460-3 grease.

Table 3
Bearing load, half contact widths (across (b) and along (a) the running direction, giving ellipticity ratio = 0.0748) and contact pressure for 6204 bearing inner ring-ball contact.

Load	Half contact width b (mm)	Half contact width a (mm)	Contact pressure (GPa)
300 N	0.849	0.0635	1.198
400 N	0.9246	0.0692	1.305
500 N	0.9874	0.0739	1.394
600 N	1.0413	0.0779	1.470

Table 4
Bearing load, half contact widths (across (b) and along (a) the rolling direction, giving ellipticity ratio = 0.0797) and contact pressure for 6206 bearing inner ring-ball contact.

Load	Half contact width 'b' (mm)	Half contact width 'a' (mm)	Contact pressure (GPa)
310 N	0.8547	0.0681	1.032
460 N	0.9618	0.0766	1.161
620 N	1.0503	0.0837	1.268

Table 5
Half contact widths (across (b) and along (a) the running direction, giving ellipticity ratio = 0.0779) and contact pressure for 6209 bearing inner ring-ball contact.

Load	Half contact width 'b' (mm)	Half contact width 'a' (mm)	Contact pressure (GPa)
513 N	1.0867	0.0846	0.972
700 N	1.1935	0.0930	1.067
900 N	1.2864	0.1002	1.151

initially increases with speed and becomes almost constant after 4000 rpm until a sudden rise in film thickness at 7000 rpm, followed by a peak at 8000 rpm. The film thickness obtained using LiM-460-3 grease is more transient (with speed) than that obtained from the LiM-100-2.5 grease, due to the higher viscosity of the LiM-460-3 grease. The effect of vibration appears more significant in the higher-viscosity base oil.

3.2. 6206 bearing

The film thickness measurements in 6206 bearings are presented in Fig. 2. Here, for the bearing lubricated with LiM-100-2.5 grease, the film thickness is measured until 9000 rpm, corresponding to 0.41 million ndm. For the bearing lubricated with 'LiM-460-3' grease, the film thickness is measured until 8000 rpm (0.37 million ndm). We could not measure the film thickness at higher speeds due to difficulty in holding the temperature at 61 °C. Similar to the 6204 results, film thickness initially increases with speed and becomes almost constant after 4000 rpm. A vibrations-induced spike in film thickness around 8000 rpm (for the 310 N load) can also be seen. The film thicknesses are measured with three different loads, the resulting contact pressure and contact widths are shown in the Table 4. A distinct film thickness profile for each different load can be observed for both greases. As load increases, the level of starvation increases, resulting in smaller film thickness at higher loads. The differences in measured film thicknesses for both greases are also attributed to differences in base oil properties such as viscosity. In these bearings, no drop in film thickness was observed at high speeds.

3.3. 6209 bearing

The film thickness for 6209, the largest bearing in this study, is shown in Fig. 3. The applied bearing load, half contact widths, and contact pressures at the inner ring contact are given in Table 5. Similar to 6204 and 6206 bearings, the film thickness in this bearing lubricated with LiM-100-2.5 and LiM-460-3 increases with speeds and becomes almost steady after 2000 rpm. Then the film thickness suddenly increases after 6000 rpm due to vibrations (for the LiM-100-2.5 grease, Fig. 3(a)). The bearings are tested at shaft speed range of 500 rpm–12 000 rpm. This results in 0.78 million ndm for the highest speed tested. These results show that film thickness does not drop with increasing speed in severely starved contacts. This is believed to be due to the film thickness dependence on side flow which is governed by the lubricant residence time and over-rolling frequencies. As the speed increases, these two factors potentially balance each other, making the film thickness almost constant at higher speeds [4,23].

4. Discussion

4.1. Relative film thickness

The transition to and level of starvation, measured by the relative film thickness h_g/h_{ff}, has been shown to be a function of speed, load, and viscosity. If $h_g/h_{ff} < 1$, the contacts are starved, or else, they are fully flooded. The fully flooded film thickness h_{ff} is calculated using Hamrock and Downson's equation. At higher speeds, where inlet shear heating effects become more significant, the Hamrock and Downson equation is adjusted by applying the correction factor proposed by Gupta et al. [24]:

$$C_T = \frac{1 - 13.2(p_m/E')Br^{0.42}}{1 + 0.213(1 + 2.23SRR^{0.83})Br^{0.64}} \quad (1)$$

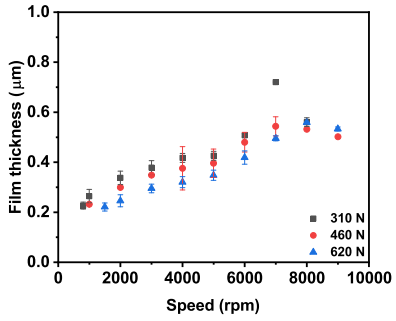

(a) Lubricated with LiM-100-2.5 grease.

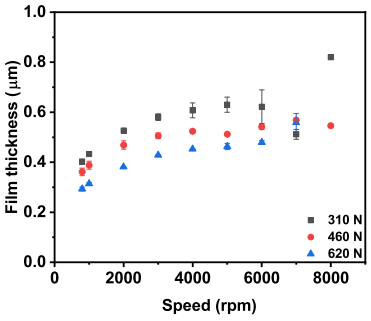

(b) Lubricated with LiM-460-3 grease.

Fig. 2. Variation of film thickness with speed in 6206 bearings lubricated with (a) LiM-100-2.5 grease and (b) LiM-460-3 grease.

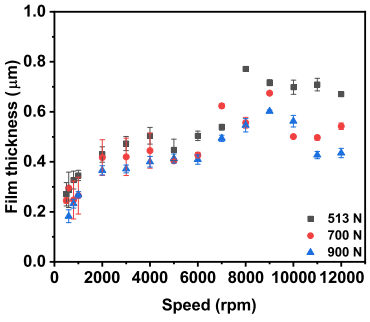

(a) Lubricated with LiM-100-2.5 grease.

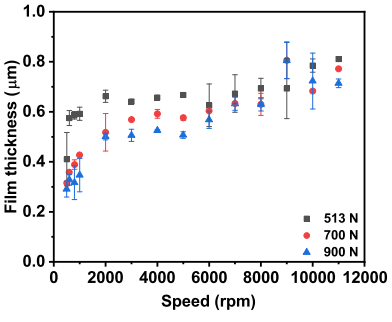

(b) Lubricated with LiM-460-3 grease.

Fig. 3. Variation of film thickness with speed in 6209 bearings lubricated with (a) LiM-100-2.5 grease and (b) LiM-460-3 grease.

where the Brinkman number is $Br \approx -\beta\eta_0 u^2/K$. Here, no slip condition is assumed, i.e., slip-to-roll ratio SRR = 0, and β is the temperature-viscosity coefficient obtained from $\eta = \eta_0 e^{-\beta(T-T_0)}$, p_m is the maximum Hertzian pressure, and K is the thermal conductivity of the lubricant. In our tests, C_T varied from approximately 0.98 to 0.63.

At low speeds, the contribution of the grease thickener could also be present in the contacts making the relative film thickness greater than 1. The film thickness after the churning phase becomes almost constant if the temperature, load, and speed are constant. This suggests a quasi-static equilibrium between the oil loss from the contact and the replenishment towards the contact. Also, we showed in our previous publication [25] that the oil layer left on the track is independent of the initial quantity of grease in the bearing, and that bleeding, therefore, does not contribute to lubricant supply to the contacts immediately after the churning phase. Following a power law equation, as found by Cen and Lugt [5], Fig. 4 plots h_g/h_{ff} vs. ηbu. All the data points – obtained from three bearing sizes and two grease types and shown in Figs. 1, 2, and 3 – are included in Fig. 4, maintaining the same power law relationship between relative film thickness and ηbu.

4.1.1. Excluding vibration effects

Some scatter can be observed at mid-range values of ηbu, particularly for the 6204 bearing–LiM-460-3 grease combination (red round points in Fig. 4). These points correspond to the vibrations-induced film thickness increase readily observed in Fig. 1(b) at shaft speeds higher than 6000 rpm. A slight shift is also seen in some points from the

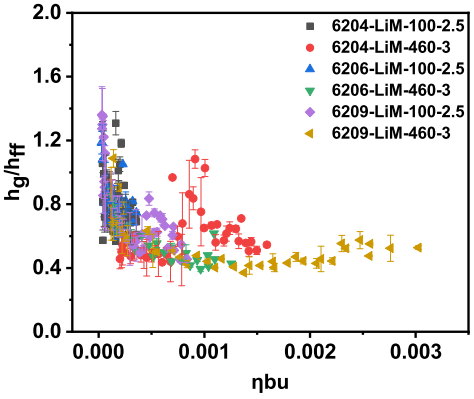

Fig. 4. Variation of relative film thickness in 6204, 6206, and 6209 bearings lubricated with LiM-100-2.5 (100 cSt) and LiM-460-3 (474 cSt) greases. Shaft speed range: 500–14 000 rpm.

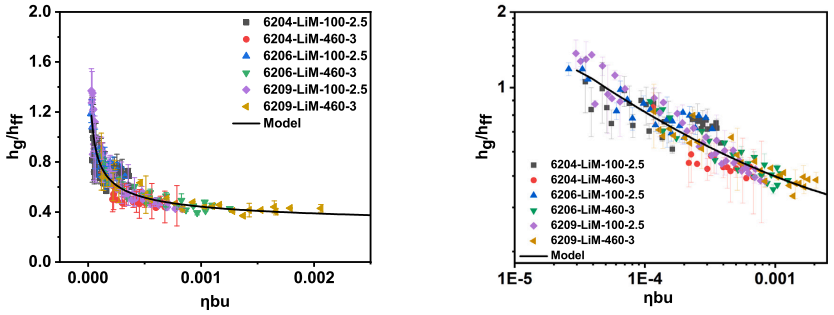

(a) Linear scale. (b) Log-log scale.

Fig. 5. Relative film thickness in 6204, 6206, and 6209 bearings lubricated with LiM-100-2.5 (100 cSt) and LiM-460-3 (460 cSt) greases.

6209 bearing–LiM-100-2.5 grease combination (purple rhombic points in Fig. 4). These correspond to the upward shift seen in Fig. 3(a) at speeds higher than 6000 rpm. Although vibration is an important film replenishment-inducing phenomenon, it is an artifact from the test rig setup, hence these points either need to be corrected [22] or removed from subsequent analysis of the h_g/h_{ff} vs. ηbu relationship.

In Ref. [22], we detailed how the vibrations in the test rig influence the film thickness. Using an empirical model, we corrected the film thickness to exclude the effects of vibrations. The corrected film thickness for 6209 bearings lubricated with LiM-100-2.5 grease and with 513 N and 900 N loads are used in this paper as well. However, in this study, vibration acceleration was not measured in other bearings, so we are unable to perform film thickness correction. Hence, in subsequent analyses, we exclude the data points described in the preceding paragraph (i.e., film thickness measurements at speeds above 6000 rpm for 6204–LiM-460-3 and 6209–LiM-100-2.5-700 N, and for 6204–LiM-100-2.5 at 7000–9000 rpm). Given we are primarily interested in identifying any bearing dimension-related parameter that could contribute to film formation and/or oil replenishment/loss, vibrations-induced artifacts are extraneous.

4.2. Bearing size and film thickness

In Fig. 5, relative film thickness is plotted against ηbu for all the three bearings tested with two greases under different loads. The power law relationship obtained by curve-fitting the data is

$$\frac{h_g}{h_{ff}} = 0.0544\ (\eta bu)^{-0.2945} \tag{2}$$

with a goodness of fit R^2 of 86.25%. It is impressive to see all three different bearings with different loads, different linear velocities, and two different greases converge on a single power law curve.

This indicates that the size of the bearing does not have an impact on the replenishment behavior in the bearing contacts.

The fully flooded film thickness h_{ff} is calculated using the Hamrock and Dowson equation where

$$h \propto u^{0.67}$$

with a correction of inlet shear heating (Eq. (1)) where the speed-dependency for somewhat higher speeds can be approximated by

$$C_T \propto u^{-0.25}$$

This gives

$$h_{ff} \propto u^{0.42} \tag{3}$$

and therefore

$$h_g \propto u^{0.12}, \tag{4}$$

showing the very weak dependency of speed at somewhat higher speeds.

Eq. (2) is not validated for extremely low speeds. For low speeds the film thickness will exceed the fully flooded "oil" film thickness but maybe only to a limited value, given by thickener deposited layers or the high viscosity of the grease at very small shear rates. The measurements in [26,27] show that h_g/h_{ff} could reach values of 1000! The fact that the transition from fully flooded to starved is again solely determined by the ηbu values strengthens the earlier conclusion from [5] that replenishment in a ball bearing is local, and bearing geometry parameters such as bearing width, and ball/groove diameter do not play a role. Cann [15] speculated that the larger bearings would have low oil replenishment because of the larger distance between the grease reservoirs and the race-ball contacts. However, since bleed evidently does not play a role in replenishing the contact in the early post-churning phase, the distance between the reservoir and the race-ball contact also does not affect the oil replenishment.

Okal et al. [17] found that the conformities of the bearing contacts – the ratios of the inner and outer race groove radii to the ball diameter – also play a role in determining the film. Each of our three bearings has different outer ring conformities. In Ref. [17] conformity varied more than in our standard bearings. Here, we do not see any influence of conformity on the film thickness.

Due to the different bearing sizes, the centrifugal effect on the lubricant flow is expectedly different but since the replenishment is similar in all the bearings, this effect appears minimal. This was also theoretically predicted by Van Zoelen et al. [23,28], who showed that the flow induced by the EHL action is more dominant than the centrifugal effects.

The film thickness in starved lubricated contacts depends mainly on the oil layer thickness on the tracks [3,14]. Van Zoelen et al. [4,23,28] showed that the oil layer thickness at the outlet of the EHL contacts, distributes equally between the rolling contacts, facilitating equal oil layer thickness in both the inner and outer rings of the bearing. The convergence of the relative film thickness in all three bearings indicates that the degree of starvation has the same dependence on the combination of viscosity, load (via the half-contact width), and speed.

Based on the equation proposed by Chevalier and Damiens, $h_\infty = \frac{h_g \rho(p)}{2\rho_0}$, which relates the film thickness h_g and the supply oil layer h_∞ near the contacts, we can estimate the thickness of the oil layer left on the track after the churning phase. Here, the measured film thickness after the churning phase h_g is taken as an input. The density $\rho(p)$ is

Table 6
Thicknesses, in μm, of the oil layers left on the track after churning.

Grease	6204	6206	6209
LiM-100-2.5	0.304	0.352	0.375
LiM-460-3	0.365	0.291	0.397

a function of pressure via the Dowson and Higginson's equation [29]. The oil layer thicknesses estimated after the churning phases for all the bearings are listed in Table 6. The approximate thicknesses of the oil layers left on the track for both the greases are slightly different for all the bearings. For the LiM-100-2.5 grease, 6209 bearing has an oil layer thickness 23% larger than 6204 bearing and about 6% larger oil layer than 6206 bearing.

5. Conclusion

The main conclusion from this work is that the relative film thickness for grease-lubricated ball bearings is a function of the product of viscosity, half contact width, and speed ηbu, a relationship that is independent of bearing size.

Additional conclusions are:

- The film thickness at very low speeds is larger than that predicted using the base oil viscosity.
- At moderate to higher speeds, film thickness becomes almost independent of speed.
- Increasing load and viscosity increases the level of starvation.
- The transition to starvation (given by $h_g/h_{ff} < 1$) can be predicted using the ηbu values in all deep groove ball bearings.
- None of the bearing dimension-related parameters appears to influence the oil replenishment under starved lubrication.
- Replenishment is a local phenomenon driven by the capillary action.
- For axially loaded deep groove ball bearings, the relative film thickness can be calculated using:

$$\frac{h_g}{h_{ff}} = 0.0544\ (\eta bu)^{-0.2945} \tag{5}$$

- The speed dependency of the absolute film thickness at higher speeds is very weak can be approximated as:

$$h_g \propto u^{0.12}, \tag{6}$$

CRediT authorship contribution statement

Pramod Shetty: Writing – original draft, Validation, Methodology, Investigation, Formal analysis, Data curation, Conceptualization. **Robert Jan Meijer:** Writing – review & editing, Supervision, Resources, Project administration. **Jude A. Osara:** Writing – review & editing, Supervision, Project administration. **Rihard Pasaribu:** Writing – review & editing, Supervision, Resources, Project administration, Funding acquisition. **Piet M. Lugt:** Writing – review & editing, Validation, Supervision, Resources, Project administration, Funding acquisition, Formal analysis, Conceptualization.

Declaration of competing interest

The authors declare that they have no known competing financial interests or personal relationships that could have appeared to influence the work reported in this paper.

Data availability

Data will be made available on request.

Acknowledgment

We thank SKF and Shell for funding this work and for the permission to publish this paper.

Appendix. Grease churning: temperature and film thickness

Fig. A.6 shows the evolution of temperature and film thickness during the churning phases in 6204 (Figs. A.6(a) & A.6(d)), 6206 (Figs. A.6(b) & A.6(e)), and 6209 (Figs. A.6(c) & A.6(f)) bearings. The churning phase is the initial phase of grease lubrication after a freshly grease-filled bearing starts running. It is typically characterized by significant heat generation leading to high temperature rise. In the measurement shown in the Appendix, the ndm – the product of rotational speed (rpm) and the mean diameter (in mm) – of all three bearings is set to 0.26 million. The linear speed of all the bearings is 6.5 m/s. The loads on the bearings are different for each bearing, generating approximately equal Hertzian pressures (0.97 GPa–1.06 GPa). These figures show different peak temperatures during churning for the differently sized bearings. In our previous paper [22], we demonstrated that successive runs under the same conditions and with the same grease can yield different churning durations in the same bearing [6]. That, in addition to the different bearing housing and contact dimensions yielding different thermal dissipation and friction levels, may prevent direct comparison of these measured temperature profiles. However, the churning temperature and film thickness profiles provide remarkable results regarding the grease churning behavior in the bearings.

During churning, the grease thickener contributes to film formation even though the relative film thickness (h_g/h_{ff}) during this phase is less than one (i.e., measured film thickness is less than the calculated fully flooded film thickness). This is attributed to the high shear rate at the inlet, dropping grease viscosity to that of its base oil. The film thickness is primarily determined by the contact inlet conditions. The high shear rate in this region could reduce the grease/base oil viscosity significantly [30]. Thus, even when the relatively fresh grease is being broken down (i.e, churned) in the film build-up, the film thickness can still be starved.

The maximum shear rate at the inlet can be approximated using the equation proposed by Dyson [30]: $\dot{\gamma}_{max} = \frac{3u}{2h_c}$, where u is linear velocity and h_c is central film thickness. The shear rates for the 6204, 6206, and 6209 bearings at their churning conditions are calculated using the final measured grease film thicknesses as the central film thicknesses, yielding 18.5×10^6 s^{-1}, 16.7×10^6 s^{-1}, and 17.1×10^6 s^{-1}, respectively. So also very similar. At such high shear rates, the grease viscosity approaches the base oil viscosity. This confirms that base oil properties are enough to estimate the film thickness at higher speeds.

After grease churning has finished in all the bearings, the film thicknesses at different speeds and loads are measured. Post-churning film thickness is nearly constant when temperature, load and speed are held constant. A sample film thickness measurement for each bearing is presented in Fig. A.7, showing the period during which the temperature is controlled using the hot air flow. A 10-min average of the stable film thickness profile yields the discrete data point used for analysis.

The entrainment velocity u is obtained by the following equation [31]:

$$u = \frac{R_i \omega_i}{2}\left(\frac{R_i + d}{R_i + 0.5d}\right) \tag{A.1}$$

where R_i is the inner race radius, ω_i is the inner race angular velocity (equal to the shaft rotational velocity), and d is the ball diameter.

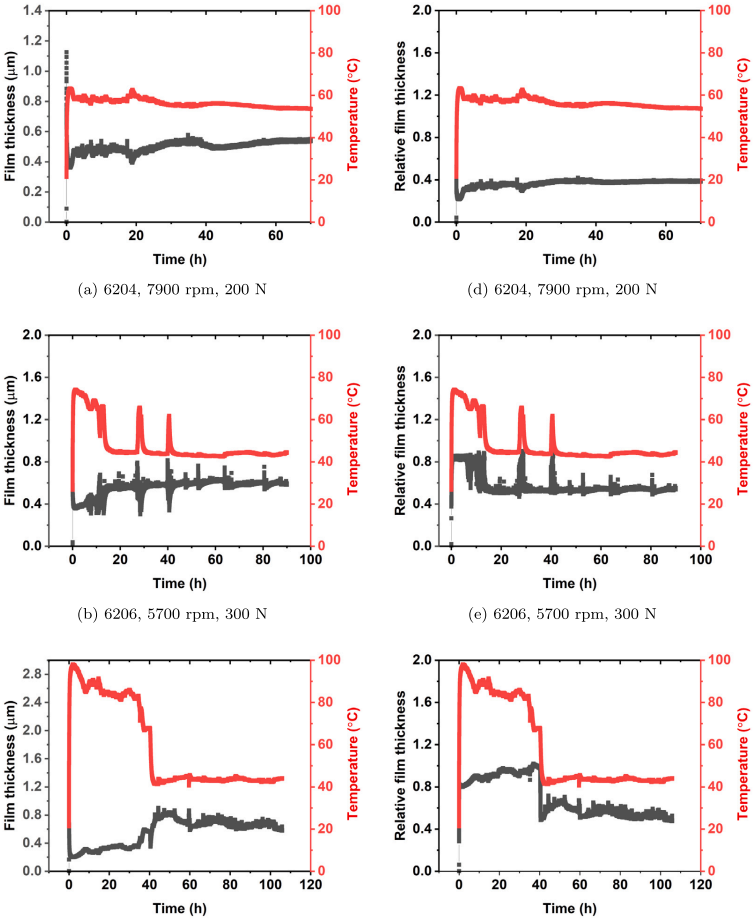

(a) 6204, 7900 rpm, 200 N

(d) 6204, 7900 rpm, 200 N

(b) 6206, 5700 rpm, 300 N

(e) 6206, 5700 rpm, 300 N

(c) 6209, 4000 rpm, 513 N

(f) 6209, 4000 rpm, 513 N

Fig. A.6. LiM-100-2.5 grease churning results for 6204, 6206, and 6209 bearings.

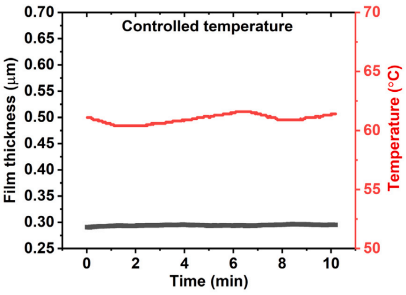

(a) 6204 bearing, LiM-100-2.5, 4000 rpm, 500 N

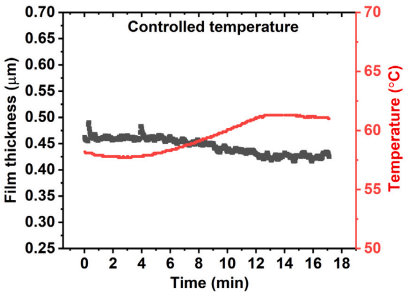

(b) 6206 bearing, LiM-460-3, 4000 rpm, 620 N

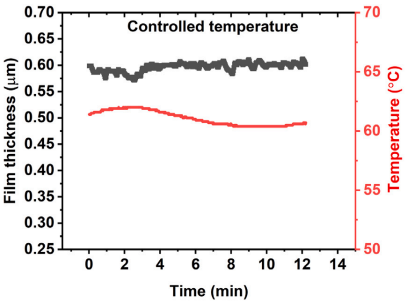

(c) 6209 bearing, LiM-460-3, 4000 rpm, 700 N

Fig. A.7. Example film thickness measurements. The film thicknesses shown here are measured at a controlled temperature of approximately 61 °C.

References

[1] Wedeven LD, Evans D, Cameron A. Optical analysis of ball bearing starvation. J Lubr Technol 1971;93(3):349–61.
[2] Hamrock BJ, Dowson D. Isothermal elastohydrodynamic lubrication of point contacts: Part IV—starvation results. J Tribol 1977;99(1):15–22.
[3] Damiens B, Venner CH, Cann P, Lubrecht A. Starved lubrication of elliptical EHD contacts. J Tribol 2004;126(1):105–11.
[4] Van Zoelen M, Venner CH, Lugt PM. Prediction of film thickness decay in starved elasto-hydrodynamically lubricated contacts using a thin layer flow model. Proc Inst Mech Eng J: J Eng Tribol 2009;223(3):541–52.
[5] Cen H, Lugt PM. Replenishment of the EHL contacts in a grease lubricated ball bearing. Tribol Int 2020;146:106064.
[6] Shetty P, Meijer RJ, Osara JA, Lugt PM. Measuring film thickness in starved grease-lubricated ball bearings: an improved electrical capacitance method. Tribol Trans 2022;65(5):869–79.
[7] Cen H, Lugt PM. Film thickness in a grease lubricated ball bearing. Tribol Int 2019;134:26–35.
[8] Cen H, Lugt PM. Effect of start-stop motion on contact replenishment in a grease lubricated deep groove ball bearing. Tribol Int 2021;157:106882.
[9] Jacod B, Pubilier F, Cann P, Lubrecht A. An analysis of track replenishment mechanisms in the starved regime. In: Tribology series. Vol. 36, Elsevier; 1999, p. 483–92.
[10] Gershuni L, Larson MG, Lugt PM. Lubricant replenishment in rolling bearing contacts. Tribol Trans 2008;51(5):643–51.
[11] Nogi T, Shiomi H, Matsuoka N. Starved elastohydrodynamic lubrication with reflow in elliptical contacts. J Tribol 2018;140(1):011501.
[12] Nogi T. Film thickness and rolling resistance in starved elastohydrodynamic lubrication of point contacts with reflow. J Tribol 2015;137(4):041502.
[13] Fischer D, von Goeldel S, Jacobs G, Stratmann A. Numerical investigation of effects on replenishment in rolling point contacts using CFD simulations. Tribol Int 2021;157:106858.
[14] Cann P, Damiens B, Lubrecht A. The transition between fully flooded and starved regimes in EHL. Tribol Int 2004;37(10):859–64.
[15] Cann P, Lubrecht A. Bearing performance limits with grease lubrication: the interaction of bearing design, operating conditions and grease properties. J Phys D: Appl Phys 2007;40(18):5446.
[16] Chiu Y. An analysis and prediction of lubricant film starvation in rolling contact systems. ASLE Trans 1974;17(1):22–35.
[17] Okal M, Kostal D, Sperka P, Krupka I, Hartl M. Effect of contact conformity on grease lubrication. Lubricants 2022;10(11):289.
[18] Damiens B, Lubrecht A, Cann P. Influence of cage clearance on bearing lubrication. Tribol Trans 2004;47(1):2–6.
[19] Liang H, Guo D, Ma L, Luo J. Experimental investigation of centrifugal effects on lubricant replenishment in the starved regime at high speeds. Tribol Lett 2015;59:1–9.
[20] Lugt PM. Grease lubrication in rolling bearings. John Wiley & Sons; 2012.
[21] Heemskerk R, Vermeiren K, Dolfsma H. Measurement of lubrication condition in rolling element bearings. ASLE Trans 1982;25(4):519–27.
[22] Shetty P, Meijer RJ, Osara JA, Lugt PM. Vibrations and film thickness in deep groove ball bearings. Tribol Trans 2023;(1):2–6.
[23] Van Zoelen MT. Thin layer flow in rolling element bearings (Ph.D. thesis), University of Twente; 2009.
[24] Gupta P, Cheng H, Zhu D, Forster N, Schrand J. Viscoelastic effects in MIL-L-7808-type lubricant, Part I: Analytical formulation. Tribol Trans 1992;35(2):269–74.
[25] Shetty P, Meijer RJ, Osara JA, Pasaribu R, Lugt PM. Effect of grease filling on the film thickness in deep groove ball bearings. Tribol Trans 2023;(just-accepted):1–12.
[26] Morales-Espejel GE, Lugt PM, Pasaribu H, Cen H. Film thickness in grease lubricated slow rotating rolling bearings. Tribol Int 2014;74:7–19.
[27] Cen H, Lugt PM, Morales-Espejel G. On the film thickness of grease-lubricated contacts at low speeds. Tribol Trans 2014;57(4):668–78.

[28] Van Zoelen M, Venner CH, Lugt PM. The prediction of contact pressure–induced film thickness decay in starved lubricated rolling bearings. Tribol Trans 2010;53(6):831–41.
[29] Venner CH, Van Zoelen M, Lugt PM. Thin layer flow and film decay modeling for grease lubricated rolling bearings. Tribol Int 2012;47:175–87.
[30] Dyson A, Wilson A. Film thicknesses in elastohydrodynamic lubrication by silicone fluids. Proc Inst Mech Eng 1965-66;180:97–112.
[31] Spikes H. Basics of EHL for practical application. Lubr Sci 2015;27(1):45–67.

APPENDIX E

Film thickness in grease-lubricated deep groove ball bearings–a master curve

Abstract

Film thickness in a grease-lubricated bearing is a critical bearing operation parameter, yet there are no models available to predict it. Our recent articles demonstrated that the relative film thickness (h_g/h_{ff}) can be predicted using the base oil viscosity (η), half contact width (b), and linear speed (u) for any axially loaded deep groove ball bearing. In this article, we extend this study to include radial loads and combined—axial and radial—loads. Radial load application causes an additional replenishment in the unloaded zone, introducing a new length variable z_r and surface tension σ. A universal power-law relationship between the relative film thickness in a deep groove ball bearing and the non-dimensional number $(\eta bu)/(z_r\sigma)$ for all loading and grease lubrication conditions is presented for use in predicting film thickness.

KEYWORDS

Grease film thickness, Axial load, Radial load, Combined load, Electrical capacitance method, Rolling Bearings.

INTRODUCTION

Rolling element bearings are some of the most important machine elements (1). The life of these bearings is mainly determined by the quality of lubrication. The film thickness determines whether the surfaces of the rolling elements will be separated enough to avoid metal-to-metal contact. Film thickness in grease-lubricated bearings is strongly determined by the level of starvation.

There are a few equations to predict film thickness in a ball-disc contact under starved lubrication conditions, proposed by Wedeven et al. (2), Hamrock and Dowson (3), Damiens et al. (4), and Van Zoelen et al. (5). These equations are either based on the inlet meniscus distance from the contact center, or the thickness of the oil layer on the track. This input parameter required by these models impedes the calculation of the film thickness in actual bearing contacts where the oil layer thickness is not readily obtainable. Currently, the grease film thickness in a bearing is estimated as a fraction of the base oil film thickness. It is evident from experiments that grease film thickness can be larger than the base oil film thickness at low speeds, almost equal to base oil film thickness at moderate speeds (6, 7), and a further increase in speed can result in a lower film thickness than that of the base oil because of lubricant starvation (8, 9). Being able to calculate the film thickness would help in selecting the right lubricant.

In a bearing, the film thickness is a function of the availability of oil in front of the rolling contacts in

addition to the operating parameters, lubricant properties and bearing geometry (4). The availability of lubricant around the contacts is mainly determined by the net lubricant supply towards the contacts via replenishment and loss of lubricant from that region. The loss of lubricant from the contact in severely starved contacts is primarily due to the side flow out of the Hertzian zone, side flow from the front of contact, and partially due to centrifugal forces induced flow (5, 10, 11). Replenishment of the contact is considered to be mainly dependent on capillary forces (9, 12–14). Cann et al. (14) studied the replenishment of starved contacts on a ball-on-disc machine, proposing an empirical equation for relative film thickness. Their proposed non-dimensional "starvation degree SD" parameter ($\eta bu/h_{\infty}\sigma$) to determine the degree of starvation also needs the oil layer thickness 'h'_{∞} (14). Computational fluid dynamics (CFD) simulation and experimental study on a ball-on-disc machine by Nogi et al. (15–17) and Fischer et al. (18, 19) showed that the meniscus position, a function of lubricant availability, correlates well with the capillary number. Based on a parametric study, an equation was proposed to find the film thickness—considering re-flow and loss of lubricant—in a starved EHL contact. These models also require the oil layer thickness on the track, an unknown parameter in bearings.

Inspired by the above-mentioned research, Cen and Lugt (20) studied the film thickness behavior in grease-lubricated 6209 bearings under axial load conditions. They showed that the relative film thickness (the ratio of grease film thickness to the calculated fully flooded base oil film thickness) depends only on the product of base oil viscosity (η), half contact width (b), and linear speed (u) (20). Our previous article (21) also showed that after the churning phase, the film thickness does not depend on the initial amount of grease in the bearing. This indicates that the oil layer thickness left on the track after churning will be independent of the initial grease quantity and oil bleed from the side reservoirs (21). The film thickness immediately after the churning phase depends solely on the oil flow dynamics in and around the contacts. Furthermore, we (22) studied the film thickness in the differently sized 6209, 6206, and 6204 bearings under axial loads and found that the ηbu concept holds well for any deep groove ball bearing. All these studies were restricted to axially loaded bearings, where the load distribution is uniform among all balls.

In a bearing under a radial load, the load distribution among all the balls is not uniform. In fact, under pure radial load, only a few balls are loaded, while the rest of the balls are unloaded depending on the radial clearance and the magnitude of the applied radial load. This causes the balls to experience cyclic loading and unloading conditions. These dynamic conditions also contribute to oil replenishment in the contacts.

Cann et al. (9) simulated the loading and unloading action on a ball-on-disc machine and found that the unloading action helped replenish the starved contacts. They argued that the unloading promotes the reflow of the lubricants from the side unto the track due to surface tension effects. Jablonka et al. (23) measured the film thickness in a radially loaded bearing lubricated with oil in fully flooded conditions

using an electrical capacitance method. They showed that the film thickness varies along the circumference of the bearing due to varying load distribution. So far, the film thickness in grease-lubricated bearings under radial loads is not yet studied.

References (14, 16, 17, 24) also observed that, in addition to the base oil viscosity, the surface tension of the base oil plays a vital role in determining film thickness. Åstöm et al. (25) write that replenishment probably mainly takes place in the inlet by squeezing the ridges/side bands of oil formed by the preceding ball.

In this study, we measure the film thickness under radial and combined (radial + axial) loads using two different greases. Then, we will show that the product ηbu is enough to describe the level of starvation for axially loaded bearings as was shown by Cen and Lugt (20) and our recent paper (22). Surface tension does not vary enough between various lubricating oils and typical temperatures compared to speed, viscosity and contact size to make it relevant to include it in a film thickness equation for (commonly used) greases. Next we will show that this is not enough when a radial load is introduced.

MATERIALS AND METHODS

Lubricant grease

Two Lithium-thickened greases with similar NLGI consistency are chosen for this study. The grease with base oil viscosity of 100 cSt at 40 $^{\circ}C$ is named 'LiM-100-2.5', and the one having base oil viscosity of 472.5 cSt at 40 $^{\circ}C$ is named 'LiM-460-3'. More information about these greases is provided in Table 1.

Property	LiM-100-2.5	LiM-460-3
Kinematic viscosity @ 40°C (cSt)	102.8	474.5
Kinematic viscosity @ 100°C (cSt)	10.3	31.4
Density @ 15°C (g/cm^3)	0.891	0.902
Pressure-viscosity coeff. @ 40°C (GPa^{-1})	31.8	27.4
Surface tension @ 61°C (N/m)	0.0171	0.0276
Thickener content (% mass)	13	17
A_{lv} (N/m)	0.0330	0.0327
B_{lv} (Pa.s)	-0.0217	-0.0219

Table 1. Thickener contents of the greases used and their base oil properties. A_{lv} and B_{lv} are used in Pelofsky's equation to determine surface tension at various temperatures.

Film thickness measurement

The film thicknesses in specially modified—one ball steel while others ceramic—hybrid bearings are measured using a device called 'Lubcheck MK3' developed by Heemskerk et al. (26). It uses an electrical capacitance method to measure the film thickness. The test rig used to measure the film thickness is outlined in our previous paper (27). In that study, only axial loads were applied. With an all-steel ball

bearing under axial load, the film thickness at each ball-ring contact is the same, hence the total measured capacitance is the sum of the capacitance contributions from all the balls. In this study, the film thickness is measured under radial and combined–axial and radial–loads. When a radial load is applied to the bearings, the loads on the rolling elements vary, hence, the capacitance (which is a function of film thickness) will also vary at the rolling element-ring contacts. This variation under radial loads necessitates instantaneous measurement of the film thickness at a single ball-ring contact. Therefore, we modified the 6209 hybrid bearings; one of the hybrid bearing's ceramic balls was replaced with a steel ball. Because the ceramic balls are non-conductive, the measured capacitance is only from this steel ball, and it varies as the ball rolls from the loaded/heavily loaded zone to the unloaded/low loaded zone. We are interested in the film thickness in the heavily loaded zone which is the most susceptible to metal-to-metal contact. The capacitance value corresponding to the highest loaded position is obtained using a peak-finding algorithm, and used for further analysis (see Section 3.2.2 & 3.2.3 for details). The film thickness, via the measured capacitance, is recorded at a frequency of 10 kHz in all tests. The procedure to obtain the film thickness from the measured capacitance is explained in our previous publication (28). The schematic diagram of the special bearing and the electrical connections are shown in Figure 1.

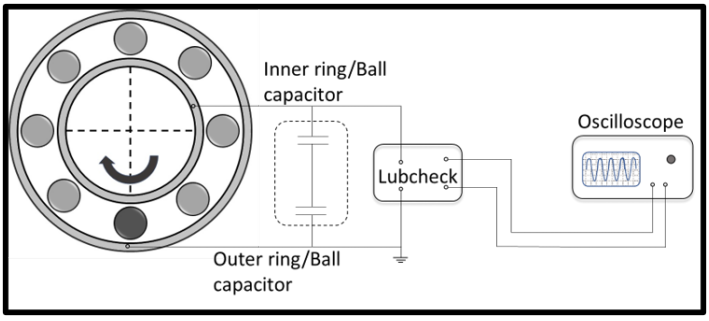

Figure 1. Hybrid bearing with single steel ball (dark gray) and electrical connections to measure film thickness.

All the tested bearings are filled up to 30 % of their free volume with grease and run at 4000 rpm for about 100 hours to finish the churning process. Film thicknesses are measured after the churning phase in a controlled temperature environment. Hot air at appropriate flow rates is used to hold the bearing outer ring temperature at 61 $\pm 0.5^{\circ}C$. Instantaneous film thickness is measured for about 10-15 minutes for each speed. The film thickness becomes stable within 1-2 minutes after setting new speed/load conditions, similar to our observation in the axially loaded bearings (21). The time average value of the measured capacitance during this period is considered for further analysis. All measurements are repeated at least twice, and the plotted error bars in the result plots are the standard deviations.

Surface tension measurement

The surface tension of each base oil is measured with a Dynamic contact angles (DCAT) machine, using a Wilhelmy plate method. Here, the oil is heated to a certain temperature, and a clean Wilhelmy plate is immersed in the test lubricant. The force acting on the plate is measured. Using this force, the surface tension of the lubricant can be calculated. A picture of the test rig is shown in Figure 2. The surface tension of the liquid is measured at different temperatures, and the measurements are repeated at least twice.

Figure 2. DCAT machine with Wilhelmy plate to measure surface tension at different temperatures.

RESULTS

Surface tension

The surface tension of the base oils σ varies with temperature and can be calculated using Pelofsky's equation (29):

$$ln\ \sigma = ln\ A_{lv} + \frac{B_{lv}}{\eta} \tag{1}$$

where η is the dynamic viscosity. A_{lv} & B_{lv} are constants specific for each liquid and are obtained by curve-fitting Pelofsky's equation with the experimentally measured surface tension at different temperatures, with the dynamic viscosity calculated using Walther's equation (30). The constants used and the estimated surface tension at $61°C$ are listed in Table 1. Figure 3 shows the measured surface tension and the estimated surface tension at different temperatures. Notice that the surface tensions of the two base oils are different at all temperatures. It is also evident that the surface tension decreases with temperature.

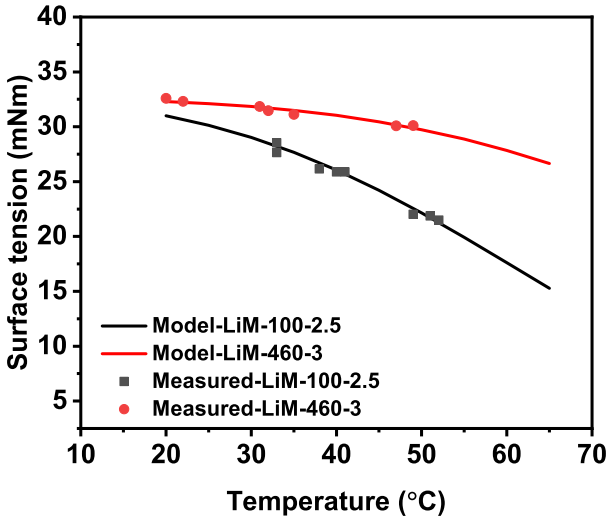

Figure 3. Surface tension variation with temperature, measured and estimated from Pelofsky's model.

Film thickness

Axial load - a review

In reference (22), film thickness was measured in three different deep groove ball bearings of varying sizes under axial load. The same two greases are also used in this article. It was observed that the film thickness after the churning phase is almost steady. Film thickness increased with speeds similar to the oil-lubricated contacts. Further increase in speed initiated starvation. The degree of starvation is measured as the ratio of the measured grease film thickness (h_g) to the fully flooded base oil film thickness (h_{ff}) calculated using Hamrock and Downson's equation (3, 31) (see Equation 5 in appendix). We also consider the inlet shear heating effect on the film thickness and correct it using the correction factor C_T proposed by Gupta et al. (32) (see Equation 6 in appendix). The relative film thicknesses at different speeds, loads, greases, and bearings were found to be dependent only on the base oil viscosity, half-contact width, and entrainment velocity, as shown in Figure 4. Via a curve fit, a power law relation between the relative film thickness and the product ηbu was obtained as

$$\frac{h_g}{h_{ff}} = 0.0544\ (\eta bu)^{-0.2945} \tag{2}$$

with R^2 86%. Figure 4 plots the relative film thickness h_g/h_{ff} against ηbu for two different greases in three different bearings at various loads and speeds. The fact that none of the bearing geometry-related parameters are required to define the relative film thickness, indicates the influence of centrifugal force on the loss/replenishment, and the replenishment in between the overrolling is not significant. Therefore, we concluded from these results that oil replenishment is a local phenomenon. It was shown that the film thickness does not reduce with speed up to moderately high speeds and its dependency on the speed in the starved regime is minimal.

Radial load

Figure 5a shows an example of the calculated normal load distribution and the capacitance variation along the bearing circumference for a radial load of 900 N. It is evident that the capacitance variation follows the load distribution in the bearings. The film thickness is inversely proportional to the measured capacitance, so the point of highest capacitance corresponds to the highest loaded point where the film thickness is lowest. This point is used in subsequent analysis. Figure 5b shows the cyclic profile and the peak values (green star) of capacitance considered. It can also be seen that the capacitance is relatively stable at its minimum value (largest ball-outer ring gap) in the unloaded zone.

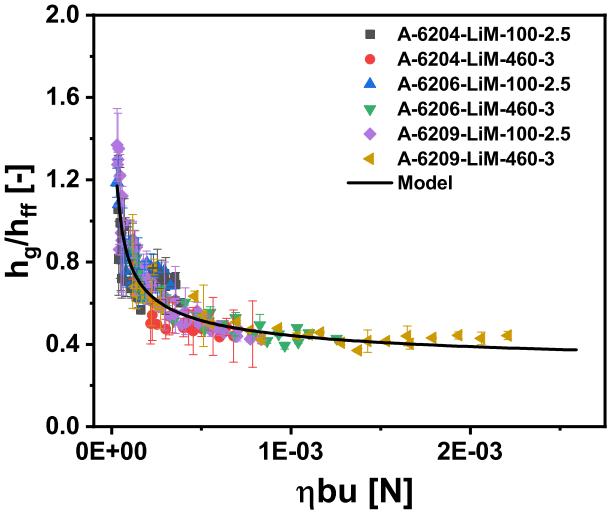

Figure 4. Variation of relative film thickness with ηbu for axially loaded 6209, 6206, and 6204 bearings.

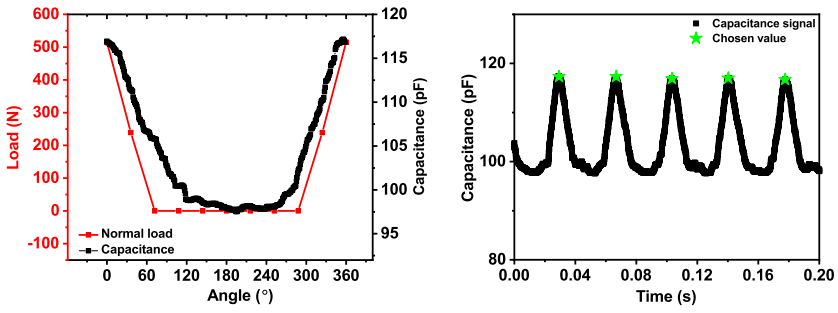

(a) (b)

Figure 5. (a) Calculated ball-ring normal load variation and capacitance signal at different angular locations as the steel ball moves along the bearing circumference, (b) cyclic capacitance signal showing the selected peaks for a LiM-100-2.5 grease-lubricated 6209 bearing under 900 N applied radial load.

Figure 6 plots the film thickness for radially loaded bearings lubricated with LiM-100-2.5 and LiM-460-3 greases. The film thickness in the bearing lubricated with LiM-100-2.5 is measured up to 6000 rpm which corresponds to 0.39 million *ndm* (*ndm* is the product of rotational speed *n* in rpm and pitch circle diameter *dm* in millimeters). The film thickness in the bearing lubricated with LiM-460-3 grease is measured up to 4000 rpm corresponding to 0.26 million ndm.

At higher speeds, the temperature could not be lowered to 61±0.5°*C* because of the higher heat

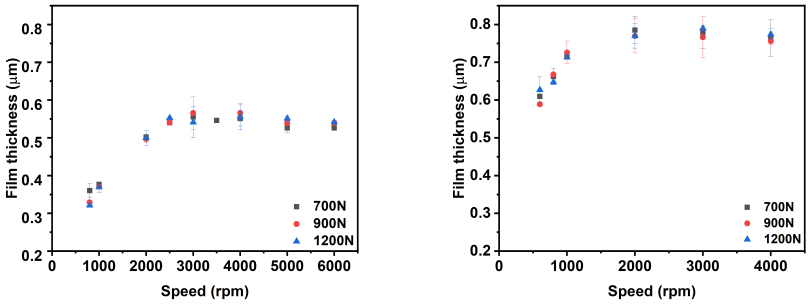

(a) Lubricated with LiM-100-2.5 grease.

(b) Lubricated with LiM-460-3 grease.

Figure 6. Film thickness variation with speed for radially loaded 6209 bearings lubricated with (a) LiM-100-2.5 grease and (b) LiM-460-3 grease.

generation from the high-viscosity base oils. For both grease types, the film thickness is measured under 700 N, 900 N, and 1200 N applied radial loads. The resulting contact load, half contact widths, and contact pressure for the highest loaded ball is shown in Table 2.

Radial load	Highest load	a (mm)	b (mm)	Contact pressure (GPa)
700 N	414.8 N	0.1103	1.417	1.27
900 N	515.3 N	0.1186	1.523	1.36
1200 N	662.8 N	0.1290	1.656	1.48

Table 2. Applied radial load on the bearing and the resulting normal load on the highest loaded ball-ring contact, half contact widths across b and along a the running direction, giving ellipticity ratio = 0.0779) and contact pressure for 6209 bearing inner ring-ball contact.

The film thickness increases with speeds up to 2500 rpm for LiM-100-2.5 grease, and up to 1000 rpm for the LiM-460-3 grease-lubricated bearing. Then the film thickness becomes almost constant with speed. Similar to what we saw under axial loads, at low speeds, the contacts are still fully flooded hence the film thickness increases with speed. But as the speed increases, contacts become starved, causing the film thickness to deviate from its fully flooded condition behavior. When an EHL contact is severely starved, the film thickness is primarily determined by the side flow, governed by the residence time and the over-rolling frequency. As the speed increases, these two effects balance each other out, making film thickness almost independent of speed (10, 28). Starvation in the LiM-460-3-greased bearing starts at speeds lower than in the LiM-100-2.5 grease bearing. This is attributed to the higher viscosity of the base oil. In starved contacts, higher viscosity makes it difficult to replenish the center of the contacts (14, 20). The overall variation of the film thickness with speed under radial loads is similar to the film thickness evolution in axially loaded bearings.

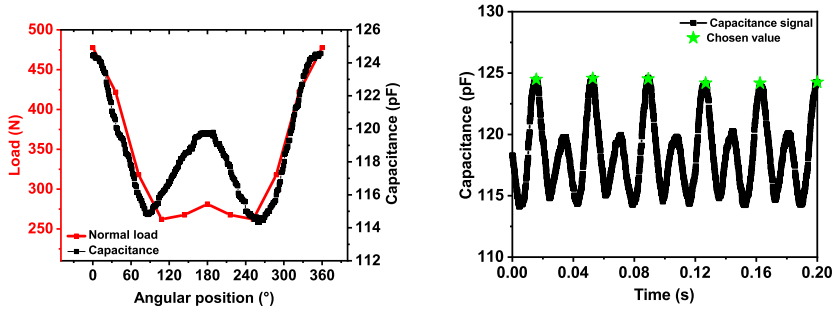

(a) (b)

Figure 7. (a) Load distribution and capacitance variation at different angular positions, (b) capacitance signal and the selected peaks for 6209 bearing lubricated with LiM-100-2.5 grease at 4000 rpm under the combined 900 N axial load and 500 N radial load.

Combined axial and radial load

When a ball bearing is subjected to both radial and axial loads, all the balls will be loaded but the magnitude of the load varies for each ball depending on the position of the ball. Figure 7a shows the normal load distribution (red plot) and the capacitance variation (black plot) at various angular positions in the bearing when 900 N axial and 500 N radial loads are applied. The first of the pair of balls carrying the lowest load is located at an angle of ±108 ° from the ball carrying the highest load. The capacitance in the bearing also varies at different positions, correlating with the load distribution. Figure 7b shows an example capacitance signal showing the selected peak values corresponding to the film thickness at the highest loaded position considered for the analysis, similar to the radial load conditions.

The film thickness is measured for three sets of load combinations: 500 N axial load + 900 N radial load; 900 N axial load + 900 N radial load; and 900 N axial load + 500 N radial load. For each combination, the resulting load on the highest-loaded ball, contact pressure, and contact widths are shown in Table 3.

Axial load	Radial load	Highest contact load	a (mm)	b (mm)	Contact pressure (GPa)
500 N	900 N	587 N	0.124	1.590	1.42
900 N	900 N	658 N	0.129	1.652	1.47
900 N	500 N	478 N	0.116	1.485	1.32

Table 3. Applied combined (axial + radial) loads on the bearing and the resulting contact loads on the highest loaded ball, half contact widths across b and along a the running direction, giving ellipticity ratio = 0.078) and contact pressures for 6209 bearing inner ring-ball contact.

The resulting film thickness as a function of speed for both greases is shown in Figure 8. Similar to the axial and radial load results, the film thickness increases with speed and then becomes almost constant. The film thickness of the LiM-460-3 grease is again higher than that of the LiM-100-2.5 grease-lubricated bearing because of the higher viscosity of LiM-460-3 base oil. These results show that the overall film thickness trend is the same for all three loading conditions (axial, radial and combined): After a critical

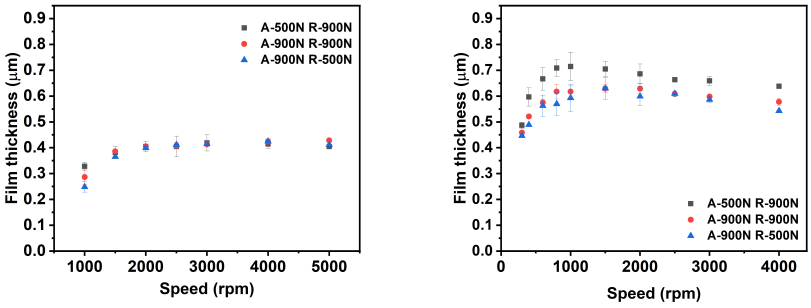

(a) Lubricated with LiM-100-2.5 grease.

(b) Lubricated with LiM-460-3 grease.

Figure 8. Film thickness variation with speed for combined axially and radially loaded 6209 bearings lubricated with (a) LiM-100-2.5 grease and (b) LiM-460-3 grease.

speed, the film thickness becomes constant.

In the next section, we will correlate the relative film thickness with different parameters derived from the base oil properties, operating conditions, and bearing deflections.

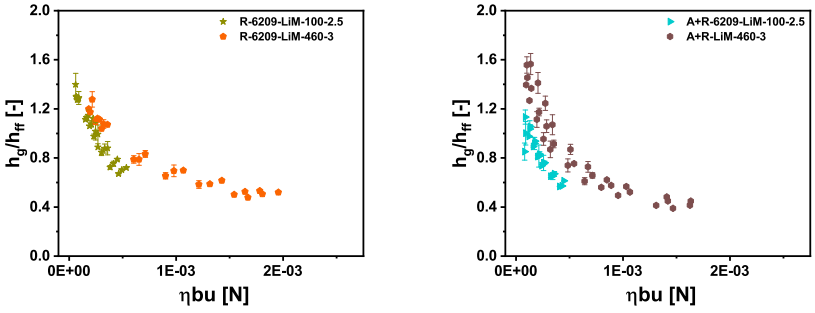

(a) Radial load

(b) Combined axial and radial load

Figure 9. Variation of relative film thickness with ηbu for (a) radially loaded bearings and (b) combined axially and radially loaded 6209 bearings and lubricated with LiM-100-2.5 grease and LiM-460-3 grease.

Relative film thickness—the effect of surface tension

Cen and Lugt (20) and our previous article (22) showed that for axially loaded bearings, the relative film thickness h_g/h_{ff} has a power law relationship with ηbu. Here, we will show that this relation no longer holds for radial and combined loads. Figure 9 plots relative film thickness against ηbu, unlike for axial loads (see Figure 4), the relative film thicknesses do not merge into a single power law relationship with ηbu for radial and combined loads. Each grease (LiM-100-2.5 or LiM-460-3) exhibits a distinct power law relationship.

This difference can be explained by the difference in contact loads in the radial and combined load situations. Here, the ball experiences continuous loading and unloading during each ball revolution, unlike in the axially loaded condition where the contact load is constant. Due to this loading and unloading cycle, the oil replenishment due to the capillary action is anticipatorily higher. Observations in the ball-on-disc experiments by Cann et al. (9) showed that during unloading, the film thickness reached the fully flooded value. They related the reflow of the lubricant to $\eta b/\sigma$. With similar considerations, Figure 10 shows the variation of the relative film thickness when surface tension σ is included as an independent variable along with ηbu for axial, radial, and combined load conditions. Now, for both radial (Figure 10b) and combined load (Figure 10c) conditions, the relative film thicknesses of both greases merge into a single power law relationship. In the next section, we will explain the physical mechanism of the surface tension effect under radial loads including oil replenishment in the unloaded zone.

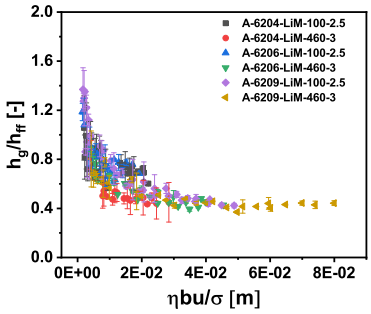

(a) Axial load

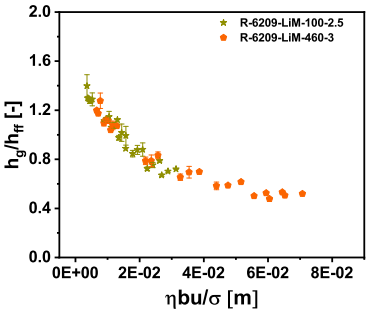

(b) Radial load

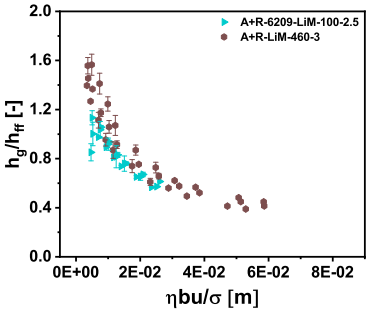

(c) Combined axial and radial load

Figure 10. Variation of relative film thickness with $\eta bu/\sigma$ for (a) axially, (b) radially, and (c) combined axially and radially loaded bearings lubricated with LiM-100-2.5 and LiM-460-3 greases.

DISCUSSION

The bearing dynamics under radial loads and combined loads are not the same as under axial loads only. In the presence of radial loads, the load carried by each ball along the circumference of the bearing varies depending on the position of the ball. In purely radially loaded bearings, only some of the balls (in the loaded zone) carry the load and the rest of the balls (in the unloaded zone) do not carry any load (see Figure 5a). In combined load conditions, all the balls are loaded but the load distribution is not uniform (see Figure 7a). This yields variations in the side flow and replenishment as ring-ball contact width changes along the bearing circumference.

As mentioned in the introduction, contact replenishment is given by the capillary pressure and the hydraulic resistance. The capillary pressure is determined by the surface tension of the lubricant and the 'fluid curvature', which is given by the gap between the ball and ring outside the Hertzian contact. In the highest loaded contact, this curvature is expected to be highest due to the smallest gap and the total resistance largest because of the large distance between the side of contact and the center of it but when the ball moves to a position where the contact load is lowest (therefore highest gap), the fluid curvature decreases and the length over which replenishment needs to take place shortest. Therefore an increase in oil replenishment in this lowest-loaded position is observed. The dependency of the hydraulic resistance on the gap is much higher than that of the capillary pressure. Since all the balls are equally loaded in axially loaded bearings, the gap is constant, hence, the capillary pressure is the same at all the contacts. Therefore, we did not need to include surface tension in determining the level of starvation under axial loads.

To show the difference in behavior we plot all the relative film thicknesses measured so far—for axial loads (all three bearings), radial loads, combined loads, and both greases—vs $\eta bu/\sigma$ in Figure 11.

Three distinct curves are evident, implying that for the same $\eta bu/\sigma$ in the highest loaded contact, the starvation degree is different for different loading types. The starvation degree in axial > combined > radial loading conditions.

The radial gap effect

The radial load does not only cause a varying Hertzian contact width b along the circumference but also a varying gap between the ball and the outer ring groove leading to a varying capillary pressure and available oil volume for replenishment. We quantify this effect by defining a gap (z_r), the radial distance between the apex of the lowest-loaded ball and the outer ring groove, as shown in Figure 12. While other locations could have been chosen, for convenience, we have chosen the apex of the ball as the reference point in determining the radial distance between the ball and the groove.

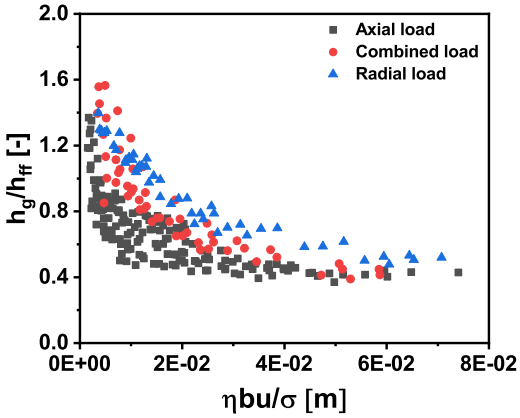

Figure 11. Relative film thickness h_g/h_{ff} vs $\eta bu/\sigma$ for all three different loading types.

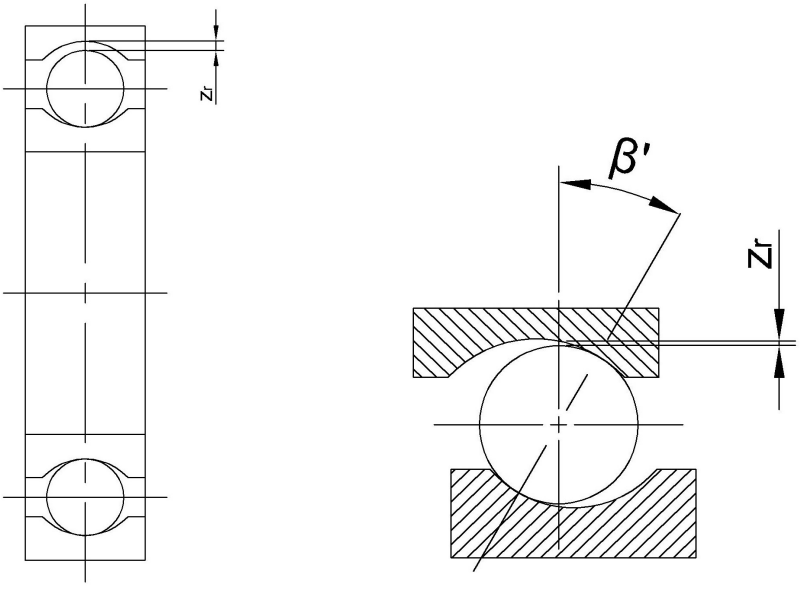

(a) Radial load

(b) Axial load and combined loads

Figure 12. Ball-ring diagram showing the gap z_r between the top of the ball and the outer ring groove

For radial load conditions, this gap is given by $z_r = P_d + \delta_i + \delta_o$, where P_d is the diametrical clearance, δ_i and δ_o are the inner ring and outer ring-ball contact deformations, respectively. As the radial load increases, further deforming the contacts, the gap z_r also increases. For axially loaded and "combined"

loaded bearings (see Figure 12b) estimating this gap requires some more parameters. With the application of axial load, the ball shifts axially and its vertical central axis forms an angle with the contact normal, commonly called the contact angle. When combined axial and radial loads are applied, there will be angular, axial and radial displacements of the inner ring. Based on these variables, the ball position with respect to the outer ring groove position can be calculated. A detailed description of this calculation is in reference (33) and in our previous article (27). Once the position of the ball is known, the gap can be calculated by assuming that the ball is perfectly spherical away from the Hertzian contact allowing the use of the equation of a circle. The outer ring is stationary while the inner ring moves. For this (static) analysis, centrifugal force is neglected, hence the contact angles in the inner ring-ball contact and the outer ring-ball contact are assumed to be equal.

For purely axial load, z_r is the same for all the balls, whereas, this will vary for combined axial and radial load conditions. We calculated z_r for all the balls along the bearing circumference considering their contact angles, loads, elastic deformations, etc, and found that the distance $z_r(\theta)$ is highest in the radially opposite position to the highest loaded ball, i.e., $z_r(\theta)$ is maximum (in the unloaded zone) at 180 degrees from the highest-loaded ball. An example calculation for combined load condition is shown in Figure 13, for comparison with the load distribution in Figure 7. Given its significance in replenishment, only the maximum value of z_r is used in subsequent analysis.

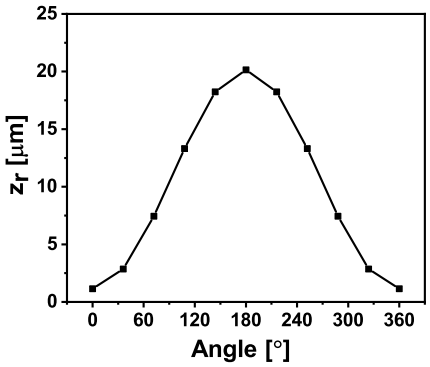

Figure 13. Vertical distance between the top of the ball and the outer ring groove for all the balls in the bearing for combined load comprising an axial load of 900 N and a radial load of 500 N in a 6209 bearing.

Table 4 presents the maximum gap z_r calculated for all the bearings at different loads. For axial loads, z_r—which is a function of bearing size via the clearance—does not vary much in each bearing, whereas for radial loads, z_r varies significantly and linearly with load. Recall that the film thickness measurements for radial load conditions showed little to no dependency on load magnitude (see Figure 6). In the starved

lubrication regime, as the load increases, the starvation level also increases proportionally to the contact width: when the contact width grows, the flow of lubricant towards the center of the contact becomes more difficult. However, for radial loads, as the load increases, the gap z_r also increases, facilitating additional replenishment which balances out the adverse effect of increasing contact width, thereby making the film thickness minimally dependent on applied load (as shown in Figure 6).

Bearing	Axial load (N)	Radial load (N)	z_r (μm)
6209	513	0	10.00
6209	700	0	10.16
6209	900	0	10.30
6206	310	0	7.50
6206	460	0	7.65
6206	620	0	7.80
6204	300	0	8.27
6204	400	0	8.43
6204	500	0	8.57
6204	600	0	8.72
6209	0	700	37.62
6209	0	900	39.28
6209	0	1200	41.52
6209	500	900	26.95
6209	900	900	25.31
6209	900	500	20.15

Table 4. Applied loads on different bearings and the calculated ball-outer ring groove gaps z_r.

Film thickness model for radial loads

Increasing z_r allows for more lubricant around the contact, reducing the starvation level, hence, film thickness starts to depend less on the applied load as the severity of starvation decreases. In fully flooded conditions, it is least dependent on the load. Therefore, under radial and combined load conditions (the latter only for LiM-100-2.5 grease-lubricated bearing), we do not see distinct load dependency. To verify this, we remove the load effect by neglecting contact width b as an independent variable. Figure 14 plots relative film thickness against the capillary number $\eta u/\sigma$ (neglecting contact width b which changes with applied load) for three different radial loads and both LiM-100-2.5 and LiM-460-3 greases, with a power law curve fit that yields $R^2 = 0.93$. Comparing this to the $R^2 = 0.92$ obtained from Figure 10b (which includes load effects via contact width b) shows that we can determine the relative film thickness in radially loaded bearings without including b. The empirical equation of Figure 14 fit is

$$\frac{h_g}{h_{ff}} = 1.8 \left(\frac{\eta u}{\sigma}\right)^{-0.31}. \tag{3}$$

The fact that, now, the contact width b is not important shows that the replenishment in the radially

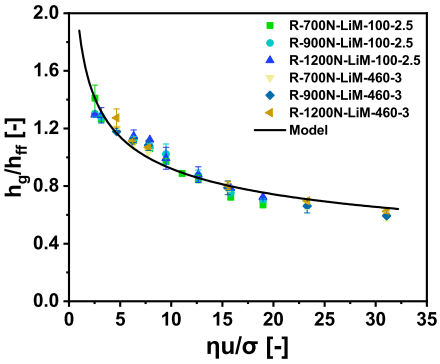

Figure 14. Relative film thickness as a function of capillary number ($\eta u/\sigma$) for three different radial loads and two different greases.

loaded bearing is dominated in the unloaded region. However, given this does not apply in the presence of axial loads, we next introduce a non-dimensional parameter to render a more universal expression including all the active mechanisms in all load conditions, such as the opposing effects of applied load on contact width b and radial gap z_r.

Film thickness master curve

The relative film thickness h_g/h_{ff} is an indicator of the level/degree of starvation: if the level of starvation is high, h_g/h_{ff} is low, and vice versa. Starvation is given by the balance of side-flow out from the Hertzian contacts and replenishment by capillary effects. This is given by the viscosity η, speed u, contact width b and surface tension σ but also by the available volume, given by the gap parameter z_r.

Considering the significance of the above effects and mechanisms, we present relative film thickness as a function of non-dimensional starvation parameter $\eta bu/(z_r\sigma)$ in Figure 15. This plot includes the film thickness measured on the three different bearings, at the different load magnitudes and types (axial, radial and combined), for both greases tested. A master curve fit yields a power law relation, rendering a universal expression for the relative film thickness as

$$\frac{h_g}{h_{ff}} = 7.305\left(\frac{\eta bu}{z_r\sigma}\right)^{-0.34} \tag{4}$$

with $R^2 = 87.7\%$. These results indicate that the film thickness in a grease-lubricated bearing immediately after the churning phase is primarily determined by the dynamics of the oil flow around the contacts.

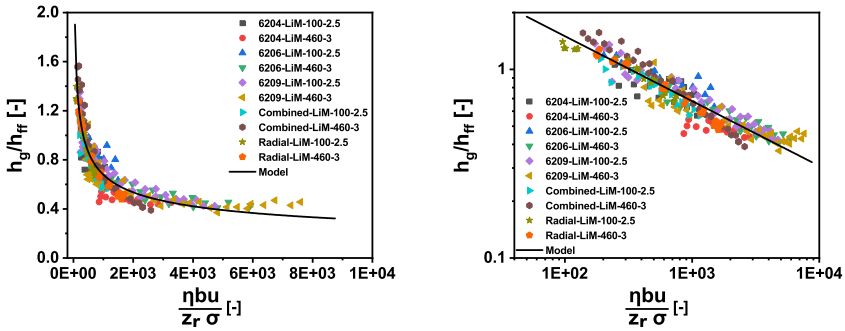

(a) Linear scale (b) Log-log scale

Figure 15. Relative film thickness as a function of non-dimensional starvation parameter $\eta bu/(z_r\sigma)$.

The film thickness does not depend on the grease bleed rate or the grease rheological properties.

The overall dependency on speed is lower than that under fully flooded conditions as discussed in our recent paper (22). The film thickness dependency on the applied load magnitude varies with the load type. When the bearings are axially loaded, the relative film thickness decreases with the load since the contact width increases but z_r does not vary considerably. But for applied radial loads and combined loads, as the radial load increases, the gap z_r also increases, nullifying the load effect on contact width and resulting in the reduced dependency. Figure 16 compares the gap z_r with the contact width b, showing a near-linear relationship. This explains why equation 3 does not contain the contact width b but includes surface tension σ.

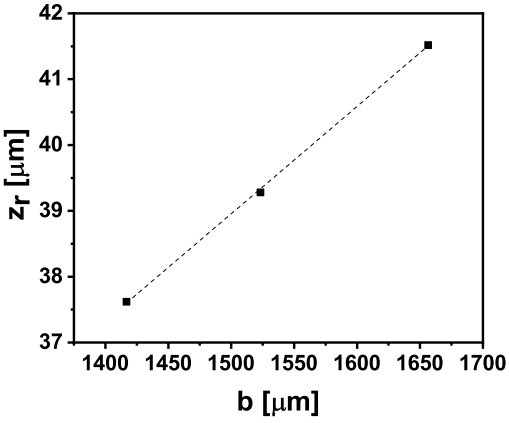

Figure 16. Radial gap z_r vs contact width b showing a linear proportionality for a 6209 bearing under 700 N, 900 N, and 1200 N radial loads.

CONCLUSION

This study showed that the film thickness in grease-lubricated ball bearings immediately after the churning phase is primarily determined by the dynamics of the oil flow in and around the contacts. In this phase, film thickness does not depend on the oil bleed. The base oil viscosity is the grease property that determines the film thickness for NLGI 2 greases (good quality ball bearing greases). This resulted in a universal relative film thickness model for grease-lubricated deep groove ball bearings under axial, radial and combined loads:

$$\frac{h_g}{h_{ff}} = 7.305 \left(\frac{\eta b u}{z_r \sigma} \right)^{-0.34}$$

This model includes all the identified active mechanisms and applies to both small and medium sized bearings.

For axial loads only, z_r does not vary very much with load and the significance of a varying surface tension is much less relevant. For pure axial load this equation reduces to:

$$\frac{h_g}{h_{ff}} = 0.0544 \, (\eta b u)^{-0.2945}$$

For radial loads only, the relative film thickness reads:

$$\frac{h_g}{h_{ff}} = 1.8 \left(\frac{\eta u}{\sigma} \right)^{-0.31}.$$

Here the ratio of contact width b to radial gap z_r is excluded because both parameters are linearly dependent on each other.

Some additional conclusions are:

- Film thickness dependency on speed in starved conditions is lower than in fully flooded conditions.
- Film thickness dependency on applied load magnitude is different for axially loaded bearings and bearings with radial loads.
- The starvation level depends on the base oil viscosity and surface tension.

The above hold for lubrication after the churning phase, before commencement of oil bleeding from the grease reservoirs.

ACKNOWLEDGMENTS

We thank SKF Research and Technology Development and Shell for funding this work and approving this publication. We also thank Dr. Norbert F. Bader for the insightful discussions during the study.

References

(1) McQueen, A., 2010. “Stathis ioannides, devoted to the fight against friction”. *Evolution: The Business and Technology Magazine from SKF*, pp. 18–20.

(2) Wedeven, L. D., Evans, D., and Cameron, A., 1971. “Optical analysis of ball bearing starvation”. *J. of Lubrication Tech,* **93**(3), pp. 349–361.

(3) Hamrock, B. J., and Dowson, D., 1977. “Isothermal elastohydrodynamic lubrication of point contacts: part iii—fully flooded results”. *J. Trib.,* **99**(2), pp. 264–275.

(4) Damiens, B., Venner, C. H., Cann, P., and Lubrecht, A., 2004. “Starved lubrication of elliptical EHD contacts”. *J. Trib.,* **126**(1), pp. 105–111.

(5) Van Zoelen, M., Venner, C. H., and Lugt, P. M., 2009. “Prediction of film thickness decay in starved elasto-hydrodynamically lubricated contacts using a thin layer flow model”. *Proceedings of the Institution of Mechanical Engineers, Part J: Journal of Engineering Tribology,* **223**(3), pp. 541–552.

(6) Morales-Espejel, G. E., Lugt, P. M., Pasaribu, H., and Cen, H., 2014. “Film thickness in grease lubricated slow rotating rolling bearings”. *Tribology International,* **74**, pp. 7–19.

(7) Cen, H., Lugt, P. M., and Morales-Espejel, G., 2014. “On the film thickness of grease-lubricated contacts at low speeds”. *Tribology transactions,* **57**(4), pp. 668–678.

(8) Cann, P., 1996. “Starvation and reflow in a grease-lubricated elastohydrodynamic contact”. *Tribology Transactions,* **39**(3), pp. 698–704.

(9) Cann, P., and Lubrecht, A., 2003. “The effect of transient loading on contact replenishment with lubricating greases”. In *Tribology Series*, Vol. 43. Elsevier, pp. 745–750.

(10) van Zoelen, M. T., 2009. “Thin layer flow in rolling element bearings”. PhD thesis, University of Twente.

(11) Van Zoelen, M., Venner, C. H., and Lugt, P. M., 2010. “The prediction of contact pressure–induced film thickness decay in starved lubricated rolling bearings”. *Tribology transactions,* **53**(6), pp. 831–841.

(12) Jacod, B., Pubilier, F., Cann, P., and Lubrecht, A., 1999. “An analysis of track replenishment mechanisms in the starved regime”. In *Tribology Series*, Vol. 36. Elsevier, pp. 483–492.

(13) Cann, P., and Lubrecht, A., 2007. “Bearing performance limits with grease lubrication: the interaction of bearing design, operating conditions and grease properties”. *Journal of Physics D: Applied Physics,* **40**(18), p. 5446.

(14) Cann, P., Damiens, B., and Lubrecht, A., 2004. “The transition between fully flooded and starved regimes in EHL”. *Tribology International,* **37**(10), pp. 859–864.

(15) Nogi, T., 2015. “An analysis of starved EHL point contacts with reflow”. *Tribology Online,* **10**(1),

pp. 64–75.

(16) Nogi, T., 2015. “Film thickness and rolling resistance in starved elastohydrodynamic lubrication of point contacts with reflow”. *Journal of Tribology,* **137**(4), p. 041502.

(17) Nogi, T., Shiomi, H., and Matsuoka, N., 2018. “Starved elastohydrodynamic lubrication with reflow in elliptical contacts”. *Journal of Tribology,* **140**(1), p. 011501.

(18) Fischer, D., von Goeldel, S., Jacobs, G., and Stratmann, A., 2021. “Numerical investigation of effects on replenishment in rolling point contacts using cfd simulations”. *Tribology International,* **157**, p. 106858.

(19) Fischer, D., von Goeldel, S., Jacobs, G., Stratmann, A., and König, F., 2021. “Investigation of lubricant supply in rolling point contacts under starved conditions using cfd simulations”. In IOP Conference Series: Materials Science and Engineering, Vol. 1097, IOP Publishing, p. 012007.

(20) Cen, H., and Lugt, P. M., 2020. “Replenishment of the EHL contacts in a grease lubricated ball bearing”. *Tribology International,* **146**, p. 106064.

(21) Shetty, P., Meijer, R. J., Osara, J. A., Pasaribu, R., and Lugt, P. M., 2023. “Effect of grease filling on the film thickness in deep-groove ball bearings”. *Tribology Transactions*, pp. 1–8.

(22) Shetty, P., Meijer, R. J., Osara, J. A., Pasaribu, R., and Lugt, P. M., 2024. “Effect of bearing size in a grease lubricated ball bearings”. *Tribology International,* **146**, p. 106064.

(23) Jablonka, K., Glovnea, R., and Bongaerts, J., 2018. “Quantitative measurements of film thickness in a radially loaded deep-groove ball bearing”. *Tribology International,* **119**, pp. 239–249.

(24) Larsson, P.-O., Jacobson, B., and Höglund, E., 1994. “Oil drops leaving an EHD contact”. *Wear,* **179**(1-2), pp. 23–28.

(25) A ström, H., Östensen, J. O., and Höglund, E., 1993. “Lubricating grease replenishment in an elastohydrodynamic point contact”. *J. Tribol,* **115**.

(26) Heemskerk, R., Vermeiren, K., and Dolfsma, H., 1982. “Measurement of lubrication condition in rolling element bearings”. *ASLE Transactions,* **25**(4), pp. 519–527.

(27) Shetty, P., Meijer, R. J., Osara, J. A., and Lugt, P. M., 2023. “Vibrations and film thickness in deep groove ball bearings”. *Tribology Transactions*(1), pp. 2–6.

(28) Shetty, P., Meijer, R. J., Osara, J. A., and Lugt, P. M., 2022. “Measuring film thickness in starved grease-lubricated ball bearings: an improved electrical capacitance method”. *Tribology Transactions,* **65**(5), pp. 869–879.

(29) Pelofsky, A. H., 1966. “Surface tension-viscosity relation for liquids.”. *Journal of Chemical and Engineering Data,* **11**(3), pp. 394–397.

(30) Lugt, P. M., 2012. *Grease lubrication in rolling bearings*. John Wiley & Sons.

(31) Hamrock, B. J., and Dowson, D., 1978. Minimum film thickness in elliptical contacts for different

regimes of fluid-film lubrication. Tech. rep., NASA.

(32) Gupta, P., Cheng, H., Zhu, D., Forster, N., and Schrand, J., 1992. "Viscoelastic effects in mil-l-7808-type lubricant, Part I: analytical formulation". *Tribology transactions,* **35**(2), pp. 269–274.

(33) Harris, T. A., and Kotzalas, M. N., 2006. *Advanced concepts of bearing technology*. CRC press.

NOTATION

Nomenclature

α	Viscosity–pressure coefficient	[Pa^{-1}]
β	Temperature-viscosity coefficient	[$1/^{\circ}C$]
β'	Contact angle	[deg]
δ_i	Elastic deformation in ball-inner ring contact	[m]
δ_o	Elastic deformation in ball-outer ring contact	[m]
η	Dynamic viscosity of the base oil	[Pa s]
σ	Surface tension	[Nm^{-1}]
a	Half contact along the rolling direction	[m]
A_{lv}	Experimentally determined constant in Pelofsky's equation	[Nm^{-1}]
b	Half contact width across the rolling direction	[m]
B_{lv}	Experimentally determined constant in Pelofsky's equation	[Pa s]
Br	Brinkman number	[/]
C_T	Non-dimensional thermal correction factor	[/]
E'	Reduced elastic modulus	[Pa]
F	Load on the contact	[N]
G	Dimensionless material parameter $G = \alpha E'$	[/]
h_g	Grease film thickness	[m]
h_c	Central film thickness	[m]
h_{ff}	Fully flooded film thickness	[m]
K	Thermal conductivity of the lubricant	[$Wm^{-1}{}^{\circ}C^{-1}$]
k_d	Ellipticity parameter $k_d = 1.03\left(\frac{R_y}{R_x}\right)^{0.63}$	[/]
P_d	Diametrical clearance	[m]
p_m	Maximum Hertzian pressure	[Pa]
R_x	Reduced radius in the direction of motion	[m]
R_y	Reduced radius normal to the direction of motion	[m]
SRR	Slip-to-roll ratio	[/]
U	Dimensionless speed parameter $U = \frac{\eta u}{2E'R_x}$	[/]
u	Entrainment velocity (average velocity)	[$\mathrm{m\,s}^{-1}$]
W	Dimensionless load parameter $W = \frac{F}{E'(R_x)^2}$	[/]
z_r	Radial distance between the ball top and the outer ring groove	[m]

APPENDIX

Fully flooded film thickness is calculated using Hamrock and Downson's film thickness equation

$$h_{ff} = 2.69 C_T R_x U^{0.67} G^{0.53} W^{-0.067} (1 - 0.61 e^{-0.73 k_d}). \tag{5}$$

Here R_x is the reduced radius in the x direction (along rolling direction), k_d is the ellipticity parameter, G, U, and W are dimensionless material, speed, and load parameters, respectively.

C_T is a correction factor for the inlet shear heating effect given by

$$C_T = \frac{1 - 13.2(p_m/E')Br^{0.42}}{1 + 0.213(1 + 2.23SRR^{0.83})Br^{0.64}}. \tag{6}$$

Where Br is the Brinkman number given by $Br \approx -\beta\eta_0 u^2/K$. We assumed no slip condition, hence $SRR = 0$, β is the temperature-viscosity coefficient obtained from $\eta = \eta_0 e^{-\beta(T-T_0)}$, p_m is the maximum Hertzian pressure, and K is the thermal conductivity of the lubricant

APPENDIX F

TRIBOLOGY TRANSACTIONS
2021, VOL. 64, NO. 5, 891–902
https://doi.org/10.1080/10402004.2021.1943088

An Evaporation Model for Base Oil from Grease-Lubricated Rolling Bearings including Breathing

Pramod Shetty[a], Robert Jan Meijer[a], and Piet M. Lugt[a,b]

[a]Engineering Technology, University of Twente, Enschede, The Netherlands; [b]SKF Research and Technology Development, Houten, The Netherlands

ABSTRACT
The film thickness decay of grease-lubricated bearings is determined by a loss of lubricant from the bearing. One of these loss mechanisms is base oil evaporation. In this article, a model is presented for evaporation where the volatiles leave the bearing by breathing. The model is applied to a typical drive cycle where the temperature is varied in time. The impact of the volatility of base oils and quality of sealing on the evaporation losses can be quantified with this model.

ARTICLE HISTORY
Received 23 March 2021
Accepted 10 June 2021

KEYWORDS
Evaporation; grease; oil loss; bearings; vapor pressure

Introduction

Evaporation is a mass transfer process in which a material from the liquid state will transform into a gaseous state below the boiling point (1, 2). This is particularly relevant in grease-lubricated bearings because of the limited volume of oil in the "grease reservoir" that is available for lubrication. Besides oxidation and leakage, evaporation is considered to be one of the loss mechanisms that would have an impact on the grease life in rolling bearings (3). The prediction of the evaporation rate becomes particularly important for predicting the bearing performance at higher temperatures and/or long times. After all, grease-lubricated bearings are running in starved lubrication conditions, where the film thickness is determined by the availability of oil in the inlet. Evaporation of lubricant is one of the mechanisms that will have an impact on this. In addition, because the oil is usually a mixture of components having different properties, unequal evaporation of oil components may also change the properties of the oil such as the viscosity (4). The variation in viscosity could lead to a change in the film thickness, wear, and friction (4).

It is estimated that within a year, 1 ml of mineral oil could be lost per square centimeter if the oil is kept at 60° C and in a vacuum (5, 6). Therefore, many researchers have been working on this topic, particularly those studying bearings for space and hard discs.

In general, the evaporation rate of an oil layer will depend on the oil layer film thickness, molecular weight, and functional groups. Very often a pragmatic approach is followed. To our knowledge, the first study on evaporation loss of lubricants from bearings was conducted by Booster and Baker (7) and Mahneke and Schwartz (8) in the 1970s. They studied the evaporative loss from bearings with different seals and used the empirical equation from Mahncke and Schwartz (8):

$$E = 1 - \exp\left(-\left(\frac{t}{3600\alpha}\right)^{\beta}\right), \quad [1]$$

where E is the ratio of evaporated and original oil present in the grease. α and β are parameters that depend on the temperature, grease type, and experimental conditions, for which the values had to be experimentally determined. Booster and and Baker (7) tested the evaporation of grease to predict the evaporation loss for 4,000 h. They found that the evaporation becomes significant for petroleum greases when the temperature is above 100° C. The evaporation loss for silicone oils was not significant. Application of these evaporation measurements to running bearings is not trivial. For example, other than in bearings, which are sealed off, their tests were conducted in an open, well-ventilated environment (9).

Evaporation also plays a role in modeling oxidation where large molecular weight molecules are transferred into low molecular weight molecules, which are much more volatile, as modeled by Naidu et al. (10). The evaporation rate in this work was estimated by a zero-order kinetic equation and the evaporation rate constant was determined experimentally. This rate constant was found to follow an Arrhenius relationship with the temperature.

Other available models for the evaporation of oil were developed specifically for magnetic recording systems. The experimental studies on the lubricant depletion from the

CONTACT Pramod Shetty p.shetty@utwente.nl
Review led by M. Dube.

Nomenclature

A	Surface area for oil layers inside the bearing $[m^2]$
A_{gap}	Surface area of the gap between shield and inner ring $[m^2]$
B	Bearing width $[m]$
b	Shield thickness $[m]$
C	Concentration $[mol/m^3]$
C_v	Concentration of volatiles $[mol/m^3]$
C_a	Concentration of air molecules $[mol/m^3]$
d	Bore diameter $[m]$
D_o	Outer diameter of the bearing $[m]$
D	Diffusion coefficient $[m^2.s^-1]$
E	Ratio of evaporated and original oil present in the grease [-]
K	Mass transfer coefficient $[m.s^-1]$
m	Molar mass $[kg/mol]$
M	Bearing mass $[kg]$
N	Evaporation mass flux $[kg/m^2.s]$
n	Number of moles of gas [mol]
n_v	Number of moles of volatiles [mol]
$n_{v,lost}$	Number of moles of volatiles lost from the bearing [mol]
n_a	Number of moles of air molecules [mol]
$n_{a,lost}$	Number of moles of air molecules lost from the bearing [mol]
p	Pressure $[Pa]$
p_{atm}	Atmospheric pressure $[Pa]$
p_v	Vapor pressure $[Pa]$
$p_{v,sat}$	Saturated vapor pressure $[Pa]$
$p_{ref,sat}$	Saturated vapor pressure $[Pa]$
t	Time $[s]$
T	Temperature $[K]$
T_a	Atmospheric temperature (air outside bearing) $[K]$
T_A	Arrhenius temperature $[K]$
T_l	Liquid-phase temperature $[K]$
T_v	Vapor-phase temperature $[K]$
T_{ref}	Reference temperature for saturation pressure determination $[K]$
$T_{\sigma,ref}$	Reference temperature for evaporation coefficient determination $[K]$
R	Gas constant $[J.mol^{-1}.K^{-1}]$
V	Volume $[m^3]$
V_b	Free volume in bearing $[m^3]$
α	Evaporation constant
β	Evaporation constant
χ_v	Mole fraction of volatiles $\chi_v = n_v/(n_a + n_v)$
χ_a	Mole fraction of air molecules $\chi_a = n_a/(n_a + n_v)$
η	Dynamic viscosity $[Pa \cdot s]$
ν	Kinematic viscosity $[mm^2/s]$
σ	Evaporation coefficient
σ_e	Evaporation coefficient
σ_c	Condensation coefficient
σ_{ref}	Reference evaporation coefficient
Δh	Enthalpy of vaporization
ΔH_{obs}	Constant
ΔS_{obs}	Constant
δ	Diffusion length $[m]$
ρ_b	Density of the bearing material $[kg/m^3]$

Subscripts

B	Subscript denoting "breathing" by temperature increase -
$diff$	Subscript denoting diffusion through the seal gap -
E	Subscript denoting evaporation -

magnetic drive systems by Tagawa et al. (12, 13) have shown that when the oil layer thickness is very thin—that is, on in the order of thickness of a monolayer (12), so typically less than 100 nm thickness—the vapor pressure will be attributed to the disjoining pressure (14–17). This change of saturated vapor pressure due to the disjoining pressure can be estimated from the Gibbs-Duhem equation (15, 18). For thicker layers, the influence of disjoing pressure can be disregarded; hence, the evaporation loss can be estimated from TGA measurements.

Although some inspiration can be obtained from these models, using them without suitable adaptations for bearing applications is not possible. For "normal" rolling bearing applications, the oil layers are thicker than those of monolayers, so the evaporation from very thin layers will not be addressed here. The evaporation rate can therefore be assumed to depend on the surface area, temperature, molecular weight, saturated vapor pressure, and vapor pressure of the lubricant only. The vapor pressure depends on the expulsion rate of evaporated products (volatiles). This is determined by diffusion and by flow caused by "breathing of the bearing." Breathing is the process of a pressure-driven flow, in and out of the bearing, caused by expansion and shrinkage of air and volatiles inside the free volume of the bearing, which is a result of the generation of volatiles itself but also by temperature fluctuations. This breathing will accelerate the evaporation of the base oil due to a reduction of the concentration of volatiles inside the bearing. Volatiles may also escape through the gap between the seal and inner ring in the absence of a pressure drop. In that case, migration is caused by a concentration difference of volatiles inside the bearing and outside the bearing. This can be described as a diffusion process and can also be called breathing. In this article, we will address all three processes.

General evaporation models for liquids

There are a variety of methods and theories that can be used to calculate the evaporation rate of liquids. The commonly used methods are based on the kinetic, diffusion, or mass transfer theories (19–21). In this section, these models will be discussed briefly, followed by selection of the model that will be used in our study.

Model based on kinetic theory of gas

In 1882, Hertz (22) came up with an equation for evaporation using the classical kinetic theory of gases. He concluded that "every substance will have a maximum evaporation rate, which depends only on the temperature of the surface and on properties of the substance" (21, 22). His equation describes the relation between the molecular weight of the liquid and the saturated vapor pressure as a function of the temperature (22, 23). The evaporation rate can be calculated from the frequency of collisions between the vapor molecules and the liquid surface (21, 24).

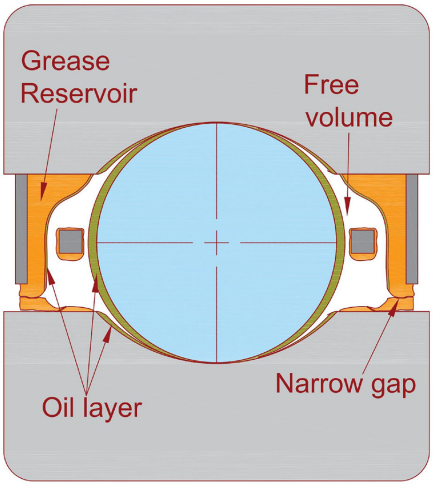

Figure 1. Schematic representation of the bearing.

The equation for the evaporation rate from Hertz was further improved by Knudsen (27) (21, 23, 25) . He noticed that the evaporation rate was over estimated by Hertz's theory. He argued that a molecule that hits the surface would not necessarily condense but could also bounce back. The evaporation rate will therefore always be lower than predicted from Hertz theory. To accommodate this, he introduced evaporation and condensation coefficients in the evaporation expression given by Hertz

$$N = \sqrt{\frac{m}{2\pi R}}\left(\sigma_e \frac{p_{v,sat}}{\sqrt{T_l}} - \sigma_c \frac{p_v}{\sqrt{T_v}}\right), \quad [2]$$

where N is the evaporation mass flux, m is molar mass, R is the gas constant, $p_{v,sat}$ is the saturated vapor pressure, p_v is the vapor pressure, T_l is the liquid phase temperature, and T_v is the vapor-phase temperature. σ_c and σ_e are condensation and evaporation coefficients, respectively, with values ranging from 0 to 1. In practice, the liquid and vapor temperatures will be almost identical, so $T_l = T_v = T$. Very often (25,28,29), this equation is further simplified by assuming $\sigma_e = \sigma_c = \sigma$, giving

$$N = \sigma\sqrt{\frac{m}{2\pi RT}}(p_{v,sat} - p_v). \quad [3]$$

Here σ is called the evaporation coefficient, sometimes also referred to as the accommodation coefficient (25). In 2012, Zhou et al. (18) experimentally showed that this evaporation coefficient follows an Arrhenius temperature relationship and proposed the following equation:

$$\sigma(T) = \exp(\Delta H_{obs} - T\Delta S_{obs}). \quad [4]$$

Here ΔH_{obs} and ΔS_{obs} are constants. These are experimentally determined and are not related to enthalpy and entropy as suggested by their symbols (18).

Evaporation model based on diffusion theory

In the absence of convection, evaporation will be limited by diffusion in the gas phase. This was addressed by Maxwell in 1877 (26 , 30), who studied the evaporation of a stationary droplet . This process is referred to as "diffusion-controlled evaporation" (30). The diffusion rate is usually estimated using Fick's first law (19, 20, 30). The following relation was used by Karis and Nagaraj (21) to derive the vapor pressure p_v from the evaporation measurements in a nitrogen environment:

$$N = \frac{D}{\delta}\left(\frac{m}{RT}\right)p_{v,sat}. \quad [5]$$

Here D is the diffusion coefficient and δ is the diffusion length. Note that this equation is quite similar to Eq. [3]. However, including a condensation term is not possible here.

Sometimes this diffusion equation [5] is further simplified by replacing the ratio of diffusion coefficient and diffusion length by a constant K, which is called the "mass transfer coefficient" and the model a "mass transfer model." This model has been applied to "oil spill evaporation," where the evaporation of oil from very thin layers on water is calculated (31) :

$$N = K\frac{mp_{v,sat}}{RT}. \quad [6]$$

Evaluation of the evaporation models

There are more models that can be used to predict the evaporation rate of oils, such as models based on the statistical rate theory (25, 32), which are still under development and are complex. These go beyond the scope of this article, in which we will use an engineering approach.

To estimate the evaporation loss of base oil from grease in a bearing, we have selected the Hertz-Knudsen model, Eq. [3]. This is because the surface speeds in a rotating bearing are generally quite high and it is assumed that by perfect mixing all evaporated molecules are distributed in a uniform manner within the bearing volume and that there will be no concentration gradients near the evaporation surface. This means that the evaporation rates will not be determined by diffusion. Because of these high speeds, the diffusion length (Eq. [5]) will approach zero. Applying the diffusion model would only be appropriate for bearings running at very low speed. However, in that case the temperatures are usually lower and evaporation is therefore less relevant for those conditions.

Evaporation loss model for rolling bearings

Bearing configuration

The model that will be outlined here describes evaporation in shielded bearings; that is, bearings that are sealed by noncontacting seals. This means that there is a thin gap between the seal and the inner ring; see Fig. 1. This gap may be closed by grease or bled oil. This closure is very "fragile," though. Even

though it is sealed by the grease, there will often be a very narrow gap that will allow some transport of volatiles from the free volume of the bearing into the atmosphere.

Evaporation will take place from the surface of the grease itself. After all, grease consists mainly (80–90%) of base oil. In addition, it will occur from the very thin base oil layers that are formed on the functional surface of the bearing by grease bleed (33). The oil layers on the grooves and rolling elements are sheared/overrolled, so it may be assumed that the surfaces of these layers are regularly "refreshed." Evaporated oil from these layers will be replenished with bled oil from the grease. The films are thin but sufficiently large (thickness on the order of magnitude 0.2 μm) to neglect the effect of disjoining pressure on the vapor pressure. Hence, it is assumed that the total surface area inside the bearing is covered with a layer of base oil or grease from where evaporation takes place. This surface area, denoted here by A, can be calculated by taking the sum of the surface areas of the inner ring, outer ring, shield, and rolling elements. The dimensions that are needed to calculate this for standard bearings can be found in rolling bearing catalogs such as SKF (34).

Evaporation model

Evaporation will take place from the surface into the free volume of the bearing, V_b, which can be approximated by using the bearing mass and outside dimensions:

$$V_b = \frac{\pi}{4} B\left(D_o^2 - d^2\right) - \frac{M}{\rho_b}, \qquad [7]$$

where B is the bearing width, d is the bore diameter, D_o is the outer diameter, M is the mass of the bearing, and ρ_b is the density of the bearing material ($\rho_b = 7,800 kg/m^3$ for a full-steel bearing).

The evaporation rate is determined by the vapor pressure, which is again determined by the concentration of volatiles inside the free volume. Evaporation will increase the vapor pressure and therefore decreases the evaporation rate. Evaporation will stop once the vapor pressure in the free volume is equal to the saturated vapor pressure of the lubricant.

The free volume of the bearing V_b is filled with n_a moles of "atmospheric molecules" and n_v "volatiles" formed by evaporation of the thin layers of oil, with surface area A, formed by grease bleed in the bearing. Evaporation continues until the air is saturated; that is, when the vapor pressure p_v has reached the saturated vapor pressure $p_{v,sat}$.

The number of molecules that are evaporating per unit of time is calculated using the Hertz-Knudsen equation [3]:

$$\frac{dn_v}{dt} = \sigma \sqrt{\frac{1}{2\pi m R T}} (p_{v,sat} - p_v) A. \qquad [8]$$

The saturated vapor pressure, $p_{v,sat}$, at temperature T, is calculated using the Clausius-Clapeyron equation (33):

$$\ln \frac{p_{ref,sat}}{p_{v,sat}} = \frac{\Delta h}{R}\left(\frac{1}{T} - \frac{1}{T_{ref}}\right), \qquad [9]$$

where $p_{ref,sat}$ is the saturated vapor pressure of the oil at temperature T_{ref} and Δh is the enthalpy of vaporization.

Loss of volatiles from the bearing

Breathing mechanisms

Even in the absence of air flow through the bearing, the volatiles that are formed in the interior of the bearing by evaporation may be lost from the bearing. This will happen through the gap between the bearing seal and shaft. There are three "breathing" mechanisms for this.

Evaporation increases the pressure, causing gas (air + volatiles) to flow out of the bearing. In our model it is assumed that the temperature fluctuations are not "abrupt" and that the resistance to gas flow through the gap between the shield and inner ring can therefore be neglected. The gas volume that is lost can then be calculated from the growth of the gas volume caused by evaporation. In this mechanism the flow is therefore only determined by expansion and shrinkage of the air inside the bearing by evaporation (or condensation), assuming a constant (ambient) pressure. This mechanism is called here "expansion by evaporation" (EE).

The second cause of migration of volatiles is flow caused by a pressure difference induced by temperature fluctuations. This may result from variations of the operating conditions in a bearing (such as load and speed), which will lead to variations in frictional heat and therefore temperature. The increase or decrease of temperature will then cause respectively "expansion or shrinkage" of the gas inside the free volume. This effect is denoted here by "isobaric thermal Expansion" (ITE).

The third mechanism is a loss of volatiles caused by diffusion, driven by a concentration difference of volatiles inside and outside the bearing. It is important to notice that this is different from the diffusion model described in section Evaporation model based on diffusion theory. This effect is denoted here by "Diffusion" (D).

The model also applies to bearings that are sealed with "contacting seals." In that case diffusion can be neglected. However, the other breathing mechanisms can still occur due to the flexibility of the (usually rubber) seals.

Expansion by evaporation

The vapor pressure is the result of the pressure caused by the evaporated molecules and is related to the number of molecules following the ideal gas law (31):

$$p_v = \frac{n_v R T}{V_b}. \qquad [10]$$

Because the bearing is sealed by a noncontacting seal, the total pressure is constant and equal to the atmospheric pressure. So

$$p_{atm} V_b = (n_v + n_a) R T \qquad [11]$$

or

$$V_b = \frac{(n_v + n_a) R T}{p_{atm}}. \qquad [12]$$

Due to evaporation during a very small time interval dt, the number of volatiles will increase with dn_v. This leads to a

virtual increase of the volume by

$$dV = \frac{RTdn_v}{p_{atm}}. \quad [13]$$

It is assumed that air and volatiles are well mixed. Hence, the fraction of volatiles, or concentration, in volume dV is the same as in volume V_b. The concentration of volatiles and air read respectively:

$$C_v = \frac{n_v}{V_b + dV} \approx \frac{n_v}{V_b} \quad [14]$$

and

$$C_a = \frac{n_a}{V_b + dV} \approx \frac{n_a}{V_b}. \quad [15]$$

The lost numbers of volatiles and air therefore are

$$\frac{dn_{v,lost}}{dV} = C_v \quad [16]$$

$$\frac{dn_{a,lost}}{dV} = C_a. \quad [17]$$

Substituting these in Eqs. [14] and [15] will result in the following equations:

$$\frac{dn_{v,lost}}{dV} = \frac{n_v}{V_b} \quad [18]$$

$$\frac{dn_{a,lost}}{dV} = \frac{n_a}{V_b}. \quad [19]$$

Replacing dV using Eq. [13] gives

$$\frac{dn_{v,lost}}{\frac{RTdn_v}{p_{atm}}} = \frac{n_v}{V_b} \quad [20]$$

$$\frac{dn_{v,lost}}{dn_v} = \frac{n_v}{V_b}\frac{RT}{p_{atm}}. \quad [21]$$

So the evaporation loss flow rates read:

$$\left.\frac{dn_{v,lost}}{dt}\right|_{EE} = \frac{n_v}{V_b}\frac{RT}{p_{atm}}\frac{dn_v}{dt} \quad [22]$$

$$\left.\frac{dn_{a,lost}}{dt}\right|_{EE} = \frac{n_a}{V_b}\frac{RT}{p_{atm}}\frac{dn_v}{dt}. \quad [23]$$

Using the Hertz-Knudsen equation [8] then gives the following for the rate of lost volatiles:

$$\left.\frac{dn_{v,lost}}{dt}\right|_{EE} = \frac{n_v}{V_b p_{atm}}\sigma\sqrt{\frac{RT}{2\pi m}}(p_{v,sat} - p_v)A. \quad [24]$$

Note that condensation causes a decrease in the gas volume and therefore does not lead to a loss of volatiles.

Isobaric thermal expansion

A change in temperature not only affects the evaporation rate but will also cause a change in volatile content in the free bearing volume. An increase in temperature will result in "breathing out" and a decrease in temperature will result in "breathing in." Breathing out will lead to a loss of volatiles. Breathing in will inhale the cold air from the atmosphere and dilute the concentration of volatiles, lowering the vapor pressure so that new evaporation can take place.

Increase in temperature. Volatiles and air molecules are present in the free volume of the bearing V_b. When the temperature changes, this gas volume will change. When the temperature increases with dT it expands with dV and will not fit inside the bearing. Again, it is assumed that there is no resistance to flow and this will therefore instantaneously be outside the bearing. This volume dV will contain a number of molecules (air and volatiles) dn that can be considered as being lost. It is assumed that the ideal gas law applies and that the total pressure remains equal to the atmospheric pressure:

$$p_{atm} = \frac{nRT}{V_b} \quad [25]$$

with

$$n = n_a + n_v. \quad [26]$$

Here n_v is the number volatiles and n_a is the number of air molecules. So when the temperature changes with dT, the volume will change with

$$dV = \frac{nR}{p_{atm}}dT. \quad [27]$$

With this change of volume, the concentration will change. When the volume increases to $V_b + dV$ the number of molecules n will remain constant. This means that the concentration now becomes

$$C = \frac{n}{V_b + dV}. \quad [28]$$

This concentration is uniform, so the number of molecules leaving the bearing in volume dV by breathing will be

$$dn_{lost}\Big|_{ITE} = \frac{n}{V_b + dV}dV \quad [29]$$

or

$$\left.\frac{dn_{lost}}{n}\right|_{ITE} = \frac{dV}{V_b + dV} \approx \frac{dV}{V_b}. \quad [30]$$

Combining Eqs. [27] and [30] gives

$$\left.\frac{dn_{lost}}{n}\right|_{ITE} = \frac{nR}{p_{atm}V_b}dT \quad [31]$$

or

$$\left.\frac{dn_{lost}}{dT}\right|_{ITE} = \frac{n^2R}{p_{atm}V_b}. \quad [32]$$

So the number of molecules that are lost by increasing the temperature depends on the number of molecules itself and on the bearing free volume. With $n = n_a + n_v$ the lost number of volatiles n_v can be calculated by

$$\left.\frac{dn_{a,lost}}{dT}\right|_{ITE} + \left.\frac{dn_{v,lost}}{dT}\right|_{ITE} = \frac{(n_a + n_v)^2R}{p_{atm}V_b}. \quad [33]$$

It is assumed that air and volatiles are perfectly mixed. The mole fraction of air and volatiles in new virtual volume dV will be equal to the mole fraction in V_b. Hence, we can use the following equations to find the air and volatiles lost during the breathing out process:

$$\left.\frac{dn_{v,lost}}{dT}\right|_{ITE} = \chi_v \frac{(n_a + n_v)^2 R}{p_{atm} V_b} \quad [34]$$

$$\left.\frac{dn_{a,lost}}{dT}\right|_{ITE} = \chi_a \frac{(n_a + n_v)^2 R}{p_{atm} V_b} \quad [35]$$

with $\chi_v = n_v/(n_a + n_v)$ and $\chi_a = n_a/(n_a + n_v)$ the mole fractions of volatiles and air molecules, respectively. This can be further simplified by substituting the values for χ_v and for p_{atm} from Eq. [25].

$$\left.\frac{dn_{v,lost}}{dT}\right|_{ITE} = \frac{n_v}{T} \quad [36]$$

and

$$\left.\frac{dn_{a,lost}}{dT}\right|_{ITE} = \frac{n_a}{T}. \quad [37]$$

Decrease in temperature. If the temperature decreases with dT, fresh air with volume dV, containing dn_a moles of air molecules, is sucked into the bearing. In that case the volatiles are not lost, as was the case with a temperature increase, but the concentration will be reduced. More specifically, at temperature T there were $n = n_a + n_v$ moles of molecules. When the temperature is now decreased with dT these will now be diluted by dn_a air molecules, originating from a volume dV. Again, it is assumed that there is no resistance to flow and this "breathing in" will therefore occur instantaneously.

The reduction of volume applies to the bearing volume $V = V_b$, filled with air and volatiles with total number of molecules $n = n_a + n_v$ (mol). It is again assumed that the ideal gas law applies and that the total pressure is equal to the atmospheric pressure. So at temperature T

$$p_{atm} = \frac{nRT}{V_b} \quad [38]$$

with $n = n_a + n_v$.

So when the temperature reduces with dT, the volume of gas inside the bearing (that will be replaced by air from outside the bearing) will be reduced by

$$dV = \frac{(n_a + n_v)R}{p_{atm}} dT. \quad [39]$$

This dV be filled with air molecules from outside the bearing. The concentration of air molecules in air is

$$\frac{n_a}{V} = \frac{p_{atm}}{RT_a}, \quad [40]$$

where T_a is the temperature outside the bearing (ambient temperature), which can be considered constant.

Hence the "inhaled" number of air molecules reads

$$dn_a = \frac{p_{atm}}{RT_a} dV. \quad [41]$$

With Eq. [39] this gives

$$dn_a = \frac{p_{atm}}{RT_a} \frac{(n_a + n_v)R}{p_{atm}} dT \quad [42]$$

or

$$\frac{dn_a}{dT} = \frac{n_a + n_v}{T_a}, \quad [43]$$

with n_a the air molecules *inside* the bearing volume V_b.

Diffusion of volatiles through the seal gap (D)

The volatiles from the bearing can also leave the bearing through the narrow gap between the shield and the bearing inner ring by diffusion. This is not pressure driven but concentration driven and can be estimated using Fick's first law,

$$\left.\frac{dn_v}{dt}\right|_D = -A_{gap} D \frac{dc}{dx}, \quad [44]$$

where dn_v is the change in number of volatiles in the bearing, A_{gap} is the surface area of the gap, D is the diffusion coefficient, and $\frac{dc}{dx}$ is the concentration gradient of the volatiles in the gap in the axial direction. Again the concentration of volatiles can be calculated using the ideal gas law:

$$C = \frac{p_v}{RT}. \quad [45]$$

The concentration is assumed to be constant in the bearing volume and linear in the shield gap, going to zero outside of the bearing. With a shield thickness b and substitution of Eq. [45] into Eq. [44] this gives

$$\left.\frac{dn_v}{dt}\right|_D = -A_{gap} D \frac{p_v}{bRT} = -A_{gap} D \frac{n_v}{bV_b}. \quad [46]$$

The lost number of volatiles by diffusion through the shield gap then reads:

$$\left.\frac{dn_{v,lost}}{dt}\right|_D = -\left.\frac{dn_v}{dt}\right|_D. \quad [47]$$

The diffusion coefficients in gases are commonly estimated using Chapman-Enskog theory (19). The simplified form of this equation for the diffusion of oil vapors into the nitrogen atmosphere is given by Karis and Nagaraj (20):

$$D = 3.55 \times 10^{-9} \left(0.0357 + \frac{1}{m \times 1000}\right)^{\frac{1}{2}} T^{\frac{3}{2}}, \quad [48]$$

with m the molar mass (kg/mol) and T the temperature (K).

Summary of the evaporation loss model

Due to evaporation, the number of volatile molecules (n_v) in the bearing increases and the number $n_{v,lost}$ leaves the bearing by thermal expansion and diffusion.

At each point in time the change in the number of volatiles in the bearing is calculated using

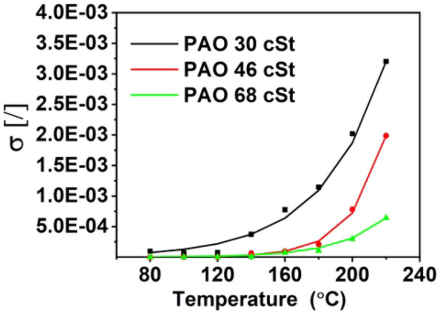

Figure 2. Evaporation coefficient for the PAO oils listed in Table 1.

$$\frac{dn_v}{dt} = \sigma\sqrt{\frac{1}{2\pi mRT}}(p_{v,sat} - p_v)A, \quad [49]$$

where σ can be estimated by,

$$\sigma = \sigma_{ref} 2^{\frac{T-T_{\sigma ref}}{T_a}}. \quad [50]$$

The saturated vapor pressure can be calculated from

$$\ln\frac{p_{ref,sat}}{p_{v,sat}} = \frac{\Delta h}{R}\left(\frac{1}{T} - \frac{1}{T_{ref}}\right). \quad [51]$$

The vapor pressure inside the bearing can be calculated from

$$p_v = \frac{n_v RT}{V_b}. \quad [52]$$

The total amount of volatiles leaving the bearing is determined by ITE, EE, and D through the seal gap:

$$\frac{dn_{v,lost}}{dt} = \frac{dn_{v,lost}}{dT}\Big|_{ITE} + \frac{dn_{v,lost}}{dt}\Big|_{EE} + \frac{dn_{v,lost}}{dt}\Big|_{D}. \quad [53]$$

For ITE, there is a difference between a temperature increase and decrease. When there is a temperature increase, $dT > 0$,

$$\frac{dn_{v,lost}}{dT}\Big|_{ITE} = \frac{n_v}{T}, \quad [54]$$

and for a temperature decrease, $dT \leq 0$,

$$\frac{dn_{v,lost}}{dT}\Big|_{ITE} = 0. \quad [55]$$

For EE there is difference between a positive and a negative dn_v/dt, as calculated in Eq. [49]. If $dn_v/dt > 0$, then

$$\frac{dn_{v,lost}}{dt}\Big|_{EE} = \frac{n_v}{V_b p_{atm}}\sigma\sqrt{\frac{RT}{2\pi m}}(p_{v,sat} - p_v)A, \quad [56]$$

For a negative flow, when $dn_v/dt \leq 0$,

$$\frac{dn_{v,lost}}{dt}\Big|_{EE} = 0. \quad [57]$$

Finally, the volatiles lost by diffusion are given by

$$\frac{dn_{v,lost}}{dt}\Big|_{D} = -A_{gap} D \frac{n_v}{bV_b}, \quad [58]$$

Table 1. Oil evaporation parameters.

Parameter	PAO 30 cSt	PAO 46 cSt	PAO 68 cSt	Unit
$T_{\sigma,ref}$	413	433	433	K
σ_{ref}	3.73×10^{-4}	9.55×10^{-5}	7.27×10^{-5}	
T_A	25.8	13.7	19.1	
Δh	14,603	21,908	27,450	J
p_{ref}	0.1347	0.2133	0.2266	Pa
T_{ref}	366.3	421.9	421.9	K
m	0.554	0.629	0.69	kg/mol

Table 2. Relevant parameters for the 6209-2Z bearing.

Sample no.	Parameter	Value	Unit
1	Surface area of evaporation	0.0166	m^2
2	Free volume	1.57×10^{-5}	m^3
3	Gap between the shield and inner ring	0.275	mm
4	Shield thickness	0.33	mm

Evaporation measurements

The evaporation model parameters from the Hertz-Knudsen equation [3] were measured using a thermogravimetric analyzer, on polyalphaolefin (PAO) oils with kinematic viscosities of 31, 47, and 63 cSt at 40° C. A droplet of oil was put in the ceramic pan where it was distributed evenly. Measurements were carried out at 80, 100, 120, 140, 160, and 180° C in a nitrogen atmosphere for 3 h. As mentioned above, the temperature dependence of the evaporation flux follows an Arrhenius behavior. Instead of using the original formulation from Zhou et al. (18), Eq. [4], we will use a more convenient formulation that is commonly used in grease life models (3):

$$\sigma = \sigma_{ref} 2^{\frac{T-T_{\sigma,ref}}{T_A}}, \quad [59]$$

where σ_{ref} is the evaporation coefficient at temperature $T_{\sigma,ref}$ and T_A, an Arrhenius temperature.

The evaporation coefficients are shown in Fig. 2. It can be seen that the evaporation coefficient increases exponentially with increasing temperature. The estimated parameters for all tested oils are listed in Table 1. Using these values we can estimate the evaporation rate of these oils at any temperatures.

Simulation results

Configuration and simulation drive cycle

All calculations will be done for a single bearing. Studying the effect of bearing type and bearing size goes beyond the scope of this article. We selected a 6209-2Z bearing and the three PAO oils for which the parameters are given in Table 1. An arbitrary temperature drive cycle was used where the bearing was run at 150° C for 10 h and at 70° C for 10 h. This cycle was repeated for 2 years. Other relevant parameters are listed in Table 2. To study the effect of different evaporation loss mechanisms, simulations were run, showing not only the total loss but also the separate loss of volatiles by volume expansion by EE, ITE, and D.

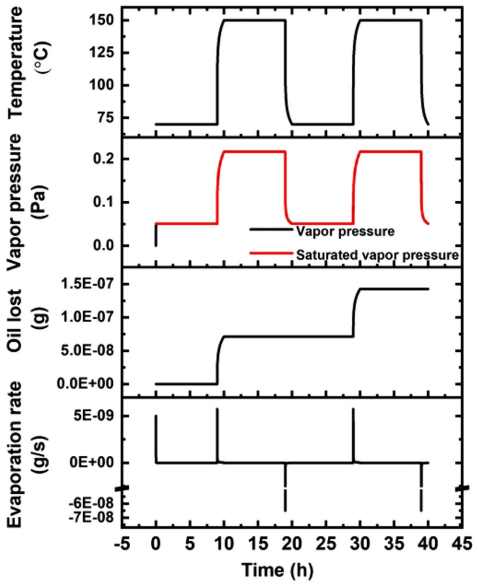

Figure 3. The variation in evaporation rate, oil remaining in the bearing, vapor pressure, and temperature cycle with only ITE as a loss mechanism.

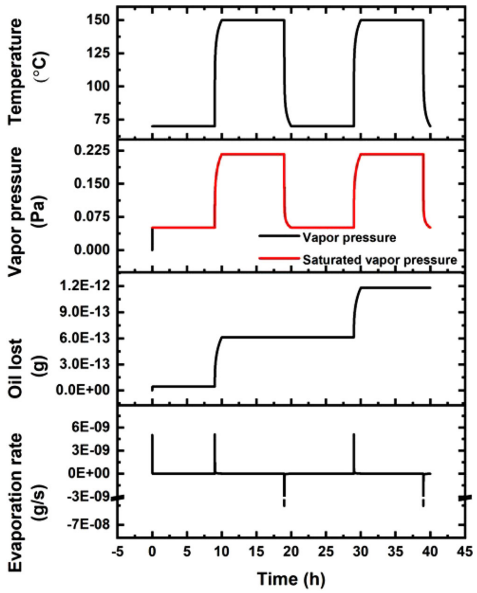

Figure 4. Response to a variation in temperature with only EE as a loss mechanism.

The significance of the various loss mechanisms

To study the significance of the various loss mechanisms, the cycle as defined above was run for various cases, where in all cases the base oil in the bearing was evaporating and could escape from the bearing by means of EE, ITE, or D. Only PAO 46 oil is considered.

Loss of volatiles only by isobaric thermal expansion

Figure 3 shows the variation of temperature, vapor pressure, remaining oil, and evaporation rate for the selected temperature cycle. Only the first two cycles are shown. At the beginning of the cycle, the vapor pressure is zero, so the oil starts to evaporate. This increases the vapor pressure inside the bearing and the evaporation rate gradually decreases. After 10 h, the temperature increases to 150° C, leading to a loss of volatiles by ITE and a reduction of the remaining oil in the bearing. It also leads to a higher saturation vapor pressure, resulting in a sudden increase in evaporation. The vapor pressure again starts to increase in the bearing and reaches the saturated vapor pressure. After 10 h, the temperature drops to 70° C. Fresh air is sucked into the bearing, which reduces the concentration of volatiles. The lower temperature also reduces the saturated vapor pressure of the oil, resulting in condensation. This leads to a gradual decrease in the vapor pressure until it reaches the saturated vapor pressure where the condensation stops. When the temperature subsequently rises to 150° C again, volatiles escape by "breathing out" (ITE), reducing the remaining oil in the bearing. Moreover, it increases the saturated vapor pressure, leading to evaporation again. This cycle repeats itself for 2 years. We can observe that at both low and high temperatures, the vapor pressure reaches the saturated vapor pressure quickly. This is because we assumed in this section that the volatiles can escape from the bearing only during an increase in temperature.

Loss of volatiles by volume expansion by evaporation

This section describes the volatiles that will escape from the bearing during evaporation by a virtual expansion of the gas volume caused by an increase of volatile molecules while keeping the pressure constant, $p = p_{atm}$. ITE and D are not considered here. The variation in vapor pressure, evaporation rate, and loss of volatiles when only this mechanism is considered are shown in Fig. 4. Volatiles escape from the bearing throughout the considered time period but the loss is more pronounced when the temperature changes. This is due to the large difference in vapor pressure and saturated vapor pressure when the temperature increases. The figure also shows that the loss induced by this mechanism is very small compared to the loss due to other mechanisms.

Loss of volatiles by diffusion

To estimate the diffusive losses, we have to define the area of the gap between the shield and the shoulder. Usually, this gap is filled with grease that partially or completely closes the gap. The actual area depends on the type of grease, seals, temperature, load, time, and other operating conditions. It is difficult to predict the exact value of this area at this point, and it is beyond the scope of this article. Hence, we considered two extreme possible conditions; that is, a gap areas of 0.01% and 100% of the total area between the shield and the

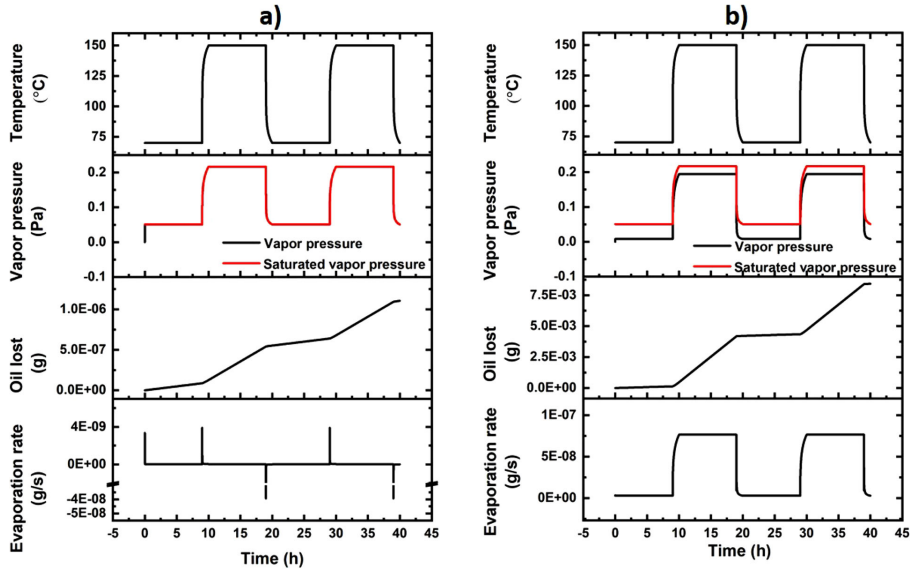

Figure 5. Response to a variation in temperature when only the diffusive loss mechanism (D) is considered. (a) 0.01% of the shield gap is open and (b) shield–inner ring gap totally opened.

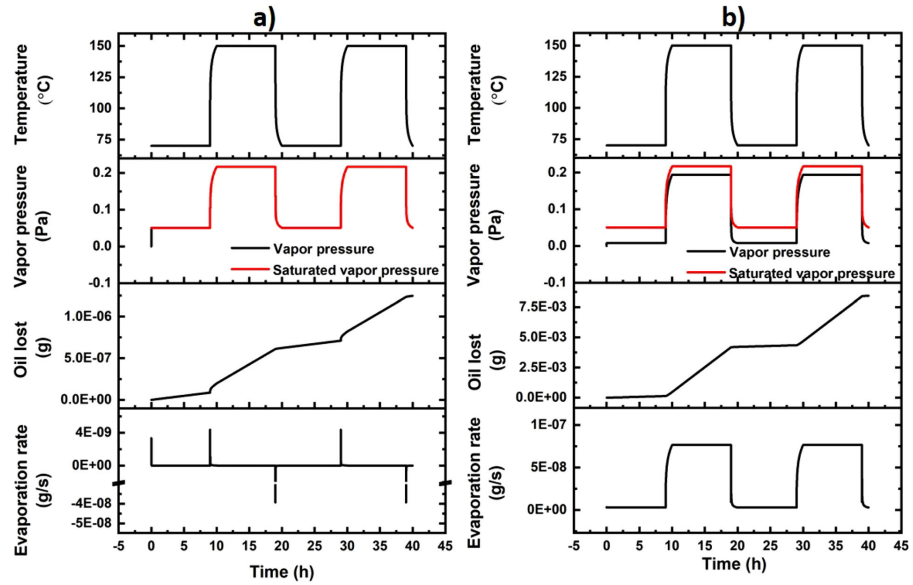

Figure 6. Response to a variation of temperature when all loss mechanisms are included. (a) 0.01% of the shield gap is open and (b) shield–inner ring gap totally opened.

inner ring shoulder. For simplicity, from here onwards, the percentile area is denoted by a prefix. The variation of evaporation rate, oil remaining, and vapor pressure are shown in Fig. 5. Unlike losses caused by ITE, the diffusion losses are continuous. When considering an area of 0.01%, the vapor pressure inside the bearing is always nearly equal to the

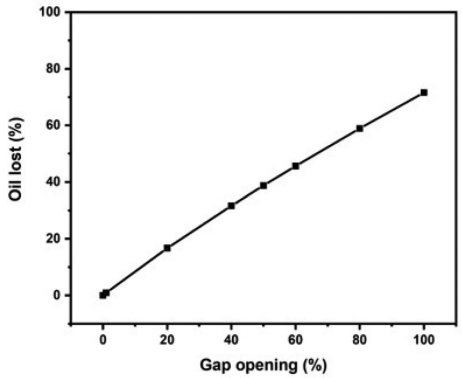

Figure 8. Effect of gap opening on the oil loss. All three loss mechanisms are taken into account.

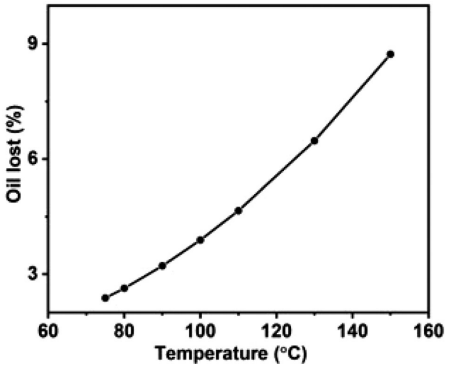

Figure 9. Oil loss at different temperatures after 2 years of drive cycles, where the bearing is running for 10 h at 70 ° C and 10 h at temperatures ranging from 75–150° C.

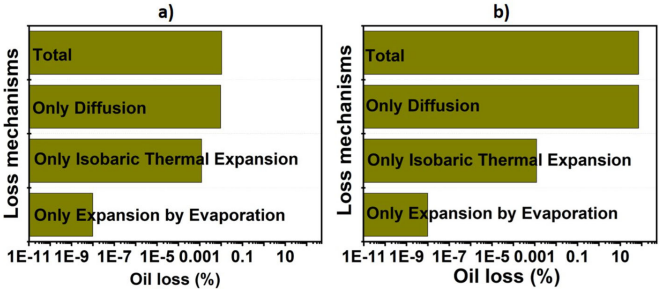

Figure 7. Percentage oil lost after 2 years by considering different loss mechanisms where "Total" refers to "including all mechanisms" (EE + ITE + D). (a) almost closed shield–inner ring gap and (b) open shield–inner ring gap.

saturated vapor pressure and the loss of volatiles is the same order of magnitude as for ITE. The evaporation rate shows a sudden short increase when the temperature increases due to an increase in the saturated vapor pressure. Because of the very small gap, hardly any volatiles can escape and the vapor pressure will therefore increase quickly, leading to a very low evaporation rate. By contrast, when the shield gap is 100% open, the diffusive losses are four orders of magnitude larger, leading to a continuous low vapor pressure. The vapor pressure never reaches the saturated vapor pressure, leading to continuous evaporation and therefore to a much higher evaporation loss.

Loss of volatiles by considering all three loss mechanisms

Figure 6 shows the evolution of vapor pressure, volatiles, mass loss, and evaporation rate when losses induced by all three mechanisms are considered. Here, the loss induced by diffusion is calculated for both 0.01% and 100% shield gap openings. It can be noticed that for 0.01% and 100%, the oil loss and the evaporation rate is clearly different, not only when the temperature changes but also for the time periods when the temperature is constant. When the seal gap is 100% open, as explained in the previous section, diffusive losses dominate. When the gap is almost closed, all three loss mechanisms should be taken into account. These results also show that for a very good sealed bearing, evaporation losses are small but both diffusive losses and ITE are on the same order of magnitude. However, the sealing quality is clearly the most important factor for preventing losses by evaporation. Note that the evaporation losses are very significant with a totally opened gap.

Impact of the different loss mechanisms on the total oil loss

The variation in vapor pressure, flow rate, and oil loss a shown in Figs. 3, 4, 5, and 6 for different mechanisms for a few cycles. Figure 7 shows the influence of different loss mechanisms on the oil lost from the bearing in 2 years; that is, after the full drive cycle. It was assumed that 30% of the free volume of the bearing is filled with grease for which the oil content is 85%. Again two cases are shown with shield–inner ring gap openings of 0.01% and 100%. For an almost closed gap (i.e., 0.01% gap opening), both diffusion and breathing effects give a comparable contribution to the total evaporation rate. However, for the 100% opened shield gap, the diffusion

loss is 71.5% and all losses combined add only 0.001%, so clearly the diffusive losses dominate in that case.

Impact of the quality of sealing

Figure 8 shows the effect of sealing by varying the gap between the shield and the inner ring with 100, 80, 60, 50, 20, 1, and 0.01%. The effect of the gap opening was been studied by considering all the loss mechanisms. The oil loss is lower than 1% for up to a 1% gap. When the 20, 40, 50, 60, 80, and 100% opening is considered the loss is 16.7, 31.6, 38.7, 45.6, 58.9, and 71.5%, respectively. It is interesting to see that the losses could be as high as 71.5% if the bearings are not sealed efficiently. The most extreme case would be an open bearing without shields. Any volatiles will be expelled from the "bearing volume" immediately and the vapor pressure will always be zero, leading to an evaporation rate that is only dependent on temperature (see Eq. [3]). The loss of oil during this situation is 100% for the 2-year cycle.

Impact of temperature

To study the impact of temperature, a 10% shield gap opening was selected. Figure 9 shows the evaporation after 2 years for different drive cycles, each with the same minimum temperature of 70° C but now with different maximum temperatures. The maximum temperatures vary from 75 to 150° C. It can be seen from this figure that the oil loss is exponentially increasing with increasing temperature. This behavior is due to an exponential increase in the saturated vapor pressure and evaporation coefficient of the oil. We can see that for the same shield gap opening, oil loss at 75° C is 2.4%, increasing to 8.7% at 150° C.

Conclusions

The Hertz-Knudsen equation was selected to estimate the evaporation rate of base oil from grease inside bearings. It was shown that three mechanisms control the flow of volatiles out of the bearing: EE, ITE, and D through the gap between the shield and inner ring. The model was applied to a shielded ball bearing undergoing an arbitrary selected temperature drive cycle. Here the loss by diffusion through the gap between the shield and inner ring is the dominating loss mechanism if this gap is not blocked by grease. For an almost closed gap, the frequency of temperature fluctuations in the bearing dominates the oil loss. Losses by evaporation will be higher in the case of high operating temperatures and high frequencies of temperature fluctuations and are related to the evaporation rate of the base oil and the quality of the bearing sealing. These conclusions suggest that contacting seals (with a 0% gap opening) are always preferred to reduce evaporation losses. However, such seals generate heat, which increases the temperature, leading to higher evaporation losses. Ideally, the grease itself should close the gap between the shield and inner ring.

Oils with low molecular weight molecules, which typically have a high saturation pressure, will show high evaporation losses. The examples that were selected here were extreme cases. Oxidation of the base oil will have a major effect on the results here and the selected example is therefore only illustrative.

Acknowledgement

We thank Wim Rouwenhorst from SKF for some of the evaporation measurements.

Funding

The authors thank SKF Research and Technology Development for funding this work.

ORCID

Pramod Shetty http://orcid.org/0000-0001-6946-2201
Piet M. Lugt http://orcid.org/0000-0001-9356-7599

References

(1) Moldoveanu, S. and David, V. (2002), *Sample Preparation in Chromatography*, Elsevier: Amsterdam.
(2) Moldoveanu, S. and David, V. (2015), *Modern Sample Preparation for Chromatography*, Elsevier: Amsterdam.
(3) Lugt, P. (2013), *Grease Lubrication in Rolling Bearings*, 1st Ed., John Wiley & Sons: Chichester, UK.
(4) Muller-Brodmann, M. and Bodden, W. (1986), "Influence of Lubricant Ageing on the Wear Characteristics of Sintered Bearings," *Horizons of Powder Metallurgy. Part II*, European Powder Metallurgy Federation, Germany, pp 793–797.
(5) Conley, P. and Bohner, J. (1990), "Experience with Synthetic Fluorinated Fluid Lubricants," **NASA Conference Publication**, pp 213–230.
(6) Totten, G. (2006), *Handbook of Lubrication and Tribology: Volume I Application and Maintenance*, Vol. 1, CRC Press: Boca Raton, FL.
(7) Booster, E. and Baker, A. (1976), "When Lubrication Fails," *Industrial Lubrication and Tribology, 28(6)*, pp 198–201. doi:10.1108/eb053120
(8) Mahncke, H. and Schwartz, A. (1974), "Grease Lubrication of Rolling Bearings in Spacecraft (I)," *ASLE Transactions*, **17**(3), pp 172–181. doi:10.1080/05698197408981454
(9) Lansdown, A., Gupta, R., and Booser, E. (1985), "The Influence of Evaporation on Grease Life," *NLGI Spokesman*, **49**(4), pp 148–153.
(10) Naidu, S., Klaus, E., and Duda, J. L. (1986), "Kinetic Model for High-Temperature Oxidation of Lubricants," *Industrial and Engineering Chemistry Product Research and Development*, **25**, pp 596–603. doi:10.1021/i300024a601
(11) Rezasoltani, A. and Khonsari, M. (2016), "On Monitoring Physical and Chemical Degradation and Life Estimation Models for Lubricating Greases," *Lubricants*, **4**(3), pp 34. doi:10.3390/lubricants4030034
(12) Tagawa, N., Kakitani, R., Tani, H., Iketani, N., and Nakano, I. (2009), "Study of Lubricant Depletion Induced by Laser Heating in Thermally Assisted Magnetic Recording Systems –Effect of Lubricant Film Materials," *IEEE Transactions on Magnetics*, **45**(2), pp 877–882. doi:10.1109/TMAG.2008.2010663
(13) Tagawa, N., Andoh, H., and Tani, H. (2010), "Study on Lubricant Depletion Induced by Laser Heating in Thermally Assisted Magnetic Recording Systems: Effect of Lubricant Thickness and Bonding Ratio," *Tribology Letters*, **37**(2), pp 411–418. doi:10.1007/s11249-009-9533-4

(14) Curry, J. and Christenson, H. (1996), "Adsorption, Wetting, and Capillary Condensation of Nonpolar Fluids in Mica Slits," *Langmuir*, **12**(23), pp 5729–5735. doi:10.1021/la960538b

(15) Sharma, A. (1998), "Equilibrium and Dynamics of Evaporating or Condensing Thin Fluid Domains: Thin Film Stability and Heterogeneous Nucleation," *Langmuir*, **14**(17), pp 4915–4928. doi:10.1021/la971389f

(16) Wayner, P., Jr. (1993), "Spreading of a Liquid Film with a Finite Contact Angle by the Evaporation/Condensation Process," *Langmuir*, **9**(1), pp 294–299. doi:10.1021/la00025a056

(17) Wu, L. (2007), "Modelling and Simulation of the Lubricant Depletion Process Induced by Laser Heating in Heat-Assisted Magnetic Recording System," *Nanotechnology*, **18**(21), p 215702. doi:10.1088/0957-4484/18/21/215702

(18) Zhou, W., Zeng, Y., Liu, B., Yu, S., and Huang, X. (2012), "A Model for Laser Induced Lubricant Depletion in Heat-Assisted Magnetic Recording," *Tribology Letters*, **45**(3), pp 411–416. doi:10.1007/s11249-011-9898-z

(19) Cussler, E. (2009), *Diffusion: Mass Transfer in Fluid Systems*, Cambridge University Press: Cambridge, UK.

(20) Karis, T. and Nagaraj, H. (2000), "Evaporation and Flow Properties of Several Hydrocarbon Oils," *Tribology Transactions*, **43**(4), pp 758–766. doi:10.1080/10402000008982405

(21) Knacke, O. and Stranski, I. (1956), "The Mechanism of Evaporation," Progress in Metal Physics, 6, pp 181–235. doi:10.1016/0502-8205(56)90007-7

(22) Hertz, H. (1882), "Über die Verdunstung der Flüssigkeiten, insbesondere des Quecksilbers, imluftleeren Raume," Annalen der Physik, 253(10), pp 177–193. doi:10.1002/andp.18822531002

(23) Boudart, M. (1961), "Rates of Evaporation of Liquids," Tech. Rep., Princeton University, Princeton, NJ, AD0255155.

(24) Eames, I., Marr, N., and Sabir, H. (1997), "The Evaporation Coefficient of Water: A Review," International Journal of Heat and Mass Transfer, 40(12), pp 2963–2973. doi:10.1016/S0017-9310(96)00339-0

(25) Persad, A. and Ward, C. (2016), "Expressions for the Evaporation and Condensation Coefficients in the Hertz-Knudsen Relation," Chemical Reviews, 116(14), pp 7727–7767. doi:10.1021/acs.chemrev.5b00511

(26) Maxwell J. C. Encyclopedia Britannica. Ency. Brit. Chicago. 1877. 2.

(27) Knudsen Martin (1950). *Kinetic Theory of Gases,* 3rd Ed. London Methuen: London.

(28) Eames, I., Marr, N., and Sabir, H. (1997), "The Evaporation Coefficient of Water: A Review," International Journal of Heat and Mass Transfer, 40(12), pp 2963–2973. doi:10.1016/S0017-9310(96)00339-0

(29) Xia, T. and Landman, U. (1994), "Molecular Evaporation and Condensation of Liquid n-Alkane Films," The Journal of Chemical Physics, 101(3), pp 2498–2507. doi:10.1063/1.467689

(30) Fuchs, N. (2013), Evaporation and Droplet Growth in Gaseous Media, Amsterdam: Elsevier.

(31) Mackay, D. and Wesenbeeck, I. (2014), "Correlation of Chemical Evaporation Rate with Vapor Pressure," Environmental Science & Technology, 48(17), pp 10259–10263.

(32) Ward, C. and Fang, G. (1999), "Expression for Predicting Liquid Evaporation Flux: Statistical Rate Theory Approach," Physical Review E, 59(1), p. 429.

(33) Lugt, P. (2009), "A Review on Grease Lubrication in Rolling Bearings," Tribology Transactions, 52(4), pp 470–480. doi:10.1080/10402000802687940

(34) SKF. (2018), "General Catalogue 17000," AB SKF: Gothenburg, Sweden.

(35) Ott, J. and Boerio-Goates, J. (2000), Chemical Thermodynamics: Advanced Applications: Advanced Applications, Amsterdam: Elsevier.